Imaging Membrane Potential

James Daniel Wilkinson, Corpus Christi College

A thesis submitted in partial fulfilment of the requirements for the degree of *Doctor of Philosophy*

Trinity Term 2014

Imaging Membrane Potential

James Daniel Wilkinson, Corpus Christi College

Doctor of Philosophy, Trinity Term 2014

Abstract

Imaging membrane potential is a promising technique in the elucidation of the interactions of large networks of neurons. The membrane potential in a neuron varies as an action potential, the basic electrical signal of neuronal communication, travels along the length of the cell. Voltage-sensitive dyes play a key role by providing an optical readout of the electric field generated across a neuron membrane by the action potential. However, none of the dyes reviewed in Chapter 1 generate sufficient signal change with changes in membrane potential; this sensitivity problem limits the ability of the imaging membrane potential technique to allow the high spatial and temporal resolution necessary for neuronal networks to be better understood. This thesis features two avenues of research that are expected to result in the necessary enhancements to voltage-sensitive dyes to improve the signal change.

The first avenue is based on the effect of an electric field upon the non-linear optical properties of a porphyrin macromolecule. The encouraging electric field sensitivity of a previous porphyrin monomer voltage sensor inspired an investigation which identified optimisations likely to enhance the voltage sensitivity (Chapter 2). The design, synthesis and initial characterisation of optimised porphyrin voltage sensors is detailed in Chapter 3.

The second avenue is based on the effect of an electric field upon the rate of intermolecular electron transfer. In a suitably designed dye, the competition between electron transfer and fluorescence, following excitation by incoming light, allows the fluorescence intensity to act as an optical indicator of the electron transfer rate, and thus of the electric field. New dyes were rationally designed and synthesised, as this effect had not been applied to voltage sensitive imaging before the research detailed in Chapter 4. The challenging purification of the new amphiphilic dyes synthesised also inspired research into a novel testing method which does not require amphiphilic dyes (Chapter 5).

Acknowledgements

I would like to thank Professor Harry Anderson, without whose enthusiasm, patience, wisdom and creativity this work would not have been possible. I could not have wished for a more approachable or talented supervisor.

I am also indebted to my collaborators - both to those in the HLA group and beyond. To coworkers past and present, I am glad to have not been in this alone. Thanks to Drs. James E. Reeve, Ismael 'loopy' Lopez-Duarte and Jan Fleischhauer for their groundbreaking work on monomeric porphyrin voltage sensors. Igor Boczarow and Wojciech Kaluza are also acknowledged for their more recent input, and I wish them the best in further advancing the IMP *via* SHG project. I am grateful to Dr. Rob Jacobs, Dr. Bríd Cronin, Jason Sengel and Dr. Mark Wallace for being helpful collaborators under the same roof. Further afield, thanks to Dr. Maria Izquierdo Arcusa and Dr. Marina Kuimova (London) for their microscopy work. Even further afield, thanks to Griet Depotter and Prof. Koen Clays (Leuven), and Geoff Wicks, Dr. Mikhail Drobizhev and Prof. Aleks Rebane (Montana) for the non-linear optical measurements they performed.

A massive thanks to each and every one of the many colleagues who have made the HLA group a fun, stimulating and enjoyable workplace for the past five years. I am hugely fortunate to have met such wonderful people, to have learnt about your languages, cultures and baking abilities, not to mention drunk copious amounts of coffee, and baffled you with my daily Marmite on toast. Particular thanks to Mel, James, Ismael, Karolina, Dima, Phil, Matthew, Julien, Levon, Patrik, Christiane, Arjen, Sophie, Guzman, Igor and Cécile. Tim and Sarah, thanks for being great Part II students, I think I learnt more from you than you did from me.

Thanks to my family and friends, old and new, for making the evenings and weekends even more fun than work. I have only got this far with their support, and the loving smile of my beautiful wife, Alice, who makes every day worthwhile.

Thank you Jesus, my saviour, my rock and my purpose.

For Ruthie, the only member of my family who stood a chance of understanding this work, who sadly passed away in April 2011. You are missed.

Glossary

1P	one-photon
1PA	one-photon absorption
2P	two-photon
2PA	two-photon absorption
2PEF	two-photon excited fluorescence
AP	action potential
BODIPY	boron dipyrromethane
CGM	chemically grafted monolayer
CS	charge-separated
DCC	dicyclohexylcarbodiimide
DDQ	2,3-dichloro-5,6-dicyano-*p*-benzoquinone
DFWM	degenerate four-wave mixing
DHB	droplet-on-hydrogel bilayer
DIPEA	*N,N*-diisopropylethylamine
DMF	*N,N*-dimethylformamide
DMSO	dimethylsulfoxide
DMAP	4-*N,N*-dimethylaminopyridine
eT	electron transfer
FRET	Förster resonant energy transfer
GUV	giant unilamellar vesicles
HEG	hexa(ethylene glycol)
HLB	hemispherical lipid bilayer
HOMO	highest occupied molecular orbital
HRMS	high resolution mass spec
HRS	hyper-Rayleigh scattering
IMP	imaging membrane potential
ITO	indium-doped tin oxide
L-B	Langmuir-Blodgett
LRMS	low resolution mass spec
LUMO	lowest unoccupied molecular orbital
MALDI	matrix-assisted laser desorption and ionisation
MS	mass spectrometry
MW	molecular weight
NBS	*N*-bromosuccinimide
NCL	native chemical ligation
NLO	non-linear optical
NMR	nuclear magnetic resonance
OMs	methanesulfonate
OPE	oligo-*p*-phenylene ethynylene
OPV	oligo-*p*-phenylene vinylene

PAMAM	poly(amidoamine)
PDT	photodynamic therapy
PE	phenylene ethynylene
PEG	poly(ethylene glycol)
PeT	photoinduced electron transfer
PPI	poly(propylenimine)
PS	polystyrene
SAM	self-assembled monolayer
SHG	second harmonic generation
SLB	supported lipid bilayer
SNR	signal-to-noise ratio
TCO	transparent conducting oxide
THF	tetrahydrofuran
THG	third harmonic generation
TIRFm	total internal reflection fluorescence microscopy
TLB	tethered lipid bilayer
TLC	thin layer chromatography
TOF	time-of-flight
UV	ultra-violet
VS	voltage-sensitive
VSD	voltage-sensitive dye

Contents

Chapter 1: Introduction

A comprehensive literature review is undertaken, presenting the necessity of imaging membrane potential using voltage-sensitive dyes against other methods. The demanding requirements to be met by such dyes are detailed, and the historical attempts to meet them are analysed and critiqued. Finally, recent advances complete the setting of the scene for the proposition of the novel dyes designed and synthesised in this thesis.

1.1 Neurophysiology & electrophysiology

Neuronal networks, such as the brain, are not well understood. Science has not yet allowed us to fully investigate the significance of the thousands of connections between a cerebral neuron and its neighbours – and with an estimated 10^{10} to 10^{12} neurons in a human brain, each with 10^4 synapse connections to other neurons, the problem is not trivial. Even at the single cell level, we have yet to unravel the mechanistic details of signal propagation in each section of a neuron, with some of the cellular compartments almost completely inaccessible to researchers. Progress in neurophysiology, the study of the physiology of the nervous system, and specifically electrophysiology, the study of electrical phenomena in physiology, is held back by the lack of appropriate methods by which neurophysiologists can interface with these microscopic circuits, as this introduction will explore.

1.1.1 The language of neuron communication

The fundamental language of neuron communication is the action potential (AP). APs are virtually identical in a wide variety of neurons, whether the cell is communicating instructions for movement, urgent environmental sensations over long distances, or integrating the input from thousands of neighbours in the myriad of proximate interconnections of a brain.

An AP is a regenerative, self-propagating electrical impulse travelling along the axon (see Figure 1.1 on the following page) as a result of changes in the transmembrane potential of the cell. It is an all-or-nothing signal with characteristic amplitude ($\approx$ 100 mV) and duration ($\approx$ 2 ms) (Figure 1.2 on the next page), although these values vary from species to species. Information is thus not encoded in the amplitude or duration, but rather in the pattern and frequency of the APs. During an AP the resting potential, the transmembrane potential maintained by the slight excess of Na^+ ions on the extracellular

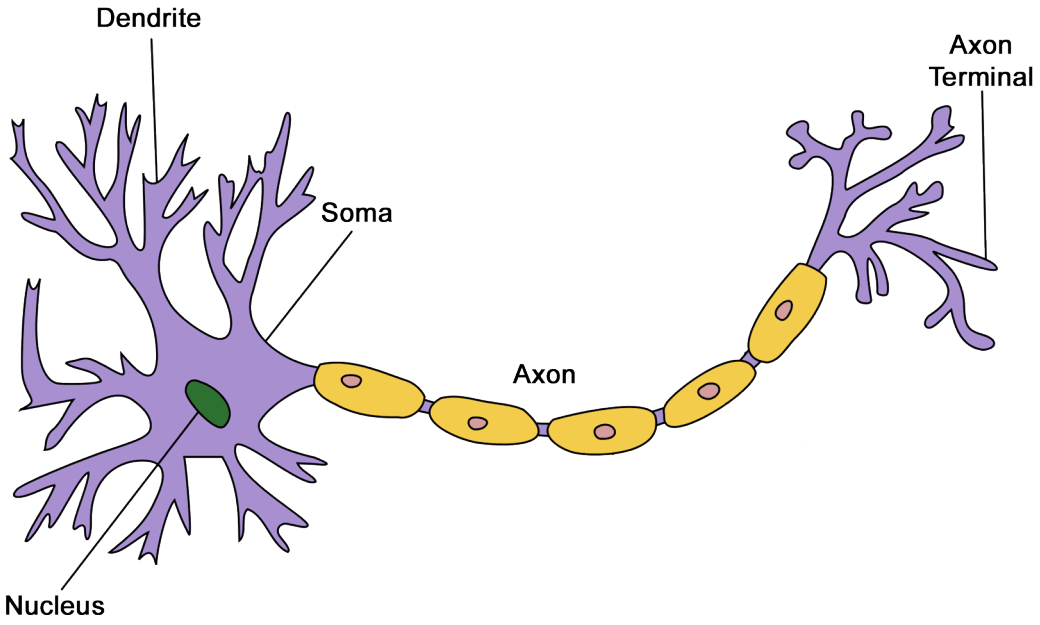

Figure **1.1** The key compartments of a neuron. Figure adapted with permission from Quasar Jarosz under a Creative Commons licence.

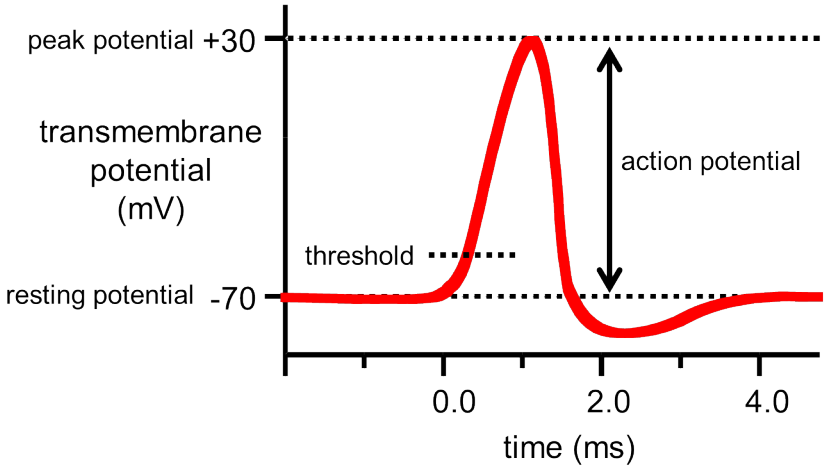

Figure **1.2** The changes in transmembrane potential on the AP timescale.

surface of the membrane of a neuron, is perturbed: an excitatory input in a dendrite, either of a sensory nature or from an AP of an adjoining cell, leads to a localised change in the transmembrane potential from its resting value. If this local graded potential shifts the transmembrane potential in the positive direction (depolarisation) sufficiently, a threshold is reached and an AP is trig-

gered. In general terms, this local potential stimulates voltage-sensitive sodium channels to allow an influx of Na^+ to the cell, causing a complete depolarisation of around 100 mV, flipping the membrane potential from -70 mv to $+30$ mV. An initially slower efflux of K^+ ions helps to repolarise (hyperpolarise) the segment of membrane back to its resting potential (Figure 1.3).

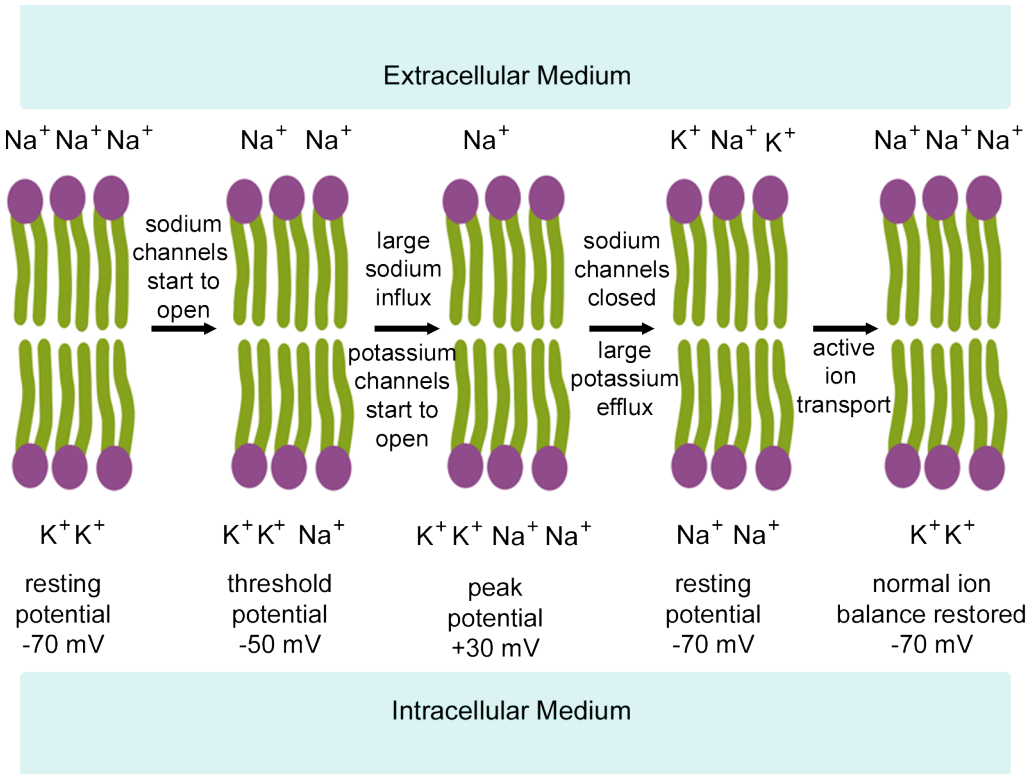

Figure **1.3** A simple depiction of the ion movements across the cell membrane at each stage of an AP.

The direct electrical effect of this change cannot propagate far along the neuron, as the membrane is a poor conductor. However, the AP propagates by triggering the threshold for the ionic activity to occur in the vicinity of the initial depolarisation. Thus a domino-effect reaction occurs – the change in transmembrane potential leads to a regenerative and rapidly self-propagating AP. In the human nervous system, the speed of propagation can reach 120 metres s^{-1}. At a given point on the membrane, the action potential lasts around 2 ms and is followed by the refractory period, a 'silent' few milliseconds where

ongoing changes in ion concentration prevent the threshold from being reached again.

Active transport of ions, as opposed to the passive transport due to concentration gradients and electrical potential, is required to maintain the resting state, and the Na^+/K^+ exchange pump uses metabolic energy to achieve this. Ca^{2+} and Cl^- are also crucial to the maintenance of and variation in transmembrane potential; the exact ions and channels involved in initiating an AP vary with species and cell type.[1]

1.2 Monitoring action potentials

1.2.1 Electrical methods

The most direct way to follow the electrical signals in a neuron or a neuronal network *in vitro* or *ex vivo* is to use electrodes to measure changes in transmembrane potential. The sensitivity of the available electronics for electrophysiology allows good temporal and potential resolution, even allowing the operation of a single ion channel to be monitored.[2] With the application of multiple electrodes or micro arrays, potential changes can be studied at up to 100 locations in a network simultaneously.[3] Direct electrical measurements have been the major tool in this field for many years, with much of the knowledgebase owing its existence to this 'gold standard' in neurophysiology.[2] However, there are several key limitations to electrophysiology that limit the scope of what can be measured. The size of microelectrodes constrains the spatial resolution of electrophysiology to around 50 μm.[4] This is too large for such electrodes to be inserted across the membrane of the dendritic spines, a key cell region in terms of excitatory signal input in the brain. The need for manual positioning of electrodes in the patch clamp technique (Figure 1.4 on the next page) also necessitates highly skilled microscopists and a certain degree

of fortuity. The inherent invasiveness makes taking measurements in 3D in a network inconceivable. Multitransistor arrays are an emerging technique that could address some of these restrictions,[5] but in its current form this approach has limited utility.

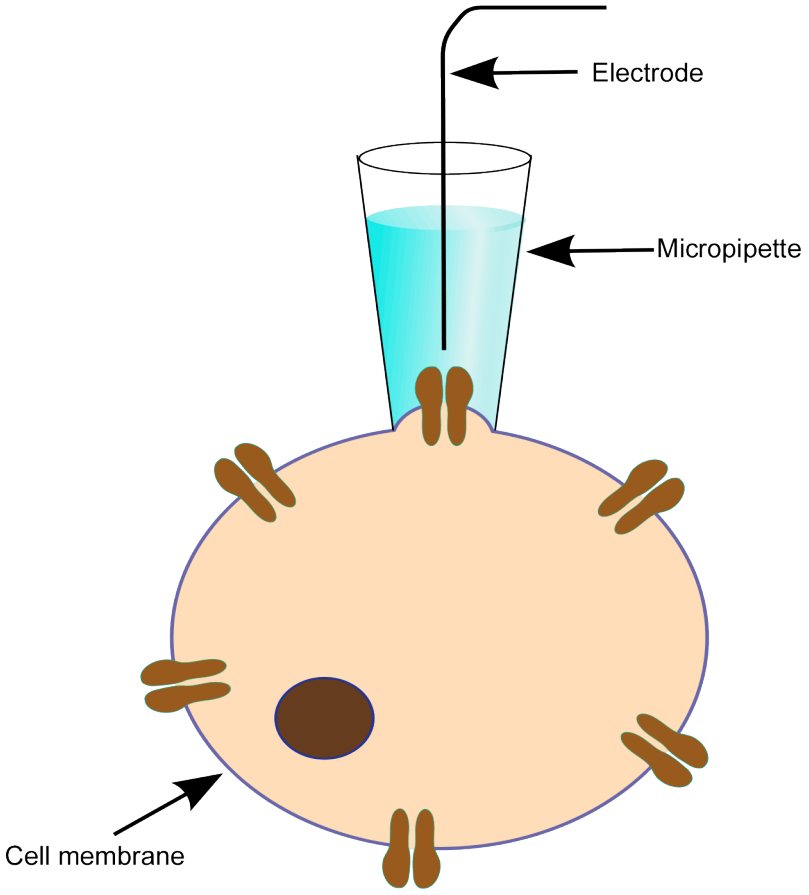

Figure **1.4** In the patch clamp technique, the cell membrane forms an electrical seal around a fine pipette. Figure adapted with permission from Maria Knott under a Creative Commons licence.

1.2.2 Alternative methods

Two alternative techniques, mainly used for *in vivo* studies, are positron-emission tomography and functional magnetic resonance imaging (fMRI). The former is limited in its application because of the dangers of radiation exposure, and both are limited by spatial (100s of μm) and temporal resolution (seconds), and are thus best suited to mapping the activity of larger regions

of a brain during complex cognitive behaviour, such as studying text or memorising objects.[1]

1.2.3 Optical methods

Since the 1950s, scientists have been interested in optical methods for monitoring membrane potential. It is immediately apparent that imaging membrane potential (IMP) is a promising approach to resolving the issue with spatial resolution in electrophysiology, as provided sufficient signal collection (the signal-to-noise ratio (SNR) obtainable with the combination of dye and microscope), the resolution is limited only by diffraction and scattering. Even with these physical constraints, optical measurements can be performed on a 1 μm scale, a 10- to 100-fold improvement.

The earliest investigations were based upon the observation that changes in membrane potential are accompanied by changes in the light scattering and birefringence (polarisation-dependent refraction) properties of the membrane, but 10^3 – 10^4 trials were necessary to gather adequate data, rendering the approach useless.[6] Another early approach to IMP relied upon monitoring changes in the intrinsic fluorescence of the membrane accompanying action potentials, caused by the presence of coenzyme NADH.[6]

1.3 Voltage-sensitive dyes

The primary approach for optically measuring membrane potential is by the addition of VSDs to an *in vitro* or *ex vivo* sample to provide a clear optical readout of electrical activity.[2,7] A VSD provides a measurable optical signal change in response to a change in membrane potential, often a change in fluorescence intensity or wavelength (Figure 1.5 on the following page). Typically, VSDs are designed to localise in the cell membrane where their specific mechanism can interact most strongly with the membrane potential. VSDs are usually in-

troduced to neurons *via* the culture medium (*in vitro*) or *via* injection through a patch clamp (*ex vivo*).

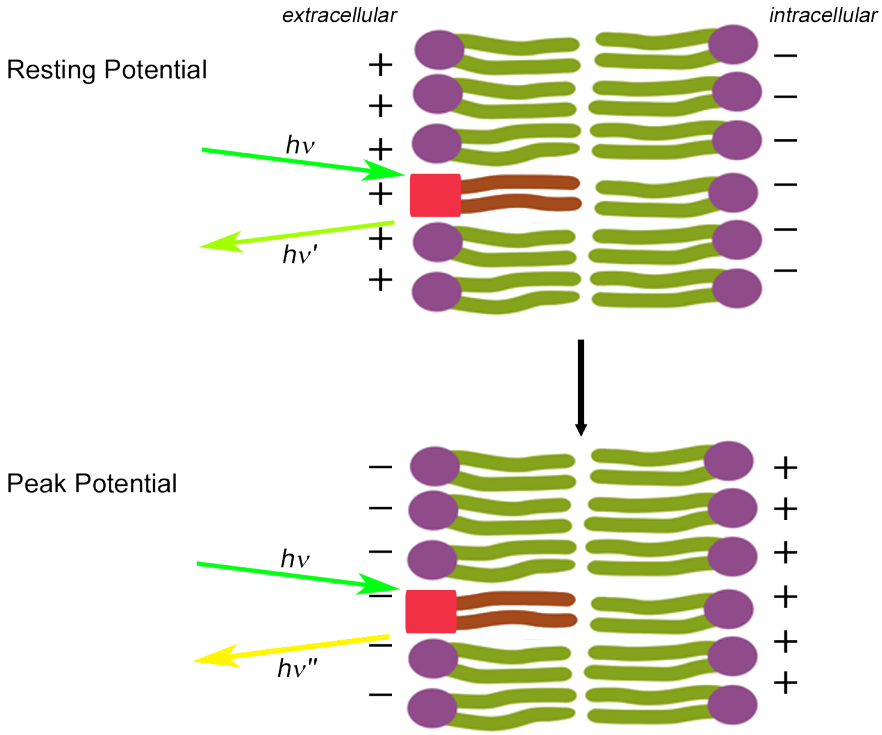

Figure **1.5** A lipid-like VSD (red/orange) embedded in a lipid bilayer (purple/green), providing an optical output of changes in membrane potential (in this case, a fluorescent readout).

Illumination of a certain spot of the sample, in conjunction with natural or stimulated nerve activity, allows the optical signal over time for that location to be collected and processed to reveal the action potentials. With improvements in microscope technology granting the possibility to monitor large numbers of locations concurrently, VSDs are promising tools in unlocking the electrical activity of neuronal networks.[2,7] However, this depends upon the sufficient sensitivity (signal change per unit voltage) of the particular optical mechanism to changes in membrane potential; poor sensitivity leads to a low SNR, limiting both temporal and potential resolution and negating the benefits of increased spatial resolution. The important variables determining the SNR are S the baseline signal (the signal at the resting potential), ΔS the change in signal

and N, the photon flux. They are related thus:

$$\text{SNR} \propto (\Delta S/S)\sqrt{N} \tag{1.1}$$

$\Delta S/S$ can be improved by increasing the sensitivity of the dye to voltage, and N can be improved by increasing the dye concentration, instrumentation sensitivity, or dye design to maximise the baseline signal. Because the dependence of the SNR upon $\Delta S/S$ is linear, whereas there is a square root relationship of SNR with N, optimising $\Delta S/S$ is a better strategy.[2] Without sufficient SNR, signal averaging across multiple trials or a larger area is required, thus resulting in a loss of important information, for example critical differences between individual action potential events. Compared to single trial measurements which capture this information, averaged measurements diminish the advantages of IMP over performing direct electrical measurements. Averaging is also undesirable as any movement of the sample or other jitter will lead to an apparent broadening of the voltage-time measurement.[8] An alternative to averaging is to increase the incident light intensity,[9] but this comes at the expense of increased phototoxicity, caused by the formation of destructive singlet oxygen by energy transfer from photoexcited dye. The generation of singlet oxygen in or near the membrane limits the duration of an experiment due to cell death. Most VSDs developed to date suffer from poor sensitivity. In order to harness the advantages of optical measurements of membrane potential, the neurophysiologists toolkit must be expanded with VSDs of improved sensitivity.

1.3.1 The ideal VSD

There are a variety of mechanisms by which a dye may exhibit a potentiometric optical behaviour, and these can be classified as direct or indirect. Direct dyes operate by sensing the large changes in electric field that accompany changes

in transmembrane potential during an action potential: a 100 mV change in potential across a dielectric medium of around 5 nm thick induces an electric field change of 10^7 V m^{-1}.[10] As the membrane itself is the capacitor and the effect of the field will diminish rapidly away from the membrane, direct dyes must be localised in the membrane to experience the field and respond to it. They can be divided into two categories, slower and faster, depending on whether there is a motion response or a rapid electro-optic response to changes in membrane potential respectively. The slower dyes operate on the order of milliseconds at best, whereas faster dyes operate on the microsecond timescale.

Indirect dyes work by sensing changes in ion concentration with membrane potential, most commonly Ca^{2+}. Although the absolute changes in ion concentration during an action potential are small (micromolar), if the cation affinity of a cation-binding dye is matched carefully to the cation concentration, measurable changes in optical properties can be obtained.[11]

The quest for effective VSDs has proved challenging due to the demanding requirements imposed by APs and the outstanding performance of electrode techniques. In order to be an excellent VSD, a dye must be capable of providing an optical signal that is sensitive to 1 mV changes in transmembrane potential on sub-ms timescales. A high sensitivity is desirable to ensure a high SNR ratio and avoid the need for signal averaging or increased illumination intensity. An ideal VSD will also have no toxic or pharmacological effects that will interfere with measurements.[7] For decades these criteria also included transferability between different species and cell types all with simple-to-calibrate responses, but these additional challenges have been deemed unsolvable.

I will now examine the match between these requirements and historical VSDs in order to provide the context for the work in this thesis towards the design of improved voltage sensors. Briefly reviewing the potentiometric mechanisms of the most significant VSDs, critically analysing their strengths and

shortcomings, I will highlight the need for continued discovery and advances in this field.

It must be noted at the outset that as microscope technologies and imaging methods have evolved along with VSDs, it is hard to draw quantitative comparisons between mechanisms across the generations of dye design. This is partly due to an evolution in the way data have been reported (the preferred scale is currently % $\Delta S/S$ per 100 mV). As a general rule, when earlier measurements boasted high sensitivities and temporal resolution, they lacked the spatial resolution that is now targeted in the age of laser microscopy, and offered few advantages over electrode techniques. However, the earliest advances in this field served to demonstrate the benefits of optical measurements in terms of monitoring networks of neurons at multiple locations and provided great inspiration for further research.

1.3.2 Indirect dyes

Ca^{2+} binding chromophores have been used for IMP for 45 years, although the earliest example was not a synthetic dye but the fluorescent protein aequorin.[12] Synthetic Ca^{2+} sensors started to become useful in the 1980s, with new tetracarboxylate dyes from Roger Y. Tsien (Nobel Laureate, Chemistry, 2008) offering improvements in metal selectivity and binding kinetics over previous dyes.[11,13] **Fura-2** (Figure 1.6 on the next page) is the most widely used of these dyes and exhibits a fluorescence wavelength change in response to changes in Ca^{2+} concentration, which can be monitored at one wavelength to give a typical $\Delta S/S$ per 100 mV of around 5%.[14,15] Later dyes have achieved much higher sensitivities, up to 150% $\Delta S/S$ per 100 mV.[16,17]

However, Ca^{2+} binding dyes suffer from the natural impediment of acting as calcium buffers, requiring careful controls to assess the effect that the dye has upon normal cellular electrical activity. Buffers can also saturate and fail

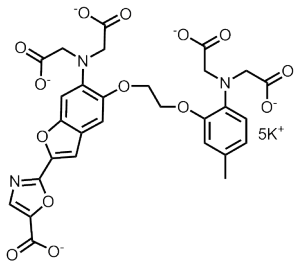

Fura-2

Figure **1.6** One of the most widely used Ca^{2+} sensing dyes.[14]

to respond to rapid successions of events.[7] The probes are also not designed to localise near the membrane and thus their response also relies upon diffusion of calcium ions. These factors lead to slow kinetics, on the order of tens to hundreds of ms.[15,18] Further, as the mechanism of repolarisation leads to a faster decrease in transmembrane potential than in Ca^{2+} concentration, the signal is strongly biased to the rise of the AP,[19] and any subthreshold post-AP activity is missed.

Ca^{2+} binding chromophores thus find their use in situations related to IMP, for example in studying the presence of voltage-sensitive calcium channels and proving their mechanistic role.[20,21] Although Ca^{2+} indicating dyes are still used in active research, their utility for multi-site resolution of APs in live systems is limited by their temporal response.

1.3.3 Direct dyes

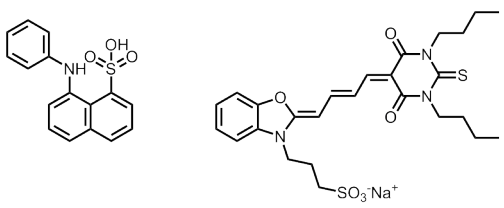

ANS **M540**

Figure **1.7** The two most significant early direct dyes.[22,23]

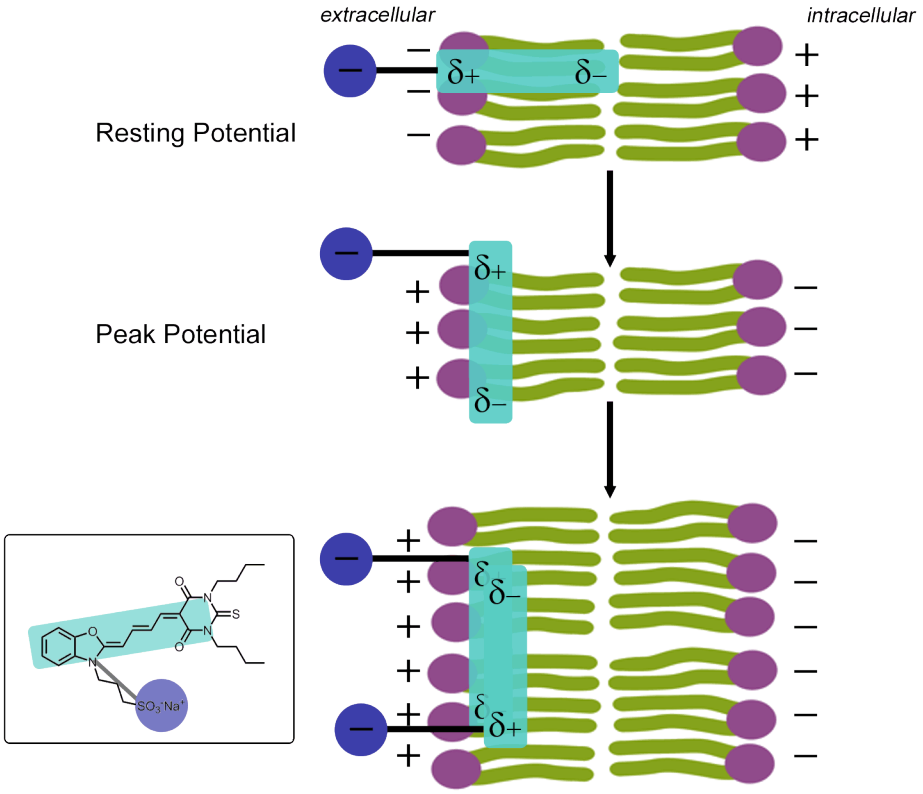

Figure **1.8** The rotation-dimerisation mechanism thought to lead to voltage-sensitivity in M-540.[27,28] As shown in the inset, the blue circle represents the sulfonate which acts as an hydrophilic anchor, and the turquoise rectangle the dipolar section of the dye which aligns preferentially with the membrane charge.

The first example of using a direct dye to monitor APs was published around the same time as the earliest Ca^{2+} sensors. 8-Anilinonaphthalene-1-sulfonate (ANS) (Figure 1.7 on the preceding page), known to be sensitive to conformational changes in a macromolecular environment, was introduced to giant squid axons and a reversible increase in fluorescence was observed during nerve excitation. However, no anatomical explanation of how conformational changes in macromolecules in the nerve are related to changes in the transmembrane potential was offered.[22] Other early examples of direct fluorescent probes emerged from the screening of large libraries of organic dyes in the search for conductance- and current-sensitive probes for monitoring membrane potential.[24,25] The researchers instead found strong correlations between

fluorescence changes and the action potential (AP) itself, and the field of IMP in a direct manner was truly born. Early developments in the field include the use of the merocyanine dye **M-540** (Figure 1.7) exhibiting absorption and emission wavelength changes detectable in a single trial,[23] and the use of dyes to enhance birefringence measurements beyond what an unstained cell allows.[26] Even at this early stage in the history of VSDs, dyes responding on sub-millisecond timescales were allowing single-trial AP measurements with SNR over 10.[24,27]

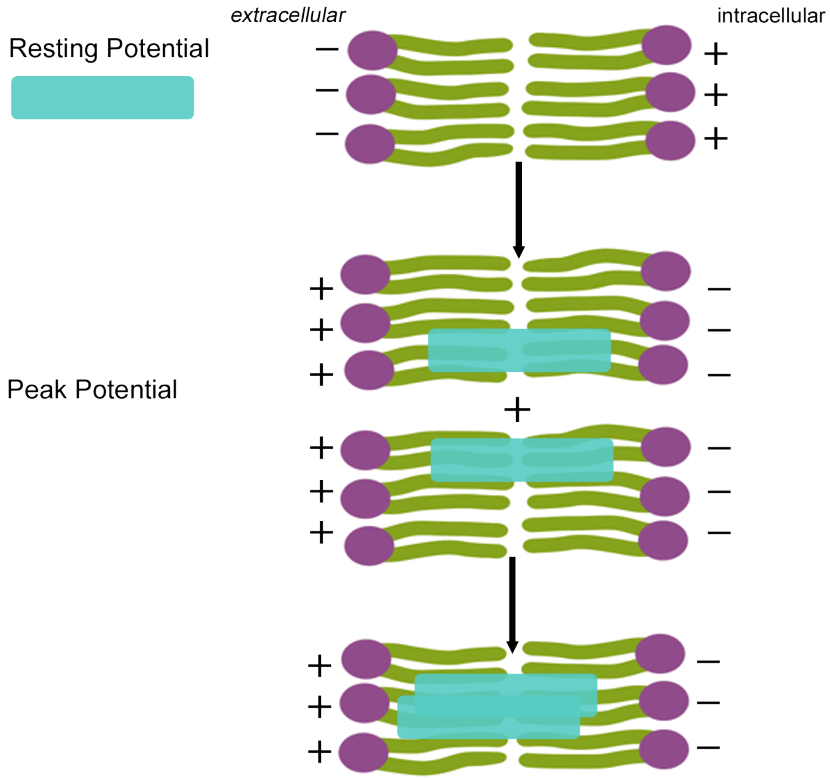

Figure **1.9** The repartitioning-aggregation mechanism.[27,28] The VSD, represented by a turquoise rectangle, undergoes electrophoresis when the membrane charge changes, followed by aggregation within the hydrophobic membrane environment.

During this period, many investigations focussed on deducing the mechanisms of voltage sensitivity, driven by the desire for calibrated signals that were transferable between species. The fastest dyes were found to operate either by a rotation-dimerisation mechanism or by a repartitioning-aggregation

mechanism, both relying upon movement. In the rotation-dimerisation mechanism (Figure 1.8 on Page 13), the dye rotates in response to voltage changes to allow a preferential dipole alignment, then proceeds to form dimer aggregates parallel to the membrane surface, the dye-dye electronic interaction leading to wavelength shifts. In the repartitioning-aggregation mechanism (Figure 1.9 on the preceding page) there is a potential-induced movement of dye from the aqueous region (intra- or extra-cellular dependent upon the loading method) into the membrane (electrophoresis), with aggregates forming inside the membrane resulting in further spectral shifts.[27,28]

Because of the role of aggregation in these mechanisms, the voltage sensitivities were found to change with loading concentration. The sensitivities were also found to vary greatly from species to species; the key factor in this was thought to be that the mechanisms relied upon movement, either *via* repartitioning or rotation.[29] The differing membrane lipid composition of different species implies that motion-based mechanisms might always result in poor transferability, inspiring the first investigations into a new dye mechanism — electrochromism.[30]

1.3.4 Electrochromic dyes

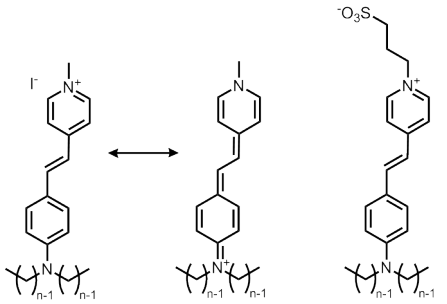

Di-n-ASP **Di-n-ASPPS**

Figure **1.10** The first rationally-designed VSDs.[30]

The electrochromic, or Stark shift, mechanism is now the most thoroughly explored and applied mechanism. Electrochromism is the shift in absorption and emission wavelengths of a chromophore as the result of a change in interaction with a local electric field between the ground and excited states. For example, **Di-5-ASP** (Figure 1.10 on the page before), featuring strongly electron-accepting and -withdrawing moieties joined by a short π-bridge, undergoes an intramolecular charge shift in the excited state. As the resultant change in dipole moment interacts with local electric fields, the energy levels are modulated and thus the absorption and emission energies are also varied (Figure 1.11). This effect is the origin of electrochromism, an electro-optic effect as the optical properties are modulated by the direct interaction between the electromagnetic field of light and the chromophore.

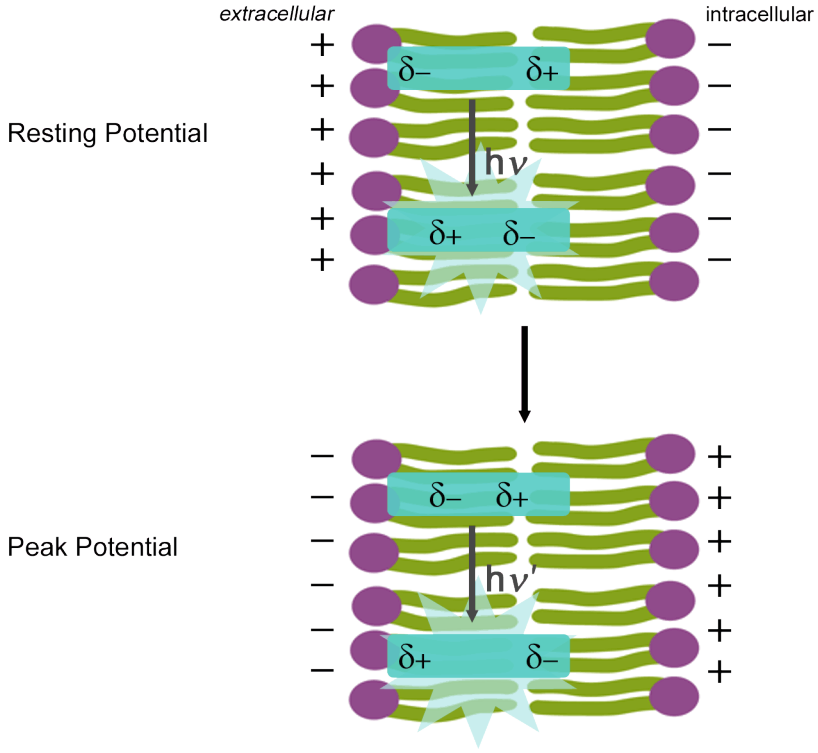

Figure **1.11** The electrochromic mechanism. The dipoles labelled on the VSD (turquoise rectangle) show the stabilisation of the change in dipole upon excitation by interaction with the transmembrane electric field, leading to shifts in the excitation and emission wavelengths when the field is changed.

Examples of electrochromic dyes were already known, but they had not been applied to IMP.[30] Mechanistic studies on existing VSDs, such as **M-540**, had previously ruled out electrochromism as an insignificant contribution.[27,28] However, computational analysis of charge shifts within a range of the best probes to date, including **M-540**, indicated that many of these dyes in fact had promising electronic structures for observing electrochromism.

A combination of theory-led design, along with the previous (and crucial) observation that **M-540** readily undergoes a voltage-sensitive rotation within a membrane, resulted in the first probe optimised for this mechanism, **Di-5-ASP**, a (*para*-aminostyryl)pyridinium dye.[30] The key design improvement over dyes like **M-540** is the use of long alkyl chains to 'fix' the orientation of the chromophore perpendicular to the membrane surface, thus suppressing the rotation-based mechanism which would drag the chromophore away from preferential alignment with the changing electric field. The overall amphiphilicity of **Di-5-ASP** is also important in order to enforce asymmetric incorporation into the lipid bilayer membrane, without which the electro-optic voltage-sensitive response will cancel to zero. Thus whereas for **M-540** there was a competition between the electrochromic and rotation-based mechanisms, **Di-5-ASP** was optimised towards the electrochromic mechanism alone.

Di-5-ASP represents a critical advance in the VSD field as the first probe rationally designed to operate *via* a specific mechanism. It was found to have 5% $\Delta S/S$ fluorescence sensitivity, attributed to arise almost entirely from electrochromism (as judged by the match of the voltage response spectrum to the first derivative of the excitation spectrum). In a model membrane hemispherical lipid bilayer (HLB) setup, the response timescale was judged to be as fast as the bilayer was chargeable, 100 μs.[31]

Initial investigations into derivatives of **Di-5-ASP**, such as **Di-6-ASP** and **Di-6-ASPPS**, revealed that changes in the charged headgroup did not

dramatically change the voltage response, implying that electrophoresis is not important, lending reinforcement to electrochromism as the sole mechanism.

However, comparing the performance of **Di-4-ASP** and its zwitterionic analogue **Di-6-ASPPS** in a model membrane setup, and a squid axon, immediately revealed complicating factors. Both dyes were greatly reduced in their sensitivity ($\sim 40\times$) as a result of strong background fluorescence, due to non-specific membrane binding and the geometric constraints of imaging a cylindrical cell membrane compared to the spherical HLB setup. **Di-4-ASP** was found to become less sensitive over time, attributed to the negative resting potential of the axon inducing dye flip-flop and eventual localisation in the internal leaflet of the bilayer. The effect of the electrochromic mechanism was thus diminished by other processes, and its sensitivity was found to be far from generalisable across different cell types. In contrast, the neutral zwitterionic chromophore **Di-6-ASPPS** only displayed a single time-component response on a very fast timescale of around 1 μs, the limit of the experiment.[32] The electrochromic mechanism was thus found to be less robust than initially hoped.

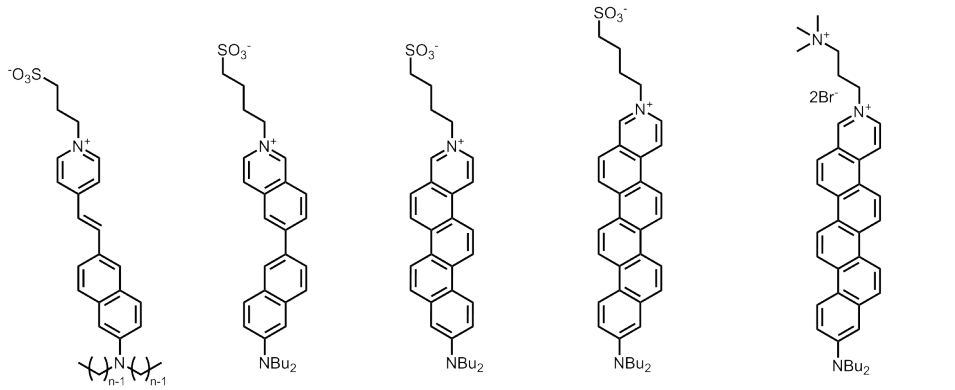

Di-n-ANEPPS **BNBIQ** **ANNINE-5** **ANNINE-6** **ANNINE-6plus**

Figure **1.12** Second-generation electrochromic dyes.[33]

Nevertheless, the use of this mechanism was furthered by the synthesis of the ANEPPS dye family (Figure 1.12), characterised by enhanced elec-

trochromic properties due to increasing the charge-shift distance relative to the ASP dyes without introducing extra flexibility.[33] The top performing dye of this family, **Di-4-ANEPPS**, exhibits a modest increase to 8% $\Delta S/S$ per 100 mV in both excitation and emission, compared to 5% of the best ASP dye.[34] Once more the localisation of an optical membrane probe was found to vary greatly from membrane to membrane. Indicative of this is the use of an ANEPPS dye to detect changes in the permanent dipoles (the strong potential change Ψ_d in a small region of the bilayer, resulting from the polarised bonds of the lipid headgroups; Figure 1.13) of bilayers of differing compositions, an effect that clearly interferes with its ability to sense the electric field changes of the transmembrane potential.[7,35,36] This result casts doubt on whether any dye could ever be truly transferable and calibrated across different species; bilayers are more complicated than early researchers could have envisaged.

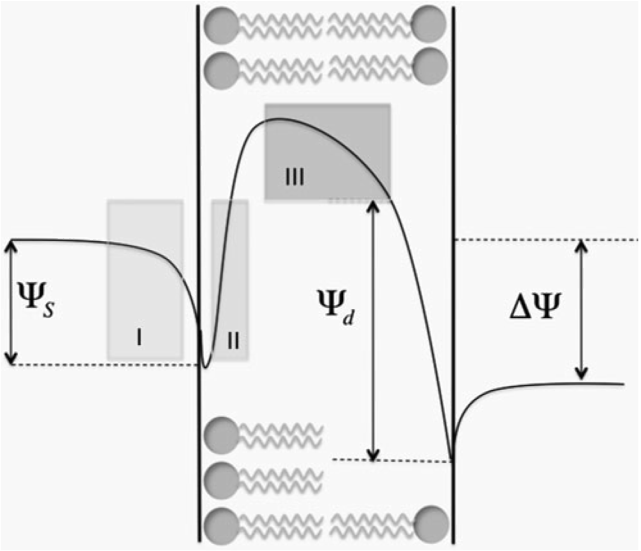

Figure **1.13** The electrostatic potential profile across the lipid bilayer with the locations of fluorescent probes used to determine surface potential (area I), dipole potential (area II) and membrane potential difference (area III). Reproduced with permission from reference 36.

Later work from the group of Peter Fromherz uncovered that the early electrochromic VSDs do not operate *via* a purely electrochromic mechanism,

exhibiting multiple contributions to their voltage-response leading to varying voltage sensitivity in different cell lines.[37,38] The free rotation about C−C bonds and the potential for photoisomerism about the C=C bonds in ANEPPS-type dyes results in other spectral shifts beyond the expected electrochromic response.[39,40] This problem has been remedied by providing greater rigidity to the system by annelating the hemicyanine structures (**BNBIQ, ANNINE-5/-6/-6plus**, Figure 1.12 on Page 18), enhancing the sensitivity by a factor of 5 to around 50% $\Delta S/S$ (although some of this enhancement is also due to the doubled charge shift distance compared to **Di-4-ANEPPS**).[41] The poor water-solubility of **ANNINE-6** was addressed by a simple modification to a doubly-charged polar headgroup (**ANNINE-6plus**).[42]

This mechanism certainly holds more promise than the earlier redistribution and reorientation mechanisms, and with a wide variety of closely related dyes available, it may be possible to find a suitable chromophore and headgroup combination to give a pure electro-optic response in each cell to be studied.

However, a general drawback of all electrochromic dyes is that the greatest sensitivity is found in the 'spectral tails' (Figure 1.14). As the change in photon count is greatest in the regions of the spectrum where the curve is steepest, to achieve a high sensitivity the intensity must be monitored at the edge of the emission band. However, this results in the wasting of photons, as the intense 'photon rich' part of the spectrum is discarded. In the process of maximising $\Delta S/S$, N, the photon count, is thus drastically reduced, leading to poor SNR (Equation 1.1 on Page 9).[41] It is also of note that the strongest electrochromic responses have been found in a family of very closely related structures, strong 'push-pull' 1D conjugated systems. Only minor changes have been possible over 30 years. In contrast, the FRET and PeT mechanisms considered next can be designed with a modular approach to choosing components.

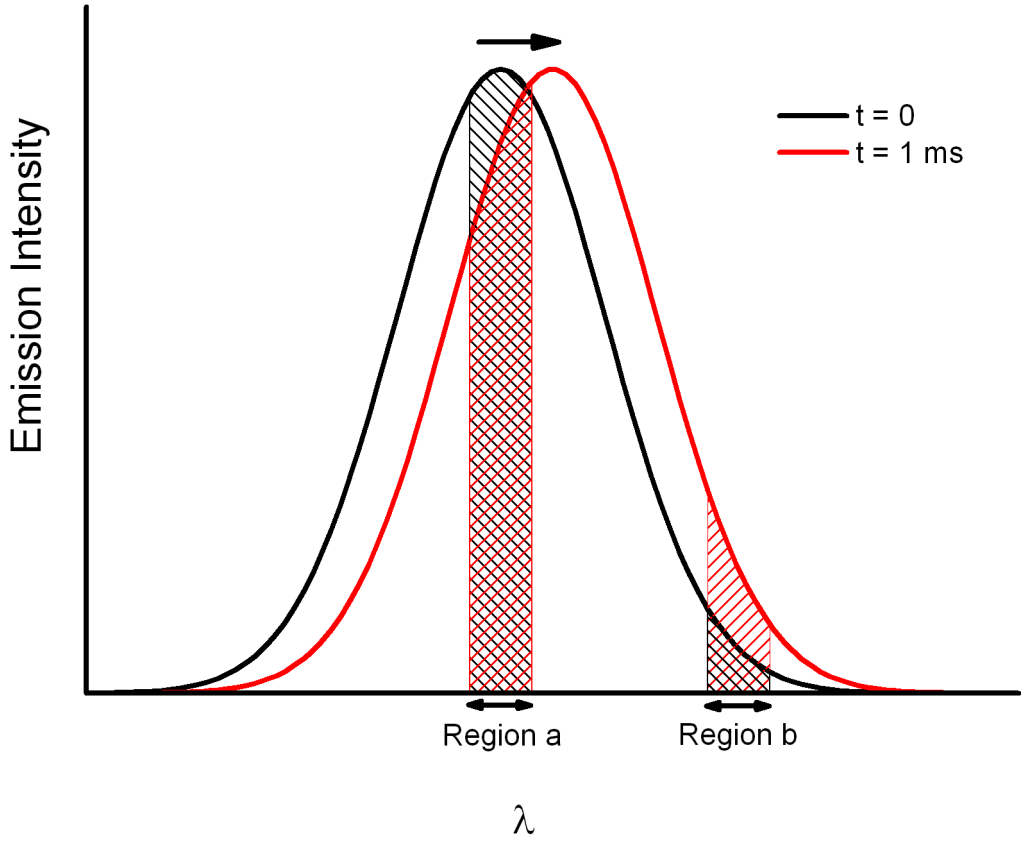

Figure **1.14** Collecting photons from the emission 'spectral tail' gives the highest voltage sensitivity for electrochromic dyes. (The black and red curves indicate the spectra at resting and peak transmembrane potential respectively. The most sensitive detection technique uses a photon-counting method which does not discriminate between wavelengths, therefore filters are necessary to choose a region of the emission wavelength to collect. Regions a and b are two wavelength regions that could be monitored in a microscope. The change in integration between resting and peak potential, the signal change, is much greater in region b than in region a.)

1.3.5 Förster resonant energy transfer systems

More recently, voltage sensing systems relying on FRET have been developed. FRET occurs between two fluorophores with appropriately matched emission (donor) and excitation (acceptor) energies and leads to a quenching of the emission of the donor along with augmented emission of the acceptor. The efficiency with which this process occurs scales with $\left[\frac{R_0}{r}\right]^6$ where r is the distance between the fluorophores, and R_0 is the Förster distance (at which the energy transfer efficiency is 50%).[43] As R_0 is typically on the order of nm, a good match with the 3 – 5 nm neuronal membrane thickness, an unbound two com-

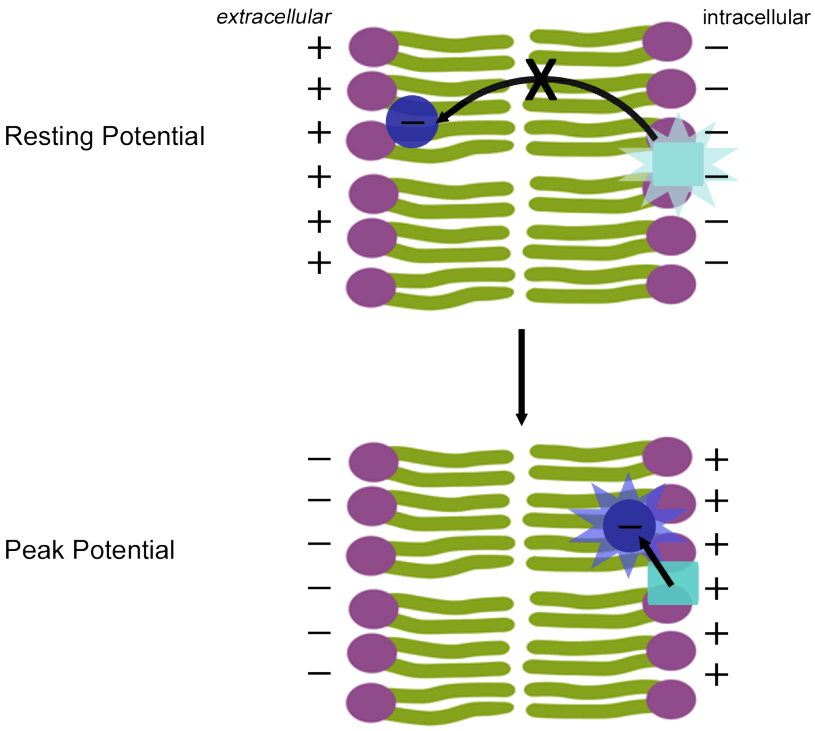

Figure **1.15** The basis of the FRET mechanism. The extent to which the mobile anionic component (blue circle) quenches the fluorescence of the static component (turquoise rectangle) depends upon the distance between the two components, which varies with the field-induced motion of the mobile component.

ponent system where one component is 'fixed' in the membrane and the other is free to translocate in response to changes in the transmembrane potential was conceived (Figure 1.15). The significant changes expected in the FRET efficiency of such a system were hoped to result in a large and ratiometric signal change between the fluorescent signals of each of the two components (see Figure 1.16), and thus a highly sensitive voltage-sensing system.

The first example of a FRET voltage-sensing system consisted of a fluorescently-labelled protein (**FL-WGA**, a commercially available lectin) and the lipophilic anion **DiSBAC$_6$(3)** acting as the anchored and mobile components respectively (Figure 1.17 on the following page). Both of these individual components were introduced to the sample tissue *via* the culture medium, **DiSBAC$_6$(3)** requiring β-cyclodextrin as a delivery agent. **DiSBAC$_6$(3)**, the

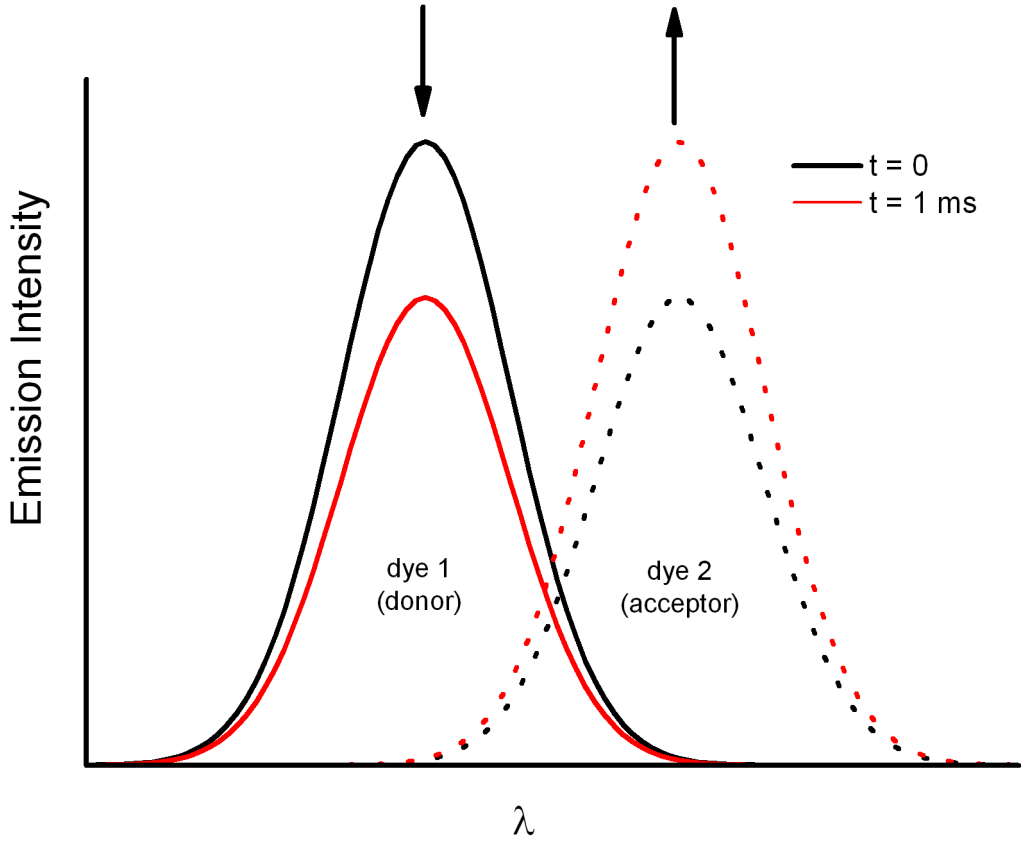

Figure **1.16** The change in emission intensity observed for each of the two fluorophores in a FRET voltage-sensor system. (solid and dashed curves represent the two individual dyes; black and red curves indicating the spectra at resting and peak transmembrane potential respectively).

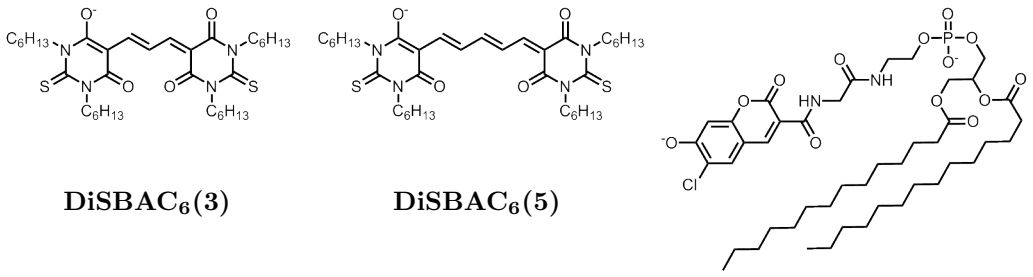

DiSBAC$_6$(3) **DiSBAC$_6$(5)** **CC1-DMPE**

Figure **1.17** Examples of the two components used in a FRET VS system.[44,45]

FRET acceptor, was found to translocate across the inside of a bilayer on a 2 ms timescale, and this movement caused a ratio change of up to 34%/100 mV in cells. The principle was also proved with an alternative fluorescently-labelled protein (**TR-WGA**), whose excitation energy aligns with the emission

of **DiSBAC$_6$(3)** such that the mobile component acts as the FRET donor instead of acceptor.[44] The sensitivity was later improved to 80% $\Delta S/S$ using **CC1-DMPE** (Figure 1.17 on the page before), a coumarin-labelled lipid, and **DiSBAC$_6$(3)**. Faster time resolution (0.3 ms) was attained with a mobile anion with improved charge delocalisation, **DiSBAC$_6$(5)**, as the activation barrier to moving the anion through the low dielectric medium of the lipid bilayer membrane is decreased.[45]

Another approach to using FRET to image membrane potential was to modify a voltage-gated ion channel, the very machinery of the cell responsible for propagating action potentials, by tagging with a FRET pair in the voltage-sensitive domain to form a voltage-sensitive fluorescent protein (VSFP). Movements in the voltage-sensitive domain during AP propagation result in a change in the relative position of the two fluorophores, modulating the FRET efficiency. This approach benefits from genetic targeting but the sensitivities are still unpractically low (<1% $\Delta S/S$).[7,46]

A key advantage of these systems over other VSDs is that a ratiometric fluorescence measurement can be made by recording the change in emission intensity of both the FRET donor and FRET acceptor (Figure 1.16). A ratiometric approach removes some sources of experimental error present in single emission measurements, for example uncertainty in signal changes caused by cell movement and photobleaching over time.

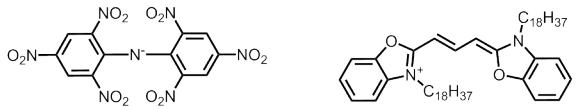

DPA **DiO**

Figure **1.18** FRET systems can also use a non-fluorescent dye, such as **DPA** as the energy acceptor, partnered with a fluorophore, such as **DiO**.[47]

However, variants of the system have also successfully used a non-fluorescent FRET acceptor, dipicrylamine (**DPA**) (Figure 1.18). The first example

of this uses a genetically encoded fluorescent farnesylated enhanced green fluorescent protein (**eGFP**), which exhibits specific binding to the inner leaflet of the plasma membrane. This hybrid system, so-called because one of its components is genetically encoded and the other loaded *via* injection or culture medium, has achieved a maximum 34% $\Delta S/S$ with 0.5 ms resolution.[48] Another example features a purely synthetic system, pairing **DiO**, a fluorescent membrane label with **DPA**, obtaining 60% $\Delta S/S$ with 0.1 ms time resolution, limited only by the translocation rate of **DPA**.[47] This FRET pair was used to demonstrate optical measurements of action potentials in different compartments of the same Purkinje neuron (the soma, dendrites and axon).

These measurements were of sufficient spatiotemporal resolution to clearly demonstrate that the AP is initiated in the axon, and also revealed differences in the temporal width of the AP in the different compartments, consistent with propagation *from* the axon. Such measurements are impossible with electrode-based methods - the electrodes measure an averaged AP response compared to the optical measurement because their size limits the spatial resolution achievable.

Despite the high voltage sensitivity of most of the FRET VS systems, and the ratiometric readout that some systems offer, there are clear disadvantages compared to other VSDs. The most significant of these is the extra capacitative burden put on the membrane by the translocation of the mobile anion. This can interfere with normal cellular electrical function, changing the resting potential of the cell, and can give misleading results due to aborted APs or extraneous subthreshold activity.[48] However this effect can be tested for, and some dyes have been assessed to give negligible capacitative load up to a certain dye concentration.[44,47]

Further, with the exception of the **VSFP** family, all of the systems require a correct stoichiometry of the two components to be established, which may

not always be simply achieved, particularly given the hydrophobic nature of the anion component. This could be solved by a tethered 'two-in-one' dye, but there are no examples of this being attempted. The mobile component also presents problems in optimising the time response of the FRET mechanism, as increasing the charge delocalisation and lipophilicity to improve the translocation kinetics come at the expense of impeding the aqueous solubility necessary for introducing the dye to the cell medium. There is thus a limit upon the time resolution achievable (tens to hundreds of μs),[44] whereas the pure electro-optical mechanisms could be 10^3 – 10^6 $\times$ faster than this, given satisfactory $\Delta S/S$ and sufficiently sensitive detection. Although the FRET mechanism has proved impressive so far, these clear disadvantages limit its utility.

1.3.6 Discussion concerning existing VSDs

Performing optical measurements of membrane potential using voltage-sensitive dyes is clearly a promising method, and essential for understanding neuronal networks. Yet the majority of the molecular probes that have been tested are flawed, and many of the advantages that optically monitoring changes in membrane potential could offer have not been fully realised. The most detrimental shortcoming of VSDs to date is low sensitivity, which requires an equally detrimental compromise from the ideal experiment to be made: temporal or spatial averaging of optical signals, which reduces the benefits of optical measurements over the electrophysiological approach. Poor voltage-time resolution due to insufficient signal change gives direct electrode measurements the upper hand. With the 'spectral tail' limitations of electrochromic dyes requiring either a signal or sensitivity compromise, and the time resolution and capacitance limits of FRET systems, there is ample room in the field for alternatives to be explored.

Optical probes introduce the problem of photodamage or phototoxicity to the experimental setup, an issue that each generation of dyes has struggled with and that no dye can be completely immune to. Some dyes have been found to be better or worse in this respect, but no clear structure-property relationships have been proposed. Exacerbating the issue has been the move away from studying robust giant squid axons to studying fragile cells, and the confined intense light used in modern high resolution laser microscopy.[27,29] An 'unphysiological' solution to the problem is to deoxygenate the cell storage medium.[26] More elegant is the nature-inspired use of the carotenoid astaxanthin as a membrane-localised singlet oxygen quencher.[45] However this problem can be best resolved by addressing the major issue of low sensitivity by developing new VSDs, as enhancements in sensitivity allow lower intensity illumination to achieve the same SNR, reducing the concentration of photoexcited dye molecules for a given SNR and thus reducing phototoxicity. The problem of photodamage can also be addressed by considering the incident wavelength, and the opportunity to lower the necessary energy and power better that VSDs could provide. It can also be tackled by considering second harmonic generation, a non-linear optical mechanism which does not involve the formation of real excited states. The rest of this introduction will consider the latest developments and ideas in this field and how they are starting to resolve the issues of poor sensitivity and photodamage.

1.4 Voltage-sensitive photoinduced electron transfer

A mechanism based upon PeT is a possible solution to these problems.[a] At the start of the research in this thesis, the proposition of this mechanism was

[a]It is noted that indirect Ca^{2+} voltage sensors in Section 1.3.2 on Page 11 operate by ion binding changing PeT efficiency, but that a direct sensitivity of PeT to the transmembrane electric field has only been recently explored, as detailed here.

known.[10] A demonstration of this mechanism in action was reported while the work in this thesis was in progress (see Section 4.7 on Page 193).[17]

Following initial excitation by a photon, the fate of an excited state dye is typically to return to its ground state by a combination of emission and non-radiative decay. However if the sum of the energy of the first excited state and the reduction potential of a nearby electron acceptor matches or exceeds the oxidation potential of the dye (see Section 4.2 on Page 158), electron transfer from the lowest unoccupied molecular orbital (LUMO) of the donor into the LUMO of the acceptor becomes a competing process of the excited state (Figure 1.19(a) on the next page). Alternatively, the fluorophore can be an electron acceptor, and the electron transfer process is from the highest occupied molecular orbital (HOMO) of the donor into the partially vacated HOMO of the fluorophore (Figure 1.19(b)). When a fluorophore undergoes the PeT process, its fluorescence is quenched to an extent depending upon the competition of the rates of PeT (k_{et}), fluorescence (k_{f}), and non-radiative decay (k_{nr}) as expressed in the equation for the fluorescence quantum yield:

$$\Phi_{\mathrm{f}} = \frac{k_{\mathrm{f}}}{k_{\mathrm{f}} + k_{\mathrm{et}} + k_{\mathrm{nr}}} \tag{1.2}$$

If the electron transfer between the donor and acceptor occurs across a molecular wire aligned with a strong electric field (Figure 1.20 on Page 30), its rate will be modulated up or down by the field. Any change in k_{et} will affect a change in the fluorescence quantum yield, and thus in the presence of the varying electric field the fluorescence intensity will vary. The large variations in transmembrane electric field can therefore lead to a fluorescent readout of changes in membrane potential in an appropriately designed system.

This mechanism presents several key advantages over other mechanisms. As the fluorescence intensity is the variable, the whole of the fluorescence band

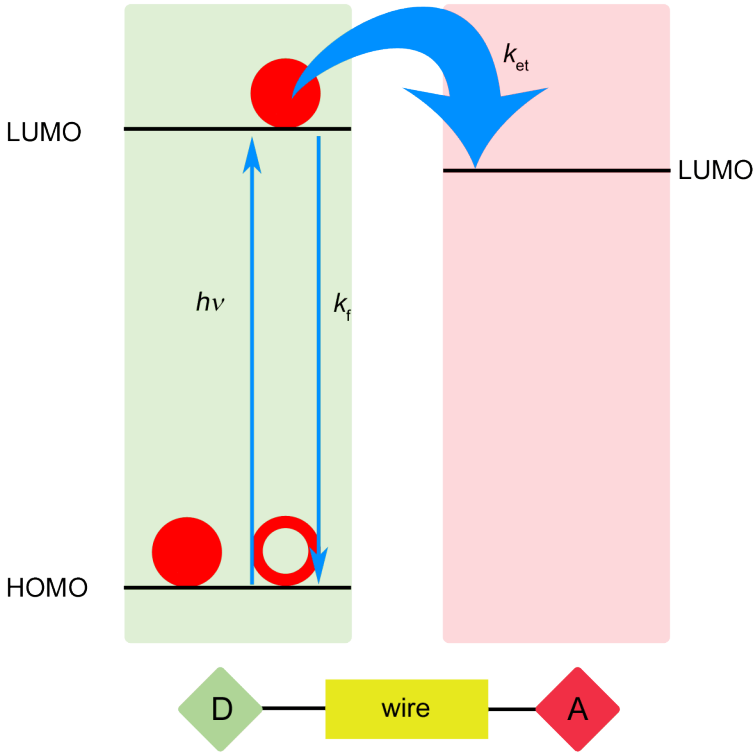

(a) The molecular orbitals involved in PeT when the fluorophore is the electron donor.

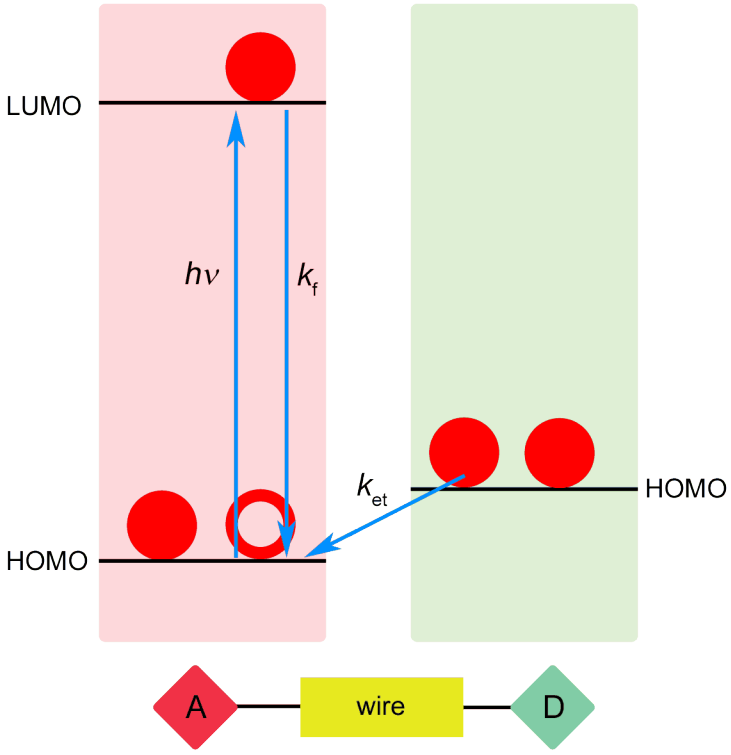

(b) The molecular orbitals and electron movements involved in PeT when the fluorophore is the electron acceptor.

Figure **1.19** The two types of PeT.

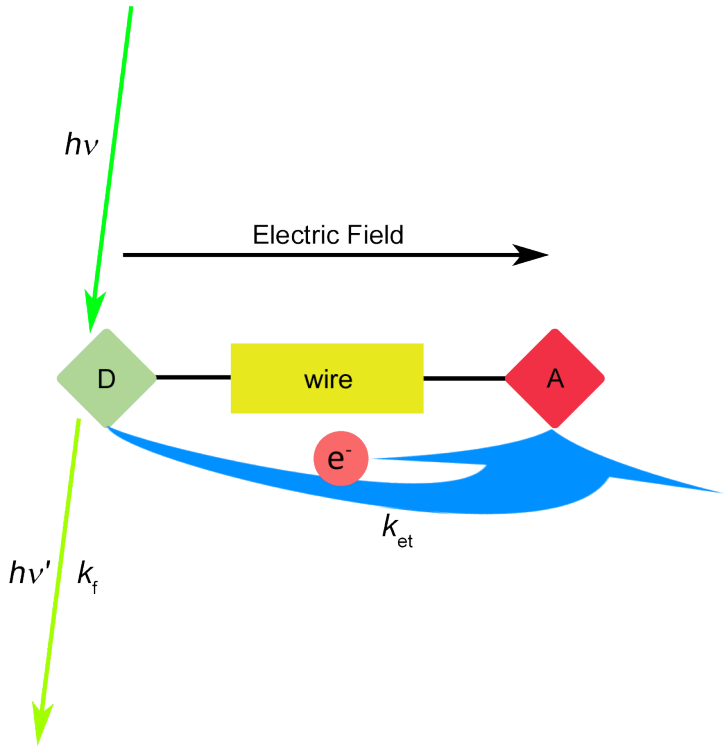

Figure **1.20** k_{f} and k_{et}, the two important rates in voltage-sensitive PeT.

can be collected, which is good for SNR. This contrasts with electrochromic dyes which are monitored by the wavelength shift in their emission spectrum, which in practical terms equates to monitoring changes in intensity of a small section at the edge of the emission band, thus 'wasting' photons by ignoring the most intense 'photon rich' parts of the spectrum (see Figure 1.14 on Page 21).

This mechanism also lends itself more readily than electrochromic dyes to variations in the molecular design, and thousands of appropriate designs could be devised from known building blocks. With the correct combination of redox potentials, excited state energy and molecular wire, PeT efficiencies can be optimised, opening up a library of readily accessible candidate dyes. The PeT principle should also work in all of the four conceivable permutations (Figure 1.21 on the following page), with the fluorophore acting as either the electron donor or acceptor, equipped with either lipophilic or hydrophilic solubilising groups. There are thus a huge number of designs possible from the

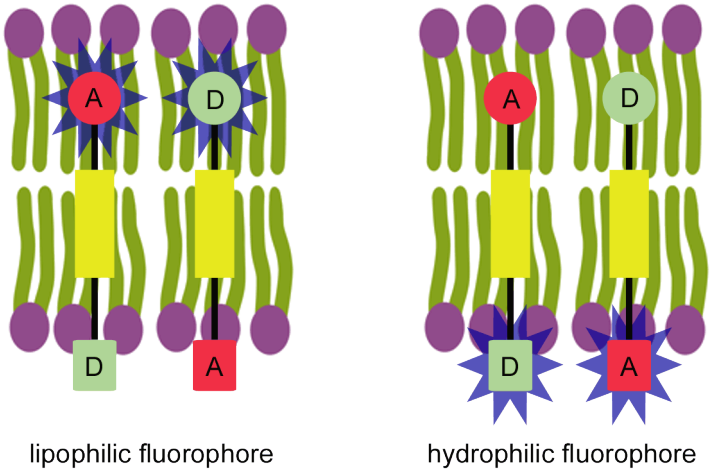

Figure **1.21** The four possible configurations of PeT dyes. Circles represent lipophilic components, squares hydrophilic components, and the yellow rectangles the molecular wire.

corpus of known dyes, electron donors and electron acceptors. Such variation has not proved possible for electrochromic dyes, which are essentially one small family of closely related structures. This scope for design also provides opportunity for maximising the voltage sensitivity by matching the donor-acceptor separation to the bilayer thickness to ensure that the system samples the greatest proportion possible of the electric field.

1.4.1 Conclusions regarding PeT VSDs

It is hoped that these advantages of this new mechanism will allow researchers to unlock enough voltage sensitivity to surpass the limits of previous mechanisms and thus also allow IMP with reduced phototoxicity. In Chapter 4 I will explore the rational design and synthesis of a family of dyes for VS imaging *via* the PeT mechanism.

1.5 Non-linear optical effects

I will now examine an alternative approach to improving IMP that also has the possibility to solve the sensitivity and photodamage problems. Non-linear

optical effects (NLO) effects, such as second harmonic generation (SHG) and two-photon absorption (2PA), only become relevant in very intense electromagnetic fields, such as in the focussed beam of a laser. SHG results in the output of frequency-doubled light by the scattering of incident light. It is an instantaneous process in which excited states are not populated. As indicated in Figure 1.22, scattering occurs *via* virtual states. 2PA leads to the population of a real excited state by the simultaneous absorption of two photons *via* an intermediate, virtual state. 2PA is followed by the usual emissive and non-radiative decay processes that one-photon (1P) excitation would lead to. 2PA can therefore often be applied to problems in imaging where a 1P solution is already known, as the same excited state is involved. With the increasing availability of lasers as an excitation source for microscopy, NLO effects have become more significant in imaging and the field of IMP.

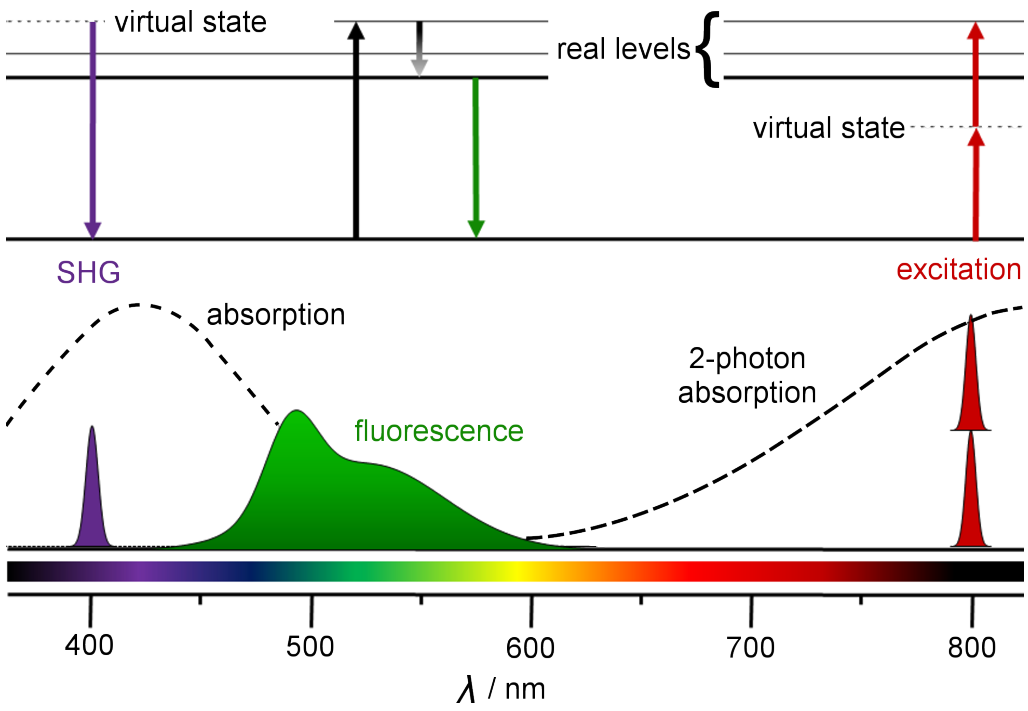

Figure **1.22** The molecular energy levels involved in fluorescence, 2PA and SHG. Reproduced from reference 49 with permission of the PCCP Owner Societies.

There are several key advantages of using two-photon (2P) excitation which

make NLO effects promising for the future of IMP. Firstly, as 2P excitation is proportional to the square of the incident light intensity, which decreases rapidly away from the focal point, there is a smaller excitation volume (the volume centred around the focal point in which the intensity is 50% or greater of that at the focal point) compared to 1P excitation at the same wavelength (Figure 1.23).[50]

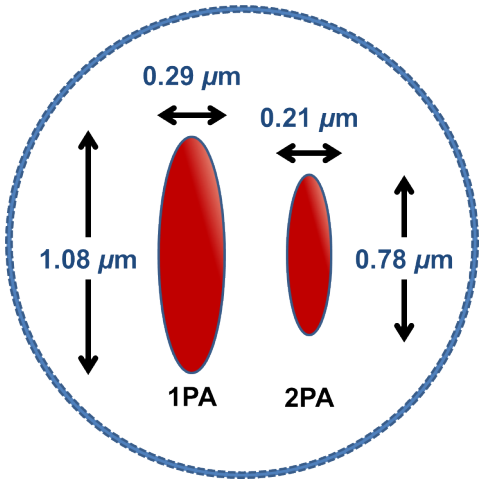

Figure **1.23** An xy cross-section of the excitation volume in the focal plane (fixed z) comparing 1PA and 2PA (at 800 nm with a lens of numerical aperture 1.4). Adapted from reference 50 with permission, copyright 2009 Wiley-VCH Verlag GmbH & Co. KGaA, Weinheim.

Secondly, the longer wavelengths used in 2P excitation are typically in the biological transparency window (700–900 nm), and thus the excitation is absorbed less by intrinsic chromophores, increasing the depth of tissue penetration and reducing background signal and photodamage.[b]

Thirdly, longer wavelength light is scattered less (scattering is proportional to λ^{-4}) and scattered light is less likely to lead to excitation away from the focal volume, reducing both losses due to scattering and extra background signal due to scattering.[51] These advantages are often collectively referred to as 'optical sectioning'. Further, photodamage should be inherently reduced

[b] Although 1P excitation at 400 nm would give a smaller excitation volume than 2P at 800 nm, the added advantage of exciting in the biological transparency window makes 2P imaging a powerful and popular technique.

as lower energy/longer wavelength light sources are used. However, to fully realise the potential advantages of NLO imaging, a suitable dye and mechanism providing voltage sensitivity must be used.

1.5.1 2P imaging with electrochromic dyes

It is possible to simply take a promising 1P electrochromic molecular probe and test it under 2P excitation conditions. As the same excited state is reached, the interactions of this state with changes in membrane potential will have the same effect upon the emission wavelength as for 1P excitation. Unfortunately, as the underlying electrochromic mechanism remains the same, using 2P excitation cannot solve the limitations of this mechanism. However, **ANNINE-6** has been found to demonstrate higher voltage sensitivity under 2P than 1P excitation, up to 70% $\Delta S/S$ at 1040 nm compared to 50% at 514 nm, but this increase in sensitivity has been attributed to the benefits of optical sectioning, particularly the reduced background fluorescence, rather than any difference in the VS mechanism.[41] The improved excitation volume of 2P imaging has also led to advances towards 3D imaging, with 2P excitation allowing discrimination between different depths in a sample that would be otherwise integrated into the signal obtained under 1P excitation.[52]

1.5.2 Second Harmonic Generation

SHG is a mechanism exclusive to 2P imaging which has great scope for solving the sensitivity and photodamage concerns. SHG is a second order NLO effect, whereby scattering of incident light by a non-centrosymmetric medium results in frequency-doubled output light (Figure 1.24 on the next page). It can be observed from unstained biological samples, due to scattering of endogenous proteins, but it can be greatly enhanced by a suitable harmonophore (a chromophore designed for SHG). The SHG response of a harmonophore is in-

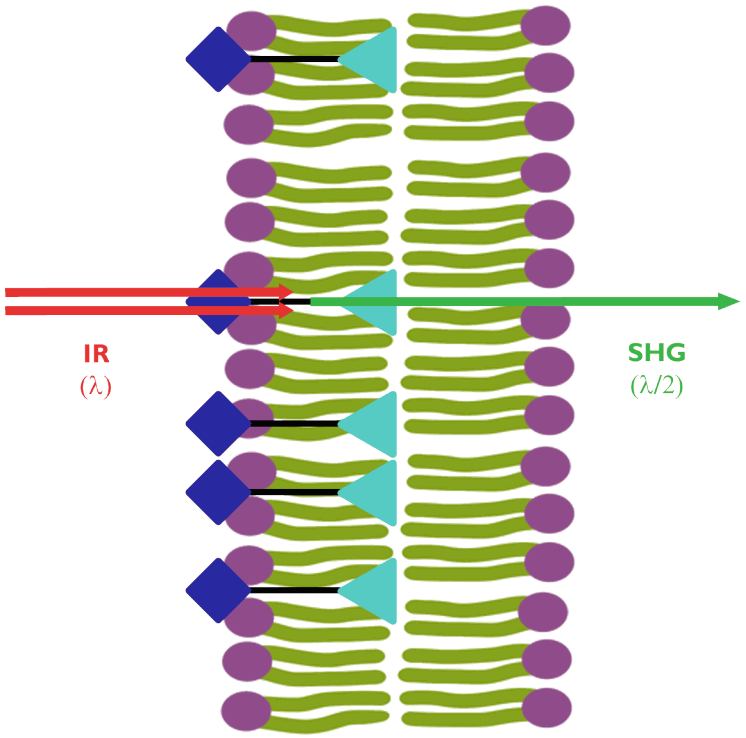

Figure **1.24** SHG is a coherent scattering process and thus results in forward propagation of the output light relative to the input light. SHG membrane probes usually feature a lipophilic (diamond) and a hydrophilic (triangle) end, and a donor-acceptor electronic architecture.

trinsically sensitive to electric fields. As an electro-optic process, SHG probes are expected to be fast, as per electrochromic probes. Although a weak effect that is only observed in the high intensity electric field of a laser, thus holding the potential to cause even greater photodamage than the alternative VS mechanisms, with advances in laser microscopy SHG is becoming readily accessible and relevant to imaging.

Despite the weakness of the SHG signal, the requirement of non-centrosymmetry reduces the background signal to zero, as harmonophores in intra- or extra-cellular media are isotropic and give negligible scattering signal compared to harmonophores inserted to one leaflet of a membrane. This provides SHG with a clear benefit over fluorescent techniques in maximising SNR; although many fluorophores are less fluorescent in aqueous solution than in an apolar lipid environment, SHG is the most strongly discriminating physical

process.

The strength of a harmonophore's ability to generate SHG is dictated by its first molecular hyperpolarisability, β, which is intrinsically sensitive to local static electric fields. The sensitivity of β to electric fields is dictated by the second molecular hyperpolarisability, γ. Molecular design principles for optimising both β, and γ, are becoming increasingly understood, and thus efficient SHG probes for membrane potential should be accessible. However despite this promise, there are few examples of SHG providing fast and sensitive molecular probes for IMP.

1.5.3 Examples of IMP *via* SHG

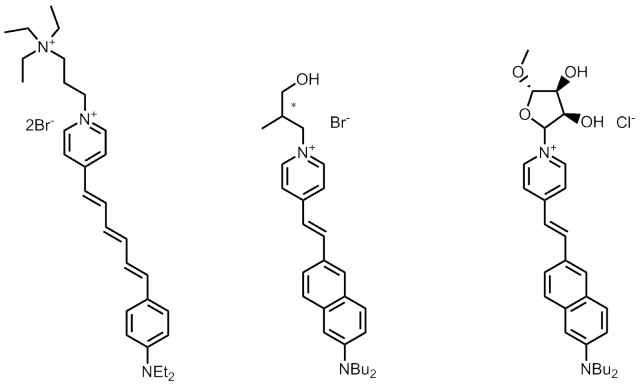

FM4-64 **JPW1234** **JPW1259**

Figure **1.25** **FM4-64**, a commercial SHG dye, and two chiral analogues of **Di-4-ANEPPS**.[53,54]

The two main examples of SHG dyes used for potentiometry are **FM4-64** (Figure 1.25) and **Di-4-ANEPPS**. Both of these dyes were originally designed for fluorescence imaging, **Di-4-ANEPPS** as an electrochromic VSD and **FM4-64** as part of a family of dyes for imaging synaptic vesicle recycling.[53,55]

Di-4-ANEPPS and its chiral analogues **JPW1234** and **JPW1259** (Figure 1.25) were initially shown to demonstrate voltage-sensitive SHG in a model

membrane setup,[54] and later provided the first demonstration of IMP using SHG in voltage-clamped cells.[56] In this case, the sensitivity of SHG to voltage under 850 nm incident light was higher than that of fluorescence, 18% vs. 10%. A greater value of 40% was subsequently obtained at higher incident wavelength of 950 nm.[57]

FM4-64 has been loaded intracellularly to specific mammalian neurons below the surface of a slice sample, and used to demonstrate the ability of multi-photon microscopy to measure deeper into samples than 1P (up to 125 μm in this example).[58] **FM4-64** has been used to image membrane potential in dendritic spines, particularly demonstrating back-propagation of the action potential into the spines for the first time.[59] These examples all exploit the improved SNR of SHG imaging to glean crucial new information beyond the scope of electrophysiology or fluorescent imaging techniques.

Nevertheless, for both of these dyes, there is some uncertainty over the exact mechanism of their voltage response. A pure electro-optic response should be rapid on the scale of membrane potential changes (sub-picosecond *vs.* sub-millisecond).[60] In many reports this phenomenon has not been readily distinguishable from a change in dye orientation, which could occur on a millisecond timescale, due to limited time resolution arising from low absolute photon counts and the resulting need for signal averaging. It has been shown that **FM4-64** can reorient within the membrane in HEK-293 cells in response to an electric field, providing either a complementary or competitive contribution to the intrinsic sensitivity of the SHG to voltage.[61] This is consistent with data gathered from a model membrane for closely related styryl dyes[62] and the slow time response found for **FM4-64** in a HLB model setup.[60] In contrast to these findings, in pyramidal neurons in neocortical brain slices no change in tilt angle with voltage was observed.[63]

Di-4-ANEPPS has been found to respond strongly to electric field changes,

exhibiting a $\Delta S/S$ of 20%, but this change is on a long timescale (200 ms). The SHG was notably slower to respond than either the one- or two-photon fluorescence, implying the electric field has an insignificant effect on the SHG: in place of the desired electro-optic mechanism and a fast response consistent with this mode of operation, a slower reorientation mechanism dominates the signal change.[64] Later studies revealed a small instantaneous response (electro-optic) which is then cancelled by a slower response (reorientation).[60]

1.5.4 Conclusions regarding SHG VSDs

Despite the utility of these SHG dyes and the advances they have allowed, there is a clear need for dyes with a stronger SHG response, such that the rapid mechanism will take precedence in providing the signal change. A critical failing of SHG dyes to date is that of low sensitivity to changes in membrane potential, necessitating signal averaging. Many of the examples published hardly achieve more than could be achieved with direct electrical measurements. It is also crucial that SHG dyes operate solely by an electro-optic mechanism, in order to exhibit a rapid and simple response to changes in membrane potential. However, the most studied dyes appear to have complicated, multi-mechanism responses to electric fields, impeding their time response and reducing their voltage sensitivity.

In addition to this mechanistic issue is the problem of photodamage. Although lower energy incident wavelengths are used, the photon flux is increased in order to allow SHG to be observed, so the light power the sample is exposed to can exceed that of a 1P experiment, increasing the likelihood of photodamage. When 2P excited fluorescence competes with SHG, the formation of real excited states can lead to singlet oxygen formation and phototoxicity. In order to minimise photodamage, laser intensities or pixel dwell times can be reduced, leading to low absolute SHG signal levels.[58]

This issue is best addressed by the development of better dyes. The current generation of SHG dyes are characterised by poor SHG efficiency as they have not been designed for either SHG or VS SHG imaging. A more efficient harmonogen will generate the same flux of SHG photons at lower laser intensity, thus making the development of enhanced efficiency SHG dyes a clear priority in tackling photodamage.

SHG dyes have led to reduced background measurements and advances in neurophysiology, and deserve more exploration. However the key observation of the field is the lack of rational design input to IMP *via* SHG; much has been learnt about SHG and other relevant NLO phenomena in different contexts, but this has yet to be applied to IMP. In Chapter 2 I will look at how to design improved SHG molecular probes, combining literature with new experimental data, and then in Chapter 3 apply this to the design and synthesis of a new family of voltage sensors.

1.6 Bibliography

1 Nicholls, J.; Martin, A. R.; Fuchs, P. A.; Brown, D. A.; Diamond, M. E.; Weisblat, D. A. *From Neuron to Brain*, 5th ed.; Sinauer Associates, Incorporated, 2012.
2 Scanziani, M.; Häusser, M. *Nature* **2009**, *461*, 930–939.
3 Churchland, M. M.; Yu, B. M.; Sahani, M.; Shenoy, K. V. *Curr. Opin. Neurobiol.* **2007**, *17*, 609–618.
4 Sacconi, L.; Mapelli, J.; Gandolfi, D.; Lotti, J.; O'Connor, R. P.; D'Angelo, E.; Pavone, F. S. *Opt. Express* **2008**, *16*, 14910–14921.
5 Hutzler, M.; Lambacher, A.; Eversmann, B.; Jenkner, M.; Thewes, R.; Fromherz, P. *J. Neurophysiol.* **2006**, *96*, 1638–1645.
6 Cohen, L. *Annu. Rev. Physiol.* **1989**, *51*, 487–490.
7 Peterka, D. S.; Takahashi, H.; Yuste, R. *Neuron* **2011**, *69*, 9–21.
8 Holthoff, K.; Zecevic, D.; Konnerth, A. *J. Physiol.* **2010**, *588*, 1085–1096.
9 Sacconi, L.; Dombeck, D. A.; Webb, W. W. *Proc. Nat. Acad. Sci.* **2006**, *103*, 3124–3129.
10 Li, L.-s. *Nano Lett.* **2007**, *7*, 2981–2986.
11 Tsien, R. Y. *Biochemistry* **1980**, *19*, 2396–2404.
12 Ashley, C. C.; Ridgway, E. B. *Nature* **1968**, *219*, 1168–1169.

13 Grynkiewicz, G.; Poenie, M.; Tsien, R. Y. *J. Biol. Chem.* **1985**, *260*, 3440–3450.
14 Ross, W. N. *Annu. Rev. Physiol.* **1989**, *51*, 491–506.
15 Lev-Ram, V.; Grinvald, A. *Biophys. J.* **1987**, *52*, 571–576.
16 Yuste, R.; Denk, W. *Nature* **1995**, *375*, 682–684.
17 Miller, E. W.; Lin, J. Y.; Frady, E. P.; Steinbach, P. A.; Kristan, W. B.; Tsien, R. Y. *Proc. Nat. Acad. Sci.* **2012**, *109*, 2114–2119.
18 Lipscombe, D.; Madison, D. V.; Poenie, M.; Reuter, H.; Tsien, R. W.; Tsien, R. Y. *Neuron* **1988**, *1*, 355–365.
19 Ashley, C. C.; Ridgway, E. B. *J. Physiol.* **1970**, *209*, 105–130.
20 Sabatini, B. L.; Svoboda, K. *Nature* **2000**, *408*, 589–593.
21 Nimchinsky, E. A.; Sabatini, B. L.; Svoboda, K. *Annu. Rev. Physiol.* **2002**, *64*, 313–353.
22 Tasaki, I.; Watanabe, A.; Sandlin, R.; Carnay, L. *Proc. Nat. Acad. Sci.* **1968**, *61*, 883–888.
23 Ross, W. N.; Salzberg, B. M.; Cohen, L. B.; Davila, H. V. *Biophys. J.* **1974**, *14*, 983–986.
24 Salzberg, B. M.; Davila, H. V.; Cohen, L. B. *Nature* **1973**, *246*, 508–509.
25 Cohen, L. B.; Salzberg, B. M.; Davila, H. V.; Ross, W. N.; Landowne, D.; Waggoner, A. S.; Wang, C. H. *J. Membr. Biol.* **1974**, *19*, 1–36.
26 Ross, W. N.; Salzberg, B. M.; Cohen, L. B.; Grinvald, A.; Davila, H. V.; Waggoner, A. S.; Wang, C. H. *J. Membr. Biol.* **1977**, *33*, 141–183.
27 Waggoner, A. S. *Annu. Rev. Biophys. Bioeng.* **1979**, *8*, 47–68.
28 Waggoner, A. S.; Wang, C. H.; Tolles, R. L. *J. Membr. Biol.* **1977**, *33*, 109–140.
29 Ross, W. N.; Reichardt, L. F. *J. Membr. Biol.* **1979**, *48*, 343–356.
30 Loew, L. M.; Bonneville, G. W.; Surow, J. *Biochemistry* **1978**, *17*, 4065–4071.
31 Loew, L. M.; Scully, S.; Simpson, L.; Waggoner, A. S. *Nature* **1979**, *281*, 497–499.
32 Loew, L.; Cohen, L.; Salzberg, B.; Obaid, A.; Bezanilla, F. *Biophys. J.* **1985**, *47*, 71–77.
33 Hassner, A.; Birnbaum, D.; Loew, L. M. *J. Org. Chem.* **1984**, *49*, 2546–2551.
34 Fluhler, E.; Burnham, V. G.; Loew, L. M. *Biochemistry* **1985**, *24*, 5749–5755.
35 Gross, E.; Bedlack, R.; Loew, L. *Biophys. J.* **1994**, *67*, 208–216.
36 Przybylo, M.; Borowik, T.; Langner, M. *J. Fluoresc.* **2010**, *20*, 1139–1157.
37 Fromherz, P.; Lambacher, A. *Bioch. et Biophys. Acta - Biomem.* **1991**, *1068*, 149–156.
38 Lambacher, A.; Fromherz, P. *J. Phys. Chem. B* **2000**, *105*, 343–346.
39 Hubener, G.; Lambacher, A.; Fromherz, P. *J. Phys. Chem. B* **2003**, *107*, 7896–7902.
40 Kuhn, B.; Fromherz, P. *J. Phys. Chem. B* **2003**, *107*, 7903–7913.
41 Kuhn, B.; Fromherz, P.; Denk, W. *Biophys. J.* **2004**, *87*, 631–639.
42 Fromherz, P.; Hubener, G.; Kuhn, B.; Hinner, M. *Eur. Biophys. J.* **2008**,

37, 509–514.
43 Wong, K. F.; Bagchi, B.; Rossky, P. J. *J. Phys. Chem. A* **2004**, *108*, 5752–5763.
44 González, J.; Tsien, R. *Biophys. J.* **1995**, *69*, 1272–1280.
45 González, J. E.; Tsien, R. Y. *Chem. & Biol.* **1997**, *4*, 269–277.
46 Akemann, W.; Mutoh, H.; Perron, A.; Rossier, J.; Knöpfel, T. *Nat. Meth.* **2010**, *7*, 643–649.
47 Bradley, J.; Luo, R.; Otis, T. S.; DiGregorio, D. A. *J. Neurosci.* **2009**, *29*, 9197–9209.
48 Chanda, B.; Blunck, R.; Faria, L. C.; Schweizer, F. E.; Mody, I.; Bezanilla, F. *Nat. Neurosci.* **2005**, *8*, 1619–1626.
49 Reeve, J. E.; Anderson, H. L.; Clays, K. *Phys. Chem. Chem. Phys.* **2010**, *12*, 13484–13498.
50 Pawlicki, M.; Collins, H. A.; Denning, R. G.; Anderson, H. L. *Angew. Chem. Int. Ed.* **2009**, *48*, 3244–3266.
51 Rumi, M.; Ehrlich, J. E.; Heikal, A. A.; Perry, J. W.; Barlow, S.; Hu, Z.; McCord-Maughon, D.; Parker, T. C.; Röckel, H.; Thayumanavan, S.; Marder, S. R.; Beljonne, D.; Brédas, J.-L. *J. Am. Chem. Soc.* **2000**, *122*, 9500–9510.
52 Fisher, J. A. N.; Barchi, J. R.; Welle, C. G.; Kim, G.-H.; Kosterin, P.; Obaid, A. L.; Yodh, A. G.; Contreras, D.; Salzberg, B. M. *J. Neurophysiol.* **2008**, *99*, 1545–1553.
53 Betz, W.; Bewick, G. *Science* **1992**, *255*, 200–203.
54 Bouevitch, O.; Lewis, A.; Pinevsky, I.; Wuskell, J. P.; Loew, L. M. *Biophys. J.* **1993**, *65*, 672–679.
55 Gaffield, M. A.; Betz, W. J. *Nat. Protocols* **2007**, *1*, 2916–2921.
56 Millard, A. C.; Jin, L.; Lewis, A.; Loew, L. M. *Opt. Lett.* **2003**, *28*, 1221–1223.
57 Millard, A. C.; Jin, L.; Wei, M.-d.; Wuskell, J. P.; Lewis, A.; Loew, L. M. *Biophys. J.* **2004**, *86*, 1169–1176.
58 Dombeck, D. A.; Sacconi, L.; Blanchard-Desce, M.; Webb, W. W. *J. Neurophysiol.* **2005**, *94*, 3628–3636.
59 Nuriya, M.; Jiang, J.; Nemet, B.; Eisenthal, K. B.; Yuste, R. *Proc. Nat. Acad. Sci.* **2006**, *103*, 786–790.
60 Reeve, J. E.; Corbett, A. D.; Boczarow, I.; Kaluza, W.; Barford, W.; Bayley, H.; Wilson, T.; Anderson, H. L. *Angew. Chem. Int. Ed.* **2013**, *52*, 9044–9048.
61 Theer, P.; Denk, W.; Sheves, M.; Lewis, A.; Detwiler, P. B. *Biophys. J.* **2011**, *100*, 232–242.
62 Pons, T.; Mongin, O.; Mertz, J.; Blanchard-Desce, M.; Moreaux, L. *J. Biomed. Opt.* **2003**, *8*, 428–431.
63 Jiang, J.; Eisenthal, K. B.; Yuste, R. *Biophys. J.* **2007**, *93*, L26–L28.
64 Millard, A.; Jin, L.; Wuskell, J.; Boudreau, D.; Lewis, A.; Loew, L. *J. Membr. Biol.* **2005**, *208*, 103–111.

Chapter 2: Investigating the non-linear optical behaviour of porphyrin dimers for optimising voltage sensitivity

In this first of two chapters on second harmonic generation VSDs, the theory of improving the voltage sensitivity of SHG is examined. Butadiyne-linked porphyrin dimers are thus proposed as the core component of rational successors to the promising porphyrin monomer voltage sensor JR1. *Structure-property effects upon the non-linear optical properties of this core are assessed for a range of electron-donating and withdrawing groups, using data from hyper-Rayleigh scattering and two-photon excited fluorescence. The ramifications of the results for voltage sensor design are discussed.*

This chapter has been published in part under DOI 10.1039/C4TC01120A.

2.1 Introduction

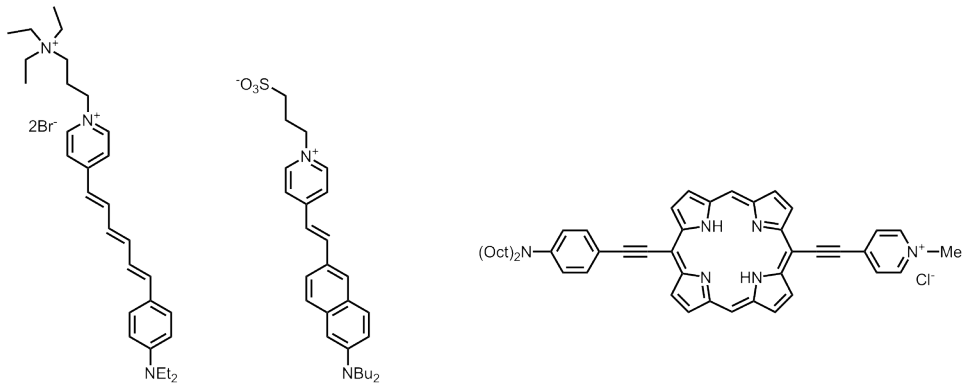

FM4-64 **Di-4-ANEPPS** **JR1**

Figure **2.1** The three main contenders in the field of IMP using SHG.

Neither of the two most studied SHG dyes for IMP, **Di-4-ANEPPS** and **FM4-64** (Figure 2.1), were designed for this purpose. Poor performance of these harmonophores is thus unsurprising, and the scope for improvement immense. The rational design of VSDs in the Anderson group has already resulted in **JR1**, a porphyrin dye with enhanced voltage sensitivity compared to the popular styryl voltage probes. **JR1** is a new benchmark in this field.

In this chapter, I will present investigations which will enable the rational design of better SHG dyes based on the hypothesis that porphyrin dimers should have optimised NLO properties compared to already successful porphyrin monomer **JR1**. I will first introduce the porphyrin chromophore and the properties that are important for optimising VS SHG dyes, then present literature supporting the use of butadiyne-linked porphyrin dimers for porphyrin voltage sensors. In the bulk of this chapter, I then detail research into the NLO properties of these dimers which will inform VSD design.

2.2 The porphyrin chromophore

The porphyrin chromophore is a large, chemically stable, aromatic heterocycle, the synthetic modification of which has been widely studied.[1] Besides modification of the porphyrin by substitution in up to twelve positions about the ring (Figure 2.2), the porphyrin macrocycle can also coordinate a variety of metals.[2] A large collection of oligomers with a wide assortment of linkages have also been investigated.[3–5] The diversity of synthetic options thus available give great potential for electronic tunability.[6]

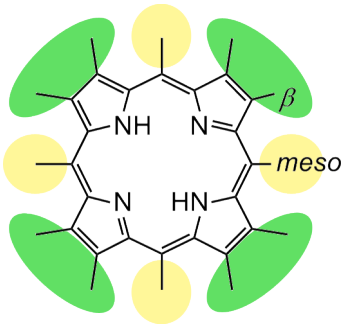

Figure **2.2** A porphyrin monomer with its substitution positions labelled with β and *meso* nomenclature.

The porphyrin ring is renowned for its strong linear and non-linear absorption,[7–9] and this chapter includes many examples of porphyrins with optimised NLO properties. The two main linear absorption bands of porphyrins are very intense and are referred to as the Soret (or B) and the Q bands (Figure 2.3 on the next page). They arise from electronic transitions from the ground state to the second (S_0–S_2) and first (S_0–S_1) excited states respectively. The Soret band absorbs around 400 nm with $\epsilon \approx 10^5$ M^{-1} cm^{-1}, and the Q band around 650 nm with $\epsilon \approx 10^4$ M^{-1} cm^{-1}. The Q band is often accompanied by vibronic satellites at higher energy, the lowest energy Q band being referred to as Q(0–0), the next as Q(0–1), Q(i–f) referring to the initial and final vibrational states accompanying the electronic transition. These features of the porphyrin chromophore make it an ideal basis for an optimised VSD.

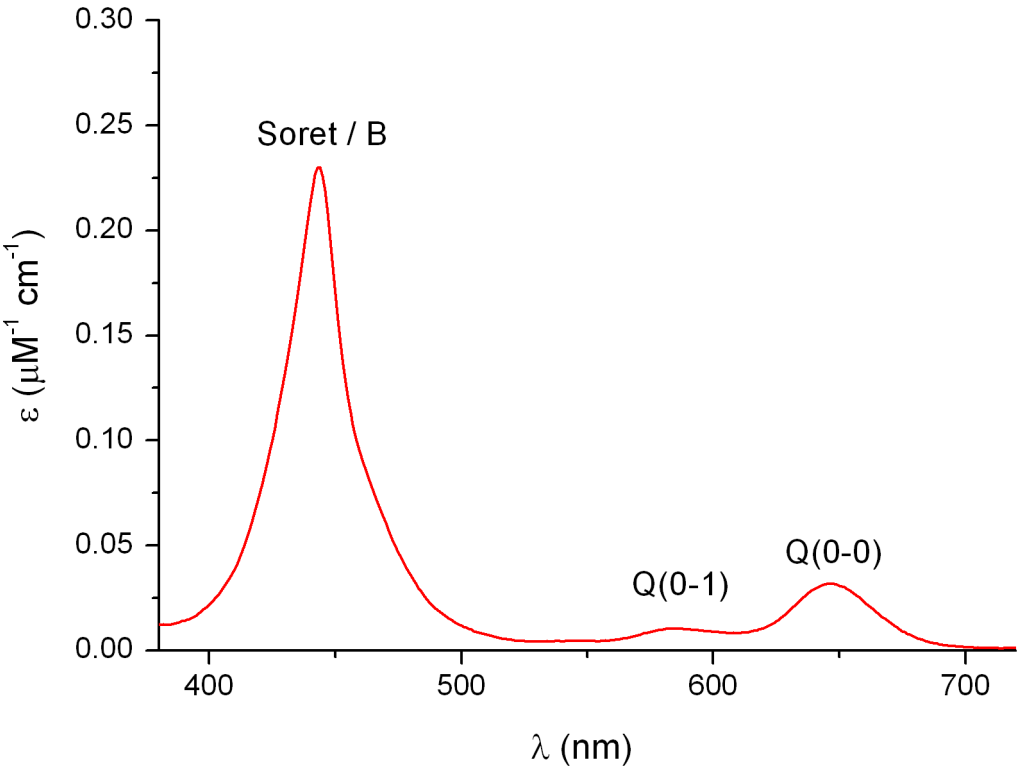

Figure **2.3** A typical UV-vis spectrum of a simple porphyrin monomer.

2.3 The important variables in optimising voltage-sensitive dyes

The polarisability of a compound under normal intensity light follows a linear relationship with the intensity E of the electromagnetic field:

$$P = \alpha E \tag{2.1}$$

where α describes the ability of an electric field, such as an oscillating electromagnetic field, to induce polarisation in the compound.

The second polarisability, or first hyperpolarisability, β, of a compound becomes significant only in a strong electromagnetic field, such as laser light. The coefficient β describes the induced polarisation with a non-linear, quadratic de-

pendence upon the field intensity:

$$P = \alpha E + \beta E^2 + \ldots \tag{2.2}$$

β is wavelength-dependent like an extinction coefficient, and resonance enhancements arising from the presence of strong linear absorption bands at energies close to the incident wavelength and the second harmonic wavelength create a non-trivial relationship between β and the wavelength. The intensity of SHG, S, depends upon β^2, and from a non-centrosymmetric ensemble of ordered dye molecules is described by the following equation:

$$S = G\beta^2 N^2 I^2 \tag{2.3}$$

where N is the number density (related to the dye concentration), I is the incident light intensity and G is a constant accounting for geometric factors. If the other variables are fixed, the efficiency of an harmonophore in generating second harmonic light depends quadratically upon β. In the presence of a static electric field, E_{static} (as opposed to the oscillating electric field of light), β is modulated thus:

$$\beta_{\text{eff}} = \beta + \gamma E_{\text{static}} \tag{2.4}$$

where γ is the second hyperpolarisability, or the cofficient of the third-order response to a polarising electromagnetic field. Assuming the electric field change with an action potential starts from $E_{\text{static}} = 0$, the electro-optic response of SHG to a change in electric field E_{static} is given by $S_{\beta_{\text{eff}}} - S_\beta$, and $\Delta S/S$ can therefore be expressed as:

$$\frac{\Delta S}{S} = \frac{S_{\beta_{\text{eff}}} - S_\beta}{S_\beta} = \frac{2\gamma E_{\text{static}}}{\beta} + \left(\frac{\gamma E_{\text{static}}}{\beta}\right)^2 \tag{2.5}$$

Equation 2.5 shows that the quantities β and γ therefore both need optimising

to improve the sensitivity of SHG to voltage. The ratio γ/β must be increased to increase $\Delta S/S$. The ratio γ/β scales with the size of a π-system.[10] In general terms, β and γ are both increased in a more polarisable molecule, such as a larger aromatic system. This understanding of the voltage-sensitivity of SHG dyes explains the success of **JR1**.

2.3.1 The promising results from JR1

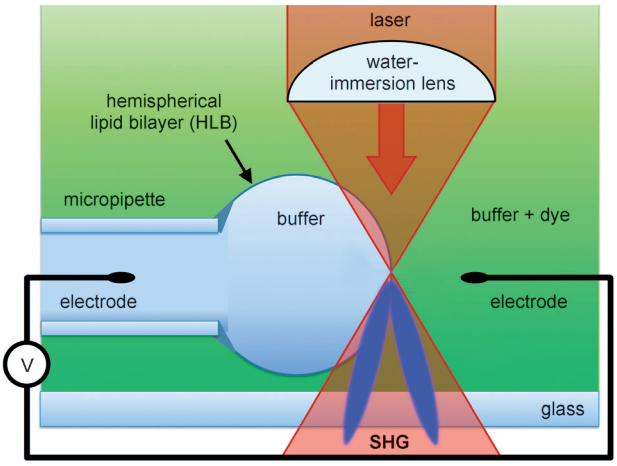

Figure **2.4** A hemispherical lipid bilayer experimental setup for testing VSDs (specifically SHG dyes in this example). VSDs insert into the outer leaflet of the HLB from the buffer bath. Adapted from reference 10 with permission, copyright 2013 WILEY-VCH Verlag GmbH & Co. KGaA, Weinheim.

In previous work in the Anderson group, under identical conditions in a hemispherical lipid bilayer (HLB) model membrane setup (Figure 2.4), **JR1** was found to be much more voltage-sensitive ($\Delta S/S$ per 100 mV of 23%) than either of the commercial dyes **FM4-64** (4.1%) or **Di-4-ANEPPS** (2.7%). The kinetic trace shown in Figure 2.5(a) reveals that **JR1** has an almost purely electro-optic response to changing transmembrane potential, its time resolution being at least as good as that of the experiment ($\sim$ 5 ms). On the other hand, **FM4-64** exhibits a small electro-optic response and a competing slow response, which results in a very poor match between the traces of the signal change ($\Delta S/S$) and the transmembrane potential (Figure 2.5(b)).[10]

JR1 is a monomeric porphyrin dye designed to manifest high values of β and γ. It has a strong 'push-pull'[a] character, as a result of its electron-donating aniline and electron-accepting pyridinium.[11] Strong interaction of the porphyrin π-system with these electronic substituents is enabled by the ethyne links.[12,13] Compared to **FM4-64** and **Di-4-ANEPPS**, **JR1** has optimised non-linear optical properties; both β and γ are increased. For example, $\beta_{800,\mathrm{HRS}}$ (β at 800 nm as measured by HRS, see Section 2.7.1)[b] is approximately doubled in **JR1** compared to **FM4-64**: 450×10^{-30} esu (for a closely related analogue of **FM4-64** in acetonitrile[14]) compared to 970×10^{-30} esu for **JR1** in $CHCl_3$.[11]

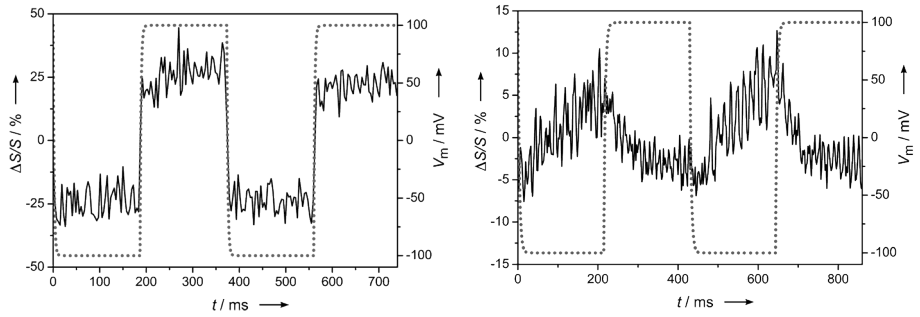

(a) **JR1** (b) **FM4-64** (averaged over 4 traces)

Figure **2.5** Kinetic traces showing the change in SHG intensity (as a percentage of the total signal) caused by an alternating transmembrane potential of ±100 mV (dotted curve). Adapted from reference 10 with permission, copyright 2013 WILEY-VCH Verlag GmbH & Co. KGaA, Weinheim.

The results of calculations deriving the $\Delta S/S$ for **JR1** and **Di-4-ANEPPS** from the second molecular hyperpolarisability γ for the two dyes match well with the observed differences in $\Delta S/S$ in the HLB setup.[10] Further, considering the two-photon cross section σ_2, the measure of the efficiency of 2PA, whose magnitude is related to the magnitude of γ, small styryl dyes such as **Di-4-ANEPPS** exhibit a peak σ_2 around 10 GM, whereas in strongly dipolar

[a] Throughout this chapter, push/donor/D refer to electron donor groups, and pull/acceptor/A refer to electron acceptor groups.

[b] β_λ is often reported as $\beta_{\lambda,\mathrm{zzz}}$, converted from $\beta_{\lambda,\mathrm{HRS}}$ to represent the value of β_λ lying along the molecular dipolar axis zzz. To simplify comparison with non-dipolar molecules, I have reported $\beta_{\lambda,\mathrm{HRS}}$ wherever possible.

porphyrins similar to **JR1**, σ_2 values of $10^2 - 10^3$ GM are found.[15,16] The increased $\Delta S/S$ of **JR1** versus **FM4-64** and **Di-4-ANEPPS** thus matches the theoretical interpretation of the voltage-sensitivity of SHG outlined in this section.

I will now examine in more detail the literature precedence for increasing β and γ and the ratio γ/β, particularly focusing on dimeric porphyrin systems because of the promising results from **JR1**.

2.4 Maximising the first hyperpolarisability

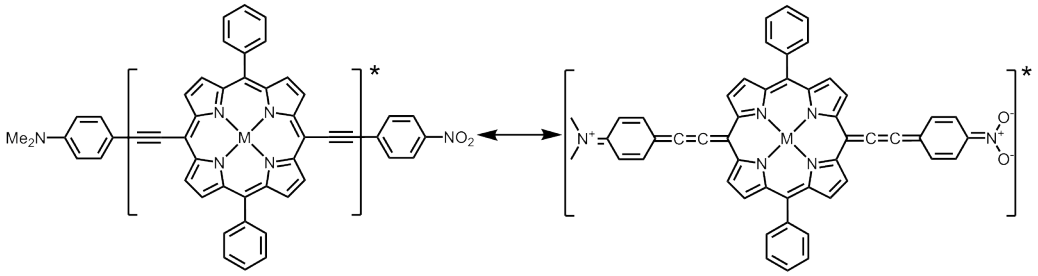

1

Figure **2.6** Cumulenic resonance form in the excited state of a porphyrin monomer.[17]

Changes in β in a dipolar system, for example an donor-π-acceptor molecule, can be rationalised via Oudar's two level model:

$$\beta \propto (\mu_{ee} - \mu_{gg}) \frac{\mu_{ge}^2}{E_{ge}^2} \tag{2.6}$$

Lengthening a simple π-system such as a polyene increases the $(\mu_{ee} - \mu_{gg})$ term, the difference between the ground and excited state dipole moments, but also decreases μ_{ge}^2, the square of the transition oscillator strength, and increases E_{ge}^2, the square of the energy gap between the ground and excited state, as a result of reduced electronic coupling between the donor and acceptor. Augmenting β values thus requires a balancing act of these factors. However, the use of a

π-bridge which itself provides a strong oscillator strength while concurrently providing a large change in dipole moment by changing the ground and excited state coupling between the donor and acceptor circumvents this problem. This is exemplified for the donor-porphyrin-acceptor system **1** in Figure 2.6, the cumulenic resonance form accessible in the excited state allowing ($\mu_{ee}-\mu_{gg}$) and μ_{ge}^2 to be increased simultaneously. $\beta_{1064,HRS}$ was reported to be 4933×10^{-30} esu.[17]

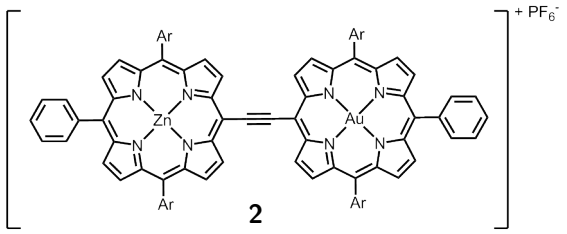

Figure **2.7** A 'push-pull' porphyrin dimer with a large value of β.[18] (Ar = 3,5-di-*t*-butylphenyl).

Porphyrin dimers are also expected to benefit from this cumulenic resonance form.[6] Calculations have shown that ethyne-linked porphyrin dimers analogous to **1** provide a suitable photonic bridge to couple a donor and acceptor, with a doubling of β predicted compared to the monomer,[19] and a further linear increase to the trimeric system.[20] Ethyne-linked dimer **2** (Figure 2.7), 'push-pull' by virtue of its mixed-metal Au-Zn coordination, gives a large experimental $\beta_{800,HRS}$ value of 1600×10^{-30} esu, compared to 970×10^{-30} esu for **JR1**.[18]

At this point a unique feature of porphyrin dimers compared to monomers must be introduced: because of the small energetic barrier to free rotation about the ethyne or butadiyne link, even compounds that look centrosymmetric on paper (such as **3** and **4**, Figure 2.8) easily adopt conformations that are non-centrosymmetric, and thus have a non-zero β value. Comparing ethyne-linked dimer **3** to a butadiyne-linked dimer **4** revealed a doubling of $\beta_{1300,HRS}$ from 410 to 830×10^{-30} esu.[21] The butadiyne linker allows a greater proportion

of non-centrosymmetric conformers to be populated compared to the ethyne linker, a clear explanation for its heightened SHG response. The weakly dipolar porphyrin monomer **5** has a $\beta_{1300,\mathrm{HRS}}$ of 40×10^{-30} esu.

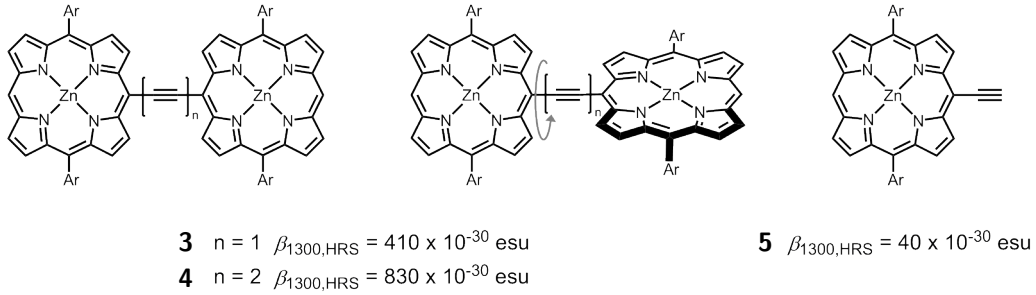

Figure **2.8** Octupolar porphyrin dimers with large values of β compared to the monomer.[21] (Ar = 2,6-bis(3,3-dimethylbutyloxy)phenyl).

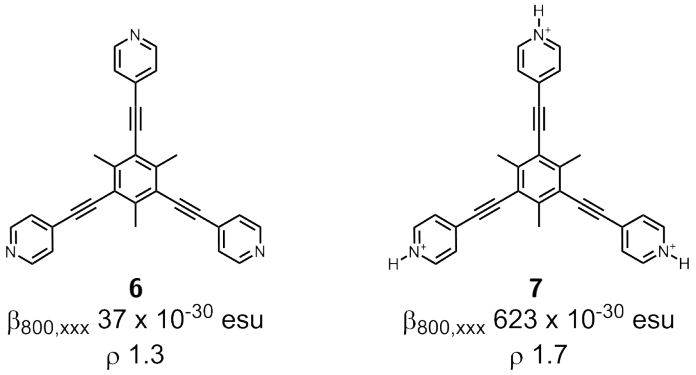

Figure **2.9** Increasing the dipolar strength of each arm leads to an increase in β without a change in symmetry.[22]

Such contributions to β arising from non-centrosymmetric systems without a dipole moment are known as octupolar, compared to the dipolar contribution of a 'push-pull' harmonophore.[22] There are many examples of octupoles with large first hyperpolarisabilities,[22–25] including octupolar butadiyne-linked porphyrin dimers (Figure 2.8). Octupolar compounds can display enhanced β when stronger individual dipoles are present, for example by the protonation of all of the three 'arms' in compound **7** compared to **6** (Figure 2.9). No change of symmetry is effected by the protonation, but β is enhanced.[22]

Resonance enhancement is another important factor to be considered in attempts to maximise β: a strong one-photon absorption band at the energy of either the second harmonic or the incident light causes dramatic growth in β at that wavelength as a result of resonance.[26] The wavelength-dependence of this effect is not easily modelled, as excited states beyond the first excited state are significant.[27] Nevertheless, it is clear that the application of monomeric and dimeric porphyrin dyes with large oscillator strengths in the region of the second harmonic (i.e. $\lambda_{\text{incident}}/2$ near the Soret band) is a good approach to achieving large, resonance-enhanced β values.

Butadiyne-linked porphyrin dimers were chosen for further investigation in this chapter on the basis of the larger β than both porphyrin monomers and ethyne-linked dimers in existing experimental results. However, the effect of 'push-pull' substitution upon these dimers has not been tested, despite the huge changes in β effected by 'push-pull' modifications in porphyrin monomers and other systems. The applicability of 'push-pull' design principles will therefore be evaluated for these systems to allow the rationally informed design of a new generation of voltage sensors. It is crucial to determine if 'push' and 'pull' substitution is important in these systems. This is particularly necessary as octupolar contributions have been largely ignored in computational studies, where calculations are performed upon one geometry.[20,28,29]

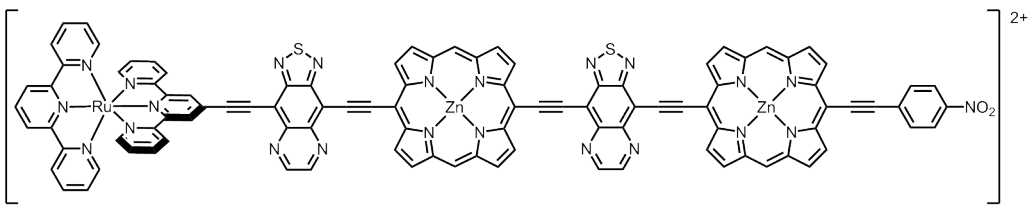

8 β_0 26000 x 10^{-30} esu

Figure **2.10** A very large β value is calculated for this compound (β_0 indicates that this is a static value not including resonance enhancements).[20]

It is noted here that while in absolute terms the β values of porphyrin

dimers cannot touch the largest known (see Figure 2.10), it is important to acknowledge the $3-5$ nm thickness of the bilayers targeted in the application of these dyes, and the need for water-solubility for introducing VSDs to cells.[20] These constraints limit the extent to which the π-system can be extended to push the limits of β; the pursuit of the largest possible β is only of interest for theoretical work.

The conclusion from this survey of published work is that butadiyne-linked porphyrin dimers can exhibit high values of the first hyperpolarisability, β. In the next section I consider their scope for high second hyperpolarisability, γ.

2.5 Maximising the second hyperpolarisability

The third order molecular polarisability, or the second molecular hyperpolarisability, γ, is responsible for many different NLO effects, including third harmonic generation (THG), degenerate four-wave mixing (DFWM), the optical and DC Kerr effects, and two-photon absorption (2PA).[30]

Measurements involving second-order nonlinear optical effects all point towards γ being vastly improved in butadiyne-linked porphyrin dimers, compared to a simple monomer. For example, DFWM revealed an hundred-fold increase in γ from compound **9** (n = 1) to butadiyne-linked dimer **10** (n = 2) (Figure 2.11).[31] Dimers and polymers of the same linkage displayed large third-order optical responses in electroabsorption measurements (DC Kerr effect) compared to a monomer.[32]

As for other NLO effects, 2PA has also revealed porphyrin dimers and higher oligomers to offer substantial increases in γ, as shown by their increased two-photon absorption cross sections, σ_2, compared to their monomeric siblings. Several varieties of conjugated porphyrin oligomers have been explored, with 10^2 –10^3 fold enhancements observed in σ_2 per porphyrin unit.[8,31,33–37]

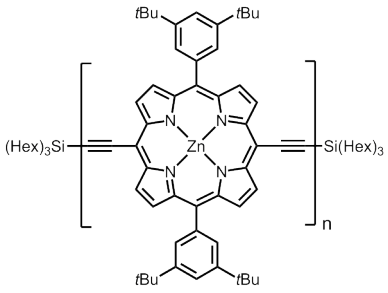

compound	n	$\lvert\chi^{(3)}_{xyyx}\rvert$ (10^{-17} m^2 V^{-2})	$\sigma_{2,\max}$ (GM)
9	**1**	0.0050	19
10	**2**	0.23	9100

Figure **2.11** Examples of large γ in porphyrin dimers.[31,33]

In recent years, there have been significant advances in the elucidation of molecular design principles for maximising σ_2.[9,38–41] 2PA is also one of the most intensely researched NLO properties of porphyrin oligomers, and is conveniently and accurately measured by the two-photon excited fluorescence (2PEF) technique.[9] However, structure-property relationships are still poorly understood for butadiyne-linked porphyrin dimers. A common design strategy for optimising σ_2 is the use of centrosymmetric quadrupolar architectures, of the type A-D-A or D-A-D, featuring strong π-conjugated 'push' and 'pull' groups.[9,38–42] Butadiyne-linked dimer **Oxdime** (Figure 2.12) with terminal pyridinium electron-acceptor groups is an example of this, and appears to exhibit enhanced 2PA ($\sigma_{2,\max} = 17,000$ GM at 916 nm) when compared with **10** ($\sigma_{2,\max} = 9,100$ GM at 873 nm),[43–47] but the effect of terminal electron acceptors and donors has not been systematically tested.[c]

To optimise butadiyne-linked porphyrin dimers for application as VSDs requires a better understanding of how their NLO properties can be optimised than the literature can currently offer. Thus in this chapter, investigations into the effect of electron-donating and electron-withdrawing groups upon β and γ in butadiyne-linked porphyrin dimers will be made, to ensure the next generation VSD design is properly informed. β is directly examined by hyper-Rayleigh scattering (HRS), whereas γ is examined *via* 2PA (measured by 2PEF).

[c]Ethyne-linked porphyrins have been studied in more detail, see reference 48.

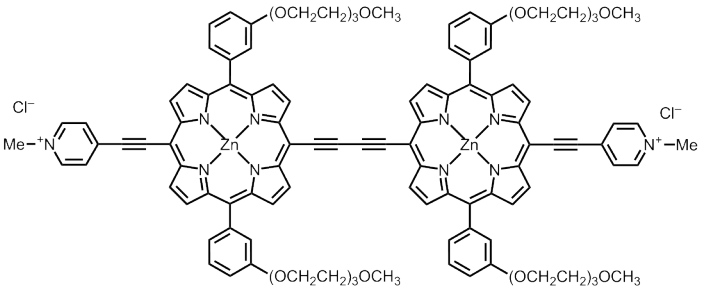

Oxdime

Figure **2.12** The porphyrin dimer **Oxdime**, a PDT sensitiser.[47]

2.6 Synthesis of butadiyne-linked porphyrin dimers

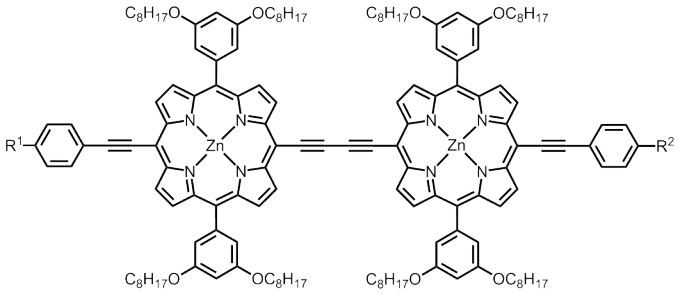

A-P2-A ($R^1 = R^2 = NO_2$)
A-P2-D ($R^1 = NO_2$, $R^2 = NBu_2$)
A-P2-R ($R^1 = NO_2$, $R^2 = Bu$)
D-P2-D ($R^1 = R^2 = NBu_2$)
D-P2-R ($R^1 = NBu_2$, $R^2 = Bu$)
R-P2-R ($R^1 = R^2 = Bu$)

Figure **2.13** The family of dimers synthesised and studied.

A family of butadiyne-linked dimers (Figure 2.13) has been chosen in order to assess the influence of strong π-conjugated 'push' (D) and 'pull' (A) groups upon β and γ for this specific π-system. A reference (R) group acts as an electronically-neutral phenyl ring. Zinc porphyrins have been used for synthetic convenience, as the coordination of pyridine to zinc helps to solvate porphyrins. This is also important in preventing aggregation in the spectroscopic studies that will be performed on these dyes. 3,5-Bis-octyloxy-phenyl *meso* groups were chosen to provide ample solubility.

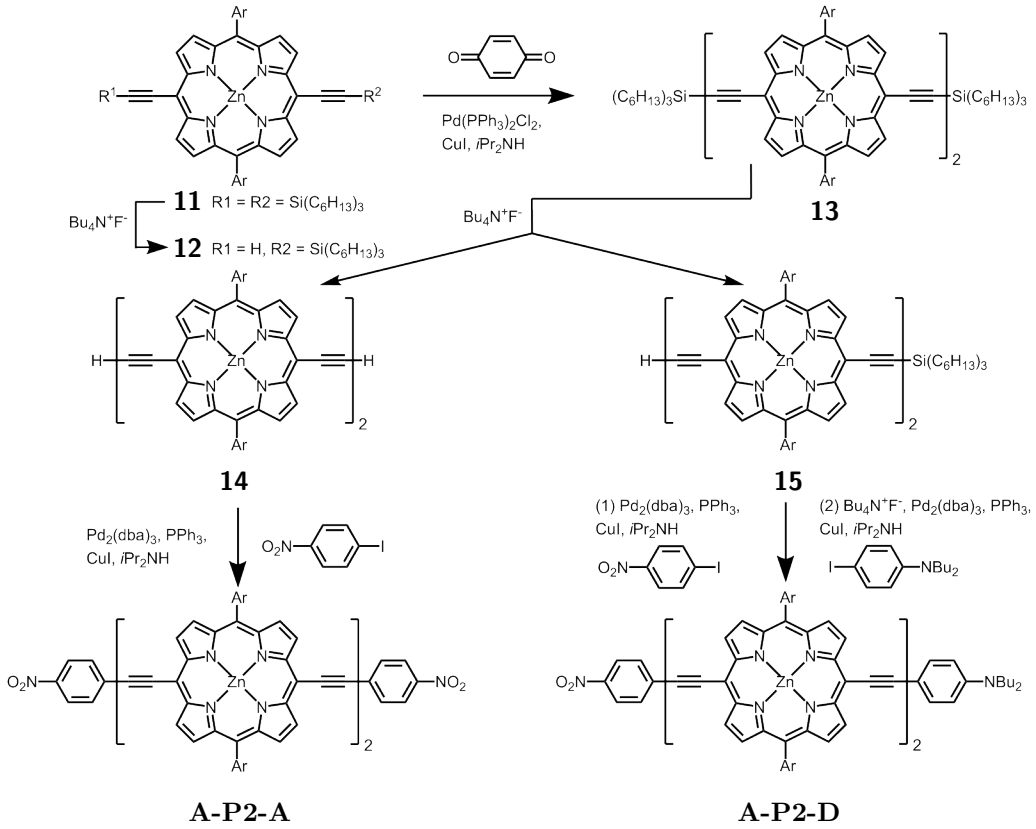

Scheme **2.1** The main synthetic steps used to access symmetric and asymmetric butadiyne-linked porphyrin dimers. (Ar = 3,5-bis-octyloxy-phenyl).

The family of six zinc porphyrin dimers shown in Figure 2.13 was synthesised from porphyrin monomer **11** using a combination of statistical desilylation and Sonogashira coupling steps, as illustrated in Scheme 2.1.[49,50] Desilylation of **11** yielded a mixture from which the singly desilylated monomer **12** was separated and subjected to a Pd catalyst in the presence of 1,4-benzoquinone as oxidant to give butadiyne-linked dimer **14**. This dimer was then similarly desilylated, and the doubly- and singly-desilylated dimers **14** and **15** separated. Coupling **14** and **15** to 4-iodonitrobenzene yielded **A-P2-A** and a silyl/nitro dimer, respectively; the latter was desilylated and in-situ coupled to *N,N*-dibutyl-4-iodoaniline yielding **A-P2-D**. The synthesis can also be performed without separating **14** and **15**, by isolating **A-P2-A** and the silyl/nitro dimer precursor **16** to **A-P2-D** one step later (Scheme 2.2).

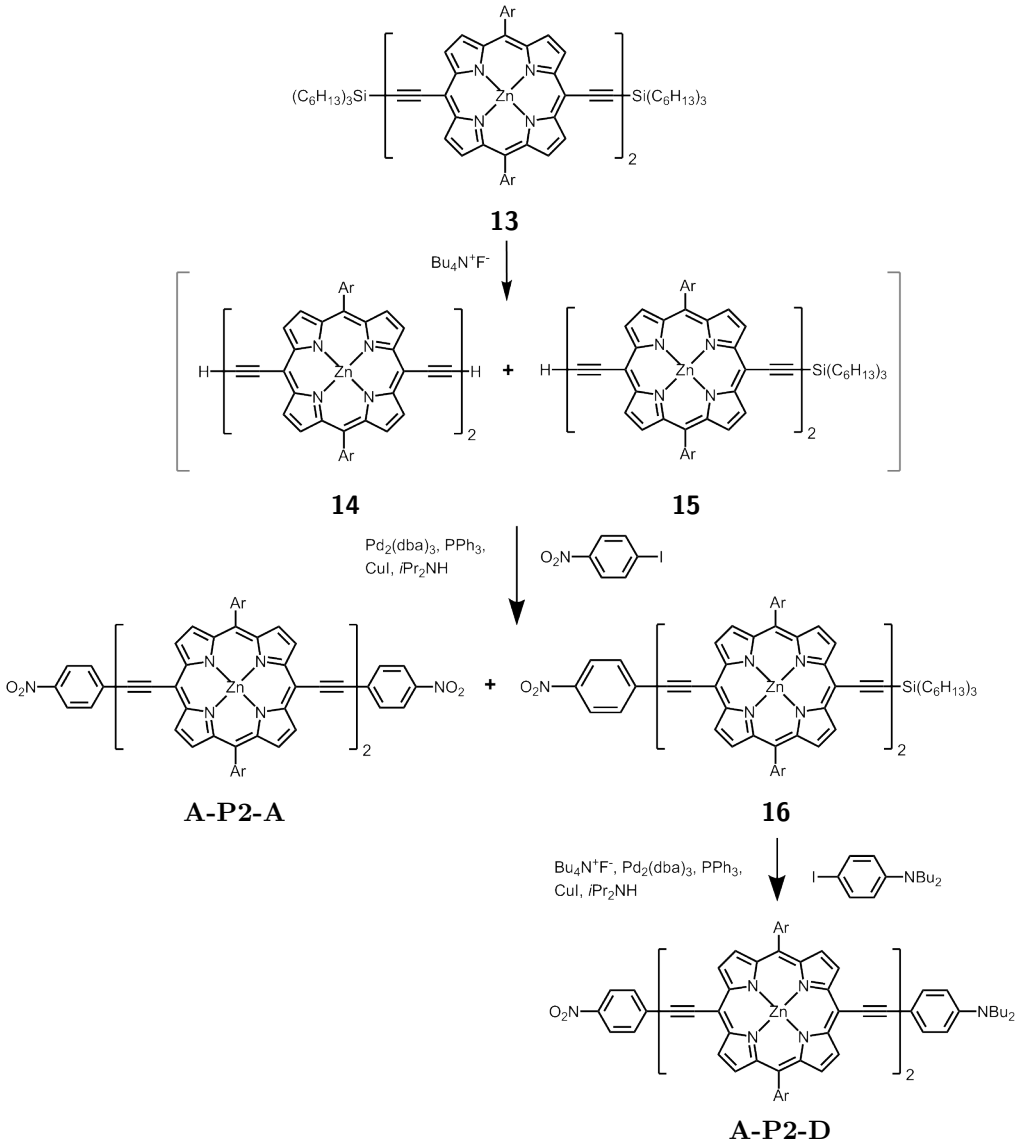

Scheme **2.2** An alternative synthetic route. (Ar = 3,5-bis-octyloxy-phenyl).

The other four compounds in the family were synthesised using analogous procedures. With pure samples of the six butadiyne-linked dimers available, studies into their NLO properties were next completed.

2.7 Investigating the first hyperpolarisability

2.7.1 Introduction to hyper-Rayleigh scattering

Hyper-Rayleigh scattering (HRS) was employed to measure values of the first hyperpolarisability β for the family of 'push-pull' porphyrin dimers. Although an isotropic solution of harmonophores might be expected to give no SHG signal as the requirement for a non-centrosymmetric ensemble appears to not be met, instantaneous fluctuations in symmetry as a result of changes in relative molecular orientation allow a weak SHG response to be observed. The main features of the practical setup required for observing this are a nanosecond or faster high-intensity pulsed laser focussed on the sample cuvette, and photon-counting apparatus to measure the intensity of the scattered light. An appropriate bandpass filter is used to prevent scattered incident light from being collected,[51] which is readily achieved as the HRS signal is at half the wavelength of the incident light. To also exclude 2P excited fluorescence from the collected signal, a frequency demodulation technique is often used to completely remove the long lifetime fluorescence component from the signal.[52] After performing the measurements across a range of concentrations and incident light intensities, I_0, the experiment yields a linear plot with slope β^2:

$$I_{\mathrm{HRS}} = GN\beta^2 I_0^2 \tag{2.7}$$

The constant G contains geometric and electronic factors but is not determined, as it is cancelled out by referencing against a standard. As β often consists of contributions from hyperpolarisability components along different molecular axes, all of which are HRS active and thus part of the total collected signal, polarisation studies are necessary help to elucidate these components.[53] By using pairs of rotatable polarisers, the parallel and perpendicular polarised components of the second harmonic signal compared to the incident light po-

larisation can be measured, and a depolarisation ratio ρ is defined from the ratio of the two detected signals. For ideal dipolar harmonophores ρ should be 5, and ρ reaches a lower limit of 1.5 for a purely octupolar HRS response. Normally values between 1 and 3.5 are found experimentally.[11]

To exemplify using Therien's compounds in Figure 2.14, monomer **5** has $\rho = 3.1$, whereas the two octupolar dimers are confirmed as such with $\rho = 1.3$ for **3** and $\rho = 1.5$ for **4**.[21]

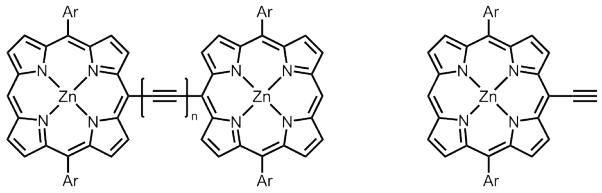

Figure **2.14** Dipolar and octupolar contributions to β revealed by depolarisation ratios.[21] (Ar = 2,6-bis(3,3-dimethylbutyloxy)phenyl)

2.7.2 Results from HRS measurements

HRS measurements on all six of the porphyrin dimers shown in Figure 2.13 were performed in collaboration with Griet Depotter and Prof. Koen Clays, KU Leuven (Belgium). I was able to assist with these experiments during a visit to Leuven. The results of these measurements for the series of dimers are shown in Table 2.1. The values vary with wavelength as expected, and there is relatively little variation of β with substitution pattern. β at 1300 nm correlate well with those of Therien and Clays *et al.* for the dimers in Figure 2.8 on Page 51.[21] The small variations within the series in Table 2.1 observed are probably attributable to differences in the extent of resonance enhancement due to differences in oscillator strengths in the regions near 420, 620 and 650 nm. Much larger variations in β with substitution pattern have been found by colleagues in the Anderson group: comparing the two monomers **17** and **18**

dimer	$\beta_{840,\mathrm{HRS}}$[a] ($\times 10^{-30}$ esu)	ρ (840 nm)	$\beta_{1240,\mathrm{HRS}}$[b] ($\times 10^{-30}$ esu)	$\beta_{1300,\mathrm{HRS}}$[b] ($\times 10^{-30}$ esu)
A-P2-A	570 ± 40	–	n.d.	940 ± 400
A-P2-D	920 ± 40	2.0	40 ± 15	400 ± 170
A-P2-R	780 ± 40	–	–	–
D-P2-D	880 ± 40	–	90 ± 40	n.d.
D-P2-R	750 ± 45	2.0	60 ± 25	440 ± 180
R-P2-R	1170 ± 50	2.3	n.d.	300 ± 120

a) frequency-demodulated HRS measurements, no contribution from 2PEF. c) spectral HRS measurements: HRS determined from a peak fitting at the wavelength of the second-harmonic. In the case of strong 2PEF/weak SHG, this peak was not determinable (n.d.). '–' indicates not measured.

Table **2.1** HRS data for the series of dimers, measured in $CHCl_3$: 1% pyridine. β is reported as $\beta_{\lambda,\mathrm{HRS}}$, where λ is the wavelength of the incident light.

reveals a factor of 50 change in β (Figure 2.15).[54] The $\beta_{840,\mathrm{HRS}}$ values measured for this family of dimers are of similar magnitude to those measured for **JR1** (2440 $\times 10^{-30}$ esu). Clearly we have not recognised an improvement over **JR1**, but investigations at different wavelengths, combined with ongoing theoretical studies may yet reveal larger β values for porphyrin dimers.

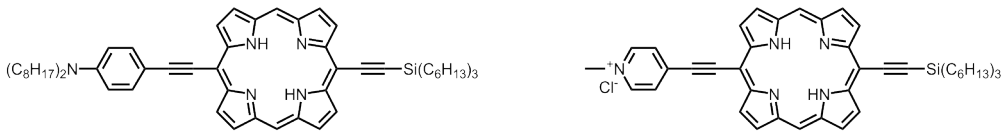

17 $\beta_{800,\mathrm{HRS}}$ 1100 x 10^{-30} esu

18 $\beta_{800,\mathrm{HRS}}$ <20 x 10^{-30} esu

Figure **2.15** Optimisation of β in porphyrin monomers by donor and acceptor substitution.[54]

The depolarisation ratios in Table 2.1 are close to 1.5 and thus indicate that β is largely but not solely due to the octupolar contribution. This is expected as non-dipolar compounds **A-P2-A**, **D-P2-D** and **R-P2-R** are only

non-centrosymmetric in a non-planar conformation of octupolar symmetry. This is also consistent with the lack of 'push-pull' substituent effect observed. In contrast to the example of strong but cancelled dipoles giving enhanced β in an octupolar compound (see Figure 2.9 on Page 51), there is no such effect found here, with the octupolar reference compound **R-P2-R** giving the largest β at 840 nm. This reflects the importance of the octupolar contribution and the inherently large polarisability of the porphyrin dimer π-system.

The conclusion of these HRS measurements is that achieving a high first hyperpolarisability in a butadiyne-linked porphyrin dimer does not necessitate strong 'push-pull' electronic substituents. Thus the design of a new generation of elongated porphyrin voltage sensors does not need to feature such groups. It is also of note that the twisted conformation of these dimers is the main source of their first hyperpolarisability, even in the dipolar dimers whose non-centrosymmetric planar conformations might also be expected to contribute to β. A voltage sensor design could therefore consider the opportunity to hinder the population of the planar conformation and thus further maximise β further, but such investigations were beyond the scope of this thesis. β_{HRS} is encouragingly large for these dimers, both in the biological transparency window (700 – 900 nm) and at higher wavelengths, and will contribute to a good $\Delta S/S$ and SNR.

2.8 Investigating the second hyperpolarisability

2.8.1 One-photon absorption properties

The main optical features of strongly coupled butadiyne-linked porphyrin dimer are broadly similar to those of the monomer, but the presence of conformations and the change in symmetry results in extra spectral features. The split Q bands result from differently polarised transitions, with the most intense

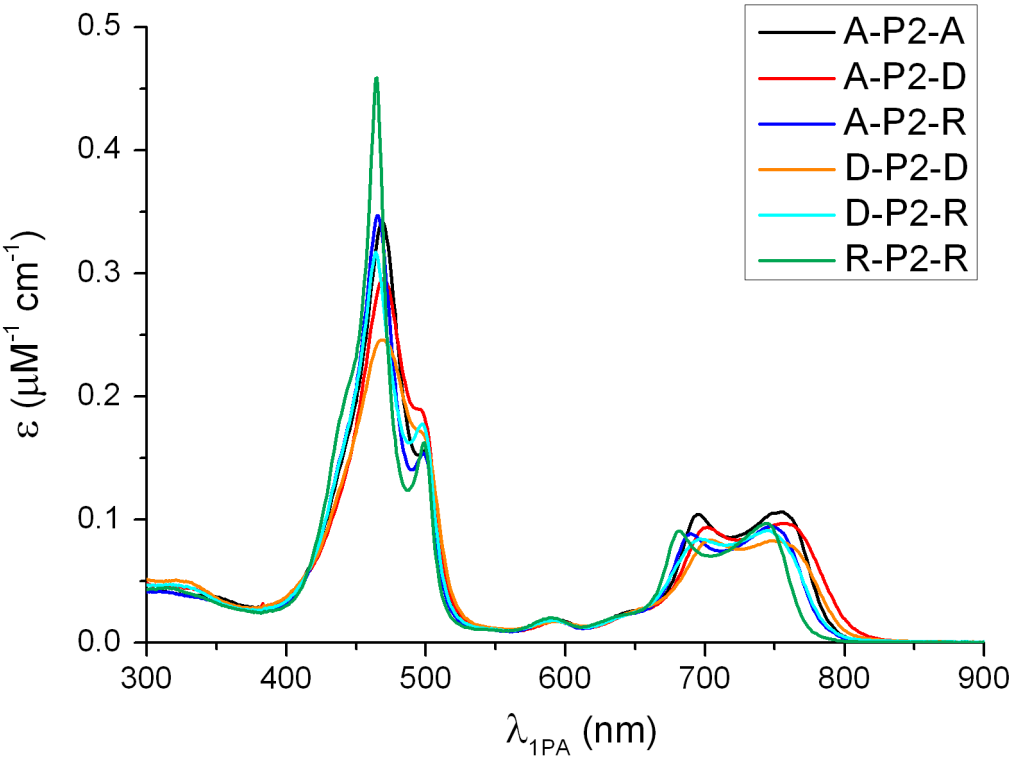

Figure **2.16** 1PA of the family of dimers, measured in $CHCl_3$: 1% pyridine.

bands, Q_x(0-0) and Q_x(0-1), due to transitions polarised along the butadiyne link, defining the x-axis.[6,33]

The absorption spectra of the series of porphyrin dimers show the spectral features typical of butadiyne-linked porphyrin dimers (Table 2.2 on Page 64 and Figure 2.16).[13,55,56] The peak of the Soret (B) band is shifted bathochromically by up to 5 nm to 469 nm in the 'pull-push' chromophore **A-P2-D**, compared to the 'push' chromophore **D-P2-R**. The trend in peak wavelength of this band (**D-P2-R** < **R-P2-R** < **A-P2-R** < **D-P2-D** ≈ **A-P2-A** < **A-P2-D**) reveals that the electron-accepting group has a greater influence on the π-system. The extinction coefficients of the Soret transition are large and correlate well with the inverse of the bandwidth; the dyes all have similar oscillator strengths (f_B and f_Q) as expected. The lowest-energy Q band transitions are more sensitive to changes in the electronic substitution, with a maximum red shift of 12 nm from **R-P2-R** to **A-P2-D**.

2.8.2 Two-photon excited fluorescence

2PEF can be used to measure accurate two photon cross-sections σ_2, and is based on the assumption that after 2PA a dye molecule will fluoresce from the same excited state with the same quantum yield as under 1P excitation. By comparing the fluorescence signal of the sample under the same energy 1P and 2P excitation ($\lambda_{1\mathrm{Pex}} = \frac{1}{2}\lambda_{2\mathrm{Pex}}$), prior measurement of the fluorescence quantum yield is not required and a source of error is removed. At each energy, the emission intensity is recorded from a solution of the analyte in a cuvette under 100 ps or faster pulsed laser excitation at $\lambda_{2\mathrm{Pex}}$ and $\lambda_{1\mathrm{Pex}}$. Comparison of the final 2P excitation spectrum with a reference sample of known 2PA cross section under identical conditions allows σ_2 to be determined. The open-aperture z-scan method can also be employed to measure σ_2, but it is more vulnerable to complications that might overestimate σ_2.[9] The 2PA behaviour of the family of dimers was thus assessed using 2PEF.

2.8.3 Results from 2PEF measurements

Two-photon absorption spectra were measured in collaboration Geoffrey Wicks, Mikhail Drobizhev and Aleks Rebane, Montana State University (USA). The entire series of dimers was found to have large σ_2 ($\sim 10^4$ GM at ~ 900 nm; Table 2.2 and Figure 2.17) with maxima lying between 890 and 904 nm, in accordance with literature values,[33–36,43,57,58] and representing an hundred-fold enhancement compared to typical porphyrin monomers.[16,33,59,60] The 2PA spectra feature a second peak at lower intensity at 1050 – 1150 nm. The strongly quadrupolar **A-P2-A** dimer exhibits a peak cross section of 1.6×10^4 GM, which is 1.7-fold larger than that of the **R-P2-R** reference system. The 2PA cross section of **A-P2-A** is similar to that of **Oxdime** (Figure 2.12).[43,47]

A three-level model (Figure 2.18 on Page 66) is often invoked to describe the 2PA spectra of centrosymmetric porphyrin dimers.[33,35] 2PA proceeds from

dimer	$\lambda_{max,1PA}$ (nm) [ϵ (μM^{-1} cm^{-1})]	f_B[a]	f_Q[a]	$\lambda_{max,2PA}$ (nm)	σ_2 (10^3 GM)
A-P2-A	468 [0.34], 494 [0.16] 694 [0.10], 748 [0.10]	2.96	0.67	904	15
A-P2-D	469 [0.30], 495 [0.19] 702 [0.09], 756 [0.10]	2.68	0.65	902	12
A-P2-R	466 [0.35], 498 [0.15] 690 [0.09], 748 [0.09]	2.67	0.58	900	13
D-P2-D	468 [0.25], 496 [0.17] 704 [0.08], 752 [0.08]	2.54	0.57	902	13
D-P2-R	464 [0.32], 497 [0.18] 697 [0.08], 745 [0.09]	2.67	0.58	900	12
R-P2-R	465 [0.46], 499 [0.16] 681 [0.09], 744 [0.10]	2.82	0.55	890	9.1

a) Calculated using $f = 4.319 \times 10^{-9} A/n$, where n is the solvent refractive index (1.45 for $CHCl_3$) and A is the integrated absorption band (units: mol^{-1} L cm^{-2}; integration range for f_B 18,020-26,670 cm^{-1}/375-555 nm; range for f_Q 11,830-16,450 cm^{-1}/608-845 nm).

Table **2.2** One- and two-photon absorption data for the family of zinc dimers, measured in $CHCl_3$: 1% pyridine. 2PA data acquired by Geoffrey Wicks.

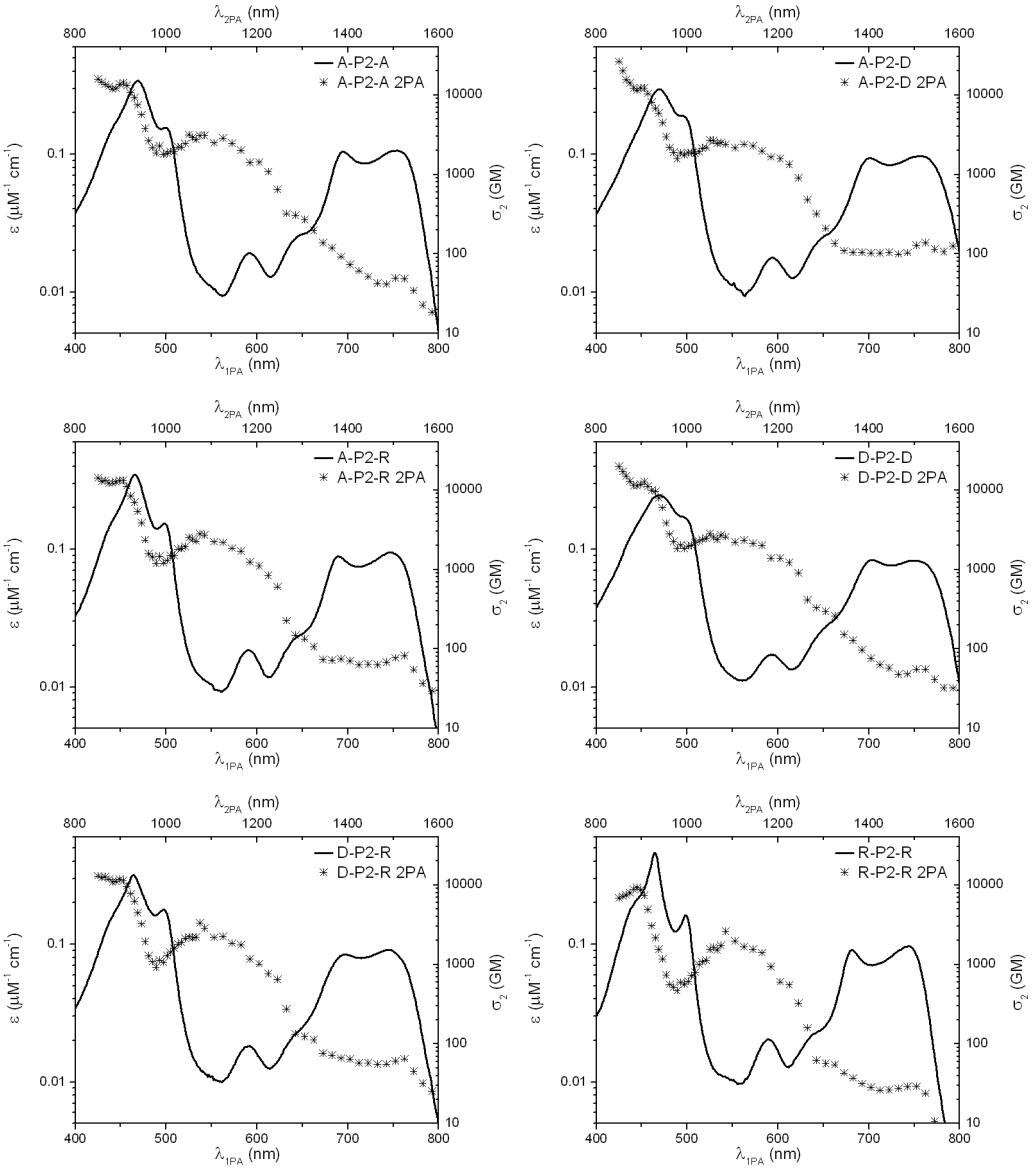

Figure **2.17** One-photon (curves) and two-photon (symbols) absorption spectra plotted on the same energy scale, measured in $CHCl_3$: 1% pyridine. 2PA data acquired by Geoffrey Wicks.

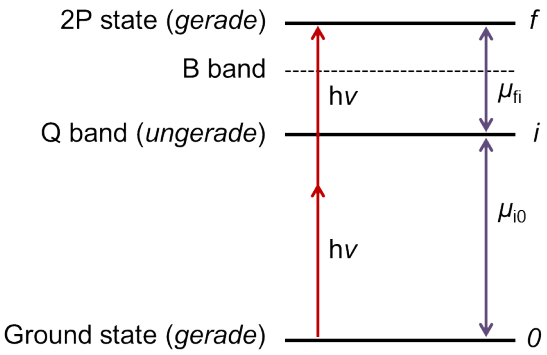

Figure **2.18** The three-level model of resonance-enhanced 2PA.[33,35]

dimer	E_{ox}	E_{ox} - $E_{ox,ref}$	E_{red}	E_{red} - $E_{red,ref}$	E_{ox} - E_{red}
A-P2-A	0.43	0.04	-1.41	0.06	1.84
D-P2-D	0.23	-0.16	-1.53	-0.06	1.76
R-P2-R	0.39	–	-1.47	–	1.86

All data are in volts against internal ferrocene (Fc/Fc^+) and were acquired using square wave voltammetry in tetrahydrofuran (THF) containing Bu_4NPF_6 (0.1 M). $E_{ox,ref}$ and $E_{red,ref}$ refer to the oxidation and reduction potentials respectively of the reference compound **R-P2-R**.

Table **2.3** Electrochemical data for selected dimers.

a *gerade* (symmetric) ground state to a *gerade* final state via an *ungerade* (asymmetric) intermediate state. The lowest-energy Q band transition, Q_x(0-0), of the porphyrin dimer is assigned to the intermediate state i; resonance enhancement due to the presence of this state is in part responsible for the large σ_2 observed for porphyrin dimers compared to monomers. Besides the centrosymmetry supporting the role of the Q_x(0-0) transition, the close match between the difference in the wavelengths of the 2PA maxima of **A-P2-A** and **R-P2-R** and the difference in the wavelengths of their lowest energy Q_x(0-0) transition further implies this state is significant in 2PA. It is also observed that the Q_x(0-0) transition is strongest in **A-P2-A**, contributing to its large σ_2.

The effect of the 'push' and 'pull' groups upon the butadiyne-linked porphyrin dimer π-core was assessed by electrochemistry. The quantity E_{ox} - $E_{ox,ref}$ defined from the electrochemical data in Table 2.3 on the page before, is the difference between the first oxidation potential of a specific dimer and that of the reference dimer **R-P2-R**. E_{ox} - $E_{ox,ref}$ thus acts as a measure of the electronic effect of the acceptor or donor groups upon the dimer core. E_{ox} - $E_{ox,ref}$ reveals that **D-P2-D** is the most strongly perturbed π-system compared to the reference dimer **R-P2-R**. On the basis of this electrochemical analysis of the 'push' and 'pull' effect alone, **D-P2-D** could be expected to exhibit the highest σ_2 as it is the most quadrupolar π-system. However, **A-P2-A** has the longest π-system due to complete conjugation of the nitro groups to the phenyl rings, and the strongest Q band oscillator strength. Although the differences in absolute σ_2 are small, it seems that desirable optical properties matter most, and the electrochemical properties do not readily correlate with other observations.

2.8.4 Discussion of 2PEF results

Overall, the 2PA cross section of the butadiyne-linked porphyrin dimer core is found to be quite insensitive to substitution. This is emphasised by comparing the factor of $\sim$ 2-fold difference between σ_2 of **A-P2-A** and **R-P2-R**, and the factor of $\sim$ 20 between analogously modified porphyrin monomers **20** and **21** from the literature (Figure 2.19 on the following page).[16]

Commonly held design principles, such as the advantage of a quadrupolar system over a dipolar system, are strongly dependent upon the core π-system and do not appear to play a strong role in butadiyne-linked porphyrin dimers. In terms of maximising γ for VSD design, the electronic substituents can be chosen for the sake of achieving other necessary design requirements, such as amphiphilicity. However, as a stronger dependence of σ_2 than β upon electronic

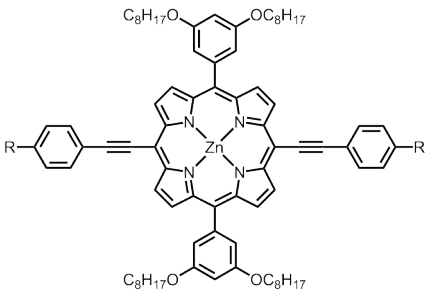

19 R = NBu_2; σ_2 = 650 GM (850 nm)
20 R= NO_2; σ_2 = 650 GM (870 nm)
21 R= Bu; σ_2 = 30 GM (850 nm)

Figure **2.19** Dramatic differences in σ_2 upon substitution are observed in porphyrin monomers.[16]

substituents was observed, it was decided to further test the 2PA behaviour of the butadiyne-linked dimer core to electronic effects. A clear way forward was to remove the coordinated zinc, as free-base porphyrins are more electron poor than zinc porphyrins. Removing the zinc to give an electron-deficient dimer core might lead to enhanced quadrupolar character with electron donor substituents (D-A-D), and augment σ_2 further. As dipolar compounds from the zinc family had shown no clear advantage in the β or σ_2 studies so far, only the symmetric free-base analogues were prepared and only σ_2 was examined.

2.9 Investigations with free-base dimers

2.9.1 Synthesis of free-base dimers

Free-base porphyrin dimers (Figure 2.20 on the next page) were prepared either by demetalation of a final zinc compound (Scheme 2.3, green route), or by demetalation of the key intermediate **13** to give **22** (blue route), followed by the application of a Cu-free Sonogashira coupling step to couple on the respective iodoaryl. The use of Cu-free conditions ensured that this coupling proceeded without the formation of Cu porphyrin impurities, which may have proved inseparable.

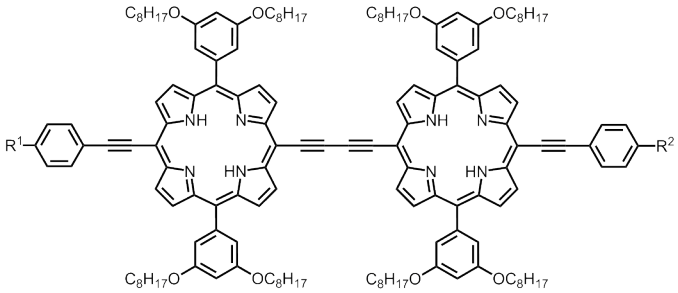

A-P2(2H)-A ($R^1 = R^2 = NO_2$)
D-P2(2H)-D ($R^1 = R^2 = NBu_2$)
R-P2(2H)-R ($R^1 = R^2 = Bu$)

Figure **2.20** The free-base dimers studied in this section.

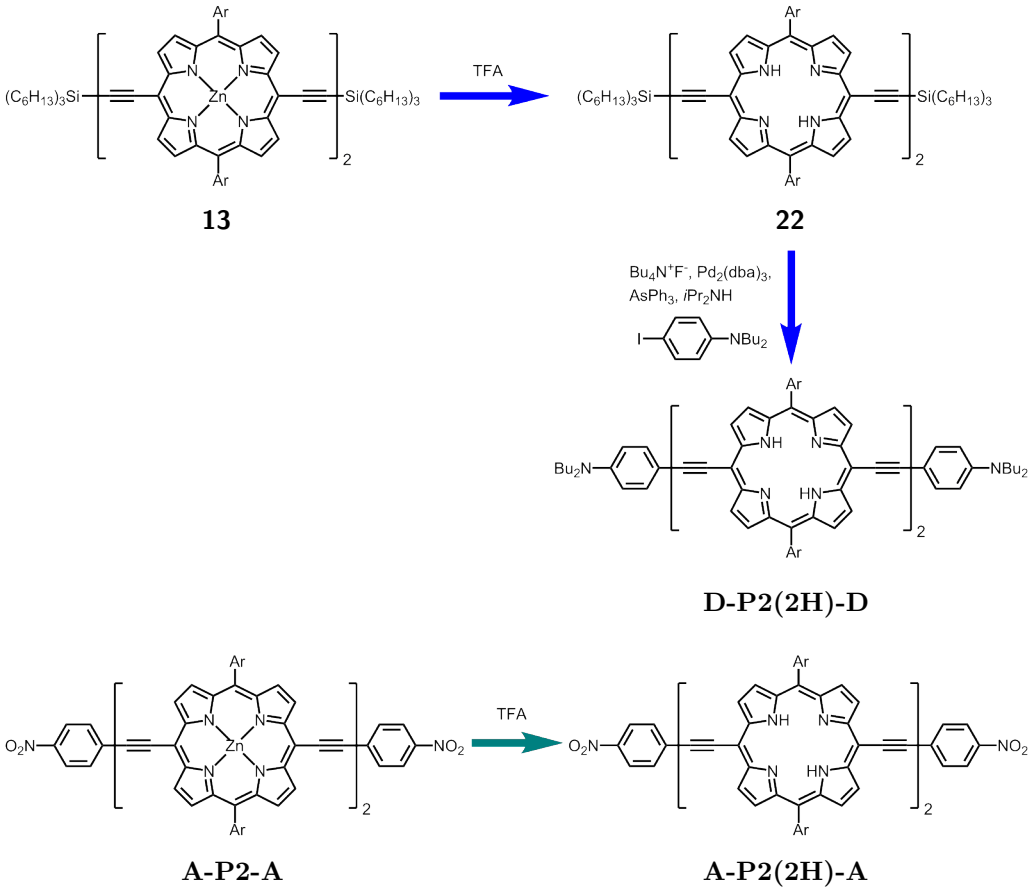

Scheme **2.3** The two approaches employed to synthesising symmetric free-base dimers. (Ar = 3,5-bis-octyloxy-phenyl)

2.9.2 One-photon absorption properties of free-base dimers

Linear electronic absorption spectra reveal that the electron-donating group has the greatest effect on the π-system, dramatically distorting the shape of

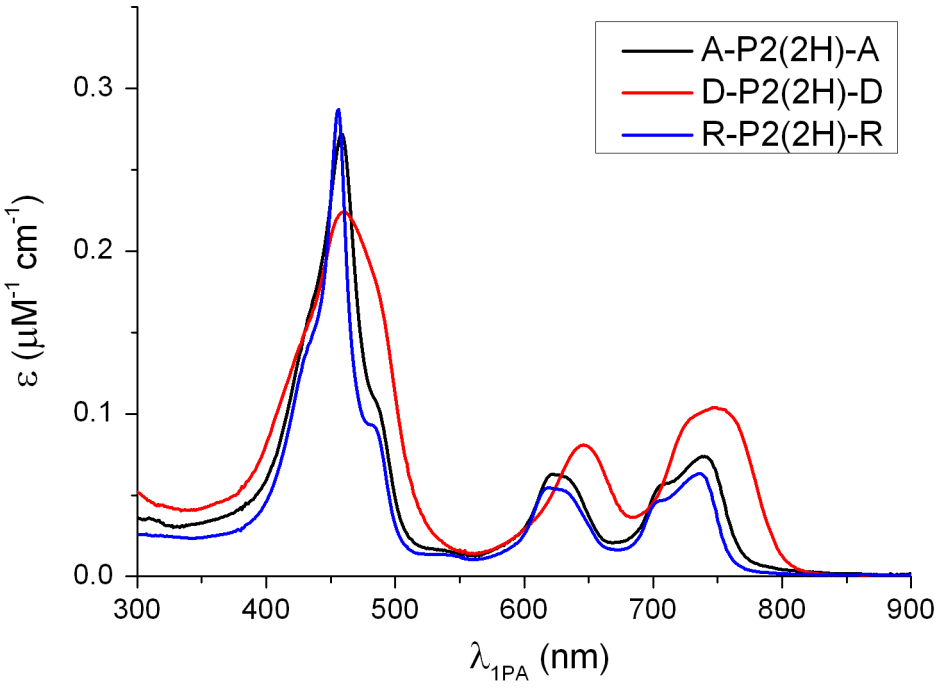

Figure **2.21** One-photon absorption spectra of the set of free-base dimers, measured in $CHCl_3$.

the Soret and Q bands (Figure 2.21). Shifts of 4 nm (Soret) and 11 nm (Q) between the reference and the bis-donor dyes complement the effect observed for the bis-acceptor dyes relative to the zinc reference. However, the oscillator strengths of **D-P2(2H)-D** are uniquely enhanced compared to any other dye in the zinc and free-base series. Due to the acidity of chloroform, tests for the effect of porphyrin or aniline protonation on this absorption spectrum were performed by the addition of a variety of bases, but no change in the spectrum was observed.

2.9.3 Two-photon absorption properties of free-base dimers

2PA cross-sections obtained by 2PEF demonstrate an increase of 2.2-fold for **D-P2(2H)-D** compared to **R-P2(2H)-R**, larger than the 1.7-fold maximum increase in the zinc series (Figure 2.22 on the following page). The shift in

dimer	$\lambda_{max,1PA}$ (nm) [ϵ (μM^{-1} cm^{-1})]	f_B[a]	f_Q[a]	$\lambda_{max,2PA}$ (nm)	σ_2 (10^3 GM)
A-P2(2H)-A	458 [0.27], 484 [0.11] 622 [0.06], 708 [0.06] 738 [0.07]	2.88	0.58	920	10
D-P2(2H)-D	460 [0.22], 646 [0.08] 747 [0.10]	3.42	0.85	925	17
R-P2(2H)-R	456 [0.29], 481 [0.09] 623 [0.05], 706 [0.05] 736 [0.06]	2.39	0.47	915	7.7

a) Calculated using $f = 4.319 \times 10^{-9} A/n$, where n is the solvent refractive index (1.45 for $CHCl_3$) and A is the integrated absorption band (units: mol^{-1} L cm^{-2}; integration range for f_B 17,699-30,030 cm^{-1}/333-565 nm; range for f_Q 11,111-17,699 cm^{-1}/565-900 nm).

Table **2.4** One- and two-photon absorption data for the free-base dimers, measured in $CHCl_3$. 2PA data acquired by Geoffrey Wicks.

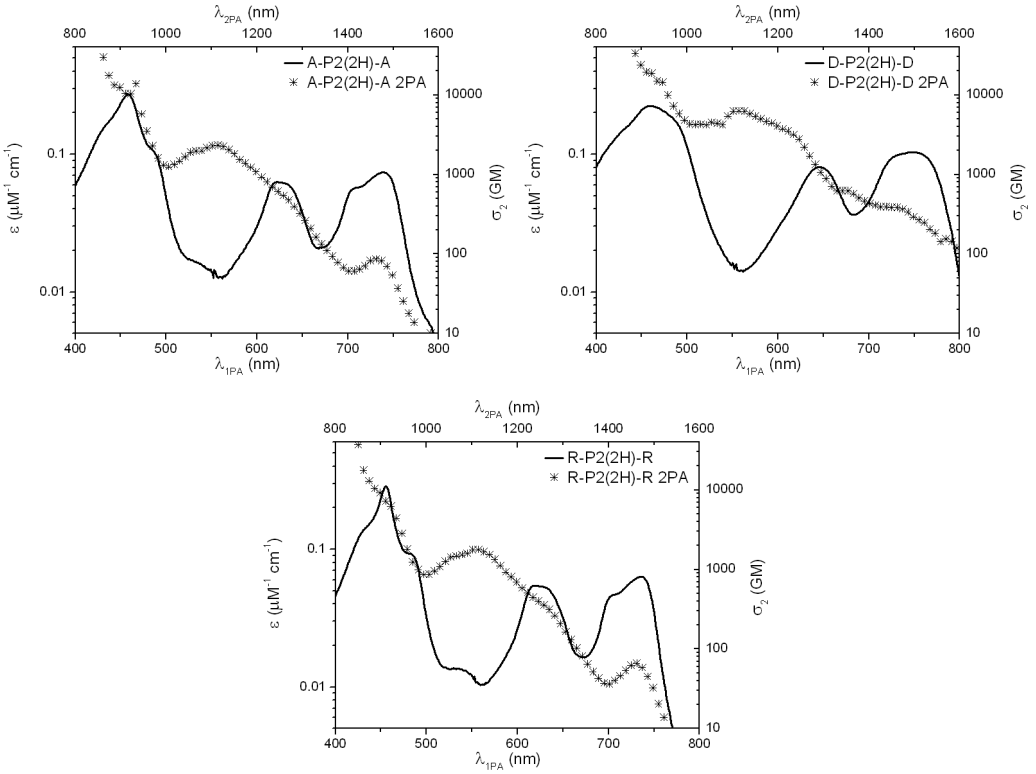

Figure **2.22** One-photon (curves) and two-photon (symbols) absorption spectra of the free-base dimers, measured in $CHCl_3$, plotted on the same energy scale. 2PA data acquired by Geoffrey Wicks.

dimer	E_{ox}	E_{ox} - $E_{ox,ref}$	E_{red}	E_{red} - $E_{red,ref}$	E_{ox} - E_{red}
A-P2(2H)-A	0.61	0.06	-1.18	0.10	1.79
D-P2(2H)-D	0.27	-0.28	-1.31	-0.03	1.58
R-P2(2H)-R	0.55	–	-1.28	–	1.83

All data are in volts against internal ferrocene (Fc/Fc^+) and were acquired using square wave voltammetry in THF containing Bu_4NPF_6 (0.1 M). $E_{ox,ref}$ and $E_{red,ref}$ refer to the oxidation and reduction potentials respectively of the reference compound **R-P2(2H)-R**.

Table **2.5** Electrochemical data for the series of free-base dimers.

wavelength of σ_2 maxima between **R-P2(2H)-R** and **D-P2(2H)-D** matches well with the difference in the lowest energy Q_x(0-0) band maxima. Therefore, as for the zinc series, these centrosymmetric dyes seem to benefit from strong resonance enhancement due to the Q band, as described by the three-level model. Again, the largest σ_2 value is also observed for the compound with the largest Q band oscillator strength.

Electrochemical measurements (Table 2.5) demonstrate that the aniline donor group induces the greatest electronic perturbation, as judged by the values of $E_{ox} - E_{ox,ref}$ on the porphyrin dimer core in **D-P2(2H)-D**, in line with the observed effects on the 1P absorption.[d] The free-base core is electron poor as expected, and **D-P2(2H)-D** is thus a stronger quadrupolar 'push-pull-push' system than **A-P2(2H)-A**; as a result, an enhanced σ_2 is observed.

2.9.4 Discussion of 2PEF properties of free-base dimers

In contrast to the zinc series, the free-base dimer 2PA cross-section is most strongly modulated by electron-donors, due to the electron-poor core. The strongest quadrupolar system has the largest σ_2. However, the variation in the series is still comparatively modest, and butadiyne-linked porphyrin dimer

[d]The quantity E_{ox} - $E_{ox,ref}$ is here defined against the free-base reference dimer **R-P2(2H)-R**.

voltage-sensors can be expected to benefit from a large σ_2 and γ compared to **JR1** regardless of electronic substitution.

2.10 Probing the effect of conformation upon two-photon absorption using high-viscosity spectroscopy

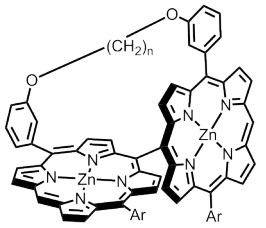

25 n = 1-6

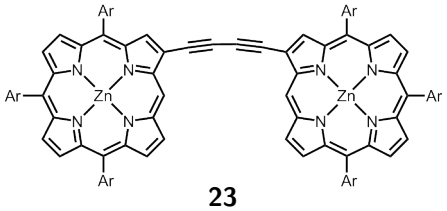

23

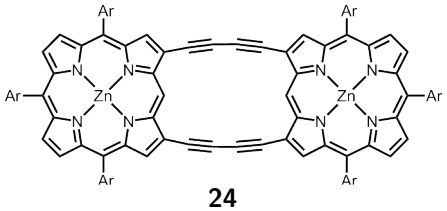

24

compound		σ_2 (GM)
23		5220
24		9620
25	n = 6	3470
	n = 5	3920
	n = 4	4830
	n = 3	6120
	n = 2	6330
	n = 1	7500

Figure **2.23** Two examples of enforcements towards planarity leading to an increase in σ_2 as a result of enhanced electronic coupling between neighbouring rings.[61,62] (Ar = 3,5-di-*t*-butylphenyl)

In the final section of this chapter, the effect of conformation upon 2PA is probed. Efficient 2PA requires strong electronic coupling over a large π-system, making it sensitive to conformational changes which alter π-overlap. Various strategies have been used to enhance 2PA by constraining the conforma-

tions of π-systems. One approach is the synthesis of multiply-linked porphyrin tapes, for example β-to-β 1,3-butadiyne doubly-linked (compounds **23** and **24**, Figure 2.23 on the page before),[61] meso-β doubly-linked and triply-linked tapes.[63,64] Other approaches are ladder-complex formation[57,65] and porphyrin-porphyrin straps (compound **25**).[62]

It has been demonstrated in this chapter (Sections 2.8.3 and 2.9.3), as in the literature, that there is a poor match between the one- and two-photon transition energies in butadiyne-linked porphyrin dimers: the values of $\lambda_{\mathrm{max,2PA}}$ do not correlate well with $2 \times \lambda_{\mathrm{max,1PA}}$.[35] This implies that 2PA involves transitions to a *gerade* final state,[33,35] and that the chromophores are effectively centrosymmetric. This is surprising because of the broad distributions of conformations that are adopted in solution, due to free rotation about the butadiyne link. Only the conformation in which both porphyrins are co-planar is centrosymmetric. The different conformations adopted by butadiyne-linked porphyrin dimers due to rotation about this link have characteristic absorption and fluorescence spectra.[49,66,67] This feature is used in this section to compare the 2PA cross sections of planar and twisted conformations.

In the ground state, the barrier to rotation about the butadiyne link is comparable to kT at room temperature ($\sim$0.7 kcal mol^{-1} vs. $\sim$0.6 kcal mol^{-1}), whereas this barrier becomes higher in the singlet excited state ($\sim$3.9 kcal mol^{-1}).[49] In low-viscosity solvents, the excited states undergo planarisation faster than radiative decay, so that most of the emission originates from the planar conformation, regardless of which conformation was excited, but in viscous media torsional rotation becomes slow on the time-scale of emission and the shape of the observed fluorescence spectrum provides information on the conformations that were excited.[66] Although there is a continuous distribution of conformations, the spectra can be adequately analysed in terms of just two extreme conformations with twisted and planar geometries.[49,66]

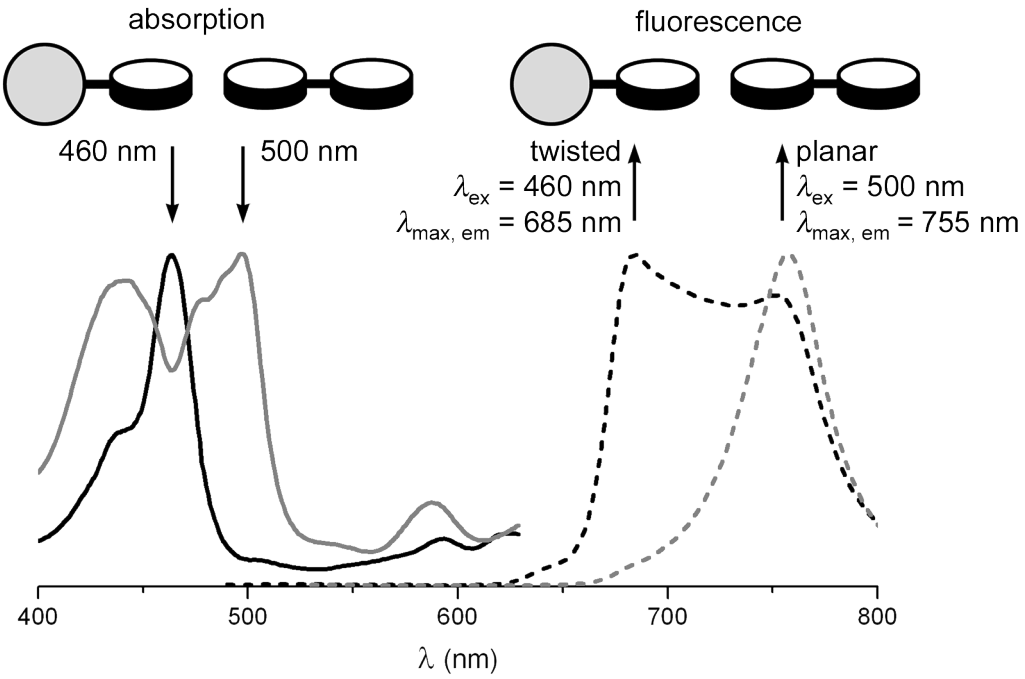

Figure **2.24** 1P excitation (solid) and emission (dashed) spectra of **R-P2-R** in viscous $CHCl_3$/polymer solution (see Experimental, Section 2.13.1) reveal the differing absorption and fluorescence behaviour of the twisted and planar conformations.

2PEF measurements lead to the same fluorescence peaks as would be observed from the sample under 1P excitation. In the case of butadiyne-linked dimers in a high viscousity medium, the emission peaks will be indicative of the state which absorbed, and therefore the emission data from the 2PEF measurement will be informative of the strength of 2PA of each conformer. This known property of butadiyne-linked porphyrin dimers was thus exploited to further demonstrate the importance of efficient conjugation upon σ_2.

The one-photon excited fluorescence spectra of **R-P2-R** in a viscous chloroform/polymer medium were analysed. The normalised one-photon excitation and fluorescence spectra of **R-P2-R** (Figure 2.24) show that twisted and planar conformations fluoresce at 685 and 755 nm respectively. One photon excitation at 500 nm generates exclusively the planar excited state, whereas excitation at 460 nm gives predominantly the twisted excited state, with also some planar excited state due to competing absorption by both conformations

at 460 nm, and possibly due to partial planarisation in the excited state. Measuring the excitation spectra of the two main emission peaks reveals where each conformer absorbs.

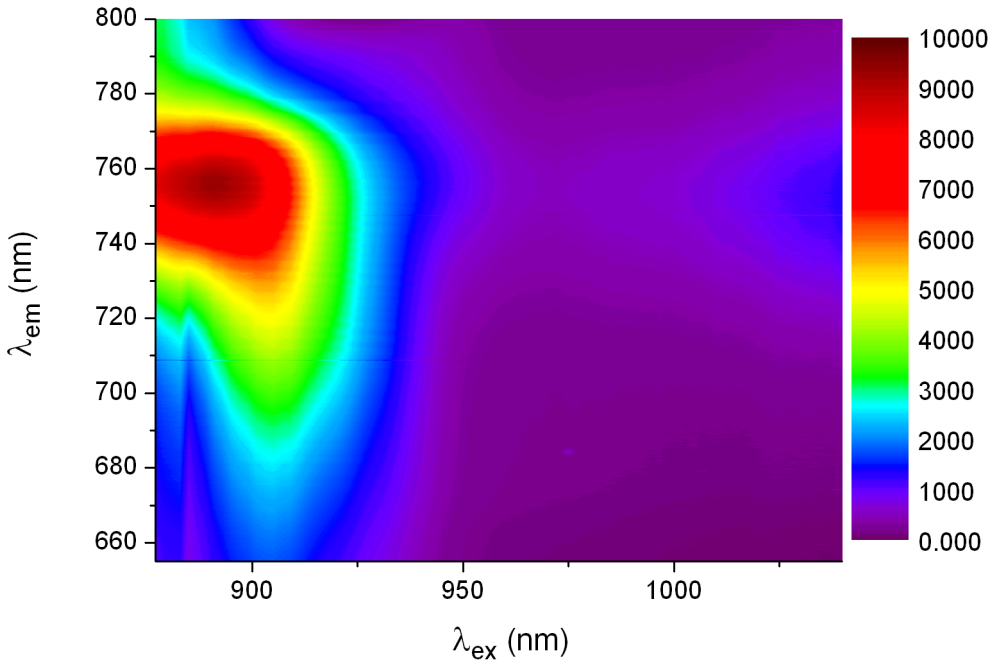

Figure **2.25** 2P excitation of **R-P2-R** in viscous $CHCl_3$/polymer solution at wavelength x leads to 1P emission at wavelength y of intensity indicated by the colour, demonstrating that the planar conformation is a stronger 2P absorber. Data acquired by Geoffrey Wicks.

This viscous solution was then used to acquire a 2D 2PEF emission-excitation spectrum shown in Figure 2.25 (measured by Geoffrey Wicks). The 2P excitation-emission map reveals that upon excitation at the 2PA maximum (890 nm), emission is seen exclusively from the planar form (755 nm), implying that this conformation is the stronger 2P absorber. The tail of the contour reveals a second 2PA peak clearly emitting at the wavelength of the twisted conformation (685 nm) with excitation shifted bathochromically by 15 nm, as expected for a twisted conformation.[68]

Whereas the one-photon excited emission spectra at various excitation wavelengths demonstrate that both conformations absorb strongly, in ratios reflected in the varying emission ratio of the two peaks (685 : 755), under 2P

excitation there is very little variation in the emission ratio, as the planar form is the dominant 2P absorber (Figure 2.26 on the following page). Plotting the individual 2P excitation spectra confirms the dominance of the planar form over the twisted form in σ_2 (Figure 2.27 on the next page). In addition to the two sets of 2PA data with spectral features strongly indicative of the importance of the centrosymmetric planar conformation, this investigation has exploited the distinct fluorescent behaviour of the two conformers to directly confirm this theory.

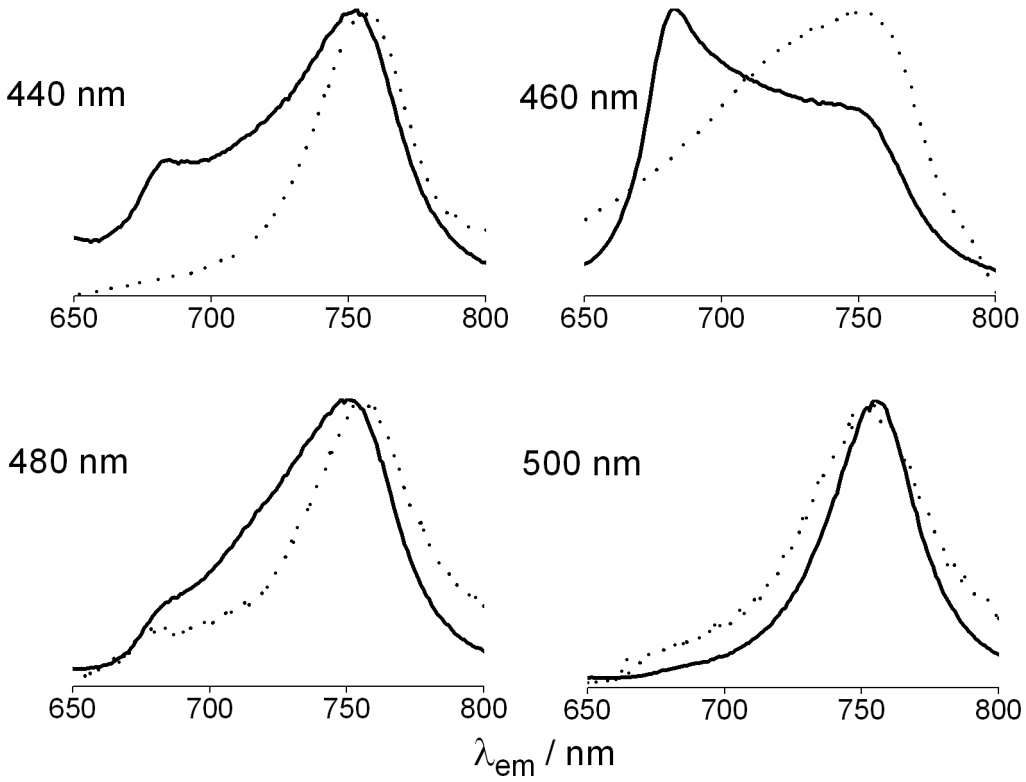

Figure **2.26** Normalised comparisons of the 1P (solid) and 2P (dashed) emission spectra, measured in the viscous $CHCl_3$/polymer solution, when exciting at the wavelength/energy indicated. Emission from the planar form dominates all of the 2P spectra. 2P data acquired by Geoffrey Wicks.

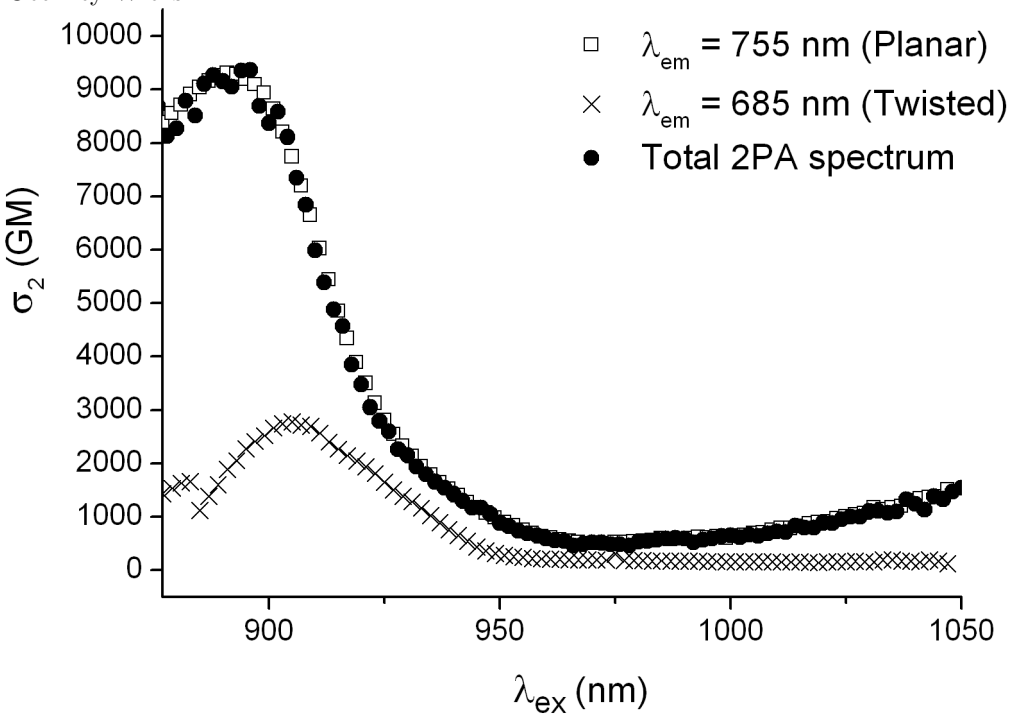

Figure **2.27** 2P excitation spectra, measured in the viscous $CHCl_3$/polymer solution, at the maximum wavelengths for the twisted and planar conformations, compared to the total 2PA spectrum ($CHCl_3$). Data acquired by Geoffrey Wicks.

2.11 Conclusion to Chapter 2

In this chapter, the second hyperpolarisability has been shown to be particularly important in optimising the sensitivity of SHG voltage sensors. Butadiyne-linked porphyrin dimers are a rational step forward in improving on the voltage sensitivity of **JR1**, as they are known to have larger second hyperpolarisabilities. The work in this chapter has revealed that both β and σ_2 are relatively insensitive to the 'push-pull' electronic substitution pattern in butadiyne-linked porphyrin dimers, although in the case of the free-base dimer σ_2 can be more than doubled by electron donors. These results suggest that the design of butadiyne-linked dimers for IMP can largely be focused on optimising other design requirements, such as amphiphilicity (adequate water-solubility and membrane binding), biocompatibility and synthetic accessibility. It has also become clear that while the twisted conformation is most important for the first hyperpolarisability, the planar is most important for the second hyperpolarisability. Thus while these dimers should offer large improvements in voltage sensitivity over their predecessors through increased hyperpolarisabilities, to optimise γ, the most significant term in increasing the SNR, by conformational restriction, a compromise with decreasing β must be made. However, the following synthetic investigation will not attempt to modify the conformational distribution in any way, as it is clear that improved voltage sensitivity compared to the porphyrin monomer **JR1** should be found even in a dimer not optimised in this way.

2.12 General Experimental

Reactions were run in dry solvents, referring to solvents (analytical- or HPLC-grade from Rathburns, Fisher or Sigma-Aldrich) dried by passing through a column of activated alumina, or freshly distilled from CaH_2 under N_2 (triethylamine, diisopropylamine). For chromatography, solvents were used as supplied. Petroleum ether refers to boiling point 40-60 °C unless specified as 60-80. $Pd_2(dba)_3$ is tris-(dibenzylideneacetone)-di-palladium(0). Solvent ratios are reported volume / volume except where specified. All reagents were commercially sourced and used as received unless specified, except for $Pd(PPh_3)_4$ which was synthesised following a literature procedure.[69]

Standard Schlenk techniques were employed for all reactions run under N_2. TLCs were run on Merck silica gel 60 F_{254} aluminium plates, visualising with UV light when needed. Flash chromatography was carried out using Merck silica gel 60 using applied pressure of N_2. Size-exclusion chromatography was performed under gravity using BioRad BioBeads grade SX1, swollen in the eluent indicated.

MALDI-ToF MS were recorded in positive reflectron mode using a Waters MALDI micro MX instrument and 1,8,9-anthracenetriol (10 mg / mL in THF) as the matrix (or for poly(ethylene glycol) (PEG) and HEG containing compounds α-cyano-4-hydroxycinnamic acid 10 mg / mL in acetone, containing 1 mg / mL NaI.). ESI measurements were performed on a Waters LCT Premier (LRMS), Agilent 6100 Single Quadrupole LC/MS (LRMS) or a Bruker μTOF (HRMS) from methanol solutions.

NMR spectra were recorded using Bruker DPX200 (200 MHz), DPX300 (300 MHz), AVII400 (400 MHz), AVIII400 (400 MHz), DRX500 (500 MHz, ^{11}B), AVII500 (500 MHz, ^{19}F) or AVII500 with ^{13}C cryoprobe (500 MHz) instruments. All peaks were referenced to $SiMe_4$ or the residual solvent peak and reported in parts per million. Coupling constants (J) are reported accurate

to ±0.1 Hz.

Absorption spectra were recorded using a Perkin Elmer Lambda20 UV-Vis spectrometer in 10 mm path quartz cuvettes at 25 C, baseline corrected against a solvent blank. Molar extinction coefficients are reported as log ϵ. Fluorescence spectra were recorded in a quartz 10 mm cuvette on a Horiba JobinYvon Fluoromax 2, using 5 nm excitation and emission slits. Quantum yields were measured in THF and established against **74** in THF as a standard ($\Phi_f = 0.76$), using the equation $\Phi_{f,\text{sample}} = \Phi_{f,\text{standard}} \times \frac{\text{Gradient}_{\text{sample}}}{\text{Gradient}_{\text{standard}}}$, where the gradient is that of a linear plot of absorption of the sample solution against integration under the fluoresence curve, with at least 5 data points.[70] The standard was cross-calibrated against Rhodamine 6G ($\Phi_f = 0.88$ in ethanol) before use.[71] A correction factor for solvent refractive index was included, $\frac{\text{n}_{\text{sample}}}{\text{n}_{\text{standard}}}$.

Electrochemical measurements were carried out using an Autolab Eco-Chemie PGSTAT12 instrument. A glassy carbon working electrode, $Ag/AgNO_3$ reference electrode (double-frit design, inner solution 0.1 M Bu_4NPF_6/0.002 M $AgNO_3$ in acetonitrile, outer solution as the flask) and a Pt counter electrode were used. The flask containing the electrolyte solution (0.1 M Bu_4NPF_6 in THF) was degassed with N_2 gas saturated with the solvent. Potentials are reported referenced to the ferrocene/ferrocenium internal standard. For the BODIPY-containing compounds, the following parameters were used: cyclic voltammetry: scan rate 0.090 V s^{-1}, step potential 100 mV; square wave voltammetry: step potential 50 mV, step amplitude 20 mV, square wave frequency 8 Hz. For the porphyrin dimers, in order to compare with literature data,[72] the following parameters were used: cyclic voltammetry: scan rate 0.25 V s^{-1}, step potential 10 mV; square wave voltammetry: step potential 2 mV, step amplitude 20 mV, square wave frequency 8 Hz.

2.13 Experimental for Chapter 2

Compound numbers correspond to those used in this chapter, except those labelled 2-A, -B etc. which are not featured in the main text. Novel compounds are denoted by an asterisk (*) after the name.

2-A (3,5-bis-octyloxy-phenyl)-methanol

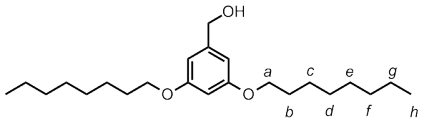

A solution of methyl 3,5-bis(octyloxy)benzoate (6.7 g, 17 mmol) in dry THF (29 mL) was added to a suspension of $LiAlH_4$ (0.71 g, 19 mmol) in THF (29 mL). The grey mixture was heated under reflux for 2 h. Hydrolysis by dropwise addition of H_2O (2.8 mL) was followed by 1.0 M NaOH solution (0.80 mL). The organic layer was washed (2 $\times$ H_2O) and the combined aqueous layers extracted (2 $\times$ Et_2O). The combined organic layers were dried over $MgSO_4$ and the solvent was evaporated to give a crude product containing (3,5-bis-octyloxyphenyl)-methanol as a colourless oil (6.0 g, 96%). ^{1}H NMR (400 MHz, $CDCl_3$) δ 6.50 (d, J=2.4 Hz, 2 H, **ortho**), 6.38 (t, J=2.3 Hz, 1 H, **para**), 4.61 (s, 2 H, **benzyl**), 3.93 (t, J=6.6 Hz, 4 H, **a**), 1.72 - 1.82 (m, 4 H, **b**), 1.40 - 1.49 (m, 4 H, **c**), 1.21 - 1.39 (m, 16 H, **d, e, f, g**), 0.89 (t, J=6.8 Hz, 6 H, **h**) ^{13}C NMR (101 MHz, $CDCl_3$) δ 160.5, 143.2, 105.0, 100.5, 68.0, 65.4, 31.8, 29.3, 29.2, 26.0, 22.7, 14.1.

2-B 3,5-bis(octyloxy)benzaldehyde

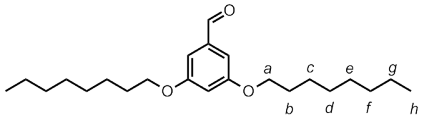

Activated MnO_2 (10.0 g, 115 mmol) was added to a solution of (3,5-bis-

octyloxyphenyl)-methanol (6.00 g, 16.5 mmol) in dry CH_2Cl_2 (55 mL). The reaction mixture was heated at reflux for 2.5 h when TLC ($CHCl_3$, $R_f = 0.9$) confirmed oxidation was complete. The cooled mixture was passed through a short silica gel column (CH_2Cl_2), to remove the oxidant, and the solvent removed to give the product as a colourless oil (5.5 g, 92%). ^{1}H NMR (400 MHz, $CDCl_3$) δ 9.89 (s, 1 H, **CHO**), 6.99 (d, J=2.4 Hz, 2 H, **ortho**), 6.70 (t, J=2.4 Hz, 1 H, **para**), 3.99 (t, J=6.6 Hz, 4 H, **a**), 1.73 - 1.84 (m, 4 H, **b**), 1.40 - 1.52 (m, 4 H, **c**), 1.21 - 1.40 (m, 16 H, **d, e, f, g**), 0.89 (t, J=6.9 Hz, 6 H, **h**) ^{13}C NMR (101 MHz, $CDCl_3$) δ 192.1, 160.7, 138.3, 108.0, 107.6, 68.4, 31.8, 29.3, 29.2, 29.1, 26.0, 22.6, 14.1.

2-C Trihexylsilylacetylene

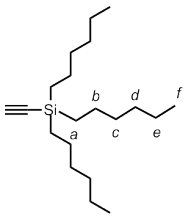

Chlorotrihexylsilane (15.2 g, 47.6 mmol) was added dropwise to ethynyl magnesium bromide (100 mL, 0.50 M in THF, 50 mmol). The mixture was refluxed with stirring for 1 h, after which HCl (aq., 10% v/v) was added dropwise. The solution was washed with water (50 mL), and extracted with $CHCl_3$ (2 $\times$ 50 mL). The combined organic layers were dried over $MgSO_4$ and concentrated to give the title compound as a yellow oil (16.0 g, quantitative). ^{1}H NMR (200 MHz, $CDCl_3$) δ 2.36 (s, 1 H, **acetylenic**), 1.17 - 1.47 (m, 24 H, **b, c, d, e**), 0.89 (t, J=6.3 Hz, 9 H, **f**), 0.62 (t, J=8.0 Hz, 6 H, **a**) ^{13}C NMR (101 MHz, $CDCl_3$) δ 94.0, 88.3, 33.1, 31.5, 23.7, 22.6, 14.1, 13.1.

2-D *N,N*-dibutyl-4-iodo-1-aniline

4-Iodoaniline (7.11 g, 32.4 mmol), *n*-butyliodide (15.0 mL, 132 mmol) and Na_2CO_3 (11.6 g, 110 mmol) were suspended in dry DMF (20 mL) in a pre-

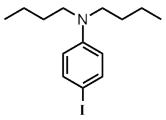

dried flask. The solution was pump-purge degassed 3 × and heated to 100 °C for 18 h. The reaction was diluted with toluene (200 mL) and washed with water (2 × 200 mL). The organic layer was dried over $MgSO_4$ and concentrated. Purification by column chromatography on silica gel, eluting 7 : 3 petrol : CH_2Cl_2 gave clean product (10 g, 78%) as a pale green oil. ^{1}H NMR (400 MHz, $CDCl_3$: 1 % d_5−pyridine) δ 7.42 (d, J=8.8 Hz, 2 H), 6.42 (d, J=8.8 Hz, 2 H), 3.23 (t, J=7.6 Hz, 4 H, **N-CH_2-**), 1.49 - 1.59 (m, 4 H), 1.34 (dq, J=14.9, 7.4 Hz, 4 H), 0.95 (t, J=7.5 Hz, 6 H, CH_3).

^{13}C NMR (101 MHz, $CDCl_3$: 1 % d_5−pyridine) δ 147.6, 137.6, 114.0, 75.3, 50.7, 29.2, 20.3, 14.0. MS Calcd for $C_{14}H_{23}IN$ (M+H): 332.1. Found (ESI QMS+): 332.1.

2-E Zinc 5,15-bis-(3,5-bis-octyloxy-phenyl)-porphyrin

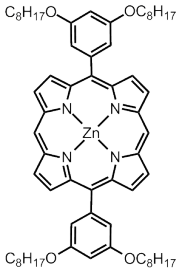

Dipyrromethane (0.80 g, 5.5 mmol) and **2-B** (2.0 g, 5.5 mmol) were dissolved in CH_2Cl_2 (1.0 L) in the dark. The reaction mixture was pump-purge degassed 3 × and TFA (0.87 mL, 11 mmol) was added. After stirring in the dark for 3 h (TLC of a worked-up aliquot shows a red spot, R_f = 0.85 in CH_2Cl_2 and green/black baseline), DDQ (2.38 g, 10.5 mmol) was added and the mixture stirred for 20 mins before NEt_3 (3.0 mL, 22 mmol) was added to quench the acid. The volume was reduced and the mixture passed through a short silica

gel column (CH_2Cl_2) to partially remove the tarry side products. The product was carried forward to the next step without further purification. (Intermediate yield, 1.0 g, max. 19%). $Zn(OAc)_2 \cdot 2\,H_2O$ (1.1 g, 5.0 mmol) was dissolved in MeOH (13 mL) and added to a solution of free base 5,15-bis-(3,5-bis-octyloxy-phenyl)-porphyrin (1.0 g, 1.0 mmol max) in $CHCl_3$ (100 mL). The reaction mixture was stirred at room temperature for 1 h. Chromatography on a short silica gel column (CH_2Cl_2) removed excess $Zn(OAc)_2$. The solution was concentrated to give an oily residue (0.80 g, 77%).

2-F Zinc 5,15-bis-(3,5-bis-octyloxy-phenyl)-10,20-dibromo-porphyrin

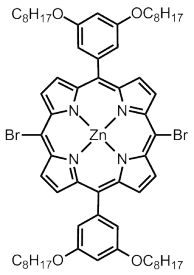

A solution of *N*-bromosuccinimide (0.28 g, 1.6 mmol) in $CHCl_3$ (18 mL) was added dropwise in the dark at room temperature using a pressure-equalising funnel to a solution of **2-E** (0.80 g, 0.77 mmol) in $CHCl_3$: 1% v/v pyridine (26 ml), then the reaction was quenched with acetone (1.0 mL). The solution was concentrated and passed through a silica plug, eluting with $CHCl_3$. The product was precipitated by layered addition of MeOH to a $CHCl_3$ solution to give a purple powder (0.71 g, 77%).

11 Zinc 5,15-bis-(3,5-bis-octyloxy-phenyl)-10,20-bis-trihexylsilyl-ethynyl-porphyrin

2-F (0.71 g, 0.59 mmol), $Pd_2(dba)_3$ (54 mg, 59 μmol), PPh_3 (46 mg, 0.18 mmol) and CuI (34 mg, 0.18 mmol) were dried under vacuum in a pre-dried Schlenk tube before dry toluene (23 mL) and Et_3N (23 mL) were added and the mixture freeze-pump-thaw degassed. Trihexylsilylacetylene **2-C** (550 mg, 1.8

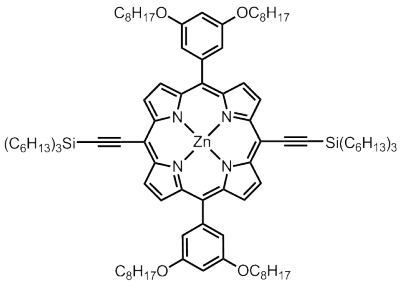

mmol) was added and the reaction stirred at 40 °C for 2 h when TLC (10 : 1 : 1 petrol ether : ethyl acetate : pyridine, $R_f = 0.90$) showed the reaction to be complete. The volume was reduced and the mixture passed through a short silica gel column (100 : 1 petrol ether : pyridine), to remove baseline impurities and excess ethynyltrihexylsilane, to give a dark green solid which was carried forward to the next step (intermediate yield assumed quantitative). ^{1}H NMR (400 MHz, $CDCl_3$: 1 % d_5−pyridine) δ 9.61 (d, J=4.5 Hz, 4 H, β-**H**), 8.94 (d, J=4.5 Hz, 4 H, β-**H**), 7.32 (d, J=2.3 Hz, 4 H, **Ar-*o*-H**), 6.87 (t, J=2.3 Hz, 2 H, **Ar-*p*-H**), 4.13 (t, J=6.7 Hz, 8 H, **O-CH_2-**), 1.83 - 1.91 (m, 9 H), 1.71 - 1.80 (m, 13 H), 1.46 - 1.57 (m, 23 H), 1.22 - 1.44 (m, 70 H), 0.95 - 1.03 (m, 13 H), 0.81 - 0.93 (m, 36 H). ^{13}C NMR (101 MHz, $CDCl_3$: 1 % d_5−pyridine) δ 158.2, 152.3, 149.9, 144.5, 132.4, 130.9, 114.5, 109.6, 100.8, 100.8, 100.5, 99.2, 68.3, 33.4, 33.0, 31.8, 31.7, 31.5, 29.4, 29.3, 26.1, 24.4, 22.7, 22.5, 14.2, 13.9. MS Calcd for $C_{104}H_{160}N_4O_4Si_2Zn$: 1652.14. Found (MALDI TOF+): 1652.14.

12 Zinc 5,15-bis-(3,5-bis-octyloxy-phenyl)-10-ethynyl-20-trihexylsilyl-ethynyl-porphyrin

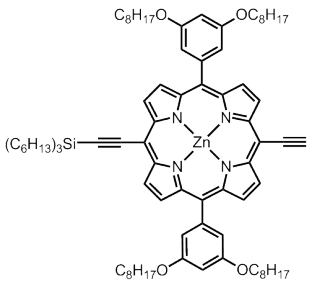

$Bu_4N^+F^-$ (1.0 M solution in THF, 0.41 mL, 0.41 mmol) was added to a so-

lution of **11** (0.98 g, 0.59 mmol) in 1 : 1 CH_2Cl_2 : $CHCl_3$ (40 mL) and the reaction mixture stirred at room temperature. The progress was monitored carefully by TLC until the starting material and mono-deprotected product (R_f = 0.90 and 0.70 respectively, 10 : 1 : 1 petrol ether : ethyl acetate : pyridine) were in roughly equal ratio (26 minutes), then AcOH (24 μL, 0.41 mmol) was added. The reaction mixture was passed immediately through a short silica gel plug (CH_2Cl_2). Chromatography on silica gel (10 : 1 : 1 petrol ether : ethyl acetate : pyridine) gave starting material (470 mg, 48%), the desired product (360 mg, 45%) and the doubly-deprotected byproduct. ^{1}H NMR (400 MHz, $CDCl_3$: 1 % d_5−pyridine) δ 9.69 (d, J=4.5 Hz, 2 H, β-**H**), 9.63 (d, J=4.5 Hz, 2 H, β-**H**), 9.00 (d, J=4.5 Hz, 2 H, β-**H**), 8.99 (d, J=4.5 Hz, 2 H, β-**H**), 7.34 (d, J=2.3 Hz, 4 H, **Ar-*o*-H**), 6.90 (t, J=2.3 Hz, 2 H, **Ar-*p*-H**), 4.11 (t, J=6.8 Hz, 8 H, **O-CH$_2$-**), 1.74 - 1.90 (m, 15 H), 1.17 - 1.60 (m, 81 H), 0.98 - 1.07 (m, 7 H), 0.77 - 0.95 (m, 29 H). ^{13}C NMR (101 MHz, $CDCl_3$: 1 % d_5−pyridine) δ 158.2, 152.3, 152.3, 150.0, 149.9, 144.5, 132.6, 132.5, 131.0, 130.7, 122.2, 114.5, 109.5, 101.0, 100.6, 99.4, 99.0, 86.8, 83.3, 68.3, 33.4, 33.4, 31.8, 31.7, 29.4, 29.2, 26.1, 24.4, 22.7, 22.6, 14.2, 14.1, 13.9. MS Calcd for $C_{86}H_{122}N_4O_4SiZn$: 1368.85. Found (MALDI TOF+): 1368.60.

13 Zinc 5,15-bis-(3,5-bis-octyloxy-phenyl)-10,20-trihexylsilyl-ethynyl-porphyrin dimer

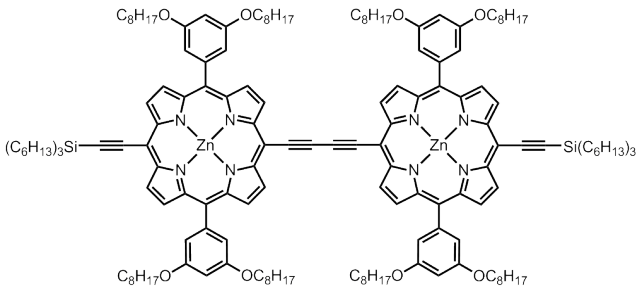

To a dried flask were added $Pd(PPh_3)_2Cl_2$ (13 mg, 19 μmol), CuI (25 mg, 0.13 mmol) and 1,4-benzoquinone (57 mg, 0.53 mmol). The reagents were dissolved in dry toluene (18 mL) and dry iPr$_2$NH (4.5 mL) and added *via* syringe to

a stirring solution of **12** (360 mg, 0.26 mmol) in dry toluene (18 mL) and dry iPr$_2$NH (4.5 mL). The solution was stirred at room temperature under N_2 and monitored by TLC (25 : 1 : 1 petrol ether : ethyl acetate : pyridine). Upon completion the solution was concentrated and passed through a short silica plug, eluting with CH_2Cl_2. The crude mixture was purified on silica, eluting with 25 : 1 : 1 to remove any unreacted starting material followed by 10 : 1 : 1 to elute the product, which was concentrated to give a green oily solid (260 mg, 70%) ^{1}H NMR (400 MHz, $CDCl_3$: 1 % d_5−pyridine) δ 9.85 (d, J=4.5 Hz, 4 H, β-**H**), 9.64 (d, J=4.5 Hz, 4 H, β-**H**), 9.05 (d, J=4.5 Hz, 4 H, β-**H**), 8.95 (d, J=4.5 Hz, 4 H, β-**H**), 7.35 (d, J=2.3 Hz, 8 H, **Ar-*o*-H**), 6.89 (t, J=2.1 Hz, 4 H, **Ar-*p*-H**), 4.13 (t, J=6.6 Hz, 16 H, **O-CH$_2$-**), 1.81 - 1.92 (m, 21 H), 1.69 - 1.81 (m, 19 H), 1.44 - 1.58 (m, 40 H), 1.13 - 1.44 (m, 18 H), 0.96 - 1.04 (m, 16 H), 0.79 - 0.93 (m, 103 H), 0.63 (dt, J=9.4, 6.7 Hz, 24 H) ^{13}C NMR (75 MHz, $CDCl_3$: 1 % d_5−pyridine) δ 157.2, 152.0, 151.3, 149.1, 148.7, 143.4, 131.9, 131.5, 130.0, 129.6, 121.8, 113.5, 108.4, 100.7, 99.7, 98.8, 98.3, 87.4, 81.2, 67.3, 32.3, 31.9, 30.8, 30.6, 30.4, 28.4, 28.2, 25.1, 21.7, 21.6, 21.5, 13.0, 12.9. MS Calcd for $C_{172}H_{242}N_8O_8Si_2Zn_2$: 2736.69. Found (MALDI TOF+): 2736.81.

14 Zinc 5,15-bis-(3,5-bis-octyloxy-phenyl)-10,20-bis-ethynyl-porphyrin dimer and 15 Zinc 5,15-bis-(3,5-bis-octyloxy-phenyl)-10-ethynyl-20-trihexylsilyl-ethynyl-porphyrin dimer

13 (260 mg, 93 μmol) was dried under vacuum in a flask then purged with N_2. $CHCl_3$ (8 mL) and CH_2Cl_2 (8 mL) were added, followed by $Bu_4N^+F^-$ (1.0 M solution in THF, 65 μL, 65 μmol). The solution was stirred at room temperature and monitored carefully by TLC. After 55 minutes, extra $Bu_4N^+F^-$ was added (35 μL). After 90 minutes, AcOH (7 μL, 0.1 mmol) was added and the reaction was immediately passed through a silica gel plug (eluting CH_2Cl_2). The crude mixture was concentrated and the starting material separated by column chromatography on silica gel, eluting with 10 : 1 : 1 petrol

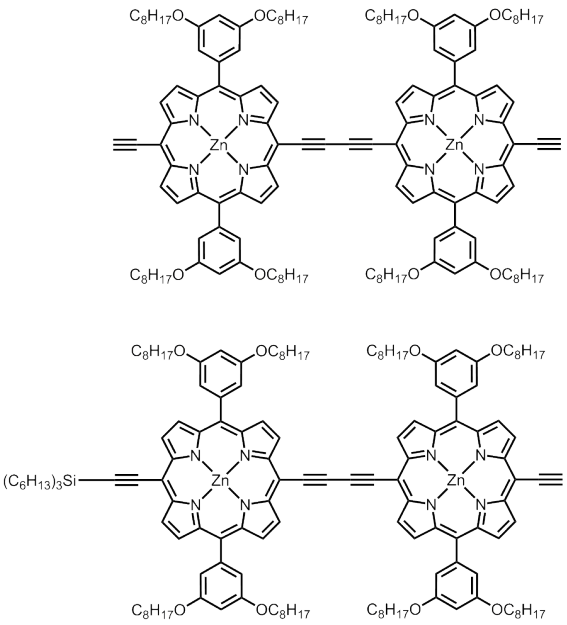

ether : ethyl acetate : pyridine. 59 mg (23%) of starting material was collected and recycled, and 105 mg of the crude product mixture. ^{1}H NMR (400 MHz, $CDCl_3$: 1 % d_5−pyridine) δ 9.76 - 9.89 (m, 4 H, β-**H**), 9.54 - 9.66 (m, 4 H, β-**H**), 8.99 - 9.08 (m, 4 H, β-**H**), 8.86 - 8.96 (m, 4 H, β-**H**), 7.31 (d, J=2.3 Hz, 6.62 H, **Ar-*o*-H**), 6.83 - 6.88 (m, J=2.0 Hz, 3.19 H, **Ar-*p*-H**), 4.09 (t, J=6.7 Hz, 16 H, **O-CH_2-**), 4.13 (s, 1.5 H, **acetylenic**), 1.78 - 1.88 (m, 15 H), 1.66 - 1.78 (m, 7 H), 1.41 - 1.55 (m, 22 H), 1.25 - 1.38 (m, 43 H), 1.15 - 1.24 (m, 33 H), 0.92 - 1.01 (m, 5 H), 0.83 - 0.89 (m, 9 H), 0.80 (t, J=6.9 Hz, 22 H) Bis MS Calcd for $C_{136}H_{166}N_8O_8Zn_2$: 2171.14. Found (MALDI TOF+): 2171.80. Mono MS Calcd for $C_{154}H_{204}N_8O_8SiZn_2$: 2453.42. Found (MALDI TOF+): 2453.81.

A-P2-A Zinc 5,15-bis-(3,5-bis-octyloxy-phenyl)-10,20-bis-(4-nitrophenyl)-ethynyl-porphyrin dimer

The crude mixture of **14** and **15** (105 mg, 43.0 μmol max. singly-deprotected porphyrin), 4-iodonitrobenzene (107 mg, 430 μmol), $Pd_2(dba)_3$ (2.0 mg, 2.2 μmol), PPh_3 (2.3 mg, 8.6 μmol) and CuI (0.4 mg, 2 μmol) were dried under vacuum in a pre-dried Schlenk tube before toluene (3.5 mL) and iPr$_2$NH (3.5

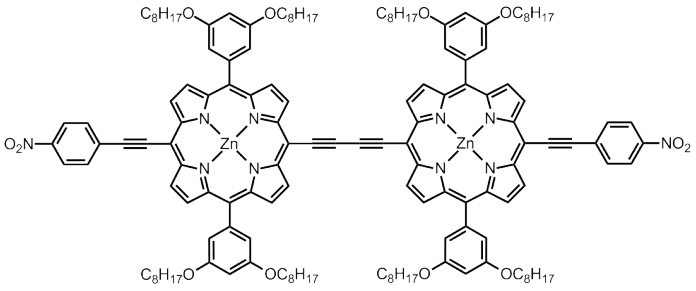

mL) were added. The mixture was freeze-pump-thaw degassed 3 × and heated to 50 °C. After 2 h, the mixture was concentrated and purified on silica gel, eluting with 10 : 1 : 1 petrol ether : ethyl acetate : pyridine. The two collected fractions were concentrated and passed through a size-exclusion column (eluting with toluene) to remove unreacted 4-iodonitrobenzene. **A-P2-A** was recovered (13 mg, 6.0% over two steps), along with **16** (42 mg, 18% over two steps). ^{1}H NMR (300 MHz, $CDCl_3$: 1 % d_5−pyridine) δ 9.80 (d, J=4.7 Hz, 4 H, β-**H**), 9.59 (d, J=4.7 Hz, 4 H, β-**H**), 9.00 (d, J=4.7 Hz, 4 H, β-**H**), 8.96 (d, J=4.7 Hz, 4 H, β-**H**), 8.33 (d, J=8.9 Hz, 4 H, **NO_2-Ar-H**), 8.04 (d, J=8.9 Hz, 4 H, **NO_2-Ar-H**), 7.30 (d, J=2.2 Hz, 8 H, **Ar-*o*-H**), 6.85 (t, J=2.3 Hz, 4 H, **Ar-*p*-H**), 4.09 (t, J=6.6 Hz, 16 H, **O-CH_2-**), 1.75 - 1.88 (m, 17 H), 1.38 - 1.52 (m, 18 H), 1.11 - 1.36 (m, 78 H), 0.74 - 0.82 (m, 27 H). MS Calcd for $C_{148}H_{172}N_{10}O_{12}Zn_2$: 2414.18. Found (MALDI TOF+): 2413.81. λ_{max}/nm (log ϵ) in $CHCl_3$: 1 % pyridine: 468 (5.53) 494 (5.21) 591 (4.30) 647 (4.44) 694 (5.01) 748 (5.02).

16 Zinc 5,15-bis-(3,5-bis-octyloxy-phenyl)-10-(4-nitrophenyl)-ethynyl-20-trihexylsilyl-ethynyl-porphyrin dimer

^{1}H NMR (400 MHz, $CDCl_3$: 1 % d_5−pyridine) δ 9.81 - 9.87 (m, 4 H, β-**H**), 9.62 (m, 4 H, β-**H**), 9.03 (d, J=4.5 Hz, 4 H, β-**H**), 9.00 (d, J=4.5 Hz, 2 H, β-**H**), 8.93 (d, J=4.5 Hz, 2 H, β-**H**), 8.34 (d, J=8.6 Hz, 2 H, **NO_2-Ar-H**), 8.05 (d, J=8.8 Hz, 2 H, **NO_2-Ar-H**), 7.34 (m, 8 H, **Ar-*o*-H**), 6.88 (m, 4 H, **Ar-*p*-H**), 4.07 - 4.16 (m, 16 H, **O-CH_2-**), 1.79 - 1.93 (m, 18 H), 1.68 - 1.79 (m, 8 H),

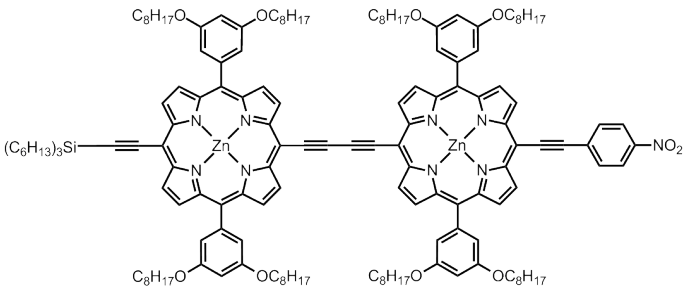

1.42 - 1.57 (m, 27 H), 1.27 - 1.41 (m, 53 H), 1.24 (m, 41 H), 0.93 - 1.03 (m, 8 H), 0.84 - 0.90 (m, 12 H), 0.82 (m, 26 H) MS Calcd for $C_{160}H_{207}N_9O_{10}SiZn_2$: 2575.44. Found (MALDI TOF+): 2575.63.

A-P2-D Zinc 5,15-bis-(3,5-bis-octyloxy-phenyl)-10-(4-nitrophenyl)-ethynyl-20-(*N,N*-di-*n*-butyl-4-aniline)-ethynyl-porphyrin dimer

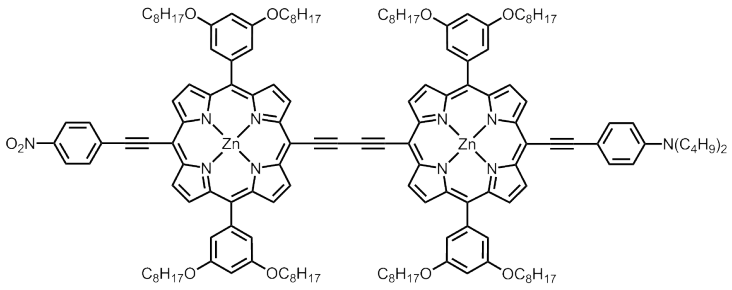

16 (20 mg, 7.8 μmol), **2-D** (13 mg, 39 μmol), $Pd_2(dba)_3$ (0.4 mg, 0.4 μmol), PPh_3 (0.4 mg, 2 μmol) and CuI (0.1 mg, 0.4 μmol) were dried under vacuum in a pre-dried Schlenk tube before toluene (0.7 mL) and iPr$_2$NH (0.7 mL) were added. The mixture was freeze-pump-thaw degassed 3 $\times$, $Bu_4N^+F^-$ (1.0 M in THF, 78 μL, 78 μmol) added, and the mixture heated to 50 °C. After 2 h, the mixture was concentrated and purified on silica gel, eluting with 3 : 1 petrol ether : CH_2Cl_2 with 1% v/v pyridine. The desired fractions were concentrated and passed through a size-exclusion column (eluting with toluene) to remove unreacted **2-D**. **A-P2-D** was recovered as a green solid (12 mg , 62%). ^{1}H NMR (300 MHz, $CDCl_3$: 1 % d_5−pyridine) δ 9.80 (d, J=4.7 Hz, 2 H, β-**H**), 9.74 (d, J=4.7 Hz, 2 H, β-**H**), 9.62 (d, J=4.5 Hz, 2 H, β-**H**), 9.59 (d, J=4.7 Hz, 2 H, β-**H**), 8.99 (d, J=4.5 Hz, 2 H, β-**H**), 8.96 (dd, J=4.5, 1.8 Hz, 4 H, β-**H**),

8.86 (d, J=4.7 Hz, 2 H, β-**H**), 8.34 (d, J=8.9 Hz, 2 H, **NO_2-Ar-H**), 8.05 (d, J=9.1 Hz, 2 H, **NO_2-Ar-H**), 7.78 (d, J=8.9 Hz, 2 H, **aniline-H**), 7.29 (dd, J=2.3 Hz, 8 H, **Ar-*o*-H**), 6.84 (dt, J=5.6, 2.3 Hz, 4 H, **Ar-*p*-H**), 6.72 (d, J=9.2 Hz, 2 H, **aniline-H**), 4.03 - 4.12 (m, 16 H, **O-CH_2-**), 3.31 (t, J=7.9 Hz, 4 H), 1.73 - 1.87 (m, 15 H), 1.52 - 1.65 (m, 4 H), 1.37 - 1.51 (m, 16 H), 1.10 - 1.37 (m, 69 H), 0.94 (t, J=7.3 Hz, 6 H), 0.73 - 0.84 (m, 23 H). MS Calcd for $C_{156}H_{190}N_{10}O_{10}Zn_2$: 2496.33. Found (MALDI TOF+): 2496.58. λ_{max}/nm (log ϵ) in $CHCl_3$: 1 % pyridine: 469 (5.47) 495 (5.28) 594 (4.25) 647 (4.38) 702 (4.97) 756 (4.99).

A-P2-R Zinc 5,15-bis-(3,5-bis-octyloxy-phenyl)-10-(4-nitrophenyl)-ethynyl-20-(4-*n*-butyl-phenyl)-ethynyl-porphyrin dimer

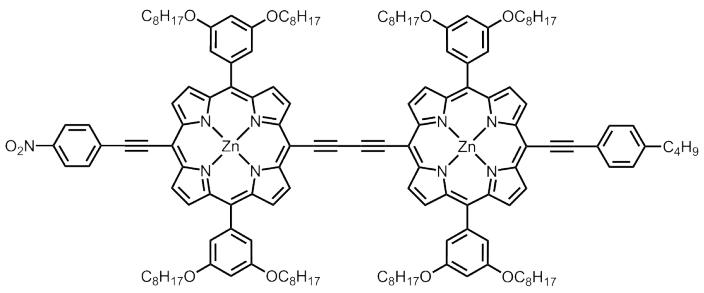

16 (40 mg, 16 μmol), $Pd_2(dba)_3$ (0.7 mg, 0.8 μmol), PPh_3 (0.8 mg, 3 μmol) and CuI (0.2 mg, 0.8 μmol) were dried under vacuum in a pre-dried Schlenk tube before toluene (1.3 mL) and iPr$_2$NH (1.3 mL) were added. The mixture was freeze-pump-thaw degassed 3 ×, $Bu_4N^+F^-$ (1.0 M in THF, 80 μL, 80 μmol) and 4-iodo-n-butylbenzene (14 μL, 80 μmol) added, and the mixture heated to 50 °C. After 2 h 30, the mixture was concentrated and passed through a plug of silica gel, eluting with CH_2Cl_2 : 1% v/v pyridine. The crude mixture was concentrated and passed through a size-exclusion column (eluting with toluene) to remove unreacted 4-iodo-n-butylbenzene. **A-P2-R** was recovered as a green solid (28 mg , 72%). ^{1}H NMR (300 MHz, $CDCl_3$: 1 % d_5−pyridine) δ 9.80 (d, J=4.7 Hz, 2 H, β-**H**), 9.78 (d, J=4.5 Hz, 2 H, β-**H**), 9.63 (d, J=4.5

Hz, 2 H, β-**H**), 9.58 (d, J=4.7 Hz, 2 H, β-**H**), 8.98 (dd, J=4.6, 1.5 Hz, 4 H, β-**H**), 8.95 (d, J=4.7 Hz, 2 H, β-**H**), 8.90 (d, J=4.7 Hz, 2 H, β-**H**), 8.35 (d, J=8.9 Hz, 2 H, **NO$_2$-Ar-H**), 8.05 (d, J=8.9 Hz, 2 H, **NO$_2$-Ar-H**), 7.87 (d, J=8.2 Hz, 2 H, ***n*Bu-Ar-H**), 7.28 - 7.33 (m, J=2.2 Hz, 10 H, **Ar-*o*-H**, ***n*Bu-Ar-H**), 6.84 (dd, J=2.6, 0.9 Hz, 4 H, **Ar-*p*-H**), 4.10 (t, J=6.7 Hz, 16 H, **O-CH$_2$-**), 2.68 (t, J=7.7 Hz, 2 H), 1.75 - 1.88 (m, 20 H), 1.58 - 1.70 (m, 2 H), 1.37 - 1.53 (m, 15 H), 1.17 - 1.37 (m, 72 H), 0.93 (t, J=7.3 Hz, 3 H), 0.74 - 0.84 (m, 26 H). MS Calcd for $C_{152}H_{181}N_9O_{10}Zn_2$: 2425.26. Found (MALDI TOF+): 2425.42. λ_{max}/nm (log ϵ) in $CHCl_3$: 1 % pyridine: 466 (5.54) 498 (5.19) 590 (4.27) 648 (4.38) 690 (4.95) 748 (4.98).

2-G Zinc 5,15-bis-(3,5-bis-octyloxy-phenyl)-10-(*N,N*-di-*n*-butyl-4-aniline)-ethynyl-20-trihexylsilyl-ethynyl-porphyrin dimer

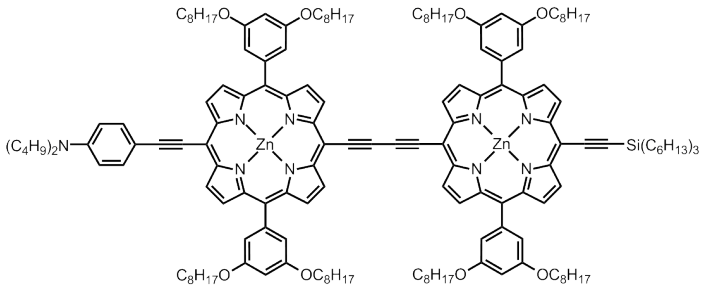

A crude mixture of **14** and **15** (72 mg, 29 μmol max. singly-deprotected porphyrin), $Pd_2(dba)_3$ (1.4 mg, 1.5 μmol), PPh_3 (1.6 mg, 6.0 μmol) and CuI (0.3 mg, 2 μmol) were dried under vacuum in a pre-dried Schlenk tube before toluene (2.4 mL) and iPr$_2$NH (2.4 mL) were added. The mixture was freeze-pump-thaw degassed 3 ×, **2-D** (96 mg, 0.29 mmol) added and heated to 50 °C. After 2 h, the mixture was concentrated and purified on silica gel, eluting with 15 : 1 : 1 petrol ether : ethyl acetate : pyridine. The desired fractions were concentrated and passed through a size-exclusion column (eluting with toluene) to remove unreacted aniline. **2-G** was recovered (20 mg, 26%), but a clean sample of the bis product was not obtainable.

^{1}H NMR (400 MHz, $CDCl_3$: 1 % d_5−pyridine) δ 9.82 (d, J=4.5 Hz, 2 H, β-**H**), 9.78 (d, J=4.5 Hz, 2 H, β-**H**), 9.65 (d, J=4.5 Hz, 2 H, β-**H**), 9.60 (d, J=4.5 Hz, 2 H, β-**H**), 9.01 (d, J=4.5 Hz, 2 H, β-**H**), 8.99 (d, J=4.5 Hz, 2 H, β-**H**), 8.92 (d, J=4.5 Hz, 2 H, β-**H**), 8.89 (d, J=4.5 Hz, 2 H, β-**H**), 7.82 (d, J=8.8 Hz, 2 H, **aniline-H**), 7.32 (d, J=1.5 Hz, 8 H, **Ar-*o*-H**), 6.85 - 6.87 (m, 4 H, **Ar-*p*-H**), 6.75 (d, J=9.1 Hz, 2 H, **aniline-H**), 4.10 (t, J=6.6 Hz, 16 H, **O-CH$_2$-**), 3.34 (t, J=7.6 Hz, 4 H), 1.79 - 1.88 (m, 16 H), 1.69 - 1.78 (m, 7 H), 1.56 - 1.67 (m, 5 H), 1.41 - 1.55 (m, 26 H), 1.18 - 1.40 (m, 90 H), 0.93 - 1.02 (m, 13 H), 0.83 - 0.89 (m, 14 H), 0.78 - 0.83 (m, 26 H). MS Calcd for $C_{168}H_{225}N_9O_8SiZn_2$: 2658.59. Found (MALDI TOF+): 2657.97.

D-P2-D Zinc 5,15-bis-(3,5-bis-octyloxy-phenyl)-10,20-bis-(*N,N*-di-*n*-butyl-4-aniline)-ethynyl-porphyrin dimer

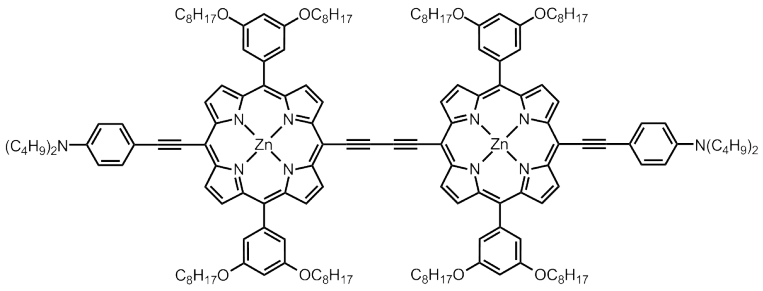

13 (15 mg, 5.5 μmol), $Pd_2(dba)_3$ (0.25 mg, 0.28 μmol), PPh_3 (0.29 mg, 1.1 μmol) and CuI (0.05 mg, 0.3 μmol) were dried under vacuum in a pre-dried Schlenk tube before toluene (0.5 mL) and iPr$_2$NH (0.5 mL) were added. The mixture was freeze-pump-thaw degassed 3 ×, $Bu_4N^+F^-$ (1.0 M in THF, 55 μL, 55 μmol) and **2-D** (36 mg, 0.11 mmol) added, and the mixture heated to 50 °C. After 2 h 30, the mixture was concentrated and passed through a plug of silica gel, eluting with CH_2Cl_2 : 1% v/v pyridine. The crude mixture was concentrated and passed through a size-exclusion column (eluting with toluene) to remove unreacted **2-D**. **D-P2-D** was recovered as a green solid (9.5 mg , 67%). ^{1}H NMR (400 MHz, $CDCl_3$: 1 % d_5−pyridine) δ 9.78 (d, J=4.5

Hz, 4 H, β-**H**), 9.65 (d, J=4.5 Hz, 4 H, β-**H**), 8.98 (d, J=4.5 Hz, 4 H, β-**H**), 8.89 (d, J=4.5 Hz, 4 H, β-**H**), 7.82 (d, J=8.8 Hz, 4 H, **aniline-H**), 7.32 (d, J=2.3 Hz, 8 H, **Ar-*o*-H**), 6.86 (t, J=2.3 Hz, 4 H, **Ar-*p*-H**), 6.75 (d, J=9.1 Hz, 4 H, **aniline-H**), 4.10 (t, J=6.6 Hz, 16 H, **O-CH_2-**), 3.34 (t, J=6.8 Hz, 3 H), 1.77 - 1.88 (m, 15 H), 1.57 - 1.67 (m, 8 H), 1.41 - 1.52 (m, 18 H), 1.15 - 1.41 (m, 88 H), 0.96 (t, J=7.3 Hz, 12 H), 0.81 (t, J=6.8 Hz, 26 H). MS Calcd for $C_{164}H_{208}N_{10}O_8Zn_2$: 2578.49. Found (MALDI TOF+): 2577.52. λ_{max}/nm ($\log \epsilon$) in $CHCl_3$: 1 % pyridine: 468 (5.39) 496 (5.24) 592 (4.24) 658 (4.47) 704 (4.92) 752 (4.92).

D-P2-R Zinc 5,15-bis-(3,5-bis-octyloxy-phenyl)-10-(*N,N*-di-*n*-butyl-4-aniline)-ethynyl-20-(4-*n*-butyl-phenyl)-ethynyl-porphyrin dimer

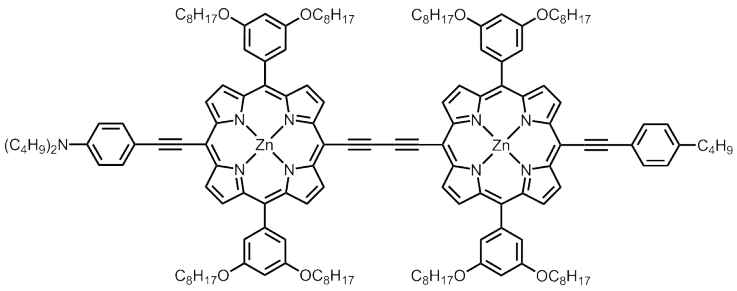

2-G (20 mg, 7.5 μmol), $Pd_2(dba)_3$ (0.4 mg, 0.4 μmol), PPh_3 (0.4 mg, 2 μmol) and CuI (0.1 mg, 0.4 μmol) were dried under vacuum in a pre-dried Schlenk tube before toluene (0.7 mL) and iPr$_2$NH (0.7 mL) were added. The mixture was freeze-pump-thaw degassed 3 ×, $Bu_4N^+F^-$ (1.0 M in THF, 37 μL, 37 μmol) and 4-iodo-n-butylbenzene (7 μL, 40 μmol) added, and heated to 50 °C. After 2 h, the mixture was concentrated and passed through a plug of silica gel, eluting with CH_2Cl_2 : 1% v/v pyridine. The crude mixture was concentrated and passed through a size-exclusion column (eluting with toluene) to remove unreacted 4-iodo-n-butylbenzene. **D-P2-R** was recovered as a green solid (11 mg , 58%). 1H NMR (300 MHz, $CDCl_3$: 1 % d_5−pyridine) δ 9.78 (d, J=4.5 Hz, 2 H, β-**H**), 9.75 (d, J=4.5 Hz, 2 H, β-**H**), 9.63 (t, J=4.5 Hz, 4 H, β-**H**),

8.97 (dd, J=7.2, 4.5 Hz, 4 H, β-**H**), 8.90 (d, J=4.7 Hz, 2 H, β-**H**), 8.86 (d, J=4.5 Hz, 2 H, β-**H**), 7.86 (d, J=8.2 Hz, 2 H, ***n*Bu-Ar-H**), 7.78 (d, J=8.9 Hz, 2 H, **aniline-H**), 7.29 (m, 10 H, **Ar-*o*-H**, ***n*Bu-Ar-H**), 6.80 - 6.85 (m, 4 H, **Ar-*p*-H**), 6.72 (d, J=8.9 Hz, 2 H, **aniline-H**), 4.07 (t, J=6.7 Hz, 16 H, **O-CH$_2$-**), 3.31 (t, J=7.8 Hz, 4 H), 2.66 (t, J=7.8 Hz, 2 H), 1.74 - 1.86 (m, 23 H), 1.52 - 1.68 (m, 8 H), 1.38 - 1.50 (m, 23 H), 1.10 - 1.37 (m, 94 H), 0.87 - 0.97 (m, 11 H), 0.78 (t, J=7.2 Hz, 32 H). MS Calcd for $C_{160}H_{199}N_9O_8Zn_2$: 2507.41. Found (MALDI TOF+): 2507.57. λ_{max}/nm (log ϵ) in $CHCl_3$: 1 % pyridine: 464 (5.50) 497 (5.25) 592 (4.26) 647 (4.38) 697 (4.93) 745 (4.96).

R-P2-R Zinc 5,15-bis-(3,5-bis-octyloxy-phenyl)-10,20-bis-(4-*n*-butyl-phenyl)-ethynyl-porphyrin dimer

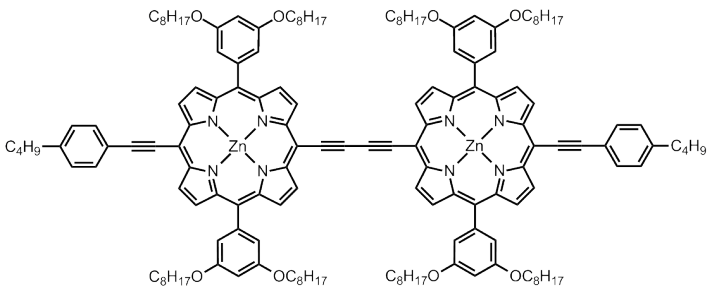

13 (15 mg, 5.5 μmol), $Pd_2(dba)_3$ (0.3 mg, 0.3 μmol), PPh_3 (0.3 mg, 1 μmol) and CuI (0.05 mg, 0.3 μmol) were dried under vacuum in a pre-dried Schlenk tube before toluene (0.5 mL) and iPr$_2$NH (0.5 mL) were added. The mixture was freeze-pump-thaw degassed 3 ×, $Bu_4N^+F^-$ (1.0 M in THF, 55 μL, 55 μmol) and 4-iodo-n-butylbenzene (10 μL, 55 μmol) added, and the mixture heated to 50 °C. After 2 h, the mixture was concentrated and passed through a plug of silica gel, eluting with CH_2Cl_2 : 1% v/v pyridine. The crude mixture was concentrated and passed through a size-exclusion column (eluting with toluene) to remove unreacted 4-iodo-n-butylbenzene. **R-P2-R** was recovered as a green solid (10 mg , 75%). ^{1}H NMR (300 MHz, $CDCl_3$: 1 % d_5−pyridine) δ 9.79 (d, J=4.7 Hz, 4 H, β-**H**), 9.64 (d, J=4.5 Hz, 4 H, β-**H**), 8.98 (d, J=4.5 Hz,

4 H, β-**H**), 8.90 (d, J=4.5 Hz, 4 H, β-**H**), 7.86 (d, J=8.2 Hz, 4 H, ***n*Bu-Ar-H**), 7.30 (d, J=2.2 Hz, 8 H, **Ar-*o*-H**), 7.30 (d, J=7.7 Hz, 4 H, ***n*Bu-Ar-H**), 6.83 (t, J=2.3 Hz, 4 H, **Ar-*p*-H**), 4.08 (t, J=6.6 Hz, 16 H, **O-CH_2-**), 2.66 (t, J=7.7 Hz, 1 H), 1.74 - 1.86 (m, 18 H), 1.57 - 1.69 (m, 5 H), 1.36 - 1.52 (m, 22 H), 1.10 - 1.35 (m, 81 H), 0.91 (t, J=7.3 Hz, 6 H), 0.71 - 0.84 (m, 30 H). MS Calcd for $C_{156}H_{190}N_8O_8Zn_2$: 2436.34. Found (MALDI TOF+): 2436.34. λ_{max}/nm (log ϵ) in $CHCl_3$: 1 % pyridine: 465 (5.66) 499 (5.21) 590 (4.31) 646 (4.37) 681 (4.96) 744 (4.99).

A-P2(2H)-A 5,15-bis-(3,5-bis-octyloxy-phenyl)-10,20-bis-(4-nitro-phenyl)-ethynyl-porphyrin dimer*

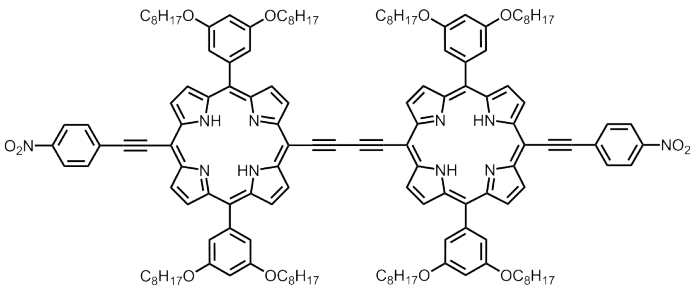

Porphyrin dimer **A-P2-A** (5 mg, 2.1 μmol) was dissolved in $CHCl_3$ (1.6 mL), and TFA (32 μL, 420 μmol) was added dropwise with stirring. The reaction was judged complete by UV-Vis after 10 min and quenched after 17 min by addition of pyridine (135 μL). The solution was immediately poured onto a short plug of silica, the product eluted with $CHCl_3$, and the solvent concentrated. The compound was precipitated from CH_2Cl_2/MeOH, giving 4.5 mg of a dark green powder (94%). ^{1}H NMR (400 MHz, $CDCl_3$: 1 % d−TFA) δ 9.52 (d, J=4.9 Hz, 4 H, β-**H**), 9.33 (d, J=4.7 Hz, 4 H, β-**H**), 8.86 (d, J=4.9 Hz, 4 H, β-**H**), 8.76 (d, J=4.6 Hz, 4 H, β-**H**), 8.47 (d, J=8.7 Hz, 4 H, **NO_2-Ar-H**), 8.19 (d, J=8.5 Hz, 4 H, **NO_2-Ar-H**), 7.57 (s, 8 H, **Ar-*o*-H**), 7.03 (s, 4 H, **Ar-*p*-H**), 4.20 (t, J=6.6 Hz, 16 H, **O-CH_2-**), 1.82 - 1.95 (m, 16 H), 1.46 - 1.58 (m, 16 H), 1.15 - 1.43 (m, 94 H), 0.81 (t, J=6.7 Hz, 32 H), free-base NH not seen due

to exchange. MS Calcd for $C_{148}H_{176}N_{10}O_{12}$: 2286.35. Found (MALDI TOF+): 2286.58. λ_{max}/nm (log ϵ) in $CHCl_3$: 458 (5.43) 484 (5.04) 622 (4.80) 708 (4.75) 738 (4.87).

22 5,15-bis-(3,5-bis-octyloxy-phenyl)-10,20-trihexylsilyl-ethynyl-porphyrin dimer*

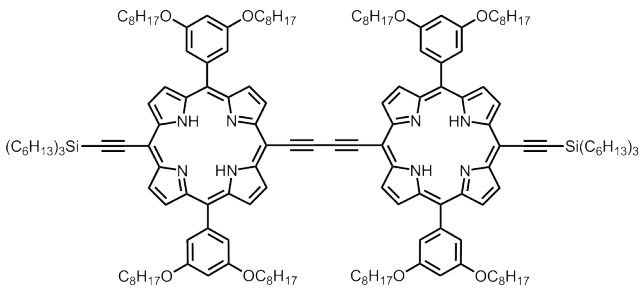

Porphyrin dimer **13** (60 mg, 22 μmol) was dissolved in $CHCl_3$ (16 mL), and TFA (0.34 mL, 4.4 mmol) was added dropwise with stirring. The reaction was quenched after 3 min by addition of pyridine (1.5 mL). The solution was immediately poured onto a short plug of silica, the product eluted with $CHCl_3$, and the solvent concentrated to yield the product (55 mg, 95%). ^{1}H NMR (400 MHz, $CDCl_3$) δ 9.78 (d, J=4.7 Hz, 4 H, β-**H**), 9.53 (d, J=4.7 Hz, 4 H, β-**H**), 8.98 (d, J=4.7 Hz, 4 H, β-**H**), 8.87 (d, J=4.7 Hz, 4 H, β-**H**), 7.31 (d, J=2.3 Hz, 8 H, **Ar-*o*-H**), 6.85 (t, J=2.3 Hz, 4 H, **Ar-*p*-H**), 4.09 (t, J=6.6 Hz, 16 H, **O-CH$_2$-**), 1.82 (quin, J=7.2 Hz, 16 H), 1.64 - 1.74 (m, 12 H), 1.40 - 1.54 (m, 34 H), 1.13 - 1.39 (m, 100 H), 0.92 - 1.01 (m, 12 H), 0.84 (t, J=7.1 Hz, 18 H), 0.79 (t, J=7.0 Hz, 32 H), -2.00 (s, 4 H, **free-base NH**). ^{1}13C NMR (126 MHz, $CDCl_3$) δ 157.5, 141.9, 131.0 (broad), 129.5 (broad), 121.2, 113.3, 106.7, 100.9, 100.8, 100.3, 98.1, 86.4, 81.8, 67.4, 32.3, 30.8, 30.6, 28.4, 28.2, 25.1, 23.3, 21.7, 21.6, 13.2, 13.1, 12.7 (peaks broadened due to exchange). MS Calcd for $C_{172}H_{246}N_8O_8Si_2$: 2609.87. Found (MALDI TOF+): 2609.44.

D-P2(2H)-D 5,15-bis-(3,5-bis-octyloxy-phenyl)-10,20-bis-(*N,N*-di-*n*-butyl-4-aniline)ethynyl-porphyrin dimer*

Porphyrin dimer **22** (10 mg, 3.8 μmol) was dissolved in THF (1 mL), and

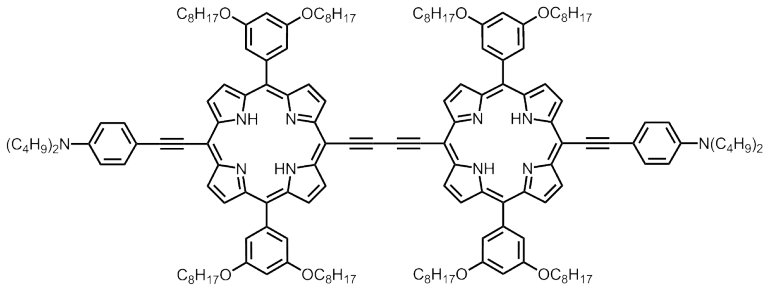

$Bu_4N^+F^-$ (1.0 M in THF, 38 μL, μmol) was added. The reaction was stirred and monitored by TLC (25 : 1 petrol ether : ethyl acetate, R_f change from 0.6 to 0.5). Upon completion (25 minutes), AcOH was added (20 μL) and the mixture passed through a short plug of silica, eluting with $CHCl_3$. The solution was concentrated in a two-neck flask and MALDI TOF MS confirmed the identity of the intermediate as the doubly-deprotected bis free alkyne. The intermediate was dried under vacuum, and the aniline **2-D** (13 mg, 38 μmol), $Pd_2(dba)_3$ (0.5 mg, 0.6 μmol) and $AsPh_3$ (0.7 mg, 2 μmol) were added under N_2. THF (0.5 mL) and iPr$_2$NH (0.5 mL) were added, the mixture freeze-pump-thaw degassed 3 $\times$ and heated to 50 °C. After 2 h, the reaction was passed through a plug of silica, eluting with $CHCl_3$. The crude residue was purified by column chromatography on silica, eluting the excess aniline with petrol and the product with 25 : 1 petrol ether : ethyl acetate. After precipitating the product from CH_2Cl_2/MeOH, 4.7 mg (51%) of clean product was obtained. ^{1}H NMR (400 MHz, $CDCl_3$) δ 9.72 (d, J=4.7 Hz, 4 H, β-**H**), 9.58 (d, J=4.7 Hz, 4 H, β-**H**), 8.94 (d, J=4.7 Hz, 4 H, β-**H**), 8.83 (d, J=4.4 Hz, 4 H, β-**H**), 7.80 (d, J=8.9 Hz, 4 H, **aniline-H**), 7.31 (d, J=2.0 Hz, 8 H, **Ar-*o*-H**), 6.85 (t, J=2.3 Hz, 4 H, **Ar-*p*-H**), 6.74 (d, J=9.2 Hz, 4 H, **aniline-H**), 4.09 (t, J=6.6 Hz, 16 H, **O-CH$_2$-**), 3.34 (t, J=7.9 Hz, 8 H, **N-CH$_2$-**), 1.78 - 1.87 (m, 16 H), 1.57 - 1.66 (m, 8 H), 1.09 - 1.47 (m, 96 H), 0.96 (t, J=7.3 Hz, 12 H), 0.79 (t, J=6.9 Hz, 24 H), -1.69 (s, 4 H, **free-base NH**). MS Calcd for $C_{164}H_{212}N_{10}O_8$: 2450.65. Found (MALDI TOF+): 2450.19. λ_{max}/nm (log ϵ) in $CHCl_3$: 460

(5.35) 646 (4.91) 747 (5.02).

R-P2(2H)-R 5,15-bis-(3,5-bis-octyloxy-phenyl)-10,20-bis-(4-*n*-butyl-phenyl)-ethynyl-porphyrin dimer*

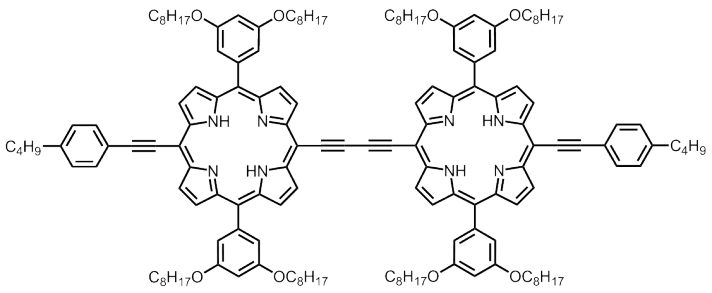

Porphyrin dimer **22** (20 mg, 7.7 μmol) was dissolved in THF (2 mL), and $Bu_4N^+F^-$ (1.0 M in THF, 77 μL, 77 μmol) was added. The reaction was stirred and monitored by TLC. Upon completion (25 minutes), AcOH was added (40 μL) and the mixture passed through a short plug of silica, eluting with $CHCl_3$. The solution was concentrated in a two-neck flask and the intermediate was then dried under vacuum, and 4-iodo-*n*-butylbenzene (14 μL, 77 μmol), $Pd_2(dba)_3$ (1.0 mg, 1.1 μmol) and $AsPh_3$ (1.4 mg, 4.6 μmol) were added under N_2. THF (1.0 mL) and iPr$_2$NH (1.0 mL) were added, the mixture freeze-pump-thaw degassed 3 × and heated to 50 °C. After 90 min, the reaction was passed through a plug of silica, eluting with $CHCl_3$. The crude residue was purified by size exclusion chromatography, eluting with $CHCl_3$: 1% pyridine. After precipitating the product from CH_2Cl_2/MeOH, 9.2 mg (52%) of a green powder was obtained. ^{1}H NMR (200 MHz, $CDCl_3$) δ 9.84 (d, J=4.6 Hz, 4 H, β-**H**), 9.69 (d, J=4.7 Hz, 4 H, β-**H**), 9.06 (d, J=4.8 Hz, 4 H, β-**H**), 8.97 (d, J=4.8 Hz, 4 H, β-**H**), 7.96 (d, J=8.1 Hz, 4 H, ***n*Bu-Ar-H**), 7.37 - 7.46 (m, 12 H, ***n*Bu-Ar-H, Ar-*o*-H**), 6.94 (t, J=2.3 Hz, 4 H, **Ar-*p*-H**), 4.18 (t, J=6.6 Hz, 16 H, **O-CH$_2$-**), 2.78 (t, J=7.7 Hz, 4 H, **Ph-CH$_2$-**), 1.82 - 2.00 (m, 16 H), 1.63 - 1.82 (m, 8 H), 1.19 - 1.62 (m, 100 H), 1.02 (t, J=7.2 Hz, 6 H), 0.88 (t, J=6.3 Hz, 24 H), -1.80 (br. s, 4 H, **free-base NH**). MS Calcd for

$C_{156}H_{194}N_8O_8$: 2308.51. Found (MALDI TOF+): 2308.14. λ_{max}/nm (log ϵ) in $CHCl_3$: 456 (5.46) 481 (4.97) 623 (4.73) 706 (4.67) 736 (4.80).

2.13.1 Viscous solution preparation

For the viscous solutions, a stock solution of **R-P2-R** at 5 μM in CHCl3 : 1% pyridine was first prepared. Then two BRAND UV micro plastic cuvettes (from Sigma-Aldrich, Z637106, batch K 175-2, mass 2.90 g) were dissolved in 2.3 mL of the stock solution and sealed in a screw-top vial. After 24 h the solution was then stirred with a spatula and centrifuged (4 k rpm, 10 mins) to give a homogeneous viscous gel. The final concentration of dye was approximately 2.5 μM due to the volume increase caused by dissolving the plastic cuvette. The gel was transferred to a fluorescence cuvette using a spatula, the lid sealed with parafilm, and centrifuged (1.5k rpm, 45 mins). For centrifugation an MSE Mistral 1000 was used.

2.14 Bibliography

1 Lindsey, J. S. *Acc. Chem. Res.* **2009**, *43*, 300–311.
2 McCarthy, J.; Weissleder, R. *ChemMedChem* **2007**, *2*, 360–365.
3 Yang, J.; Yoon, M.-C.; Yoo, H.; Kim, P.; Kim, D. *Chem. Soc. Rev.* **2012**, *41*, 4808–4826.
4 Holten, D.; Bocian, D. F.; Lindsey, J. S. *Acc. Chem. Res.* **2002**, *35*, 57–69.
5 Ryan, A.; Gehrold, A.; Perusitti, R.; Pintea, M.; Fazekas, M.; Locos, O. B.; Blaikie, F.; Senge, M. O. *Eur. J. Org. Chem.* **2011**, *2011*, 5817–5844.
6 Beljonne, D.; O'Keefe, G. E.; Hamer, P. J.; Friend, R. H.; Anderson, H. L.; Bredas, J. L. *J. Chem. Phys.* **1997**, *106*, 9439–9460.
7 Senge, M. O.; Fazekas, M.; Notaras, E. G. A.; Blau, W. J.; Zawadzka, M.; Locos, O. B.; Mhuircheartaigh, E. M. N. *Adv. Mater.* **2007**, *19*, 2737–2774.
8 Kim, K. S.; Lim, J. M.; Osuka, A.; Kim, D. *J. Photochem. Photobiol., C* **2008**, *9*, 13–28.
9 Pawlicki, M.; Collins, H. A.; Denning, R. G.; Anderson, H. L. *Angew. Chem. Int. Ed.* **2009**, *48*, 3244–3266.
10 Reeve, J. E.; Corbett, A. D.; Boczarow, I.; Kaluza, W.; Barford, W.; Bayley, H.; Wilson, T.; Anderson, H. L. *Angew. Chem. Int. Ed.* **2013**, *52*, 9044–9048.

11 Reeve, J. E.; Collins, H. A.; Mey, K. D.; Kohl, M. M.; Thorley, K. J.; Paulsen, O.; Clays, K.; Anderson, H. L. *J. Am. Chem. Soc.* **2009**, *131*, 2758–2759.
12 Lin, V. S.-Y.; DiMagno, S. G.; Therien, M. J. *Science* **1994**, *264*, 1105–1111.
13 Anderson, H. L. *Inorg. Chem.* **1994**, *33*, 972–981.
14 Coe, B. J.; Harris, J. A.; Hall, J. J.; Brunschwig, B. S.; Hung, S.-T.; Libaers, W.; Clays, K.; Coles, S. J.; Horton, P. N.; Light, M. E.; Hursthouse, M. B.; Garn, J.; Orduna, J. *Chem. Mater.* **2006**, *18*, 5907–5918.
15 Fisher, J. A.; Salzberg, B. M.; Yodh, A. G. *J. Neurosci. Methods* **2005**, *148*, 94–102.
16 Nowak-Król, A.; Wilson, C. J.; Drobizhev, M.; Kondratuk, D. V.; Rebane, A.; Anderson, H. L.; Gryko, D. T. *ChemPhysChem* **2012**, *13*, 3966–3972.
17 LeCours, S. M.; Guan, H.-W.; DiMagno, S. G.; Wang, C. H.; Therien, M. J. *J. Am. Chem. Soc.* **1996**, *118*, 1497–1503.
18 Fortage, J.; Scarpaci, A.; Viau, L.; Pellegrin, Y.; Blart, E.; Falkenstrm, M.; Hammarstrm, L.; Asselberghs, I.; Kellens, R.; Libaers, W.; Clays, K.; Eng, M.; Odobel, F. *Chem. Eur. J.* **2009**, *15*, 9058–9067.
19 Priyadarshy, S.; Therien, M. J.; Beratan, D. N. *J. Am. Chem. Soc.* **1996**, *118*, 1504–1510.
20 Jiang, N.; Zuber, G.; Keinan, S.; Nayak, A.; Yang, W.; Therien, M. J.; Beratan, D. N. *J. Phys. Chem. C* **2012**, *116*, 9724–9733.
21 Duncan, T.; Song, K.; Hung, S.-T.; Miloradovic, I.; Nayak, A.; Persoons, A.; Verbiest, T.; Therien, M.; Clays, K. *Angew. Chem. Int. Ed.* **2008**, *47*, 2978–2981.
22 Asselberghs, I.; Hennrich, G.; Clays, K. *J. Phys. Chem. A* **2006**, *110*, 6271–6275.
23 Quintiliani, M.; Perez-Moreno, J.; Asselberghs, I.; Vazquez, P.; Clays, K.; Torres, T. *J. Phys. Chem. B* **2010**, *114*, 6309–6315.
24 Ayhan, M. M.; Singh, A.; Hirel, C.; Grek, A. G.; Ahsen, V.; Jeanneau, E.; Ledoux-Rak, I.; Zyss, J.; Andraud, C.; Bretonnire, Y. *J. Am. Chem. Soc.* **2012**, *134*, 3655–3658.
25 Ishizuka, T.; Sinks, L. E.; Song, K.; Hung, S.-T.; Nayak, A.; Clays, K.; Therien, M. J. *J. Am. Chem. Soc.* **2011**, *133*, 2884–2896.
26 Reeve, J. E.; Anderson, H. L.; Clays, K. *Phys. Chem. Chem. Phys.* **2010**, *12*, 13484–13498.
27 Hu, X.; Xiao, D.; Keinan, S.; Asselberghs, I.; Therien, M. J.; Clays, K.; Yang, W.; Beratan, D. N. *J. Phys. Chem. C* **2010**, *114*, 2349–2359.
28 Ray, P. C.; Bonifassi, P.; Leszczynski, J. *J. Phys. Chem. A* **2008**, *112*, 2870–2879.
29 Zhang, L.; Qi, D.; Zhao, L.; Chen, C.; Bian, Y.; Li, W. *J. Phys. Chem. A* **2012**, *116*, 10249–10256.
30 Nalwa, H. S. *Adv. Mater.* **1993**, *5*, 341–358.
31 Thorne, J. R. G.; Kuebler, S. M.; Denning, R. G.; Blake, I. M.; Taylor, P. N.; Anderson, H. L. *Chem. Phys.* **1999**, *248*, 181–193.

32 Anderson, H. L.; Martin, S. J.; Bradley, D. D. C. *Angew. Chem. Int. Ed. Engl.* **1994**, *33*, 655–657.
33 Drobizhev, M.; Stepanenko, Y.; Dzenis, Y.; Karotki, A.; Rebane, A.; Taylor, P. N.; Anderson, H. L. *J. Phys. Chem. B* **2005**, *109*, 7223–7236.
34 Karotki, A.; Drobizhev, M.; Dzenis, Y.; Taylor, P. N.; Anderson, H. L.; Rebane, A. *Phys. Chem. Chem. Phys.* **2004**, *6*, 7–10.
35 Drobizhev, M.; Stepanenko, Y.; Dzenis, Y.; Karotki, A.; Rebane, A.; Taylor, P. N.; Anderson, H. L. *J. Am. Chem. Soc.* **2004**, *126*, 15352–15353.
36 Ogawa, K.; Ohashi, A.; Kobuke, Y.; Kamada, K.; Ohta, K. *J. Phys. Chem. B* **2005**, *109*, 22003–22012.
37 Pawlicki, M.; Morisue, M.; Davis, N. K. S.; McLean, D. G.; Haley, J. E.; Beuerman, E.; Drobizhev, M.; Rebane, A.; Thompson, A. L.; Pascu, S. I.; Accorsi, G.; Armaroli, N.; Anderson, H. L. *Chem. Sci.* **2012**, *3*, 1541–1547.
38 He, G. S.; Tan, L.-S.; Zheng, Q.; Prasad, P. N. *Chem. Rev.* **2008**, *108*, 1245–1330.
39 Albota, M. et al. *Science* **1998**, *281*, 1653–1656.
40 Kim, H. M.; Sik Seo, M.; Jeon, S.-J.; Rae Cho, B. *Chem. Commun.* **2009**, 7422–7424.
41 Terenziani, F.; Katan, C.; Badaeva, E.; Tretiak, S.; Blanchard-Desce, M. *Adv. Mater.* **2008**, *20*, 4641–4678.
42 Mongin, O.; Porrés, L.; Charlot, M.; Katan, C.; Blanchard-Desce, M. *Chem. Eur. J.* **2007**, *13*, 1481–1498.
43 Collins, H. A.; Khurana, M.; Moriyama, E. H.; Mariampillai, A.; Dahlstedt, E.; Balaz, M.; Kuimova, M. K.; Drobizhev, M.; Yang, V. X. D.; Phillips, D.; Rebane, A.; Wilson, B. C.; Anderson, H. L. *Nat. Photonics* **2008**, *2*, 420–424.
44 Dahlstedt, E.; Collins, H. A.; Balaz, M.; Kuimova, M. K.; Khurana, M.; Wilson, B. C.; Phillips, D.; Anderson, H. L. *Org. Biomol. Chem.* **2009**, *7*, 897–904.
45 Kuimova, M. K.; Collins, H. A.; Balaz, M.; Dahlstedt, E.; Levitt, J. A.; Sergent, N.; Suhling, K.; Drobizhev, M.; Makarov, N. S.; Rebane, A.; Anderson, H. L.; Phillips, D. *Org. Biomol. Chem.* **2009**, *7*, 889–896.
46 Balaz, M.; Collins, H. A.; Dahlstedt, E.; Anderson, H. L. *Org. Biomol. Chem.* **2009**, *7*, 874–888.
47 Khurana, M.; Ulrich, S.; Kim, A.; Moriyama, Y.; Netchev, G.; Akens, M. K.; Anderson, H. L.; Wilson, B. C. *Photochem. Photobiol.* **2012**, *88*, 1531–1538.
48 Fisher, J. A. N.; Susumu, K.; Therien, M. J.; Yodh, A. G. *J. Chem. Phys.* **2009**, *130*, 134506.
49 Winters, M. U.; Kärnbratt, J.; Eng, M.; Wilson, C. J.; Anderson, H. L.; Albinsson, B. *J. Phys. Chem. C* **2007**, *111*, 7192–7199.
50 Kuimova, M. K.; Hoffmann, M.; Winters, M. U.; Eng, M.; Balaz, M.; Clark, I. P.; Collins, H. A.; Tavender, S. M.; Wilson, C. J.; Albinsson, B.; Anderson, H. L.; Parker, A. W.; Phillips, D. *Photochem. Photobiol. Sci.* **2007**, *6*, 675–682.
51 Clays, K.; Persoons, A. *Phys. Rev. Lett.* **1991**, *66*, 2980–2983.

52 Olbrechts, G.; Munters, T.; Clays, K.; Persoons, A.; Kim, O.-K.; Choi, L.-S. *Opt. Mater.* **1999**, *12*, 221–224.
53 Kaatz, P.; Shelton, D. P. *J. Chem. Phys.* **1996**, *105*, 3918–3929.
54 Lopez-Duarte, I.; Reeve, J. E.; Perez-Moreno, J.; Boczarow, I.; Depotter, G.; Fleischhauer, J.; Clays, K.; Anderson, H. L. *Chem. Sci.* **2013**, *4*, 2024–2027.
55 Lin, V. S.-Y.; Therien, M. J. *Chem. Eur. J.* **1995**, *1*, 645–651.
56 Taylor, P. N.; Huuskonen, J.; Rumbles, G.; Aplin, R. T.; Williams, E.; Anderson, H. L. *Chem. Commun.* **1998**, 909–910.
57 Drobizhev, M.; Stepanenko, Y.; Rebane, A.; Wilson, C. J.; Screen, T. E. O.; Anderson, H. L. *J. Am. Chem. Soc.* **2006**, *128*, 12432–12433.
58 Wilson, G. S.; Anderson, H. L. *Chem. Commun.* **1999**, 1539–1540.
59 Goyan, R. L.; Cramb, D. T. *Photochem. Photobiol.* **2000**, *72*, 821–827.
60 Koszelewski, D.; Nowak-Król, A.; Drobizhev, M.; Wilson, C. J.; Haley, J. E.; Cooper, T. M.; Romiszewski, J.; Górecka, E.; Anderson, H. L.; Rebane, A.; Gryko, D. T. *J. Mater. Chem. C* **2013**, *1*, 2044–2053.
61 Hisaki, I.; Hiroto, S.; Kim, K. S.; Noh, S. B.; Kim, D.; Shinokubo, H.; Osuka, A. *Angew. Chem. Int. Ed.* **2007**, *46*, 5125–5128.
62 Ahn, T. K.; Kim, K. S.; Kim, D. Y.; Noh, S. B.; Aratani, N.; Ikeda, C.; Osuka, A.; Kim, D. *J. Am. Chem. Soc.* **2006**, *128*, 1700–1704.
63 Yoon, M.-C.; Noh, S. B.; Tsuda, A.; Nakamura, Y.; Osuka, A.; Kim, D. *J. Am. Chem. Soc.* **2007**, *129*, 10080–10081.
64 Tanaka, T.; Lee, B. S.; Aratani, N.; Yoon, M.-C.; Kim, D.; Osuka, A. *Chem. Eur. J.* **2011**, *17*, 14400–14412.
65 Screen, T. E. O.; Thorne, J. R. G.; Denning, R. G.; Bucknall, D. G.; Anderson, H. L. *J. Am. Chem. Soc.* **2002**, *124*, 9712–9713.
66 Kuimova, M. K.; Botchway, S. W.; Parker, A. W.; Balaz, M.; Collins, H. A.; Anderson, H. L.; Suhling, K.; Ogilby, P. R. *Nat. Chem.* **2009**, *1*, 69–73.
67 Kuimova, M. K.; Balaz, M.; Anderson, H. L.; Ogilby, P. R. *J. Am. Chem. Soc.* **2009**, *131*, 7948–7949.
68 Ohira, S.; Brédas, J.-L. *J. Mater. Chem.* **2009**, *19*, 7545–7550.
69 Coulson, D. R.; Satek, L. C.; Grim, S. O. *Inorganic Syntheses*; John Wiley & Sons, Inc., 1972; Vol. 13; pp 121–124.
70 Coskun, A.; Akkaya, E. U. *J. Am. Chem. Soc.* **2005**, *127*, 10464–10465.
71 Olmsted, J. *J. Phys. Chem.* **1979**, *83*, 2581–2584.
72 Winters, M. U.; Dahlstedt, E.; Blades, H. E.; Wilson, C. J.; Frampton, M. J.; Anderson, H. L.; Albinsson, B. *J. Am. Chem. Soc.* **2007**, *129*, 4291–4297.

Chapter 3: Design and synthesis of novel porphyrin dimer voltage-sensitive dyes

With the butadiyne-linked porphyrin dimer core identified as a starting point for improved SHG VSDs, the work in this chapter describes the design and synthesis of novel dyes. The literature is first examined to inform the choice of water-solubilising groups, before the synthetic methodology is presented. A collection of new porphyrin monomer and dimer VSDs emerges from the synthetic trials, and initial characterisation of these dyes suggests they are sufficiently water soluble for biological use.

3.1 Introduction

As concluded in Chapter 2, butadiyne-linked porphyrin dimers are the rational progression in VSD design in order to improve upon the sensitivity of the benchmark dye **JR1**. The 'push' and 'pull' electronic substituents have some effect upon the NLO properties, but are relatively unimportant compared to the choice of the butadiyne-linked porphyrin dimer as the π-core, and so the actual molecular design can focus on other factors such as the biocompatibility, solubility, and the synthetic accessibility and variability. The major final design feature of the novel porphyrin dimer voltage sensor to be considered is thus the amphiphilicity, and the choices made regarding this will meet the needs for biocompatibility and synthetic accessibility. In this chapter the molecular design considerations focus on amphiphilicity, with a literature review of water-soluble porphyrins providing design inspiration. The synthesis and initial characterisation of a family of novel voltage-sensors is then presented.

3.2 Designing amphiphilic dyes

It is necessary to introduce VSDs into aqueous media, requiring hydrophilicity, but VSDs also need a strong affinity for lipid bilayer membranes, requiring hydrophobicity. Both conditions can be met in an amphiphilic, lipid-like molecule. If either of these requirements is favoured too strongly, the dye will partition into membranes too slowly, or be insoluble in aqueous media to start with. Borrowing terminology from the field of lipids, if the hydrophilic headgroup can pass through the hydrophobic region of the membrane too readily, the dye will 'flip–flop' too easily, and the asymmetry necessary for SHG will gradually diminish. However, this factor should be less important for porphyrin dimers due to the weaker dependence upon dipolar non-centrosymmetry in their β response compared to monomers. As a butadiyne-linked porphyrin

dimer is inherently hydrophobic, most of this section will consider the hydrophilic headgroup design; the hydrophobic end will not be changed from previous dye designs. The basic starting point for a design is shown in Figure 3.1, where the length of a butadiyne-linked porphyrin dimer is also compared to the thickness of a typical biological membrane.

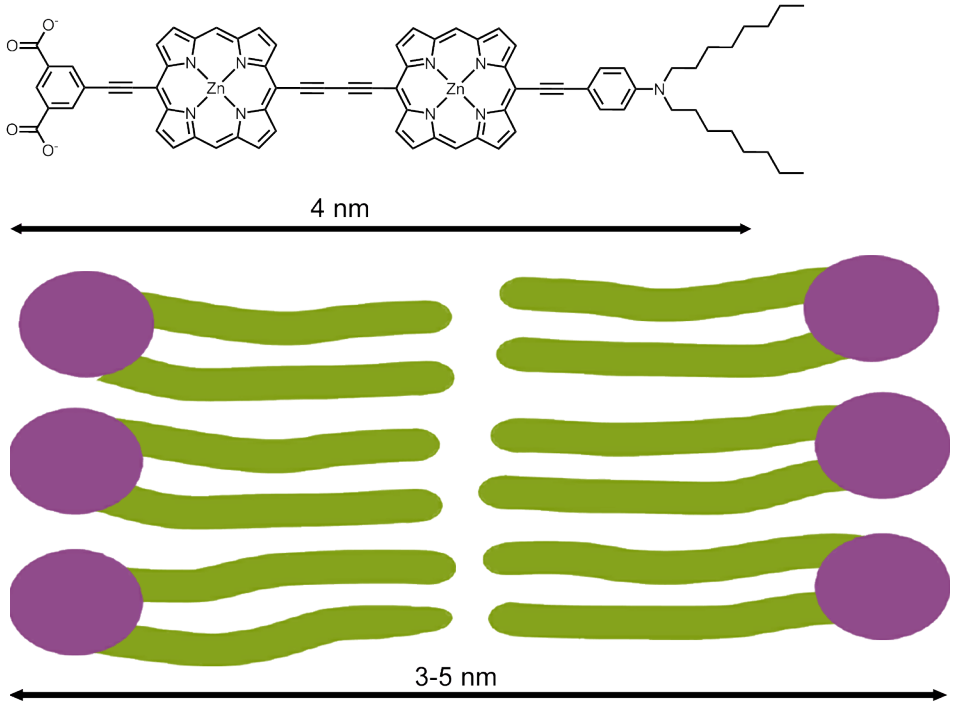

Figure **3.1** The length of a butadiyne-linked porphyrin dimer compared to the thickness of a lipid bilayer membrane.

3.2.1 Hydrophilic headgroup design

3.2.1.1 Charged groups

There are numerous examples in the literature of water-solubilising strategies applied to porphyrins to inspire the design of a hydrophilic headgroup. The first strategy uses charged or readily ionisable groups, such as ammonium or pyridinium groups, or carboxylic, phosphonic or sulfonic acids, to induce water-solubility. The sodium salt of zinc benzoporphyrin **26** (Figure 3.2) is

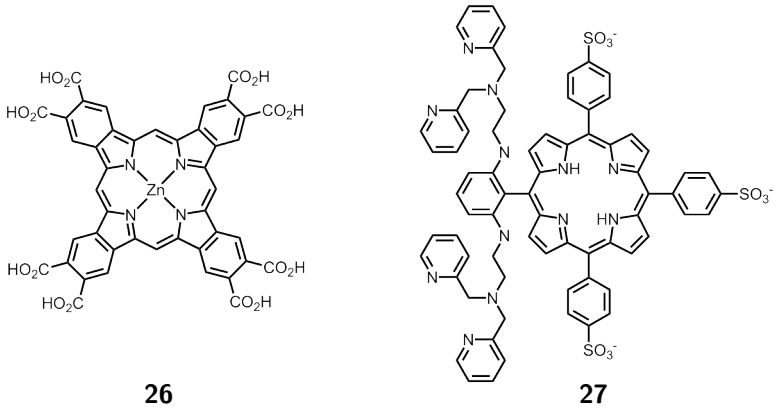

26 **27**

Figure **3.2** Other researchers have used charged or ionisable groups to provide water-solubility to porphyrins.[1,2]

soluble at up to $\sim 100\ \mu$M in water, but the neutral form is only sparingly soluble.[1] The sulfonate groups of dipicolylamine-porphyrin **27** facilitate its use for imaging at 5 μM in buffer.[2] In previous work from the Anderson group, two pyridinium groups aided the aqueous solubility of porphyrin dimer **Oxdime** (Figure 2.12 on Page 55), whereas the benchmark monomeric porphyrin SHG dye **JR1** (Figure 2.1 on Page 43) features just one pyridinium group. Dendrimeric systems, regularly branched three-dimensional architectures, such as Aida's porphyrin **28** (Figure 3.3), bearing a 32-arm Fréchet dendrimer, feature many charged or ionisable groups on their periphery in order to improve water-solubility.[3–6]

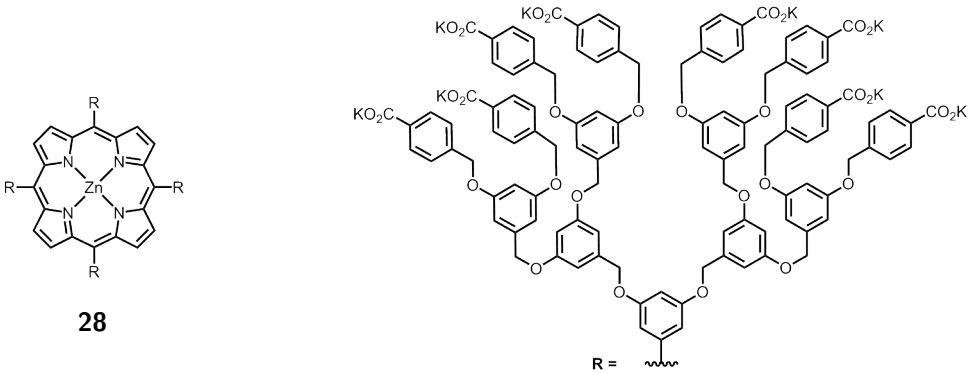

28

Figure **3.3** 32 charged groups confer water-solubility upon this porphyrin monomer.[3]

Charged groups can confer sufficient aqueous solubility to porphyrins, but

the key drawback is that the solubility then depends upon the ionic composition of the buffer solution chosen. The differing solubilities of benzoporphyrin **26** in aqueous sodium hydroxide compared to pure water are an example of this drawback,[1] as is the buffer-dependent solubility of **JR1**.[a] Charged groups can also increase the rate of endocytosis, a process by which a cell membrane ruptures and then reforms in order to internalise large molecules from outside of the cell.[7,8]

3.2.1.2 Sugars

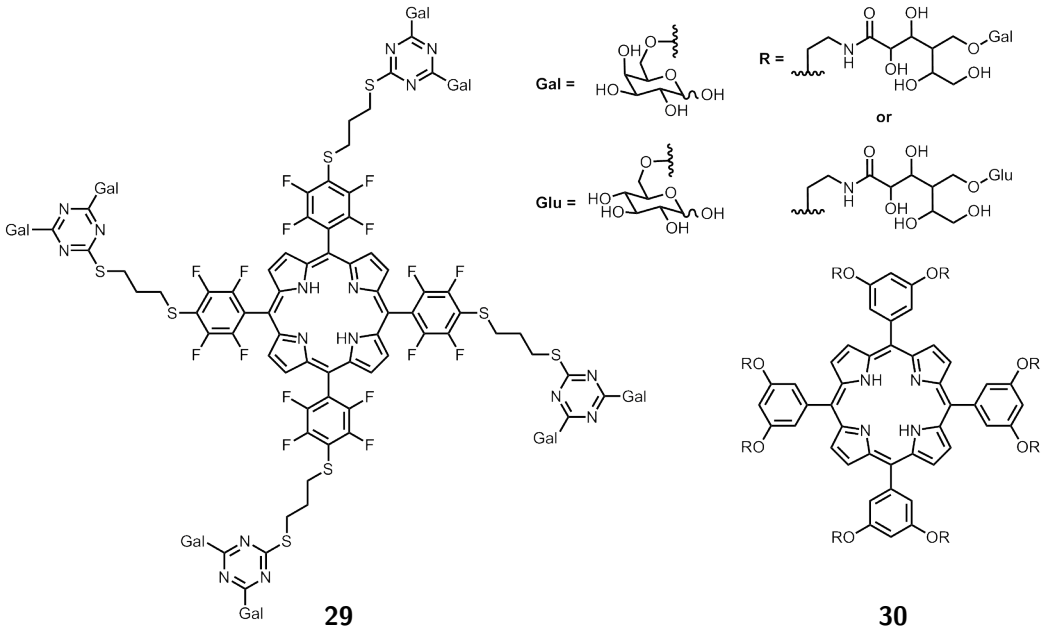

Figure **3.4** Galactose and glucose as hydrophilic water-solubilising groups.[9–11]

A second strategy reported for the water-solubilisation of porphyrins is the use of mono- or oligo-saccharides. Octa(galactose)- and octa(glucose)-porphyrins **30** (Figure 3.4) were found to be soluble in cell culture media at 250 μM,[9] exhibiting much greater water-solubility than related di(saccharide)-porphyrins. The octa(galactose) approach of compound **29** was also applied to phthalocyanines, structural siblings of porphyrins.[10,11] As with charged groups,

[a] J. E. Reeve, W. Kaluza and H. L. Anderson, unpublished results

the use of dendrimers can allow further multiples of sugar units to be added, enhancing the water-solubility (compound **31**, Figure 3.5).[12]

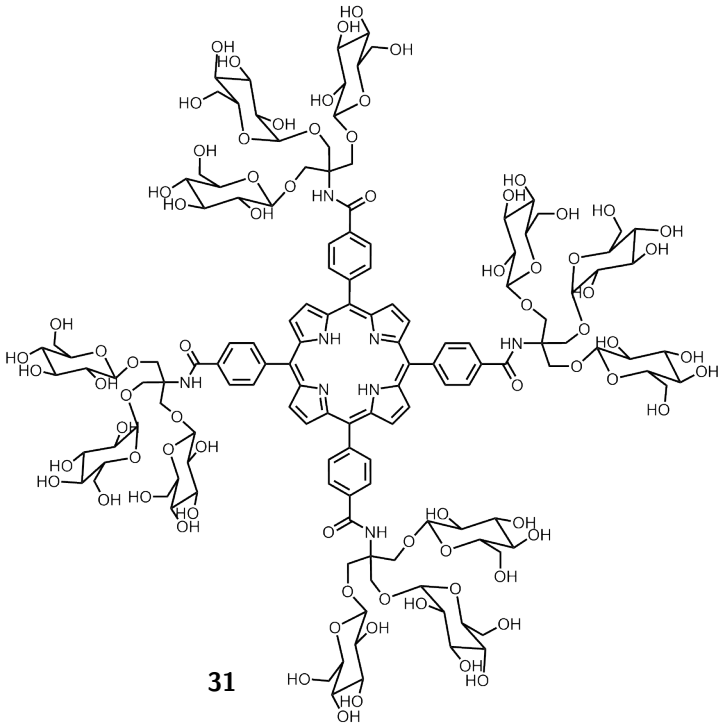

Figure **3.5** Sugars appended to a porphyrin in a dendrimeric fashion.[12]

Cyclodextrins have also been employed to impart water-solubility, in a host-guest strategy, but have also been noted (and deliberately used) for triggering the formation of new aggregates or self-assembled structures.[13–15] This is due to the possibility of more than one guest molecule entering the hydrophobic cavity, dependent upon the type of cyclodextrin and the size of the guests. This ability of cyclodextrin to promote aggregation at low concentrations in aqueous media detracts from its use as a solubilising group.

3.2.1.3 Water-soluble polymers

The third strategy other research groups have employed that can inspire the hydrophilic headgroup design is the use of water-soluble biocompatible polymers, PEG being the major example. PEG chains can uniquely induce water-

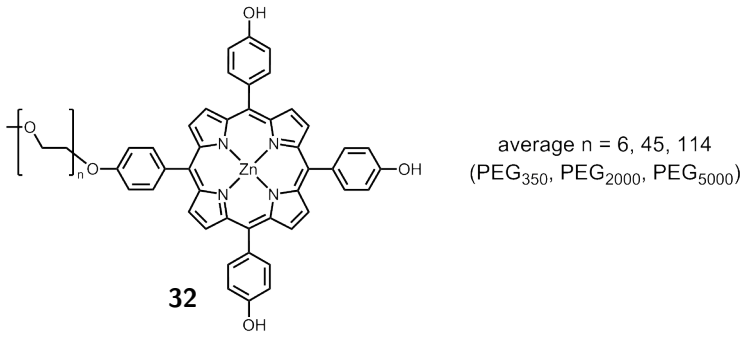

Figure **3.6** A single PEG chain used to water-solubilise a porphyrin monomer.[16,17]

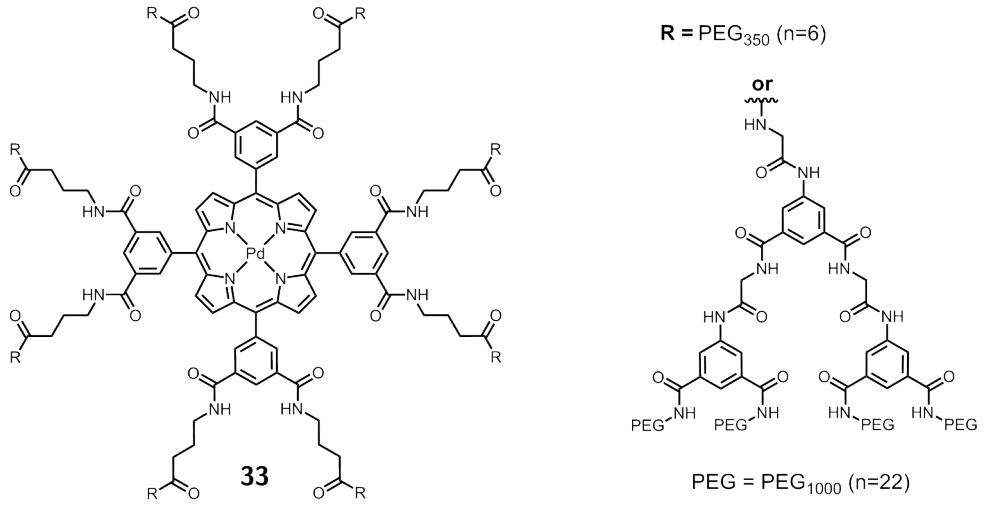

Figure **3.7** Eight or thirty-two PEG chains used to water-solubilise a porphyrin monomer.[18]

solubility without reducing organic solubility, and are thus synthetically more easily handled than charged or saccharide groups. They have been used extensively for drug delivery as they lengthen the blood circulation lifetime of the functional molecule, and also for reducing the cytotoxicity of other delivery systems, such as the cationic polymers poly(amidoamine) (PAMAM) and poly(propylenimine) (PPI), by preventing endocytosis.[19] PEG chains have also been used to render small molecules membrane-impermeable.[20] Even modestly decorated porphyrin monomers thus benefit from PEGylation.[21–23] The effect of chain length upon aqueous solubility and aggregation in monomer **32** has been thoroughly studied (Figure 3.6).[16,17]

PEG chains have also been used in a wide variety of dendrimeric systems

(compound **33**, Figure 3.7 on the preceding page, is an example) to provide solubility and enclose porphyrins in a 'microenvironment' to prevent undesired biological interactions.[3,24,25] Even very large PEGylated dendrimers do not induce endocytosis and thus allow extracellular localisation of the encapsulated dye.[18,26] PEGylated porphyrins have been used in PDT and biological imaging (pH sensors and O_2 sensors).[18,26–28]

3.3 Synthetic targets & disconnections

3.3.1 PEG headgroup

PEG chains were thus identified as the best solubilising group for this project. They are non-ionic and thus less sensitive to changes in the salt components of a buffer solution, and therefore present a better choice than using charged groups. They can confer sufficient aqueous solubility upon a porphyrin monomer without the need for symmetric substitution about the entire porphyrin ring or large dendrimeric systems, thus presenting a better option than either charged groups or saccharides. PEG is also commercially available in a variety of molecular weights, both poly- and mono-disperse, thus with an appropriate molecular design and synthetic route, the amphiphilicity of the target compound could be tuned to deliver sufficient water-solubility and membrane partitioning. The biocompatibility and poor cellular internalisation of PEGylated compounds also suits this project.

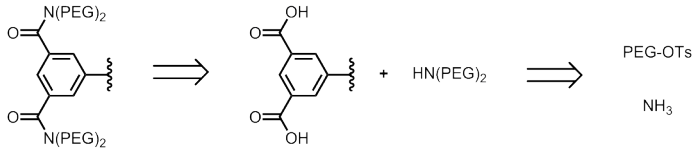

Scheme **3.1** The hydrophilic headgroup chosen for this work and a disconnection strategy.

As porphyrin monomers have previously been water-solubilised using one, eight or thirty-two PEG chains (Figures 3.6 and 3.7),[16–18,24,26] it was decided

to work with four PEG chains as an intermediate number, as illustrated in Scheme 3.1 on the page before. Because of the increased size of the hydrophobic part of the molecule moving from a porphyrin monomer to a dimer, one or two PEG chains of similar length are unlikely to provide sufficient water-solubility, but higher multiples of polymer chains may provide unnecessary bulk and too much water-solubility to allow membrane partitioning. Four chains were deemed a sensible starting point. The headgroup is based around 5-iodoisophthalic acid. The use of an iodophenyl facilitates clean Sonogashira coupling to the alkynyl porphyrin core, and the two carboxylic acid groups will allow amide bonds to be formed with the PEG-amine branches, the amide bond being chosen for its resistance to hydrolysis under physiological conditions. The bis(PEG)amine moiety was chosen as the method of branching into

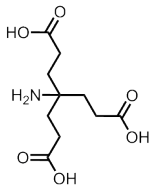

34

Figure **3.8** Behera's amine, a possible dendritic branch.[29]

two chains after the amide bond, allowing four PEG chains to be connected around one phenyl ring.[18,30] As amide bonds are also commonly used in dendrimer branches, this design has extensibility in mind if this is found to be necessary. For example, if the water-solubility of the final compounds is insufficient, the three-armed Behera's amine **34** (Figure 3.8) could be coupled between the central phenyl ring and the bis(PEG)amine to make a second generation dendrimer system with twelve PEG chains.

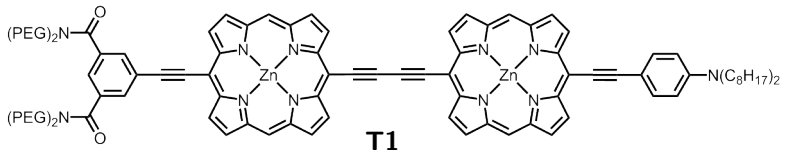

Figure **3.9** The target butadiyne-linked porphyrin dimer.

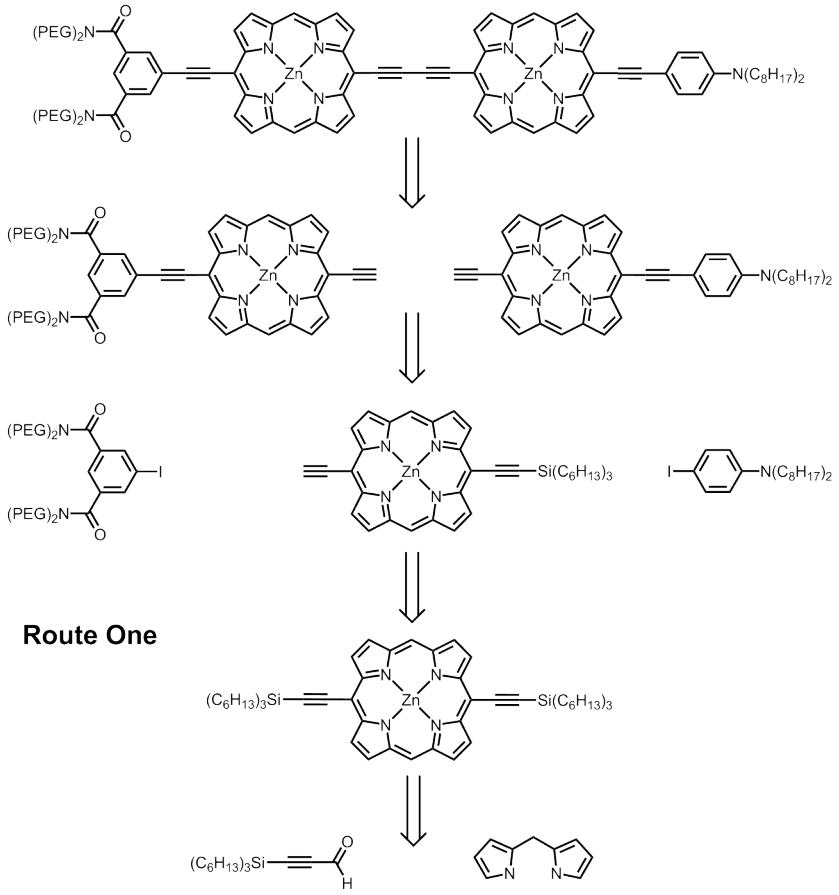

Scheme **3.2** The first of two viable disconnections of the target dimer.

3.3.2 Butadiyne-linked porphyrin dimer

For the target dimer itself, **T1**, it was decided to work with zinc porphyrins as these can coordinate THF and pyridine, which might prove useful during the synthesis if the solubility in other organic solvents was found to be poor. This is particularly important for **T1** as the design does not feature *meso*-aryl groups, often used to provide solubilising chains (either for organic or aqueous solubility).[31] The steric bulk of these groups could reduce the number

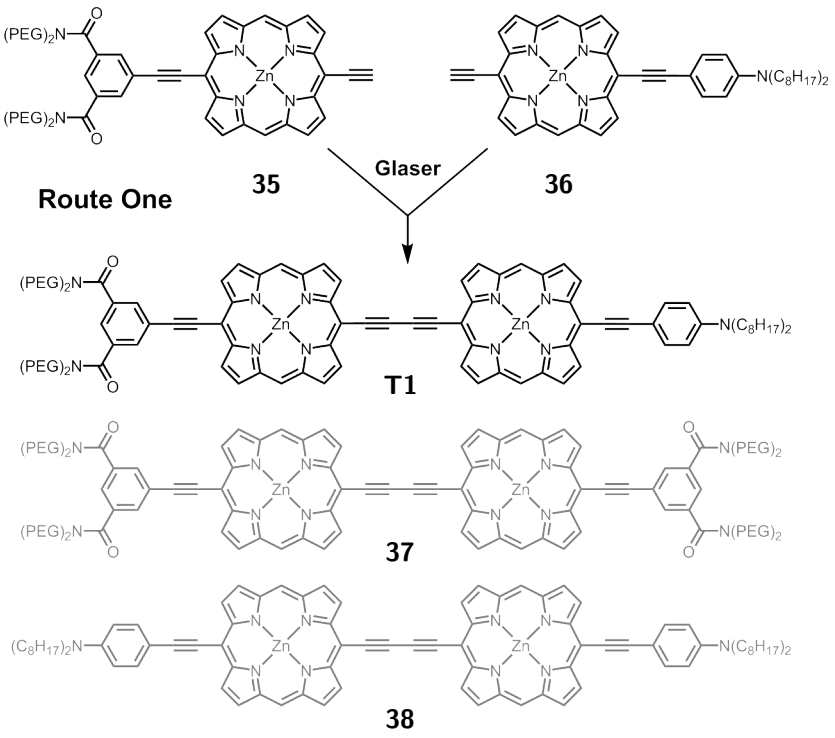

Scheme **3.3** The final step of route one, a statistical Glaser coupling with a mixture of products formed. Grayed out products indicate byproducts.

density N and thus the SHG intensity of the voltage probe in a bilayer membrane (Equation 2.3 on Page 46), justifying their omission.[32] The lipophilic and hydrophilic aryl groups can be coupled onto an alkynyl porphyrin using Sonogashira coupling, and are thus disconnected as iodoaryls. The butadiyne-link is readily formed under Glaser or other oxidative coupling conditions and it presents a natural disconnection opportunity. These disconnections allow for future flexibility in modifying this synthesis, as different hydrophilic head-groups and hydrophobic tails based upon iodoaryls could be included. Three synthetic routes can be conceived based on this disconnection. In the first, the two halves of the target dimer are connected by the formation of the butadiyne bond during the final step of the synthesis (Scheme 3.2 on the preceding page). As this step would be a statistical coupling reaction, it is clear that undesired byproducts will be formed (see the reaction of **35** and **36** in Scheme 3.3). This route carries synthetic interest as there are few literature examples of crossed

Glaser-type reactions.[33,34]

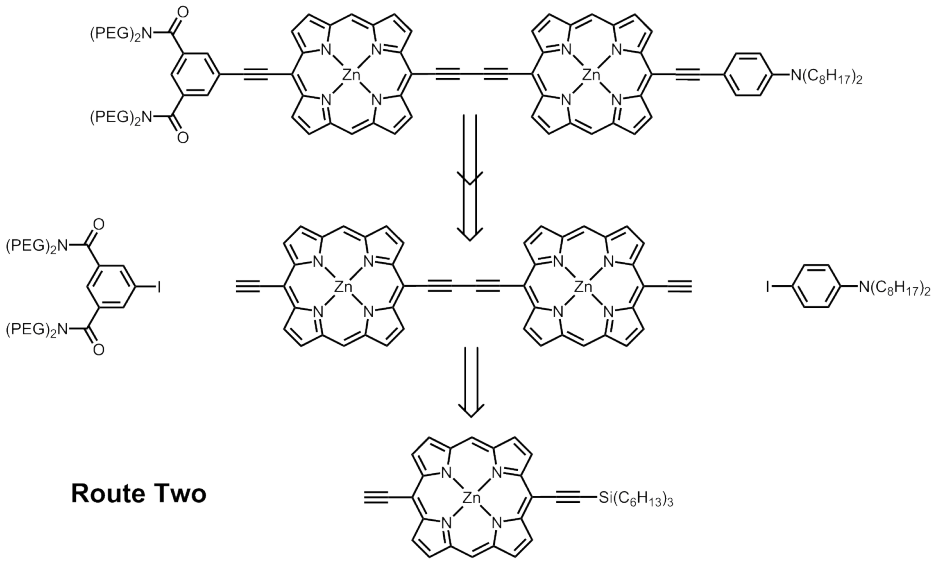

Scheme **3.4** The key disconnections of the second viable route to the target dimer.

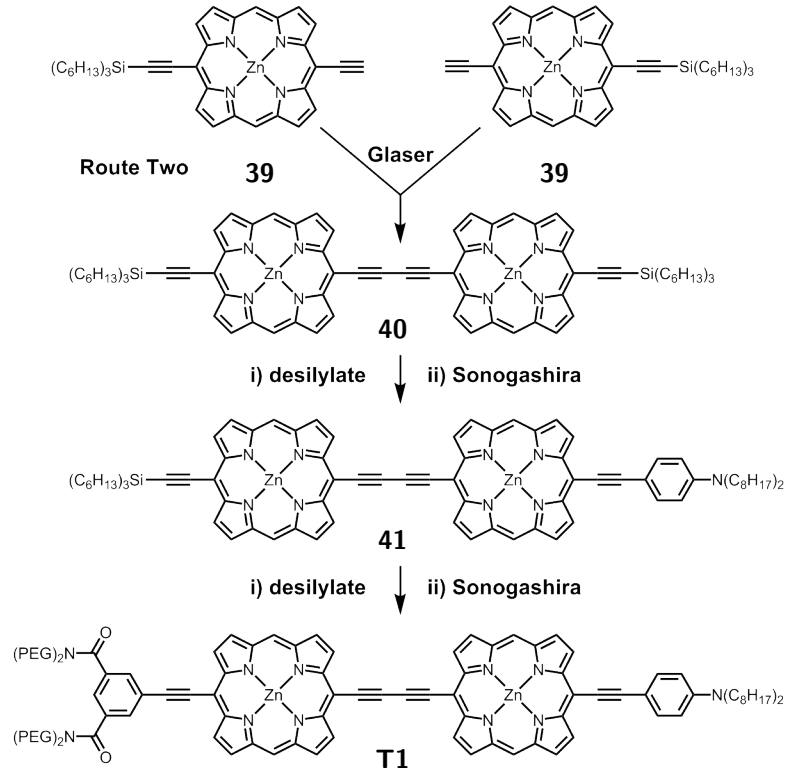

Scheme **3.5** A possible order of steps following route two.

In the second route, the butadiyne link is formed earlier, leaving the desym-

metrisation to the statistical removal of the silyl protecting groups (Scheme 3.4 on the preceding page). The opportunity for recycling of intermediates in this route could lead to improved overall yields compared to the first route. However, the dimer **40** (Scheme 3.5) without *meso*-aryl groups has not been prepared before, and may suffer from poor organic solubility. This is not an issue in route one as the dimer is formed as the final step of the synthesis and the desired target has the solubilising headgroup in place, but route two requires intermediate synthetic steps to be performed with this potentially insoluble dimer **40**.

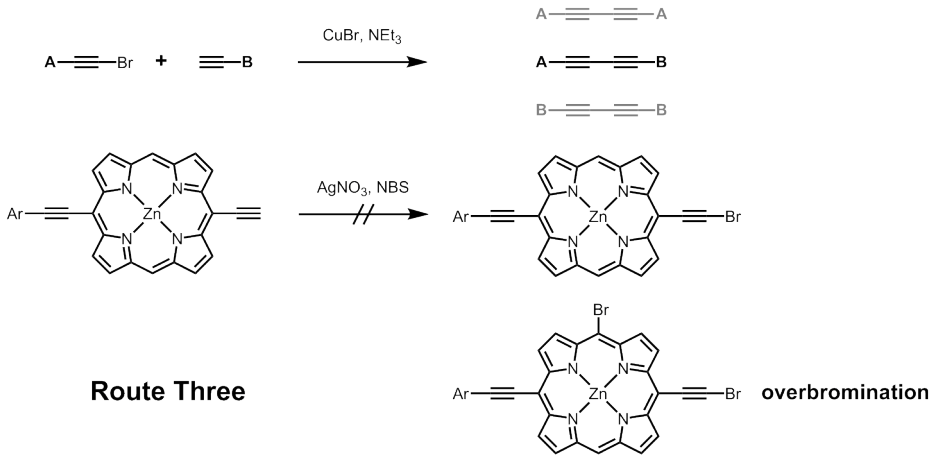

Scheme **3.6** Top: Cadiot-Chodkiewicz coupling leading primarily to heterocoupled butadiyne product; Grayed out products indicate low yield. Bottom: An example of a likely overbrominated product, ruling out the Cadiot-Chodkiewicz coupling as the basis of a viable synthetic route.

As a third potential route, Cadiot-Chodkiewicz coupling of an alkyne and a bromoalkyne has been found to lead to a greater selectivity for the heterocoupled product than a statistical Glaser-type reaction (Scheme 3.6).[35] However the preparation of a bromoalkyne porphyrin in the presence of free *meso* and β positions is non-trivial due to the likelihood of overbromination. There is one literature example of brominating an alkynylporphyrin, but this is a nickel porphyrin with the reactive *meso* positions blocked.[36]

It was decided to follow route one first, due to the expected poor solubility

of intermediate **40** of route two, and the poor prospects for forming the requisite bromoalkyne porphyrin for route three. As the intermediates of route one are common with the synthesis of a porphyrin monomer version of the final compound (one step from **35** or **36**), PEGylated monomers were prepared also (see Scheme 3.8).

3.4 Synthesis of PEGylated dyes

3.4.1 PEG headgroup

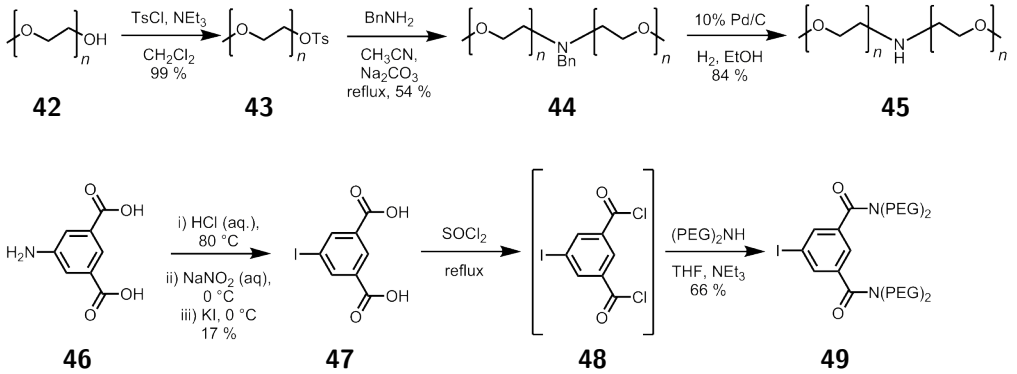

Scheme **3.7** The synthetic steps followed to access the PEG headgroup. $n = 11$ average.

Mono-methyl PEG with an average molecular weight (MW) of 500 (11 repeat units, PEG_{500}) was used for this synthesis. Bis(PEG)amine was prepared by first condensing an excess of PEG_{500}-tosylate **43** onto benzylamine in the presence of base, followed by the facile removal of the benzyl-protecting group using H_2 and Pd/C heterogeneous catalysis. A Sandmeyer reaction was used to prepare 5-iodoisophthalic acid **47**, from which 5-iodoisophthaloyl dichloride **48** was freshly prepared in small batches when needed. This intermediate was then reacted with the bis(PEG_{500})amine **45** to give the desired PEG_{500}-headgroup **49**.

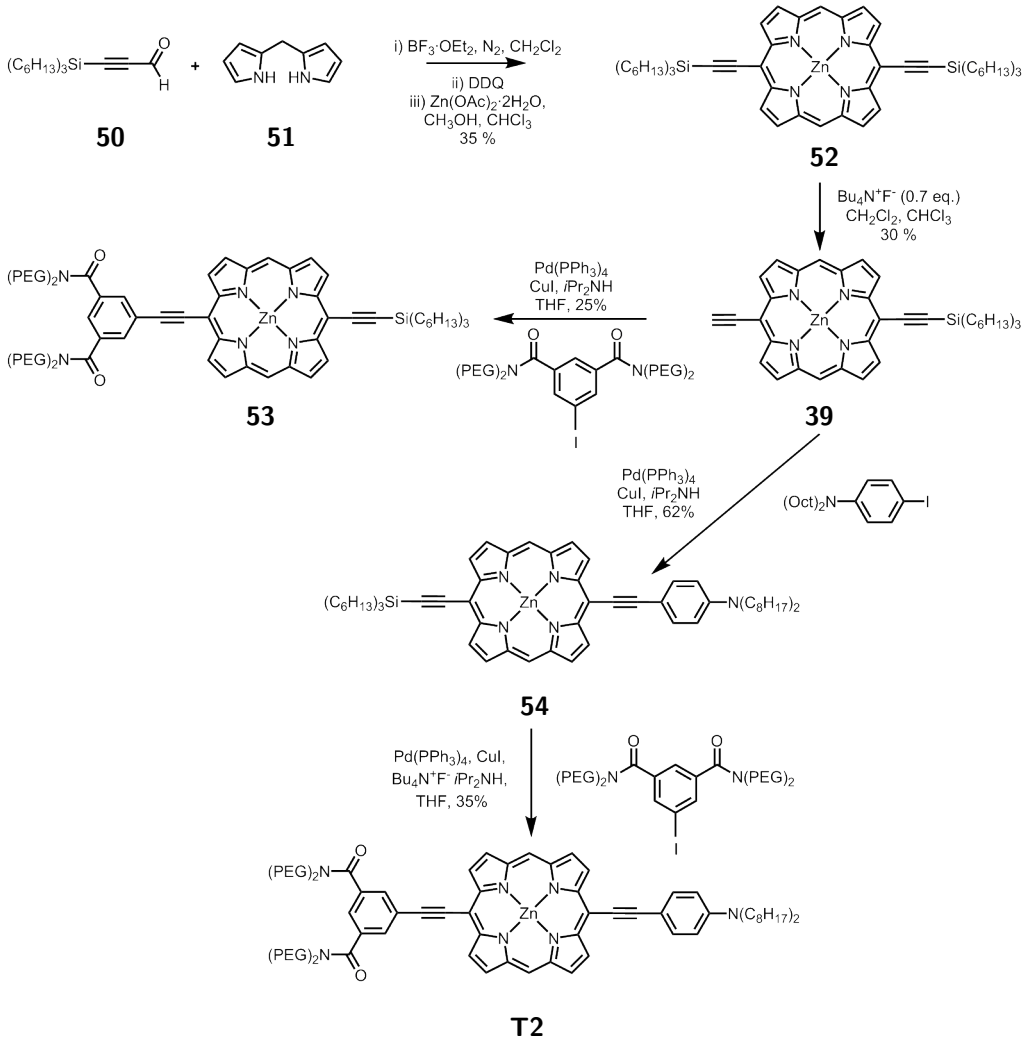

Scheme **3.8** Synthesis of the monomer target compound and useful intermediates for route one towards the dimer.

3.4.2 Porphyrin monomer

The basic porphyrin monomer building block **52** was prepared by the condensation of trihexylsilylpropynal **50** with dipyrromethane **51** under acid catalysis at high dilution, followed by oxidation with 2,3-dichloro-5,6-dicyano-*p*-benzoquinone (DDQ). Statistical desilylation gave a separable product mixture, and the singly-deprotected product **39** was typically isolated in 30% yield along with 30% recovery of the starting material **52**. This intermediate would then be coupled to an iodoaryl under catalytic Sonogashira conditions to give intermediate **53** or **54**. While the separation of **54** from *N,N*-dioctyl-4-iodo-1-aniline

was straightforward, allowing a large excess of the iodoaryl to be used to suppress side-reactions such as homo-coupling of two free alkynes, separating the PEG_{500}-headgroup from **53** required careful use of size-exclusion chromatography, and thus this reaction was most conveniently run at 1:1 stoichiometry. In-situ desilylation and Sonogashira coupling of **54** to the PEG_{500}-headgroup yielded the target amphiphilic porphyrin monomer **T2**.

3.4.3 Route one

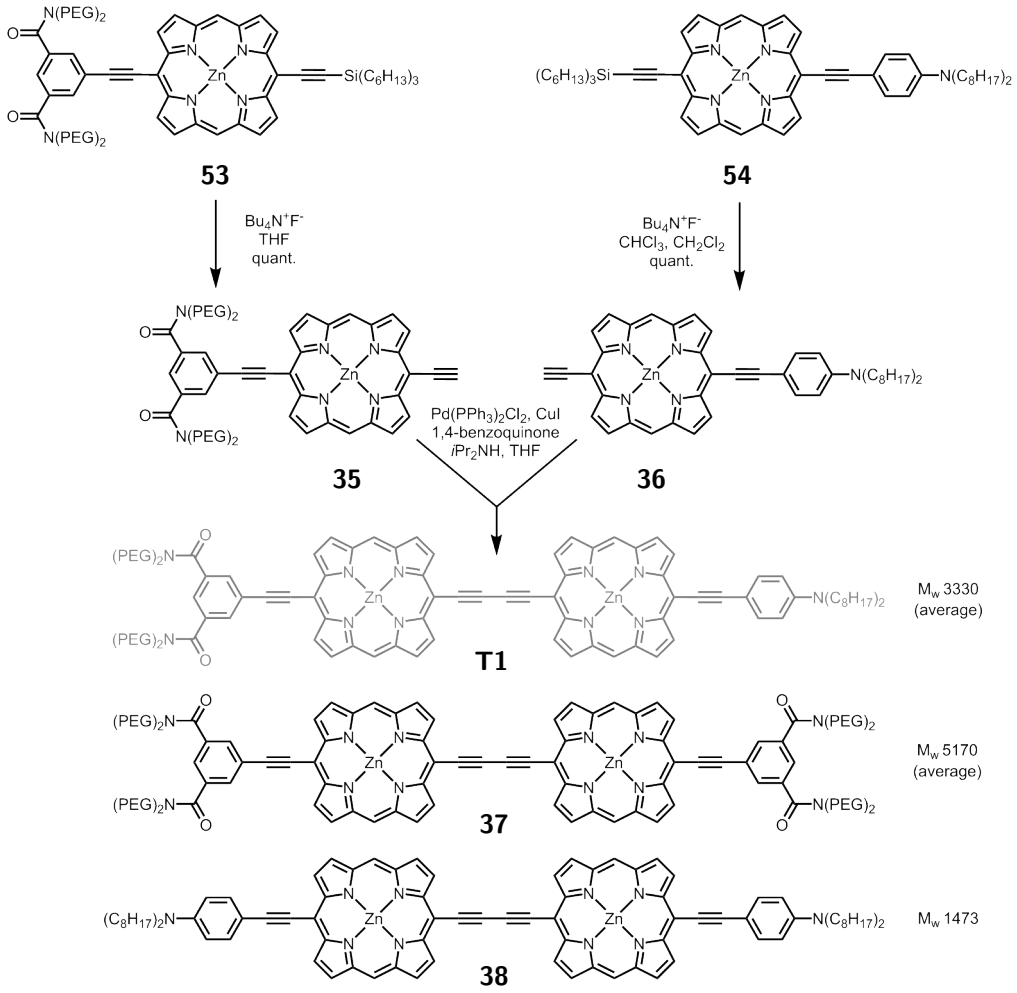

Scheme **3.9** The final steps of route one towards the dimer. Grayed out products indicate low yield.

Monomers **53** and **54** were desilylated individually before the statistical Glaser-type step was performed. The oxidative coupling reaction was attempted

several times, and size-exclusion chromatography readily allowed separation of the mixture of products, as indicated by the large differences in molecular weight in Scheme 3.9 on the page before (averages for the two PEG-containing compounds). Analysis of the fractions collected from the column revealed that the middle fraction by weight, expected to be the asymmetric dimer **T1**, was the least abundant product. This implied that one of the two homocoupling reactions proceeded faster than either the heterocoupling reaction or the other homocoupling reaction, skewing the product distribution away from statistical, and critically impacting the yield of the desired heterocoupled dimer **T1**.

The fraction expected to be the target dimer could also not be identified as the pure dimer. Apparent impurities in the NMR spectrum were initially suspected to arise from aggregation, but no change was observed in high-temperature acquisitions. HPLC confirmed that the sample was free from the heavier acceptor-acceptor dimer **37**, the lighter donor-donor dimer **38** or from excess PEG_{500}-headgroup **49**. Due to the polydispersity of the headgroup and the presence of several different M^+ ions of each unique peak in the MALDI-TOF MS, the identity of the impurity was not found here either. With these two problems plaguing route one, initial investigations into route two were carried out.

3.4.4 Route two

Intermediate **39**, already used in route one and the target monomer synthesis, was coupled under Pd-catalysed conditions to yield the dimer **40** (Scheme 3.10 on the following page). Contrary to expectations, this dimer is readily soluble in THF, and $CHCl_3$ or CH_2Cl_2 in the presence of pyridine. Unlike the analagous bis(trihexylsilyl)-protected monomer **52**, the dimer could be precipitated as a powder by the addition of methanol or pentane to a concentrated CH_2Cl_2 solution. With this promising intermediate in hand, statistical desily-

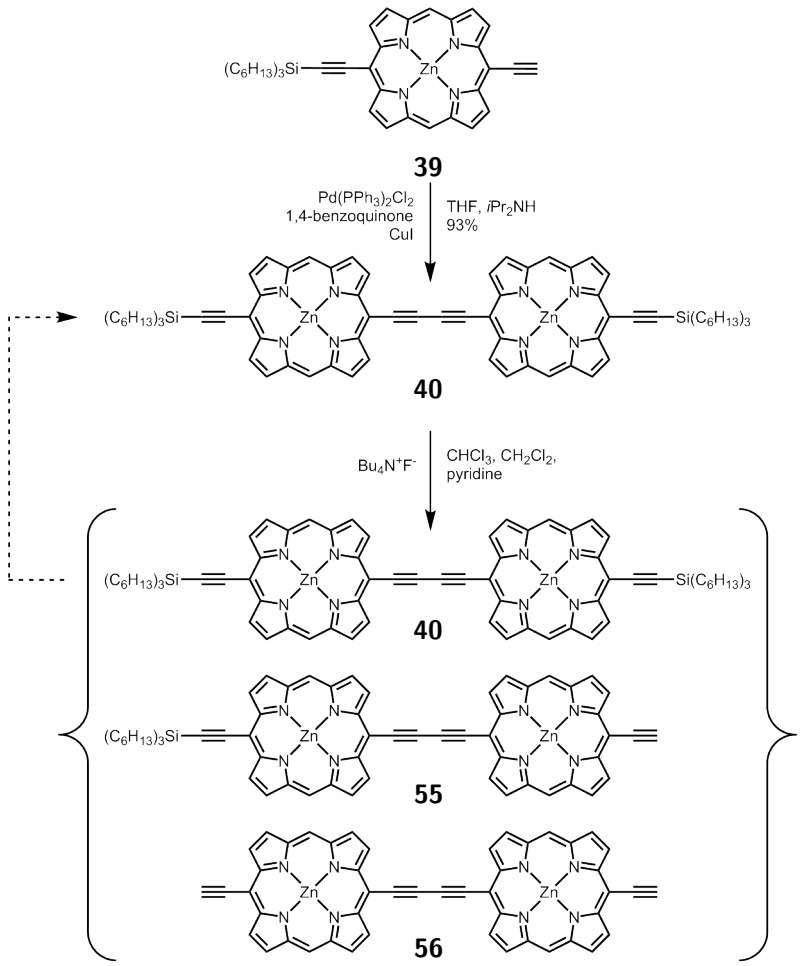

Scheme **3.10** Initial investigations into route two, with an inseparable mixture of dimers in parentheses.

lation was then attempted. Using THF for the reaction solvent, as the best solvent for the starting material, the reaction proceeded uncontrollably to the doubly-deprotected byproduct, which was fairly insoluble and identified by MS and TLC only. The reaction was then trialled in a 1:1 mixture of $CHCl_3$:CH_2Cl_2 with 1% pyridine, and was found to proceed more slowly. Monitoring by TLC allowed the reaction to be quenched when the desired ratio of products was observed. However the statistical mixture was found to be inseparable, largely as a result of poor solubility; the eluent mixtures required to resolve the products on a TLC plate caused precipitation on a silica column.

However, two ways forward were conceived that would still allow this route

with its key statistical desilylation step to be used. The idea was to subject the crude mixture of desilylated intermediates to Sonogashira coupling conditions with either dioctylaniline or the PEG_{500}-headgroup, assuming that either of these groups would yield products soluble enough to allow chromatographic separation.

The reaction of the mixture of dimers **40**, **55** and **56** with *N,N*-dioctyl-4-iodo-1-aniline was attempted first as the aniline is a less precious compound than the PEG_{500}-headgroup. The stoichiometry was estimated to ensure correct catalyst loading from the NMR spectrum of the mixture by comparing the ratio of the integrations of the porphyrinic environments with the acetylenic environment (although an excess of the aniline was used). The reaction worked well on the crude mixture and gave the expected products (Figure 3.10) according to MS, but again these were found to be inseparable on a silica column as the compounds are not sufficiently soluble in the eluent mixture necessary to resolve the components.

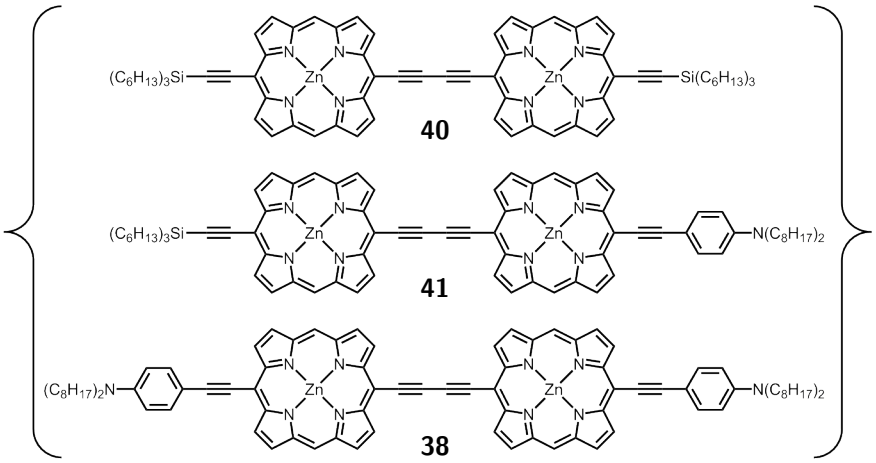

Figure **3.10** Another inseparable mixture of dimers after the dioctylaniline was added in an attempt to improve separation.

Thus the coupling of the PEG_{500}-headgroup onto the crude mixture of desilylated dimers **40**, **55** and **56** was investigated. An advantage of this approach is that the resulting products should be highly soluble in organic solvents because

of the PEG chains, and the difference in MW (or average MW for compounds containing the PEG_{500}-headgroup) should allow size-exclusion chromatography as an alternative to separating by polarity. A disadvantage was wasting the PEG_{500}-headgroup stock upon forming the bis-headgroup dimer **37**. It was most desirable to isolate compound **41** as a precursor to **T1** in order to use the headgroup as efficiently as possible, but this was not possible.

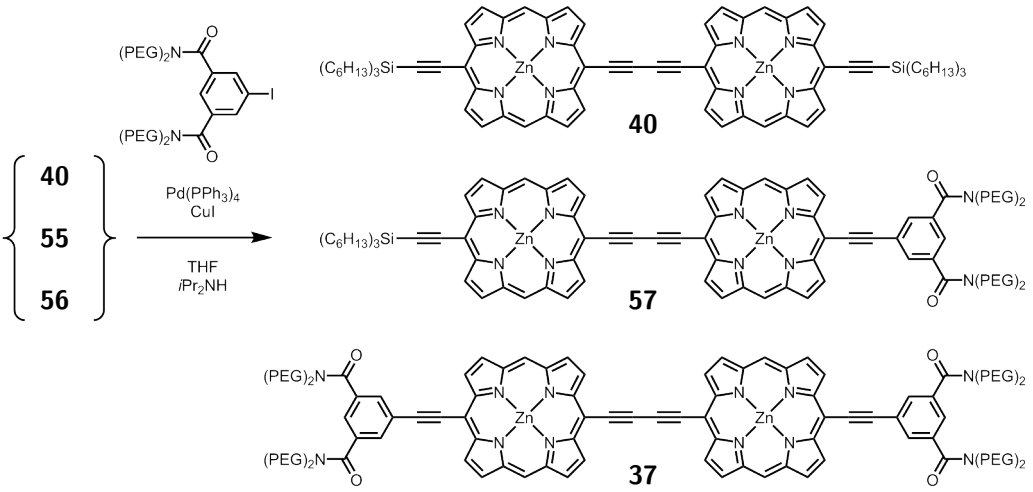

Scheme **3.11** A separable mixture of porphyrin dimers was obtained by coupling the crude desilylation mixture with the PEG_{500}-headgroup.

Thus the PEG_{500}-headgroup was coupled to the dimer mixture **40**, **55** and **56** using Sonogashira conditions (Scheme 3.11), and the mixture of porphyrin dimer products obtained were found to be separable by both silica and size-exclusion chromatography due to the polarity and mass introduced by the headgroup. The bis-silylated dimer starting material **40** was recycled, a key advantage over route one.

However, this route was hampered by a new problem, namely the separation of the PEG_{500}-headgroup from the asymmetric dimer **57**. The polydisperse nature of the headgroup impeded the ability of size-exclusion chromatography to fully resolve these two compounds (illustrated by the MS in Figure 3.11), and little difference in polarity was seen by TLC or silica column, both normal-

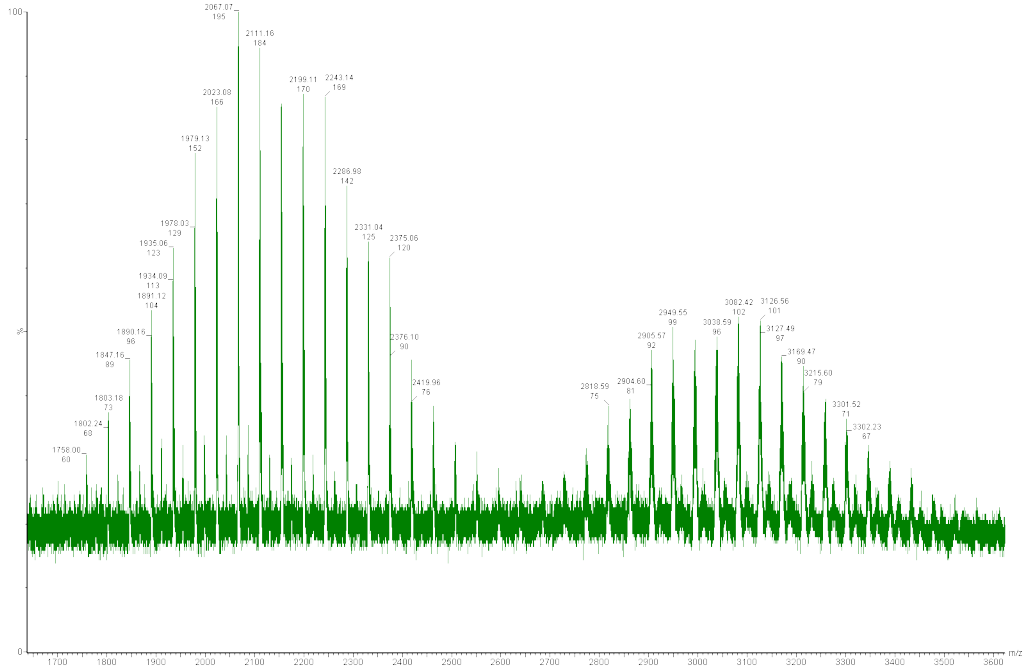

Figure **3.11** The overlapping mass distributions of the PEG headgroup **49** (centred around $\sim$ 2130) and the asymmetric dimer **57** (centred around $\sim$ 3080).

and reversed-phase. A potential solution to this problem was to run the coupling step at 1:1 stoichiometry to eliminate the need to separate these two compounds. Attempts at this methodology could reduce but not eliminate the headgroup impurity, with 10-20 molar % typically remaining after initial separation of the three dimers. This is likely due to the error in the NMR integrations used to estimate the stoichiometry. Pure samples of the desired dimer **57** were thus isolated only in small quantities, representing low yields for this two-step conversion.

Sufficient material was nonetheless obtained in order to test the final step of this route, and thereafter compare the results with those found for route one. In-situ desilylation and coupling of the precursor **57** to the dioctylaniline (Scheme 3.12) allowed the first spectroscopic glimpses at a clean sample of the target dimer **T1**. As shown in Figure 3.12 on Page 127, the NMR spectra of **T1** obtained *via* the two routes differ significantly. The porphyrinic protons (*meso* and β region) of the route two sample reveal the correct number of envi-

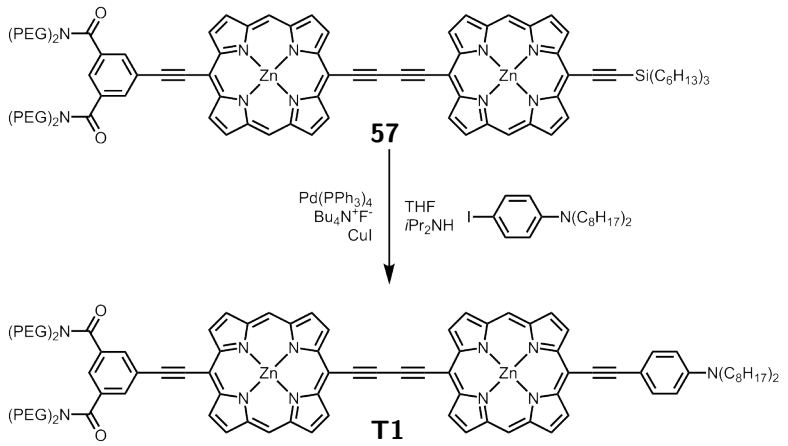

Scheme **3.12** The final step of route two.

ronments with good integrals, along with some minor impurities. On the other hand, route one seems to feature similar symmetry but several of the integrals exceed what is expected (leading to 3 *meso* and 12 β and environments, instead of the 2 and 8 observed for the route two sample) suggesting that the sample is unclean as discussed in Section 3.4.3.

3.4.5 Discussion of the PEGylated dye synthesis

Route two was identified to hold advantages over route one, particularly in the recycling of the bis-protected dimer and the early statistical step reducing wasteful byproducts. However the yields of the desired dimer **T1** were very low due to the extensive purification required. As the PEG chains dominate the polarity, size-exclusion chromatography was found to be particularly useful in these syntheses. It was thus proposed that repeating the route two methodology using a monodisperse version of the PEG_{500}-headgroup should allow more facile purification, and access to a more substantial stock of the target compound. Mono-methyl hexa(ethylene glycol) (HEG) chains were chosen for this investigation because they were readily commercially available.

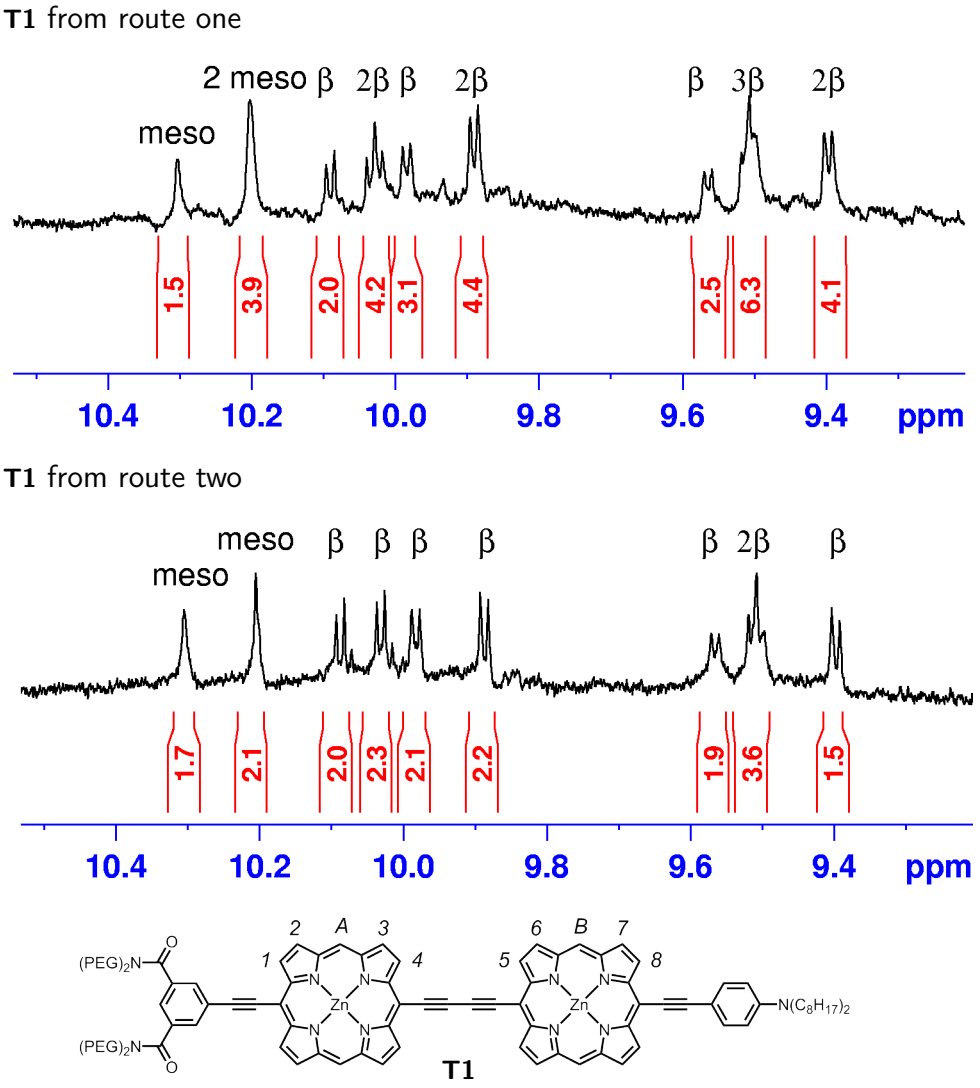

Figure **3.12** Top: Comparison of the ^{1}H NMR spectra in the porphyrinic region for the product **T1** obtained from the two routes (measured in d_8-THF/5% pyridine at 400 MHz); Bottom: the inequivalent β (1-8) and *meso* (A,B) environments of **T1**.

3.5 Synthesis of HEGylated variants

The hexa(ethylene glycol) (HEG) variants of the original targets (Figure 3.13 on the following page) were synthesised using analogous methods as already presented for the PEGylated compounds. The syntheses proceeded well *via* the routes already identified. Monomer **T4** was made first, as shown in Scheme 3.13. The dimer synthesis benefited greatly from the monodisperse headgroup, the separation of intermediate **63** from the HEG-headgroup (Scheme 3.14 on Page 129)

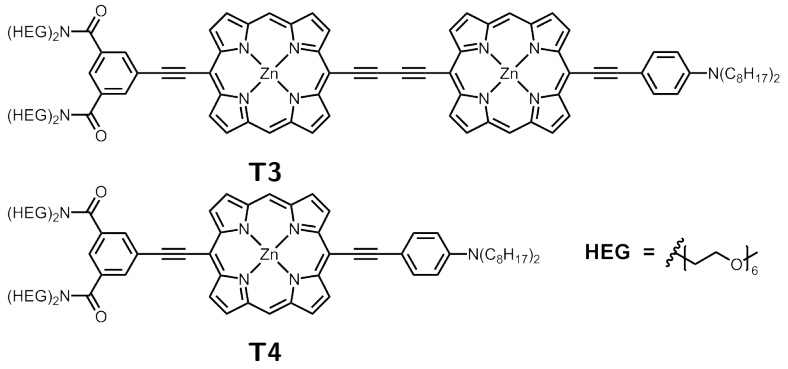

Figure **3.13** New targets identified after route two was confirmed as a viable route.

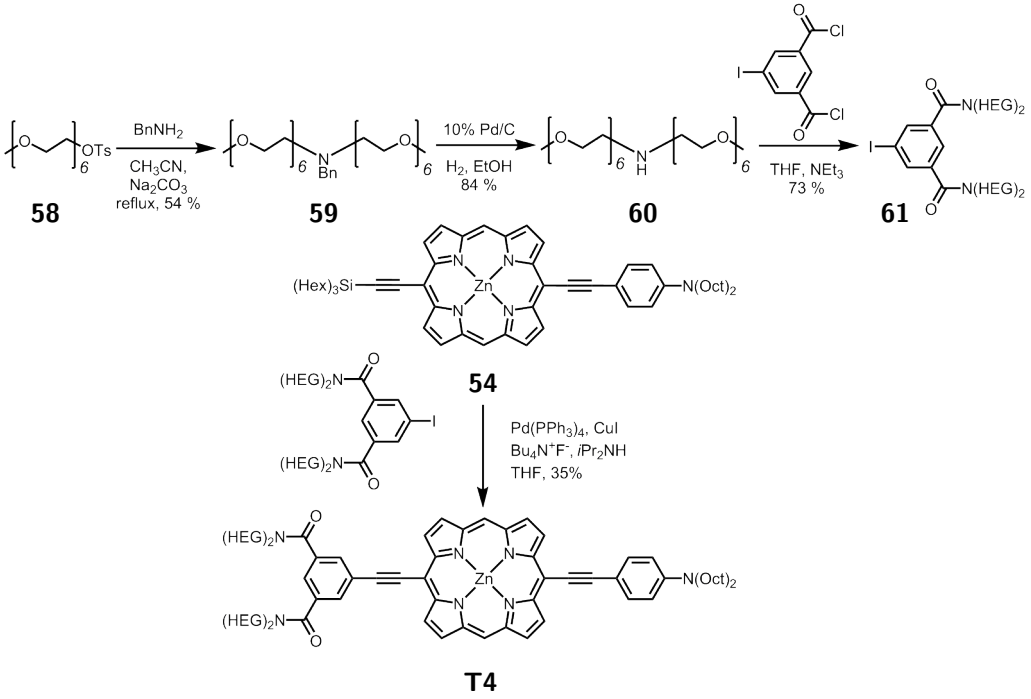

Scheme **3.13** Synthesis of the HEG-headgroup and the HEG-monomer **T4**.

being straight forward. This improved separation allowed a more realistic determination of the relative yields of the statistical step; pleasingly, a 20% yield of **63**, the precursor to the target dimer, was obtained, along with 50% recovery of starting dimer **40**, which was recycled. The final Sonogashira step was found to occur reliably when performed at room temperature; it was suspected that the starting material and products were sensitive to $Bu_4N^+F^-$ at elevated temperature, leading to the formation of inseparable impurities.

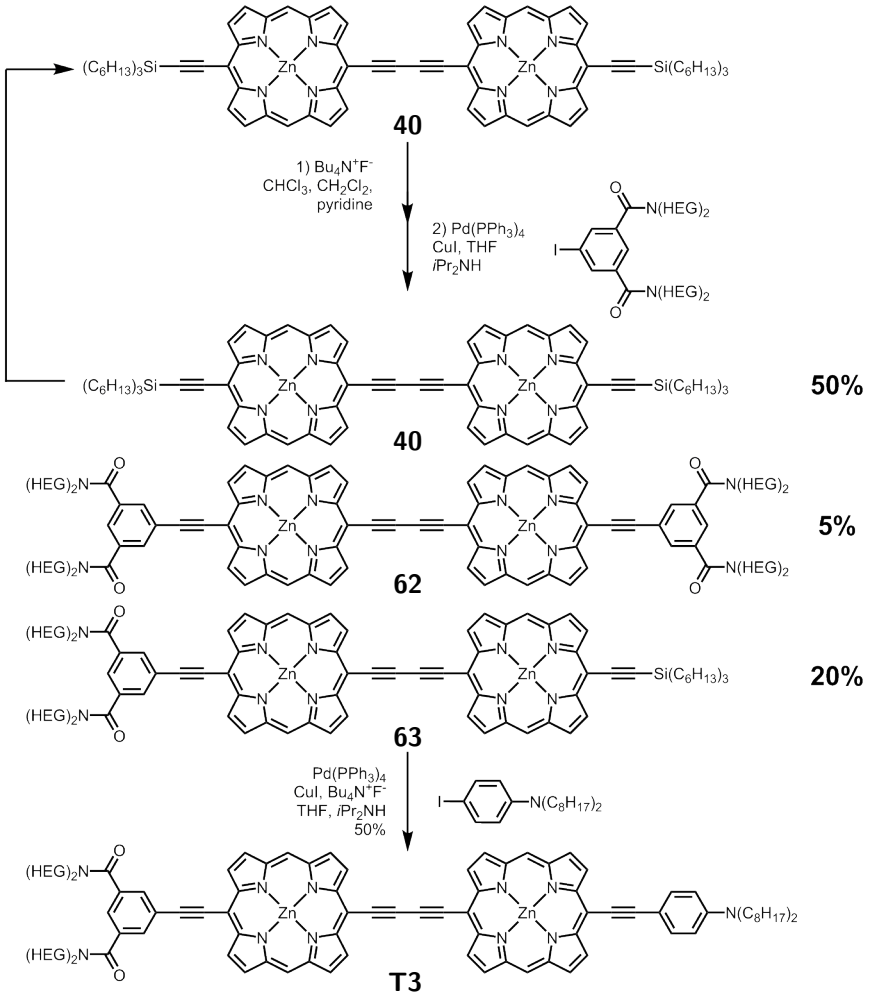

Scheme **3.14** Synthesis of the HEG-dimer **T3**.

3.6 Synthesis of free-base dyes

As discussed in Chapter 2, the coordinated metal inside the porphyrin ring can have significant effects on the electronic nature of a porphyrin, and was demonstrated to influence the NLO properties of porphyrin dimers. Thus we decided to synthesise free-base analogues of the target dyes in order to double the library of available compounds and ultimately test the effect of metalation upon the voltage-sensitivity.

Free-base porphyrin monomers **T5** and **T6** were accessed via demetalation of the final zinc compounds (Scheme 3.15 on the following page), with an

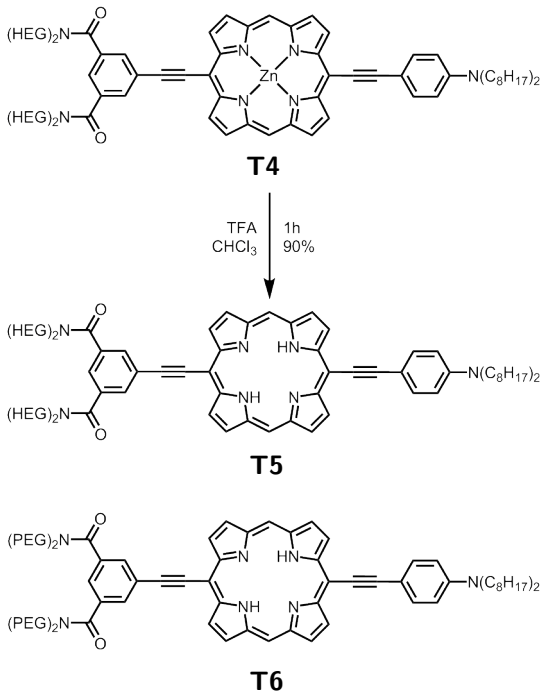

Scheme **3.15** Synthesis of the free-base HEG monomer. This methodology was also applied to the give the free-base PEG monomer shown.

extraction and precipitation necessary as the only purification. However, in the case of the final dimer **T3** which was synthesised only on a small scale (with a total stock of $\sim$ 10 mg), demetalation was first tested on the less precious compound **40** (Scheme 3.16).

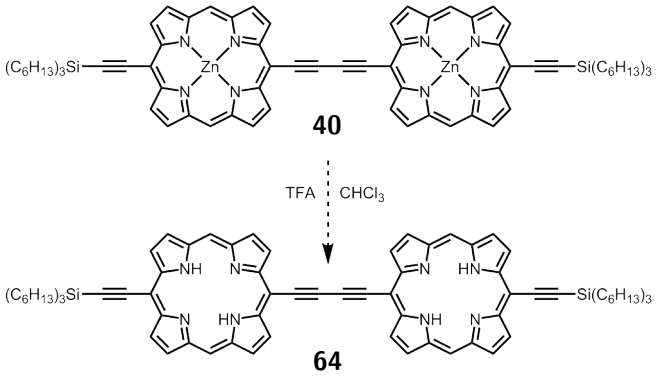

Scheme **3.16** A test reaction attempted to test the viability of making a free-base version of the final dimer.

Demetalation of the bis-trihexylsilyl protected porphyrin dimer **40** was at-

tempted but appeared to be non-trivial, with the formation of more than one product and unidentified impurities (by MS and TLC). It is noted that the desired free-base product **64** of this reaction would likely be poorly soluble and lacks the coordinating group of the zinc starting material. Ironically the demetalation, and subsequent purification and characterisation, may actually be trickier to achieve in this test situation because of poor solubility than it would be using a HEGylated dimer later in the synthesis. Due to the small stocks of pure HEGylated compounds it was decided not to attempt demetalation of the final dimer. If the zinc dimer shows promising voltage-sensitivity, the incorporation of other metals should be investigated.[b]

3.7 Optical characterisation of the synthesised dyes

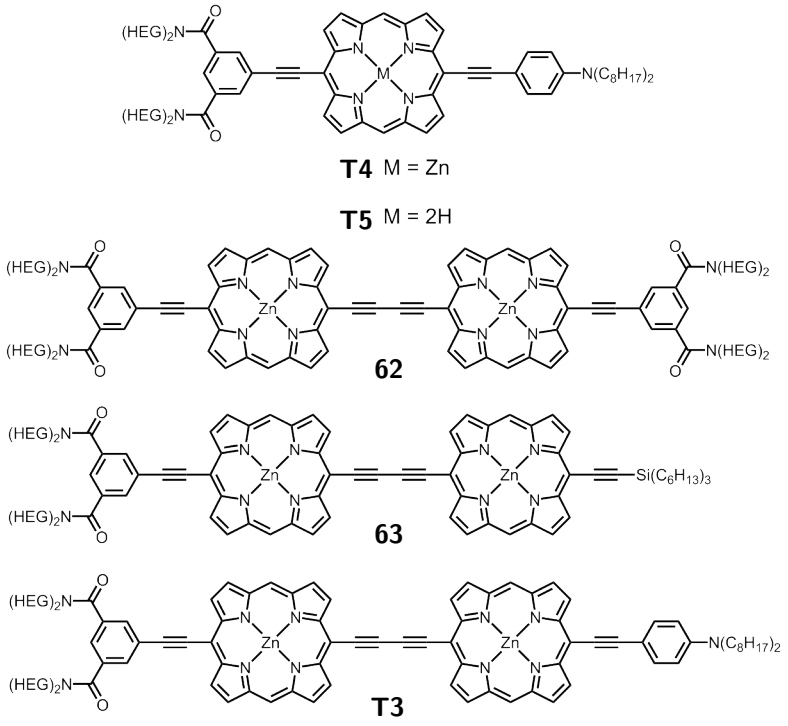

Figure **3.14** The family of HEG dyes used in optical experiments.

[b] A coworker, Igor Boczarow, is investigating alternative synthetic routes to allow the demetalation to be performed at an earlier step.

The 1P optical properties of the family of novel HEGylated porphyrin dyes (Figure 3.14) were then assessed, both in $CHCl_3$ and water. The spectral features and extinction coefficients found in Figure 3.15 are as expected and typical for diethynyl porphyrin monomers and butadiyne-linked dimers. By comparing these measurements with those in water, inferences can be made about the dye aggregation in water which will assist in the interpretation of future membrane localisation studies. The byproduct **62** and intermediate **63** were included to study the effects of an extra HEG-headgroup or the trihexylsilyl group (compared to dioctylaniline) respectively on the aqueous solubility and aggregation behaviours.

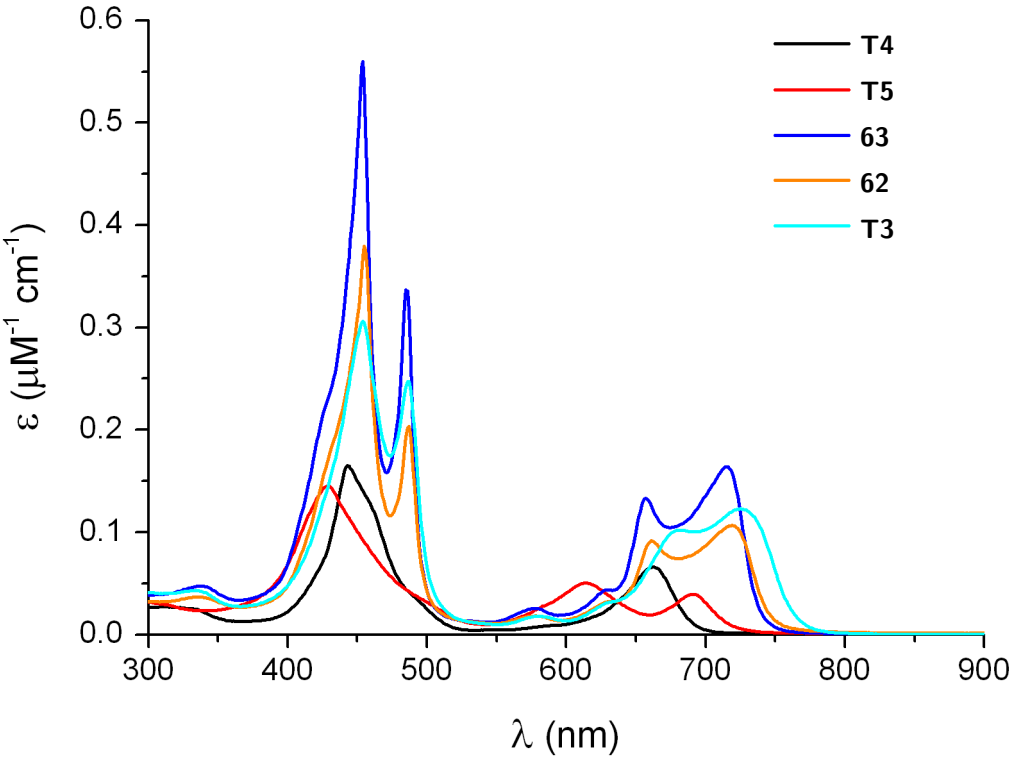

Figure **3.15** Extinction coefficients of the family of HEG dyes, measured in $CHCl_3$ (with 1% pyridine for zinc-containing compounds).

3.7.1 Aqueous studies on the porphyrin monomers

Both the zinc monomer **T4** and the free-base monomer **T5** were found to be readily soluble in pure water at $\sim$ 130 μM. Very slight broadening of the Soret band was observed for both compounds in aqueous solution compared to $CHCl_3$ (with 1% pyridine for **T4**), as well as a reduction in extinction coefficient (Figures 3.16(a) and 3.16(b)). Both dyes obeyed the Beer-Lambert law[c] across the range of concentrations tested (up to 50 μM), implying either that only a single species was involved in the absorption and aggregation is not significant,[11] or that the extent of aggregation does not change over this concentration range.

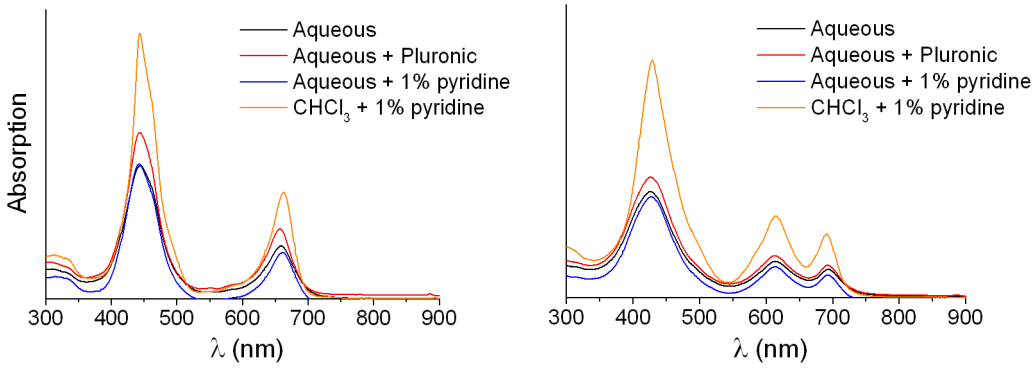

(a) Zinc monomer **T4**

(b) Free-base monomer **T5**

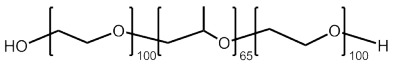

(c) Pluronic F-127 (number of units are approximate averages).

Figure **3.16** Comparison of the absorption spectra of the HEG monomers at 5 μM in different solvents.

As a further test for aggregation, Pluronic F-127 (Figure 3.16(c)), a detergent commonly used in biological imaging for preparing aqueous solutions of poorly soluble dyes, was added to the dye solutions. Such an amphiphile in large concentration would reduce the likelihood of dye-dye interactions by

[c]The Beer-Lambert law is $A = \epsilon l C$, where A is the absorption, ϵ is the molar extinction coefficient, l is the path length and C is the concentration. A linear change in A with C at constant l was observed, implying constant ϵ.

preferentially solubilising the dye. 5 mM solutions of the dyes in DMSO were mixed with an equal volume of a 20% w/v Pluronic F-127 DMSO solution, and absorption spectra were acquired after dilution to 5 μM dye concentration. Comparison with the spectra in pure water revealed no difference, suggesting no aggregation. A further check was performed by the addition of 1% of the coordinating ligand pyridine to water, which would also be expected to break up aggregates, and little change was observed. Identical results were found for the PEG-monomer (**T2**, Scheme 3.8 on Page 119) and its free-base analogue (**T6**, Scheme 3.15 on Page 130), and it is thus concluded that there is no advantage in the length and polydispersity; four HEG chains provide ample aqueous solubility for the porphyrin monomers.

3.7.2 Aqueous studies on the porphyrin dimers

Bolamphiphilic byproduct **62** featuring two HEG-headgroups was also found to be readily soluble in water at 130 μM after brief sonication, but amphiphilic dimers **T3** and **63** yielded only slightly coloured solutions after extensive sonication in pure water. To access aqueous solutions of **T3** and **63**, 3 mM DMSO solutions were diluted to 30 μM with water; no precipitation was observed from these after 24 h. In the absorption measurements (Figure 3.17 on the following page), some broadening of the Soret band was observed for the double headgroup dimer **62** and the target dimer **T3**, but this was more pronounced for the trihexylsilyl dimer **63**. Adherence to the Beer-Lambert law was tested up to 30 μM and again linearity was observed.

Applying the same protocol as for the monomers, with Pluronic F-127 only subtle changes were found in the spectra for both the two dimers with only slightly broadened Soret bands, **62** and the target dimer **T3**, suggesting these dimers are not aggregated in water in this concentration range. However the trihexylsilyl dimer **63** with more pronounced broadening in pure water matched

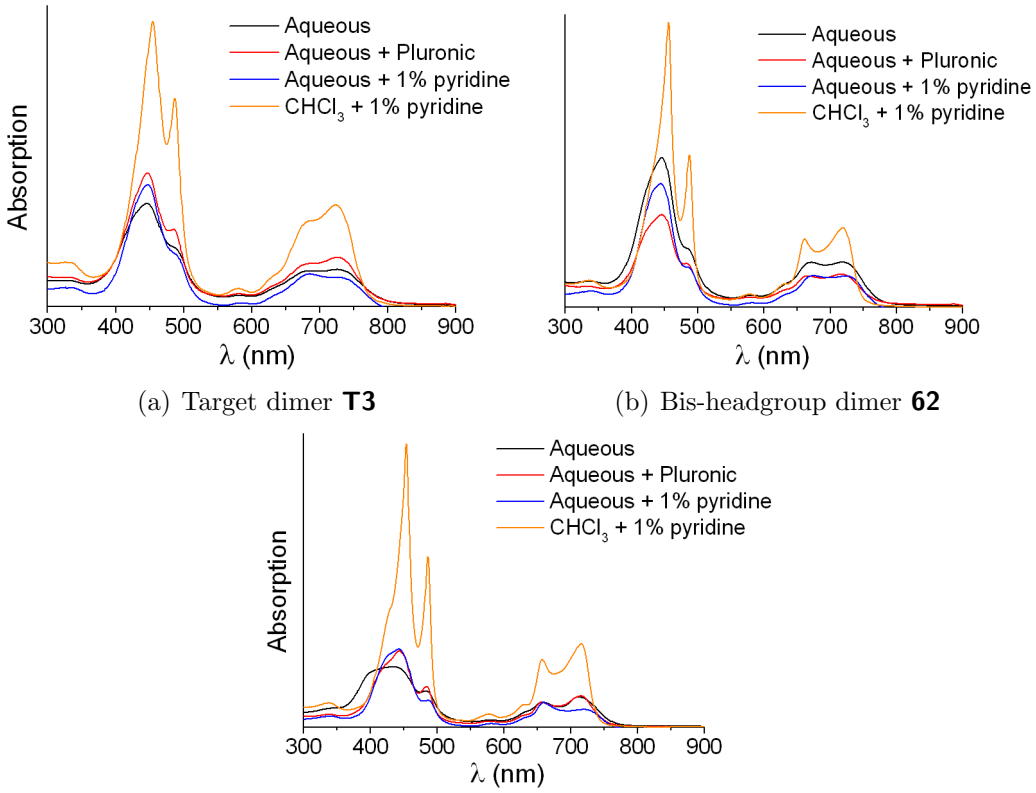

(a) Target dimer **T3**

(b) Bis-headgroup dimer **62**

(c) Trihexylsilyl dimer **63**

Figure **3.17** Comparison of the absorption spectra of the HEG dimers at 5 μM in different solvents.

the aqueous/Pluronic spectra of the other dimers in the presence of Pluronic. It was therefore concluded that this dye existed in an aggregate form across the whole concentration range of the Beer-Lambert linearity test (up to 30 μM), but that the aggregation was successfully prevented by the Pluronic detergent. This adds weight to the argument that the lack of change in the spectra of the other dyes in the presence of Pluronic is because these dyes are not aggregated to start with. As a final check, the absorption spectra were acquired in water containing 1% pyridine, and match well with the spectra in the presence of Pluronic. It is desirable to corroborate these findings against ^{1}H NMR spectra acquired in D_2O, but at such low concentrations this was not feasible.[d]

[d] ^{1}H NMR of **62** at the higher concentration of 0.8 mM in D_2O featured poorly resolved aromatic signals, indicative of aggregation.

3.8 Conclusion to Chapter 3

Novel water-soluble, amphiphilic butadiyne-linked porphyrin dimers were designed after considering literature precedence for water-solubilising porphyrins. Although the synthesis provided several challenges, an efficient synthetic route was established, particularly after the switch to monodisperse oligo(ethyleneglycol) chains was made, allowing purification to be performed more effectively. The potential adaptability of this route by the use of alternative iodoaryls adds value to its eventual elucidation. As a sensible and slight deviation from the synthesis of porphyrin dimers, novel monomers taking advantage of uncharged hydrophilic headgroups were also prepared.

The synthesised family of PEGylated and HEGylated dyes have been fully characterised and their aggregation behaviour in aqueous media studied by absorption spectroscopy. These results indicate minimal aggregation of the target dimer **T3** in the concentration range typically used for introducing dyes to cell samples.

Based on the study in Chapter 2, it is believed that these new dimeric porphyrin dyes will exhibit greater voltage-sensitivity in SHG imaging of membrane potential, and the work in this chapter is thus a significant step towards providing dyes that meet the challenging brief. In addition, the novel monomers may rectify the shortcoming in solubility of the current benchmark SHG dye **JR1**.

Collaborative studies aiming to characterise the sensitivity of these new dyes are ongoing. These include both the testing of the voltage-sensitivity under identical conditions to **JR1** in a model membrane hemispherical lipid bilayer (HLB) setup (see Figure 2.4 on Page 47), and cell viability and electrophysiological investigations. The latter tests would ideally be performed in cultured neurons and brain slices, but other cells may allow for more straightforward initial testing.

3.9 Experimental for Chapter 3

Compound numbers correspond to those used in this chapter, except those labelled 3-A, -B etc. which are not featured in the main text. Novel compounds are denoted by an asterisk (*) after the name. General experimental details can be found in Section 2.12 on Page 80.

3-A *N,N*-dioctyl-4-iodo-1-aniline

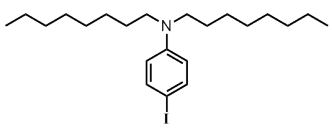

1-Iodo-4-amino-benzene (3.05 g, 13.9 mmol), *n*-octyliodide (10.0 mL, 55.4 mmol) and Na_2CO_3 (4.00 g, 37.7 mmol) were suspended in dry DMF (30 mL) in a pre-dried flask. N_2 was bubbled through for 15 mins, then the reaction was heated to 100 °C under N_2. After 21 h the reaction mixture was diluted with toluene (300 mL) and added to 200 mL of water in a separatory funnel. The organic layer was washed with water 3 ×, before being concentrated and purified on silica (eluting with 3 : 7 CH_2Cl_2 : petrol ether). The desired fractions were combined and concentrated to give the product as a pale yellow oil (5.6 g, 91%). ^{1}H NMR (200 MHz, $CDCl_3$) δ 7.42 (dt, J=9.0, 2.0 Hz, 2 H), 6.41 (dt, J=9.2, 2.2 Hz, 2 H), 3.21 (t, J=7.6 Hz, 4 H), 1.45 - 1.69 (m, 4 H), 1.13 - 1.44 (m, 20 H), 0.90 (t, J=6.5 Hz, 6 H) ^{13}C NMR (101 MHz, $CDCl_3$) δ 147.6, 137.6, 114.0, 75.3, 51.0, 31.8, 29.5, 29.3, 27.1, 27.1, 22.7, 14.1.

50 Trihexylsilyl propynal

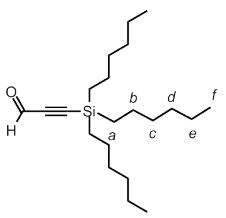

n-Butyllithium (3.0 mL, 1.6 M in hexanes, 4.9 mmol) was added dropwise to a stirring solution of **2-C** (1.5 g, 4.9 mmol) in dry THF (20 mL) in a pre-dried flask. The mixture was refluxed for 5 mins before being transferred by canula to a stirring solution of dry DMF (2.3 mL) in dry THF (20 mL) in a pre-dried flask. The reaction was refluxed for 5 mins, allowed to cool, then quenched with 1.0 M HCl (10 mL), washed with water (40 mL), extracted with Et_2O (3 × 150 mL), dried over $MgSO_4$ and concentrated to give the product as a yellow oil (1.5 g, 89%). ^{1}H NMR (200 MHz, $CDCl_3$) δ 9.18 (s, 1 H), 1.10 - 1.54 (m, 24 H, **b,c,d,e**), 0.78 - 1.00 (m, 9 H, **f**), 0.47 - 0.75 (m, 6 H, **a**). ^{13}C NMR (101 MHz, $CDCl_3$) δ 176.7, 103.5, 102.4, 33.0, 31.4, 23.7, 22.6, 14.1, 12.5.

43 Polyethyleneglycol-monomethylether tosylate

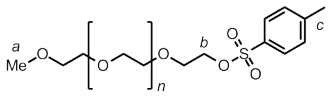

A suspension of tosyl chloride (5.0 g, 26 mmol) in dry CH_2Cl_2 (20 mL) was cooled in an ice bath. A solution of poly(ethyleneglycol) 500 methyl ether **42** (M_n = 438, M_w = 483) (10 g, 20 mmol) in CH_2Cl_2 (20 mL) and Et_3N (5.6 mL, 40 mmol) was added dropwise. The mixture was allowed to warm to room temperature and stirred. After 22 h, the mixture was poured into H_2O (50 mL) and extracted with $CHCl_3$ (600 mL). The organic layer was concentrated to give the product as a yellow/brown oil (13 g, 99%). ^{1}H NMR (400 MHz, $CDCl_3$) δ 7.80 (d, J=8.3 Hz, 2 H), 7.34 (d, J=8.3 Hz, 2 H), 4.13 - 4.18 (m, 2 H, **b**), 3.53 - 3.71 (m, 44 H), 3.38 (s, 3 H, **a**), 2.45 (s, 3 H, **c**). ^{13}C NMR (101 MHz, $CDCl_3$) δ 144.8, 133.0, 129.8, 128.0, 71.9, 70.7, 70.6, 70.6, 70.5, 69.3, 68.7, 59.1, 21.7. MALDI TOF MS shows major peaks at intervals of 44 Da, corresponding to the mass of the repeat unit. The major peaks are assigned to M+H_2O (e.g. 513 gives n=5).

44 *N,N*-bis(polyethyleneglycol-monomethylether)benzylamine

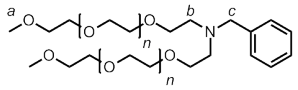

This reaction was inspired by a literature procedure.[37] Benzylamine (0.28 mL, 2.5 mmol) and MeCN (5 mL) were added to Na_2CO_3 (0.27 g, 2.5 mmol) in a two-neck flask equipped with a condensor. **43** (5.0 g, 7.6 mmol) in MeCN (5 mL) was added dropwise at room temperature and the mixture brought to reflux under N_2. After 5 d, the mixture was allowed to cool, CH_2Cl_2 (20 mL) was added, and the precipitate was filtered. The filtrate was washed with 2 M aq. HCl 5 ×. The combined aqueous layers were then basified with aq. Na_2CO_3. The product was extracted into CH_2Cl_2 3 × (until the washes no longer contained any compound visible on a TLC plate). The organic fractions from the basic extraction were dried over $MgSO_4$ and concentrated to a give the product as a brown/yellow oil (1.5 g, 54%). The product contained <10% impurity of **43**, which was carried forward. ^{1}H NMR (300 MHz, $CDCl_3$) δ 7.22 - 7.32 (m, 3 H), 7.09 - 7.20 (m, 2 H), 3.63 (s, 2 H, **c**), 3.36 - 3.61 (m, 82 H), 3.31 (s, 6 H, **a**), 2.67 (t, J=6.3 Hz, 4 H, **b**). ^{13}C NMR (75 MHz, $CDCl_3$) δ 139.8, 128.8, 128.1, 126.8, 71.9, 70.6, 70.3, 69.9, 59.7, 59.0, 53.8. MALDI TOF MS shows major peaks corresponding to the desired product at 617 (average n =3.5), 663 (average n=4), 707 (average n=4.5)...

45 *N,N*-bis(polyethyleneglycol-monomethylether)amine

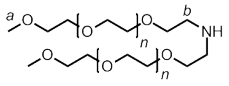

44 (1.3 g, 1.2 mmol), Pd/C (10%, 130 mg) and ethanol (absolute, 3 mL) were added to a flask and degassed thoroughly, purging first with N_2 3 × then H_2 3 ×. The reaction was stirred vigorously under baloon pressure of H_2 for 9 h, then passed through celite (eluting with ethanol), and concentrated to give the

product as a pale yellow oil (1.0 g, 84%) ^{1}H NMR (400 MHz, DMSO−d_6) δ 3.38 - 3.72 (m, 84 H), 3.23 (s, 6 H, **a**), 2.83 (t, J=5.4 Hz, 4 H, **b**) ^{13}C NMR (101 MHz, DMSO−d_6) δ 72.1, 70.6, 70.6, 70.5, 70.4, 58.9, 48.7. MALDI TOF MS shows major peaks corresponding to M+Na of the desired product at 816 (average n=6.5), 860 (average n=7)...

47 5-iodoisophthalic acid

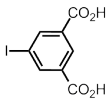

5-Aminoisophthalic acid **46** (10.9 g, 60.0 mmol) was dissolved in 80 mL 1.5 M HCl (required heating to 80 °C). The solution was cooled to 0 °C, and an aqueous solution of $NaNO_2$ (4.6 g, 66 mmol, in 60 mL) was added slowly, to maintain the temperature at 0 °C. The resulting creamy white precipitate solution was stirred at 0 °C for 30 min, after which an aqueous solution of KI (19.9 g, 120 mmol, in 60 mL) was added dropwise. The solution turned dark brown and evolution of I_2 was observed. The reaction was allowed to warm to room temperature. After 20 h, the precipitate was filtered and dried under vacuum to remove I_2. The product was recrystallised from 150 mL of hot 70 : 30 AcOH : H_2O, filtered, washed with 50 mL of cold 70 : 30 AcOH : H_2O, and dried under high vacuum. Precipitation of the product was achieved by layered addition of 10 mL 60-80 petrol ether to a hot acetone solution (50 mL), yielding 3.0 g (17%) of a pale powder. ^{1}H NMR (400 MHz, DMSO−d_6) δ 13.44 (br. s, 2 H), 8.41 (s, 3 H). ^{13}C NMR (101 MHz, DMSO−d_6) δ 166.1, 142.3, 134.0, 130.0, 95.7.

49 5-iodo-(*N,N*-bis(polyethyleneglycol-monomethylether))-isophthalamide*

47 (0.50 g, 1.7 mmol) was refluxed in $SOCl_2$ (15.0 mL, 207 mmol) for 16 h to form **48**. $SOCl_2$ was removed on a rotavapor and the brown/red oily residue

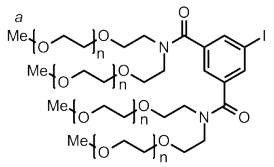

dried under high vacuum for several hours. The oil was stored under N_2 and used within 24 h. 180 mg (0.45 mmol) of the oil was dissolved in THF (3 mL) and added dropwise to a solution of **45** (1.0 g, 0.99 mmol) in THF (3 mL) and NEt_3 (140 μL, 0.99 mmol) at 0 °C. The reaction was stirred at room temperature for 17 h, then concentrated. The crude residue was dissolved in CH_2Cl_2, washed with 2.0 M HCl and extracted with CH_2Cl_2. The organic layers were dried over $MgSO_4$ and concentrated to give the desired product in 90% purity by NMR (1.0 g, 81%). Size-exclusion chromatography used to remove trace impurities of the mono-substituted amine product to yield 0.68 g of the desired product (66 %). ^{1}H NMR (400 MHz, DMSO−d_6) δ 7.76 (s, 2 H), 7.34 (s, 1 H), 3.30 - 3.71 (m, 194 H), 3.25 (s, 12 H). ^{13}C NMR (101 MHz, DMSO−d_6) δ 169.2, 139.4, 136.1, 124.7, 94.7, 71.8, 70.3, 70.1, 68.3, 68.1, 58.5, 49.4, 44.5. MALDI TOF MS shows major peaks corresponding to M+Na of the desired product at 2264 (average n=9.75), 2308 (average n=10).

52 Zinc 5,15-bis-trihexylsilyl-ethynyl-porphyrin

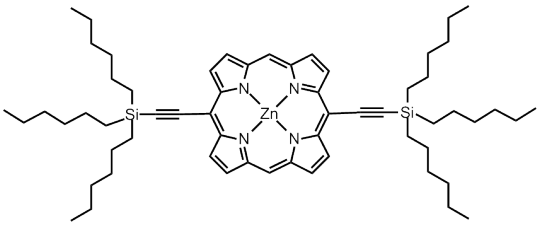

Dipyrromethane (632 mg, 4.32 mmol) was dried under vacuum in the reaction vessel for 1 h, then CH_2Cl_2 (245 mL) and **50** (1.45 g, 4.32 mmol) were added under N_2. The mixture was freeze-pump-thaw degassed thoroughly then $BF_3 \cdot OEt_2$ (0.18 mL, 1.5 mmol) was added *via* syringe. The reaction was

stirred for 45 mins in the dark at room temperature. DDQ (1.47 g, 6.46 mmol) was added and the reaction stirred for 10 mins under air before concentrating and passing through a silica plug, eluting with CH_2Cl_2. The crude mixture was concentrated and redissolved in $CHCl_3$ (200 mL). $Zn(OAc)_2 \cdot 2\,H_2O$ (2.30 g, 10.8 mmol) was dissolved in MeOH, and this was added to the porphyrin solution. The reaction was stirred for 2 h, before concentrating and passing through a silica plug, eluting with CH_2Cl_2. The mixture was concentrated to give **52** as a dark green sticky solid (0.74 g, 35%). ^{1}H NMR (200 MHz, $CDCl_3$: 1 % d_5−pyridine) δ 10.07 (s, 2 H, **meso-H**), 9.78 (d, J=4.4 Hz, 4 H, β-**H**), 9.31 (d, J=4.4 Hz, 4 H, β-**H**), 1.69 - 1.91 (m, 13 H), 1.50 - 1.68 (m, 14 H), 1.36 - 1.50 (m, 25 H), 0.99 - 1.13 (m, 13 H), 0.93 (t, J=6.9 Hz, 18 H). ^{13}C NMR (101 MHz, $CDCl_3$: 1 % d_5−pyridine) δ 152.3, 149.5, 132.0, 131.5, 109.3, 107.5, 99.8, 99.1, 33.4, 31.7, 24.4, 22.7, 14.2, 13.9. MS Calcd for $C_{60}H_{88}N_4Si_2Zn$: 985.59. Found (MALDI TOF+): 985.33.

39 Zinc 5-ethynyl-15-trihexylsilyl-ethynyl-porphyrin

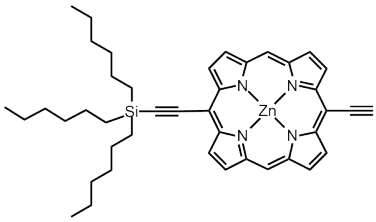

$Bu_4N^+F^-$ (1.0 M solution in THF, 0.61 mL, 0.61 mmol) was added to a solution of **52** (0.60 mg, 0.61 mmol) in 1 : 1 $CHCl_3$: CH_2Cl_2 (60 mL) and the reaction mixture stirred at room temperature under N_2. The progress was monitored carefully by TLC until the starting material and mono-deprotected product (R_f 0.75 and 0.50 respectively, 10 : 1 : 1 petrol ether : ethyl acetate : pyridine) were in roughly equal ratio (26 minutes), then (35 μL, 0.61 mmol) was added. The reaction mixture was passed immediately through a short silica gel plug ($CHCl_3$). Chromatography on silica gel (4 : 1 through 2 : 3 petrol : CH_2Cl_2)

gave starting material (200 mg, 33%), the desired product (129 mg, 30%) and the doubly-deprotected byproduct. ^{1}H NMR (400 MHz, $CDCl_3$: 1 % d_5−pyridine) δ 10.03 (s, 2 H, **meso-H**), 9.83 (d, J=4.5 Hz, 2 H, β-**H**), 9.75 (d, J=4.3 Hz, 2 H, β-**H**), 9.31 (d, J=4.3 Hz, 2 H, β-**H**), 9.28 (d, J=4.3 Hz, 2 H, β-**H**), 4.19 (s, 1 H, , **acetylenic**), 1.82 - 1.94 (m, 6 H), 1.59 - 1.69 (m, 6 H), 1.39 - 1.56 (m, 12 H), 1.07 - 1.17 (m, 6 H), 0.99 (t, J=6.8 Hz, 9 H). ^{13}C NMR (101 MHz, $CDCl_3$: 1 % d_5−pyridine) δ 152.2, 152.2, 149.5, 149.4, 132.3, 132.1, 131.5, 131.2, 109.3, 107.4, 100.0, 99.3, 97.8, 86.7, 83.0, 33.5, 31.8, 24.5, 22.8, 14.3, 14.0. MS Calcd for $C_{42}H_{50}N_4SiZn$: 703.32. Found (MALDI TOF+): 703.19.

54 Zinc 5-(*N,N*-di-*n*-octyl-4-aniline)-ethynyl-15-trihexylsilyl-ethynyl-porphyrin

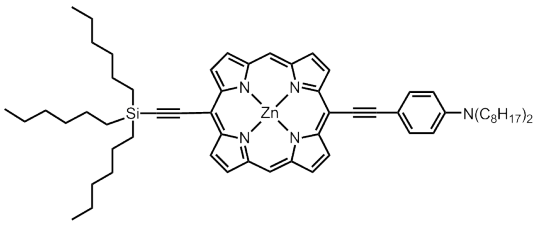

To a pre-dried schlenk tube were added **39** (126 mg, 179 μmol), tris-(dibenzylideneacetone)-di-palladium(0) (16 mg, 18 μmol), PPh_3 (19 mg, 72 μmol) and CuI (3.4 mg, 18 μmol). These were dried under vacuum for 30 mins, then the flask purged with N_2 to allow addition of THF (4 mL), iPr$_2$NH (4 mL) and **3-A** (794 mg, 1.08 mmol). The mixture was freeze-pump-thaw degassed 3 × and then heated to 50 °C under N_2. After 90 mins, the reaction was passed through a silica plug, eluting with CH_2Cl_2 : 1% pyridine, concentrated then the residue purified on silica, eluting with 20 : 1 : 1 petrol : ethyl acetate : pyridine. After precipitation from layered addition of MeOH to a CH_2Cl_2 solution of the compound, a green powder was obtained by filtration (0.11 g, 62%). ^{1}H NMR (400 MHz, $CDCl_3$: 1 % d_5−pyridine) δ 9.86 (s, 2 H, **meso-H**), 9.72 (d, J=4.4

Hz, 2 H, β-**H**), 9.64 (d, J=4.4 Hz, 2 H, β-**H**), 9.15 (dd, J=4.4, 2.0 Hz, 4 H, β-**H**), 7.78 (d, J=8.8 Hz, 2 H, **Aniline**), 6.64 (d, J=8.8 Hz, 2 H, **Aniline**), 3.18 (t, J=7.8 Hz, 4 H, **N-CH$_2$**), 1.67 - 1.78 (m, 6 H), 1.43 - 1.56 (m, 11 H), 1.27 - 1.40 (m, 13 H), 1.15 - 1.25 (m, 22 H), 0.93 - 1.00 (m, 7 H), 0.78 - 0.88 (m, 15 H). ^{13}C NMR (101 MHz, $CDCl_3$: 1 % d_5−pyridine) δ 152.7, 151.7, 149.3, 149.2, 148.2, 133.1, 132.1, 131.7, 131.3, 131.2, 111.6, 109.9, 109.7, 107.5, 102.3, 98.9, 98.7, 98.2, 91.2, 51.1, 33.5, 32.0, 31.8, 29.6, 29.4, 27.4, 27.3, 24.5, 22.8, 22.8, 14.3, 14.2, 14.1. MS Calcd for $C_{64}H_{87}N_5SiZn$: 1018.61. Found (MALDI TOF+): 1018.38.

T2 Zinc 5-(*N,N*-di-*n*-octyl-4-aniline)-ethynyl-15-(4-ethynyl-(*N,N*-bis(polyethyleneglycol-monomethylether))-isophthalamide)-porphyrin*

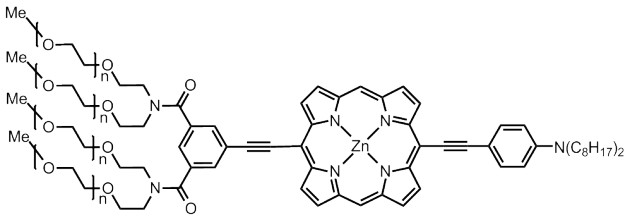

To a pre-dried schlenk tube were added **54** (55 mg, 54 μmol), **49** (124 mg, 54 μmol) tris-(dibenzylideneacetone)-di-palladium(0) (5.0 mg, 5.4 μmol), PPh_3 (5.8 mg, 22 μmol) and CuI (1.0 mg, 5.4 μmol). These were dried under vacuum for 30 mins, then the flask purged with N_2 to allow addition of THF (1.8 mL) and iPr$_2$NH (1.8 mL). The mixture was freeze-pump-thaw degassed 3 ×, then $Bu_4N^+F^-$ (1.0 M solution in THF, 0.54 mL, 0.54 mmol) was added and the reaction heated to 50 °C under N_2. After 17 h, the reaction was concentrated and initial purification was carried out by column chromatography on silica, eluting with $CHCl_3$: MeOH 0-5%. The polar fractions were then further purified by size-exclusion chromatography ($CHCl_3$). 55 mg (35%) of the desired product was isolated after drying. ^{1}H NMR (400 MHz, $CDCl_3$: 1 % d_5−pyridine) δ 9.98 (s, 2 H, **meso-H**), 9.78 (d, J=4.4 Hz, 2 H, β-**H**), 9.70 (d, J=4.4 Hz, 2 H, β-**H**),

9.25 (d, J=4.4 Hz, 2 H, β-**H**), 9.23 (d, J=4.4 Hz, 2 H, β-**H**), 8.06 (d, J=1.7 Hz, 2 H, **Aryl-ortho**), 7.84 (d, J=9.0 Hz, 2 H, **Aniline**), 7.43 - 7.47 (m, 1 H, **Aryl-para**), 6.74 (d, J=9.0 Hz, 2 H, **Aniline**), 3.19 - 3.89 (m, 198 H, **PEG, N-CH_2-C_7H_{15}, O-CH_3**), 1.63 (t, J=7.8 Hz, 4 H), 1.19 - 1.41 (m, 22 H), 0.85 (t, J=6.8 Hz, 6 H). ^{13}C NMR (126 MHz, $CDCl_3$: 1 % d_5−pyridine) δ 170.9, 152.1, 151.7, 149.2, 149.2, 148.2, 137.7, 133.0, 132.4, 131.8, 131.4, 130.8, 130.5, 125.0, 124.7, 111.5, 109.6, 107.7, 102.8, 98.4, 97.6, 94.9, 94.2, 91.0, 71.9, 70.5, 70.5, 70.3, 70.3, 70.2, 69.2, 69.0, 59.0, 51.1, 49.9, 45.3, 31.8, 29.5, 29.3, 27.3, 27.2, 22.7, 14.1. MALDI TOF MS shows major peaks corresponding to M+Na of the desired product, with a maximum at 2740 (average n=10). λ_{max}/nm (log ϵ) in $CHCl_3$: 1 % pyridine: 443 (5.33) 663 (4.93).

40 Zinc 10,20-trihexylsilyl-ethynyl-porphyrin dimer*

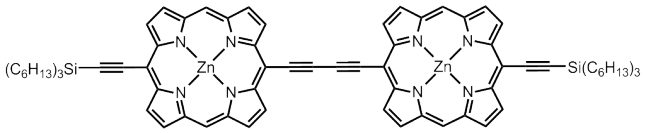

39 (30 mg, 43 μmol), $Pd(PPh_3)_2Cl_2$ (2.0 mg, 2.9 μmol), CuI (3.8 mg, 20 μmol) and 1,4-benzoquinone (8.9 mg, 82 μmol) were dried under vacuum in a pre-dried flask. THF (4 mL) and iPr$_2$NH (1 mL) were added, and the mixture stirred at room temperature for 90 mins. The mixture was then passed through a plug of silica, eluting with $CHCl_3$: 1% pyridine. After concentrating, the product was precipitated by layered addition of MeOH to a CH_2Cl_2 solution of the crude residue, to yield **40** as a dark green powder (28 mg, 93 %). ^{1}H NMR (400 MHz, d_8−THF : 5 % d_5−pyridine) δ 10.28 (s, 4 H, **meso-H**), 10.09 (d, J=4.3 Hz, 4 H, β-**H**), 9.85 (d, J=4.3 Hz, 4 H, β-**H**), 9.55 (d, J=4.3 Hz, 4 H, β-**H**), 9.45 (d, J=4.5 Hz, 4 H, β-**H**), 1.89 - 2.00 (m, 12 H), 1.64 - 1.73 (m, 12 H), 1.43 - 1.60 (m, 24 H), 1.14 - 1.21 (m, 12 H), 1.01 (t, J=7.1 Hz, 18 H). ^{13}C NMR (126 MHz, d_8−THF : 5 % d_5−pyridine) δ 153.0, 152.3, 149.9, 149.6,

132.7, 132.1, 131.2, 130.8, 109.5, 108.1, 100.3, 98.8, 98.1, 87.8, 81.7, 33.4, 31.7, 24.5, 22.7, 13.8, 13.6. MS Calcd for $C_{84}H_{98}N_8Si_2Zn_2$: 1406.60. Found (MALDI TOF+): 1407.26.

59 *N,N*-bis(hexaethyleneglycol-monomethylether)-benzylamine*

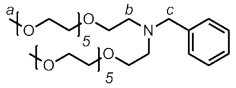

Hexaethyleneglycol-monomethylether tosylate **58** (0.90 g, 2.0 mmol), Na_2CO_3 (0.21 g, 2.0 mmol) and acetonitrile (3.0 mL) were added to a flask fitted with a condensor. Benzylamine (98 μL, 0.93 mmol) was added and the mixture stirred vigorously at reflux for 48 h. The mixture was allowed to cool and the precipitate filtered. The filtrate was concentrated then dissolved in CH_2Cl_2 (6 mL). This organic phase was washed 5 × with water / 2 M aq. HCl, with the pH maintained <2. The combined aqueous washings were then basified by addition of solid Na_2CO_3 until the pH >10. The product was extracted from the aqueous phase with 5 × 12 mL CH_2Cl_2. The washings were dried over $MgSO_4$ and concentrated to give the product as a brown/yellow oil (440 mg, 71 % with respect to benzylamine). ^{1}H NMR (400 MHz, $CDCl_3$) δ 7.11 - 7.30 (m, 5 H), 3.63 (s, 2 H, ***c***), 3.45 - 3.62 (m, 44 H), 3.31 (s, 6 H, ***a***), 2.67 (t, J=6.2 Hz, 4 H, ***b***). ^{13}C NMR (101 MHz, $CDCl_3$) δ 139.5, 128.9, 128.1, 126.9, 71.9, 71.3, 70.6, 70.5, 70.5, 70.3, 69.8, 59.7, 59.0, 53.8. MS Calcd for $C_{33}H_{61}NO_{12}$ (M + Na): 686.4086. Found (ESI TOF+): 686.4065.

60 *N,N*-bis(hexaethyleneglycol-monomethylether)-amine*

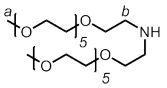

59 (440 mg, 0.66 mmol) and ethanol (3.0 mL) were added to a flask and pump-purge degassed with N_2 3 ×. 10% Pd/C (88 mg) was added under N_2, and the

vessel was pump-purge degassed with H_2 3 ×. The reaction was vigorously stirred for 3 days, monitoring by ESI-MS. The completed reaction was purged with N_2 then passed through a pad of celtie, eluting with 2-propanol. The solution was concentrated to yield a brown/yellow oil (340 mg, 90%). ^{1}H NMR (400 MHz, $CDCl_3$) δ 3.51 - 3.69 (m, 44 H), 3.37 (s, 6 H, ***a***), 2.84 (t, J=5.4 Hz, 4 H, ***b***) ^{13}C NMR (75 MHz, $CDCl_3$) δ 71.9, 70.6, 70.5, 70.3, 59.1, 59.0, 49.1. MS Calcd for $C_{26}H_{55}NO_{12}$ (M + Na): 574.3797. Found (ESI TOF+): 574.3781.

61 4-iodo-(*N,N*-bis(hexaethyleneglycol-monomethylether))-isophthalamide*

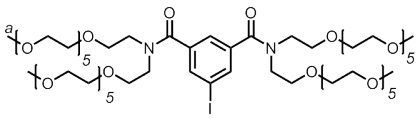

47 (73 mg, 0.25 mmol) was refluxed in $SOCl_2$ (2.2 mL, 30 mmol) for 16 h. $SOCl_2$ was removed on a rotavapor and the brown/red oily residue dried under high vacuum for 2 h. The oil was stored under N_2 and used within 24 h. A solution of the freshly prepared *p*-iodoisophthaloyl dichloride (81 mg, 0.25 mmol) in THF (1.7 mL) was added dropwise to a solution of **60** (340 mg, 0.59 mmol) in THF (1.7 mL) and triethylamine (83 μL, 0.59 mmol) at 0 °C. The mixture was allowed to warm to room temperature and stirred for 3 h before the precipitate was filtered. The filtrate was concentrated and then dissolved in CH_2Cl_2 (3 mL), washed with 1 M aq. HCl (3 × 3 mL) then 1 M aq. Na_2CO_3 (3 × 3 mL), dried over $MgSO_4$ and filtered. The solution was concentrated to give a crude yellow oil which was purified using size-exclusion chromatography (planned removal of trace hexaethyleneglycol monomethyl ether tosylate), yielding 0.26 g (73%). ^{1}H NMR (400 MHz, $CDCl_3$) δ 7.74 (d, J=1.2 Hz, 2 H), 7.31 (t, J=1.2 Hz, 1 H), 3.36 - 3.72 (m, 96 H), 3.31 (s, 12 H) ^{13}C NMR (101 MHz, $CDCl_3$) δ 169.7, 138.8, 136.5, 124.7, 93.6, 71.9, 70.6, 70.5, 70.4, 69.1,

68.6, 59.0, 49.8, 45.0. MS Calcd for $C_{60}H_{111}IN_2O_{26}$ (M + 2Na)^2+: 724.3127. Found (ESI TOF+): 724.3110.

T4 Zinc 5-(*N,N*-di-*n*-octyl-4-aniline)-ethynyl-15-(4-ethynyl-(*N,N* bis(hexaethyleneglycol-monomethylether))-isophthalamide)-porphyrin*

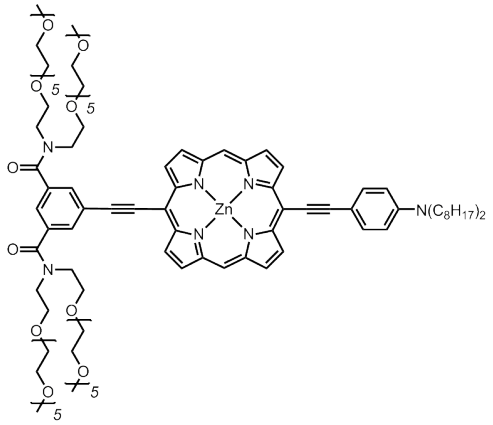

To a pre-dried schlenk tube were added **54** (25 mg, 25 μmol), **61** (35 mg, 25 μmol), $Pd(PPh_3)_4$ (2.9 mg, 2.5 μmol) and CuI (0.5 mg, 3 μmol). These were dried under vacuum for 30 mins, then the flask purged with N_2 to allow addition of THF (1 mL) and iPr$_2$NH (1 mL). The mixture was freeze-pump-thaw degassed 3 ×, then $Bu_4N^+F^-$ (1.0 M solution in THF, 0.25 mL, 0.25 mmol) was added and the reaction heated to 50 °C under N_2. After 2 h, the reaction was passed through a column of silica, eluting with THF : 1% pyridine then $CHCl_3$: 10% MeOH : 1% pyridine. The crude mixture was concentrated and purified by size-exclusion chromatography ($CHCl_3$). 25 mg (50%) of the desired product was isolated as a green solid after drying. ^{1}H NMR (400 MHz, $CDCl_3$) δ 10.05 (s, 2 H, **meso-H**), 9.85 (d, J=4.3 Hz, 2 H, β-**H**), 9.78 (d, J=4.5 Hz, 2 H, β-**H**), 9.33 (d, J=4.5 Hz, 2 H, β-**H**), 9.31 (d, J=4.3 Hz, 2 H, β-**H**), 8.14 (d, J=1.5 Hz, 2 H, **Ar-ortho-H**), 7.91 (d, J=8.8 Hz, 2 H, **aniline-H**), 7.52 (t, J=1.5 Hz, 1 H, **Ar-para-H**), 6.82 (d, J=9.1 Hz, 2 H, **aniline**), 3.10 - 3.93 (m, 112 H, **HEG, N-*CH*$_2$-C$_7$H$_{15}$, O-CH$_3$**), 1.29 - 1.44 (m, 20 H), 0.93 (t, J=6.3 Hz, 6 H). ^{13}C NMR (126 MHz, $CDCl_3$: 1 % d_5−pyridine) δ 170.9, 152.1, 151.8, 149.2,

148.2, 137.7, 133.0, 132.4, 131.8, 131.4, 130.8, 130.5, 125.0, 124.7, 111.5, 109.6, 107.7, 102.8, 98.4, 97.6, 94.9, 94.2, 91.0, 71.8, 71.8, 70.6, 70.5, 70.3, 70.2, 70.2, 69.2, 69.0, 59.0, 58.9, 51.1, 49.9, 45.3, 31.8, 29.5, 29.3, 27.3, 27.2, 22.7, 14.1. MS Calcd for $C_{106}H_{159}N_7O_{26}Zn$ (M + Na): 2035.05. Found (MALDI TOF+): 2034.94. λ_{max}/nm (log ϵ) in $CHCl_3$: 1 % pyridine: 443 (5.22) 662 (4.82).

62 Zinc 10,20-bis-(4-ethynyl-(*N,N*-bis(hexaethyleneglycol-monomethylether))-isophthalamide)-porphyrin dimer*

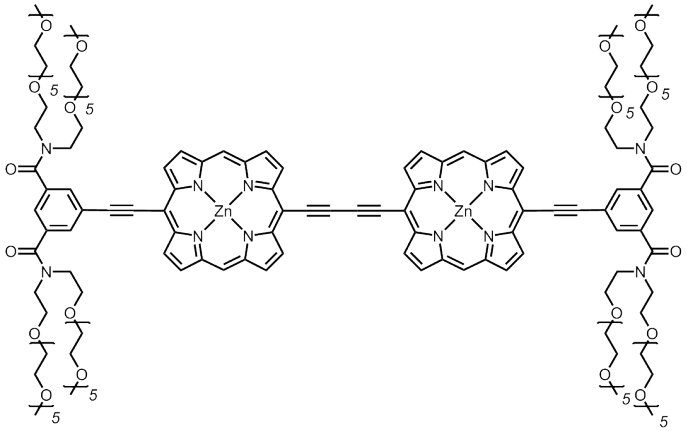

This compound was isolated in 8% yield from the procedure below. ^{1}H NMR (400 MHz, d_8−THF : 1 % d_5−pyridine) δ 10.16 (s, 4 H, **meso-H**), 9.95 (d, J=4.4 Hz, 4 H, β-**H**), 9.84 (d, J=4.4 Hz, 4 H, β-**H**), 9.42 (d, J=4.4 Hz, 4 H, β-**H**), 9.35 (d, J=4.4 Hz, 4 H, β-**H**), 8.12 (d, J=1.1 Hz, 4 H, **Ar-ortho-H**), 7.53 - 7.55 (m, 2 H, **Ar-para-H**), 3.09 - 3.81 (m, 216 H, **HEG**). ^{13}C NMR (126 MHz, $CDCl_3$: 1 % d_5−pyridine) δ 169.9, 152.2, 150.9, 148.7, 148.5, 136.8, 131.8, 131.5, 130.4, 130.3, 129.7, 124.0, 123.8, 107.4, 98.6, 97.7, 93.9, 93.6, 87.1, 81.2, 70.9, 70.8, 69.6, 69.5, 69.5, 69.5, 69.4, 69.3, 69.3, 68.2, 68.0, 58.0, 52.4, 48.9, 44.3. MS Calcd for $C_{168}H_{242}N_{12}O_{52}Zn_2Na$ (M + Na): 3415.52. Found (MALDI TOF+): 3413.14. λ_{max}/nm (log ϵ) in $CHCl_3$: 1 % pyridine: 455 (5.58) 487 (5.31) 578 (4.26) 631 (4.51) 661 (4.96) 719 (5.03).

63 Zinc 10-(4-ethynyl-(*N,N*-bis(hexaethyleneglycol-monomethylether))-isophthalamide),20-trihexylsilyl-ethynyl-porphyrin dimer*

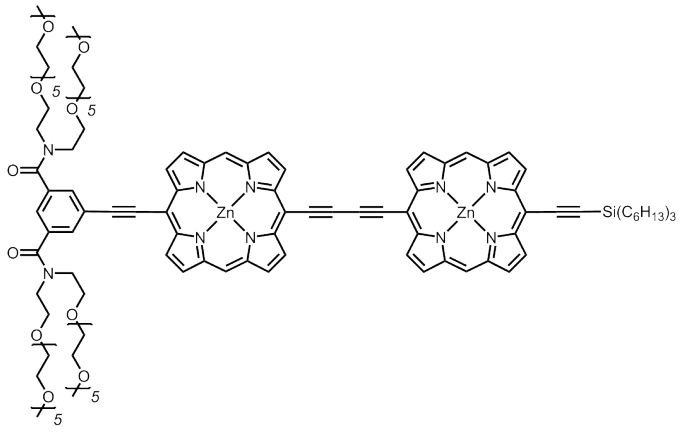

40 (38 mg, 27 μmol) was dissolved in $CHCl_3$ (5.7 mL), CH_2Cl_2 (5.7 mL) and pyridine (0.11 mL). $Bu_4N^+F^-$ (1.0 M in THF, 27 μL, 27 μmol) was added, and the reaction was stirred and carefully monitored by TLC (5 : 1 : 1 petrol ether : ethyl acetate : pyridine, mono desilylated product R_f=0.4) until the desired ratio was achieved. After 30 mins, the reaction was passed through a plug of silica, eluting with $CHCl_3$: 1% pyridine. The crude mixture was concentrated and the molar ratio of deprotected acetylene to porphyrin was measured by NMR (integration of singlet at 4.7 ppm (0.66 H) vs. meso proton at 10.2 (4 H), d8-THF : 1% d5-pyridine). The crude mixture was transferred to a schlenk tube and dried under vacuum for 30 mins. The flask was purged with N_2 and then **61** (27 mg, 19 μmol, 0.7 eq.), $Pd(PPh_3)_4$ (6.3 mg, 5.4 μmol) and CuI (1.0 mg, 5.4 μmol) were added. THF (1.8 mL) and iPr$_2$NH (1.8 mL) were added under N_2, and the mixture was freeze-pump-thaw degassed 3 $\times$ before the reaction was heated to 50 °C under N_2 for 2 h, after which the mono deprotected intermediate was no longer seen by TLC. The mixture was concentrated and the initial purification was performed on silica, eluting the unreacted starting material with $CHCl_3$: 1% pyridine then the asymmetric product with 5% MeOH and the symmetric product with 10% MeOH. The two products were then purified further using size-exclusion chromatography (eluting with $CHCl_3$: 1% pyridine). The products were precipitated by the

addition of 60-80 petrol ether to a CH_2Cl_2 solution, followed by careful removal of the CH_2Cl_2 on a rotary evaporator and addition of pentane, to give the product as a film on the flask. The title compound was isolated in 24% yield (16 mg). ^{1}H NMR (400 MHz, d_8−THF : 1 % d_5−pyridine) δ 10.17 (s, 2 H, **meso-H**), 10.16 (s, 2 H, **meso-H**), 9.96 (d, J=4.3 Hz, 4 H, **2** β-**H**), 9.86 (d, J=4.5 Hz, 2 H, β-**H**), 9.72 (d, J=4.5 Hz, 2 H, β-**H**), 9.43 (dd, J=4.3, 2.0 Hz, 4 H, **2** β-**H**), 9.37 (d, J=4.3 Hz, 2 H, β-**H**), 9.31 (d, J=4.5 Hz, 2 H, β-**H**), 8.14 (d, J=1.5 Hz, 2 H, **Ar-ortho-H**), 7.56 (t, J=1.5 Hz, 1 H, **Ar-para-H**), 3.26 - 3.83 (m, 114 H, **HEG**), 3.12 - 3.17 (s, 12 H, **O-CH$_3$**), 1.75 - 1.86 (m, 6 H), 1.50 - 1.60 (m, 6 H), 1.28 - 1.46 (m, 12 H), 1.00 - 1.07 (m, 6 H), 0.87 (t, J=7.1 Hz, 9 H). ^{13}C NMR (126 MHz, d_8−THF : 1 % d_5−pyridine) δ 170.7, 153.8, 153.8, 153.0, 152.8, 150.7, 150.4, 150.4, 139.2, 133.5, 133.5, 133.2, 132.9, 132.1, 132.0, 131.6, 131.1, 126.7, 124.7, 110.2, 109.0, 108.8, 101.1, 100.9, 99.6, 98.8, 96.2, 94.5, 88.6, 82.5, 82.5, 72.7, 71.4, 71.3, 71.3, 71.1, 58.7, 34.2, 32.5, 25.2, 23.4, 14.5, 14.4 (98.8 and 82.5 are for 2 x alkyne by integration). MS Calcd for $C_{126}H_{170}N_{10}O_{26}SiZn_2$ (M + Na): 2423.06. Found (MALDI TOF+): 2423.49. λ_{max}/nm (log ϵ) in $CHCl_3$: 1 % pyridine: 454 (5.75) 485 (5.53) 577 (4.41) 630 (4.64) 657 (5.12) 715 (5.22).

T3 Zinc 10-(4-ethynyl-(*N*,*N*-bis(hexaethyleneglycol-monomethyl-ether))-isophthalamide),20-(*N*,*N*-di-*n*-octyl-4-aniline)-ethynyl-porphyrin dimer*

63 (6 mg, 2.5 μmol) was dried in a schlenk tube. Aniline **3-A** (11 mg, 25 μmol), $Pd(PPh_3)_4$ (0.6 mg, 0.5 μmol) and CuI (0.1 mg, μmol) were added under N_2, followed by THF (0.4 mL) and iPr$_2$NH (0.4 mL). The mixture was freeze-pump-thaw degassed 3 × then $Bu_4N^+F^-$ (1.0 M in THF, 10 μL, 10 μmol) was added. The reaction was stirred at room temperature for 90 min then passed through a long plug of silica without concentrating first, eluting with $CHCl_3$: 1% pyridine to remove the excess aniline followed by the addition of 5% MeOH to elute the product. Trace impurities related to the catalyst were removed by

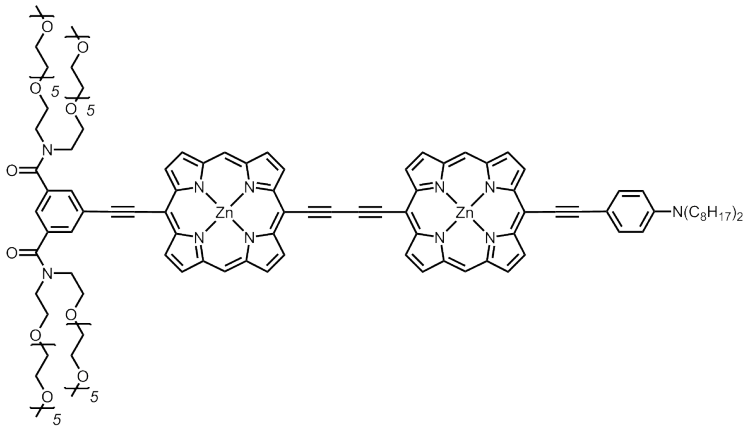

using a size exclusion column, eluting with $CHCl_3$: 1% pyridine. The product was precipitated by the addition of pentane to a CH_2Cl_2 solution, to give the product as a film on the flask (4.5 mg, 74%). ^{1}H NMR (400 MHz, d_8−THF) δ 10.24 (s, 2 H, **meso-H**), 10.15 (s, 2 H, **meso-H**), 10.03 (d, J=4.4 Hz, 2 H, β-**H**), 9.97 (d, J=4.4 Hz, 2 H, β-**H**), 9.92 (d, J=4.4 Hz, 2 H, β-**H**), 9.83 (d, J=4.4 Hz, 2 H, β-**H**), 9.51 (d, J=4.3 Hz, 2 H, β-**H**), 9.46 (d, J=4.4 Hz, 2 H, β-**H**), 9.44 (d, J=4.6 Hz, 2 H, β-**H**), 9.34 (d, J=4.4 Hz, 2 H, β-**H**), 8.20 (d, J=1.4 Hz, 2 H, **Ar-ortho-H**), 7.89 (d, J=8.7 Hz, 2 H, **aniline-H**), 7.62 (br. s, 1 H, **Ar-para-H**), 6.87 (d, J=9.0 Hz, 2 H, **aniline-H**), 3.18 - 3.88 (m, 112 H, **HEG**), 1.29 - 1.46 (m, 22 H), 0.91 (t, J=6.7 Hz, 6 H). ^{13}C NMR (126 MHz, d_8−THF) δ 170.4, 153.7, 153.4, 152.4, 152.1, 150.3, 150.1, 150.0, 149.8, 149.5, 148.9, 138.9, 135.9, 133.3, 133.1, 132.9, 132.1, 131.8, 131.6, 131.3, 130.9, 130.9, 125.0, 124.5, 112.1, 110.3, 108.6, 108.4, 103.9, 100.5, 99.4, 98.8, 97.3, 95.9, 94.1, 91.2, 88.5, 87.9, 82.4, 81.9, 72.4, 71.1, 71.0, 70.9, 67.5, 58.5, 51.3, 32.4, 30.1, 29.9, 27.9, 27.6, 23.1, 14.0. MS Calcd for $C_{126}H_{170}N_{10}O_{26}SiZn_2$ (M + Na): 2455.07. Found (MALDI TOF+): 2452.24. λ_{max}/nm (log ϵ) in $CHCl_3$: 1 % pyridine: 454 (5.49) 486 (5.39) 580 (4.26) 631 (4.50) 682 (5.01) 725 (5.09).

T6 Free-base 5-(*N,N*-di-*n*-octyl-4-aniline)ethynyl-15-(4-ethynyl-(*N,N*-bis(polyethyleneglycol-monomethylether))-isophthalamide)-porphyrin*

T2 (10 mg, 3.4 μmol) was dissolved in $CHCl_3$ (3 mL) and the solution stirred.

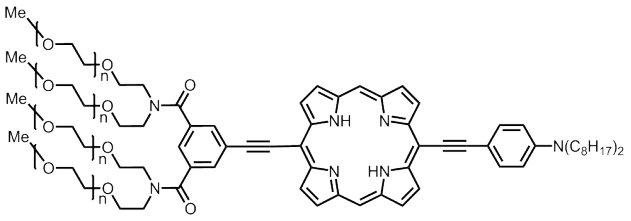

TFA (60 μL, 780 μmol) was added and the reaction stirred for 1 h, after which aq. sat. $NaHCO_3$ was added (1 mL). The product was washed with water (2 × 3 mL), extracted with $CHCl_3$ (2 × 3 mL), dried over $MgSO_4$ and concentrated. The product was precipitated as a film by addition of 60-80 petrol ether to a CH_2Cl_2 solution, followed by careful evaporation of the CH_2Cl_2 and addition of pentane, yielding 8.8 mg of clean product (91%). ^{1}H NMR (400 MHz, $CDCl_3$) δ 10.04 (s, 2 H, **meso-H**), 9.70 (d, J=4.4 Hz, 2 H, β-**H**), 9.63 (d, J=4.6 Hz, 2 H, β-**H**), 9.27 (d, J=4.7 Hz, 2 H, β-**H**), 9.24 (d, J=4.7 Hz, 2 H, β-**H**), 8.07 (d, J=1.2 Hz, 2 H, 2 H, **Ar-ortho-H**), 7.84 (d, J=8.7 Hz, 2 H, **aniline-H**), 7.47 - 7.50 (m, 1 H, **Ar-para**), 6.75 (d, J=9.0 Hz, 2 H, **aniline-H**), 3.18 - 3.85 (m, 251 H, **PEG, N-CH_2-C_7H_{15}, O-CH_3**), 1.15 - 1.39 (m, 33 H), 0.86 (t, J=6.9 Hz, 6 H), -2.30 (br. s., 2 H). ^{13}C NMR (126 MHz, $CDCl_3$) δ 169.8, 147.5, 144.2 (broad), 136.8, 132.3, 131.4, 130.6, 129.8, 129.4, 128.8, 124.2, 123.4, 110.5, 107.9, 106.1, 102.2, 99.5, 96.9, 94.4, 91.7, 88.5, 70.9, 69.5, 69.5, 69.3, 69.2, 69.2, 68.2, 67.9, 58.0, 50.1, 48.9, 44.3, 30.9, 28.5, 28.3, 26.3, 26.2, 21.7, 13.1 (peaks broadened due to exchange). MALDI TOF MS shows major peaks corresponding to M+Na of the desired product, with a maximum at 2635 (average n=9.75). λ_{max}/nm (log ϵ) in $CHCl_3$: 429 (5.22) 614 (4.78) 691 (4.68).

T5 5-(*N,N*-di-*n*-octyl-4-aniline)-ethynyl-15-(4-ethynyl-(*N,N*-bis(hexaethyleneglycol-monomethylether))-isophthalamide)-porphyrin*

T4 (10 mg, 5 μmol) was dissolved in $CHCl_3$ (4.4 mL) and the solution stirred. TFA (88 μL, 1.2 mmol) was added and the reaction stirred for 1 h, after which

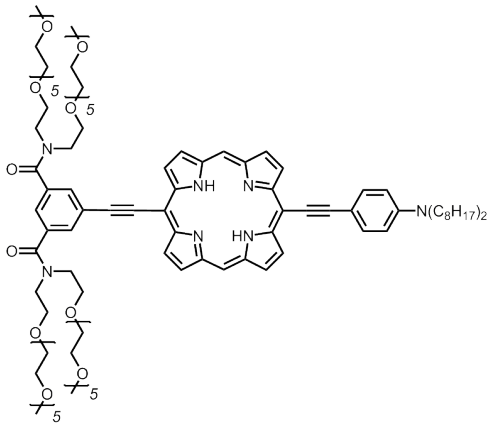

aq. sat. $NaHCO_3$ was added (2 mL). The product was washed with water (2 × 5 mL), extracted with $CHCl_3$ (2 × 5 mL), dried over $MgSO_4$ and concentrated. The product was precipitated as a film by addition of 60-80 petrol ether to a CH_2Cl_2 solution, followed by careful evaporation of the CH_2Cl_2 and addition of pentane, yielding 8.7 mg of clean product (90%). ^{1}H NMR (400 MHz, $CDCl_3$) δ 10.03 (s, 2 H, **meso-H**), 9.69 (d, J=4.4 Hz, 2 H, β-**H**), 9.63 (d, J=4.7 Hz, 2 H, β-**H**), 9.26 (d, J=4.6 Hz, 2 H, β-**H**), 9.23 (d, J=4.3 Hz, 2 H, β-**H**), 8.07 (br. s, 2 H, **Ar-ortho-H**), 7.84 (d, J=8.5 Hz, 2 H, **aniline-H**), 7.49 (s, 1 H, **Ar-para-H**), 6.76 (d, J=8.9 Hz, 2 H, **aniline-H**), 3.16 - 3.87 (m, 112 H, **HEG, N-CH_2-C_7H_{15}, O-CH_3**), 1.58 - 1.68 (m, 9 H), 1.15 - 1.38 (m, 33 H), 0.86 (t, J=6.8 Hz, 6 H), -2.32 (br. s., 2 H, **N-H**). ^{13}C NMR (126 MHz, $CDCl_3$) δ 169.8, 147.5, 144.1, 136.7, 132.3, 131.3, 130.6, 129.8, 129.4, 128.8, 124.2, 123.4, 110.5, 107.9, 106.0, 102.1, 99.4, 96.9, 94.4, 91.7, 88.5, 70.9, 70.8, 70.8, 69.6, 69.5, 69.5, 69.3, 69.3, 69.2, 68.2, 67.9, 58.0, 57.9, 52.4, 50.1, 48.9, 44.3, 30.8, 28.5, 28.3, 26.3, 26.2, 21.7, 13.1. MS Calcd for $C_{106}H_{161}N_7O_{26}Na$ (M + Na): 1972.14. Found (MALDI TOF+): 1971.77. λ_{max}/nm (log ϵ) in $CHCl_3$: 429 (5.16) 614 (4.70) 691 (4.60).

3.10 Bibliography

1 Murashima, T.; Tsujimoto, S.; Yamada, T.; Miyazawa, T.; Uno, H.; Ono, N.; Sugimoto, N. *Tetrahedron Lett.* **2005**, *46*, 113–116.

2 Zhang, X.-a.; Lovejoy, K. S.; Jasanoff, A.; Lippard, S. J. *Proc. Nat. Acad. Sci.* **2007**, *104*, 10780–10785.

3 Li, W.-S.; Aida, T. *Chem. Rev.* **2009**, *109*, 6047–6076.

4 Sadamoto, R.; Tomioka, N.; Aida, T. *J. Am. Chem. Soc.* **1996**, *118*, 3978–3979.

5 Tomioka, N.; Takasu, D.; Takahashi, T.; Aida, T. *Angew. Chem. Int. Ed.* **1998**, *37*, 1531–1534.

6 Nishiyama, N.; Stapert, H. R.; Zhang, G.-D.; Takasu, D.; Jiang, D.-L.; Nagano, T.; Aida, T.; Kataoka, K. *Bioconjugate Chem.* **2002**, *14*, 58–66.

7 Hamblin, M. R.; Miller, J. L.; Rizvi, I.; Loew, H. G.; Hasan, T. *Br. J. Cancer* **2003**, *89*, 937–943.

8 Basu, S. K.; Goldstein, J. L.; Anderson, G. W.; Brown, M. S. *Proc. Nat. Acad. Sci.* **1976**, *73*, 3178–3182.

9 Fujimoto, K.; Miyata, T.; Aoyama, Y. *J. Am. Chem. Soc.* **2000**, *122*, 3558–3559.

10 Soares, A. R.; Tom, J. P.; Neves, M. G.; Tom, A. C.; Cavaleiro, J. A.; Torres, T. *Carbohydr. Res.* **2009**, *344*, 507–510.

11 Silva, S.; Pereira, P. M. R.; Silva, P.; Almeida Paz, F. A.; Faustino, M. A. F.; Cavaleiro, J. A. S.; Tome, J. P. C. *Chem. Commun.* **2012**, *48*, 3608–3610.

12 Ballardini, R.; Colonna, B.; Gandolfi, M. T.; Kalovidouris, S. A.; Orzel, L.; Raymo, F. M.; Stoddart, J. F. *Eur. J. Org. Chem.* **2003**, 288–294.

13 Carofiglio, T.; Fornasier, R.; Gennari, G.; Lucchini, V.; Simonato, L.; Tonellato, U. *Tetrahedron Lett.* **1997**, *38*, 7919–7922.

14 Fathalla, M.; Li, S.-C.; Diebold, U.; Alb, A.; Jayawickramarajah, J. *Chem. Commun.* **2009**, 4209–4211.

15 Kiba, T.; Suzuki, H.; Hosokawa, K.; Kobayashi, H.; Baba, S.; Kakuchi, T.; Sato, S.-i. *J. Phys. Chem. B* **2009**, *113*, 11560–11563.

16 Nawalany, K.; Kozik, B.; Kępczyński, M.; Zapotoczny, S.; Kumorek, M.; Nowakowska, M.; Jachimska, B. *J. Phys. Chem. B* **2008**, *112*, 12231–12239.

17 Nawalany, K.; Rusin, A.; Kępczyński, M.; Mikhailov, A.; Kramer-Marek, G.; Śnietura, M.; Połtowicz, J.; Krawczyk, Z.; Nowakowska, M. *J. Photochem. Photobiol. B: Biol.* **2009**, *97*, 8–17.

18 Esipova, T. V.; Karagodov, A.; Miller, J.; Wilson, D. F.; Busch, T. M.; Vinogradov, S. A. *Anal. Chem.* **2011**, *83*, 8756–8765.

19 Cheng, Y.; Zhao, L.; Li, Y.; Xu, T. *Chem. Soc. Rev.* **2011**, *40*, 2673–2703.

20 Delacruz, J.; Mikulski, R.; Tu, C.; Li, Y.; Wang, H.; Shiverick, K. T.; Frost, S. C.; Horenstein, N. A.; Silverman, D. N. *Anal. Biochem.* **2010**, *403*, 74–78.

21 Hornung, R.; Fehr, M. K.; Walt, H.; Wyss, P.; Berns, M. W.; Tadir, Y.

Photochem. Photobiol. **2000**, *72*, 696–700.
22 Ueda, T.; Kitagishi, H.; Kano, K. *Org. Biomol. Chem.* **2012**, *10*, 4337–4347.
23 Sibrian-Vazquez, M.; Jensen, T. J.; Hammer, R. P.; Vicente, M. G. H. *J. Med. Chem.* **2006**, *49*, 1364–1372.
24 Lebedev, A. Y.; Cheprakov, A. V.; Sakadzic, S.; Boas, D. A.; Wilson, D. F.; Vinogradov, S. A. *ACS Appl. Mater. Interfaces* **2009**, *1*, 1292–1304.
25 Caminade, A.-M.; Hameau, A.; Majoral, J.-P. *Chem. Eur. J.* **2009**, *15*, 9270–9285.
26 Pimenta, F. M.; Jensen, R. L.; Holmegaard, L.; Esipova, T. V.; Westberg, M.; Breitenbach, T.; Ogilby, P. R. *J. Phys. Chem. B* **2012**, *116*, 10234–10246.
27 Thyagarajan, S.; Leiding, T.; rskold, S. P.; Cheprakov, A. V.; Vinogradov, S. A. *Inorg. Chem.* **2010**, *49*, 9909–9920.
28 Ceroni, P.; Lebedev, A. Y.; Marchi, E.; Yuan, M.; Esipova, T. V.; Bergamini, G.; Wilson, D. F.; Busch, T. M.; Vinogradov, S. A. *Photochem. Photobiol. Sci.* **2011**, *10*, 1056–1065.
29 Newkome, G. R.; Behera, R. K.; Moorefield, C. N.; Baker, G. R. *J. Org. Chem.* **1991**, *56*, 7162–7167.
30 Conroy, C. W.; Wynns, G. C.; Maren, T. H. *Bioorg. Chem.* **1996**, *24*, 262–272.
31 Balaz, M.; Collins, H. A.; Dahlstedt, E.; Anderson, H. L. *Org. Biomol. Chem.* **2009**, *7*, 874–888.
32 Reeve, J. E.; Collins, H. A.; Mey, K. D.; Kohl, M. M.; Thorley, K. J.; Paulsen, O.; Clays, K.; Anderson, H. L. *J. Am. Chem. Soc.* **2009**, *131*, 2758–2759.
33 Youngblood, W. J.; Gryko, D. T.; Lammi, R. K.; Bocian, D. F.; Holten, D.; Lindsey, J. S. *J. Org. Chem.* **2002**, *67*, 2111–2117.
34 Drew, S. L.; Lawrence, A. L.; Sherburn, M. S. *Angew. Chem. Int. Ed.* **2013**, *52*, 4221–4224.
35 Bandyopadhyay, A.; Varghese, B.; Sankararaman, S. *J. Org. Chem.* **2006**, *71*, 4544–4548.
36 Nath, M.; Huffman, J. C.; Zaleski, J. M. *J. Am. Chem. Soc.* **2003**, *125*, 11484–11485.
37 Selve, C.; Ravey, J.-C.; Stebe, M.-J.; El Moudjahid, C.; Moumni, E.; Delpuech, J.-J. *Tetrahedron* **1991**, *47*, 411–428.

Chapter 4: Design and synthesis of photoinduced electron transfer voltage sensors

In this chapter, the design requirements for photoinduced electron transfer (PeT) voltage sensors are outlined. From this analysis, a first generation of PeT dyes are designed, synthesised and characterised. Clear competition between PeT and fluorescence was found, as desired, and thus amphiphilic variants of the first generation were produced. Attempts to observe voltage sensitive fluorescence from the second generation have so far proved unsuccessful. Possible factors in these results are discussed. The dyes are also compared to the first literature examples of PeT voltage sensors, published after the research in this chapter was completed.

4.1 Introduction

The key problem identified with existing VSDs is poor voltage sensitivity. Electrochromic dyes have only been tweaked from their original designs in over 35 years, with limited improvement and limited scope for further improvement. FRET VS systems have inherent issues, namely capacitative loading and the necessity of introducing two sensor molecules to a cell for testing, which deter further investigations. Alongside optimising SHG dyes for IMP, this thesis concerns the pursuit of a new mechanism based on photoinduced electron transfer (PeT), introduced in Section 1.4 on Page 27. In this chapter, I outline the precedence for this mechanism, the design, synthesis and characterisation of two generations of PeT dyes, followed by the initial characterisation of their voltage sensitive fluorescence behaviour.

4.2 The PeT mechanism

PeT is a widely applied phenomenon in the field of chemical sensors, with systems designed to monitor specific ion and reagent concentrations,[1–3] pH,[4–6] and solvent polarity.[7] In all cases, the desired sensitivity is achieved by the modulation of PeT efficiency effecting a change in fluorescence intensity, due to the competition between PeT and fluorescence (Equation 1.2 on Page 28). PeT has also attracted significant interest because of its importance in nature, as scientists have sought to understand and mimic the electron transfer (eT) pathways found in the bacterial photosynthetic reaction centre.[8]

As outlined in Section 1.4 on Page 27, PeT requires an electron donor and an electron acceptor (hereafter donor or D and acceptor or A respectively), one of which must be a fluorophore.[a] PeT can occur either inter- or intra-molecularly, but fluorescent sensors benefit from the disambiguation of the donor and ac-

[a]PeT does not strictly *require* a fluorophore, but a chromophore. However, for sensing applications fluorophores are used so the fluorescence output can be monitored.

ceptor distance that an intramolecular process offers. Either a σ- or π-bonded spacer (S) can be used to achieve this. Spacers featuring greater rigidity and less conformational heterogeneity are commonly employed in PeT sensor designs; although simple alkyl chains have been used in some studies,[4,9,10] aromatic systems and alkyl rings with enforced conformations are more usual.[11–13]

The feasibility of the PeT process can be estimated by using a simplified Rehm-Weller equation:[7,14]

$$\Delta G = E_{\text{ox,donor}} - E_{\text{red,acceptor}} - E_{00} \tag{4.1}$$

ΔG is the free energy change for the PeT process, $E_{\text{ox,donor}}$ and $E_{\text{red,acceptor}}$ are the oxidation and reduction potentials respectively of the donor and acceptor, which can be measured by voltammetry, and E_{00} is the excited state energy of the fluorophore, defined as the energy of the first excited state, measured by the intersection of the normalised absorption and emission curves of the fluorophore. It is evident from Equation 4.1 that the balance between the oxidation and reduction potentials for a given fluorophore (approximately fixed E_{00}) is crucial for the PeT process of a system to have $\Delta G < 0$. The pairing up of donors and acceptors to achieve this forms part of the rational design process of a PeT system.

In solution, the rate of PeT is described by Marcus' theory, where k_{et} is related to the activation energy (ΔG^*) and ΔG by the following equations:

$$k_{\text{et}} = \rho(r) Z \exp\left(-\Delta G^*/RT\right) \tag{4.2}$$

$$\text{where } \Delta G^* = (\lambda + \Delta G)^2/4\lambda \tag{4.3}$$

The pre-exponential factor Z represents the vibrational frequency for an intramolecular eT reaction, and $\rho(r)$ is the probability of the eT step occuring,

normalised to the number of times the correct nuclear configuration is achieved. λ is the reorganisation energy of the system (solvent and solute) that accompanies the eT, R is the gas constant, T is the temperature, and the vibrations of the donor and acceptor are assumed to be well described by harmonic oscillators. A major result of the Marcus model is that ΔG^* is related to ΔG with a quadratic dependence, resulting in the 'inverted region' where the rate slows down with increasing driving force.[15–17]

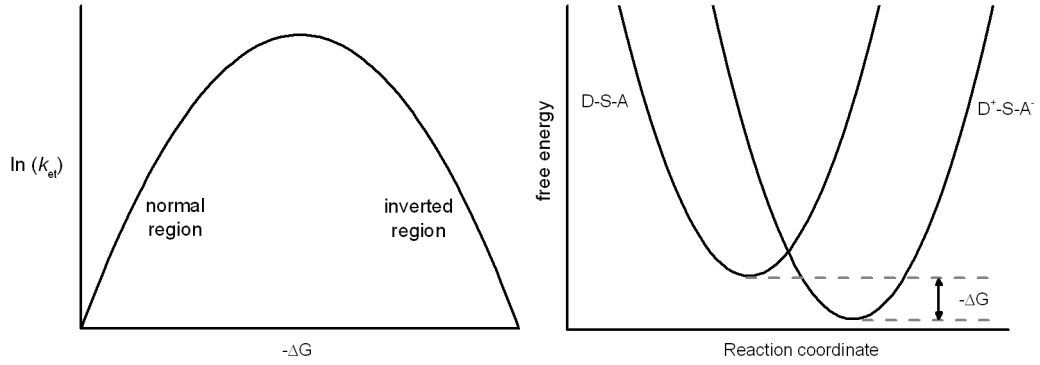

(a) Change in eT rate with free-energy. (b) A typical eT reaction profile.

Figure **4.1** The results of the Marcus model of eT.[16,17]

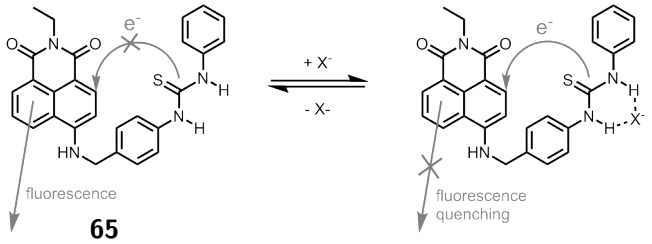

Figure **4.2** Reversible binding of certain anions to compound **65** changes the eT rate and therefore the fluorescence intensity, making **65** an ion concentration sensor.[2]

The equations outlined above can be used to explain the successful operation of PeT sensors. For example, the binding of X^- (F^-, AcO^-, $H_2PO_4^-$) to compound **65** results in decreased fluorescent output related to the concentration of X^-.[2] The oxidation potential of the thiourea binding site is decreased by the presence of an anion, thus according to Equation 4.1 ΔG will also decrease, and PeT to the 4-amino-1,8-naphthalimide fluorophore becomes more

energetically favourable. More favourable ΔG results in increased k_{et} (normal region, Figure 4.1(a)), hence compound **65** displays decreased fluorescence with increased [X^-].

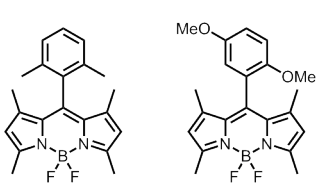

66 **67** **68**

	E_{red} (acceptor/BODIPY)	E_{ox} (donor/aromatic group)	
solvent	**66**	**67**	**68**
CH_3CN	-1.56	0.88	0.67
CH_2Cl_2	-1.76	0.89	0.64
Fluorescence 'on'	–	CH_2Cl_2	benzene
Fluorescence 'off'	–	acetone	CH_2Cl_2

Figure **4.3** The effect of solvent upon PeT is demonstrated by dyes **67** and **68** and reference dye **66**. The quoted reduction and oxidation potentials (in V *vs.* Fc/Fc^+) were measured in the solvent indicated. Fluorescence 'on' indicates the least polar solvent which prevents PeT. Fluorescence 'off' indicates the least polar solvent which allows PeT.[7]

A second example is shown in Figure 4.3, where the BODIPY dye acts as an acceptor and the appended aromatic group as a donor. The aromatic groups featured in the dyes **67** and **68** demonstrate the effect of redox potentials upon eT and thus fluorescence intensity. The increase in reduction potential for reference compound **66** from CH_2Cl_2 to CH_3CN reflects the solvent stabilisation of the charge-separated (CS) state. The different oxidation potentials of the aromatic groups of **67** and **68** imply a different driving force for eT in each of these dyes. Combining these two factors allows the eT rate to be varied as a result of changes in ΔG to allow the dyes to act as solvent polarity sensors. As these dyes have different driving forces, they each require a different solvent polarity for the eT rate to increase sufficiently to turn off the fluores-

cence. For example, the stronger electron donor of **68** (less positive oxidation potential) will be oxidised by a PeT process in all but the least polar solvents, whereas the weaker electron donor of **67** requires a more polar solvent to stabilise the CS state. These dyes come from a larger family of dyes developed to allow the solvent polarity of biological environments to be probed using their fluorescence turn on/turn off behaviour.

4.2.1 PeT and electric fields

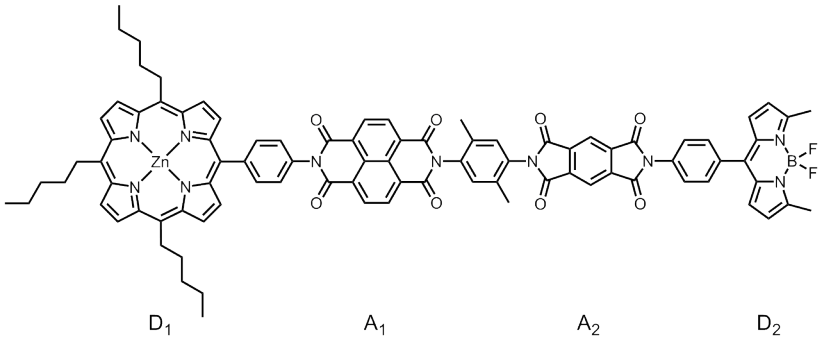

69

Figure **4.4** A four-dye system in which the excitation of D_1 leads to a CS state $D_1^+-A_1^-$ that retards the formation of a CS state in D_2-A_2 when D_2 is subsequently excited.[18]

PeT has also been used in the development of photo-activated switches, where a PeT process leads to the switching on or off of some other process. For example in Wasielewski's four-dye system **69** (Figure 4.4), formation of the CS state of the left-hand D−A pair D_1-A_1 retards the rate of formation of the CS state of the right-hand D−A pair A_2-D_2. The excitation of one dye D_1 can be used to increase the fluorescence intensity of the other dye D_2, and thus the compound acts as a photo-activated switch. This switching effect has been assigned to resulting from the effect of intramolecular electric fields upon PeT rates - the dipole created by the initial CS state changes the energy of the second PeT process and inhibits it.[18] These charge-separating tetrads and

related systems therefore provide support to the idea of sensing the changing electric field across a neuronal membrane using PeT.[8,18–22]

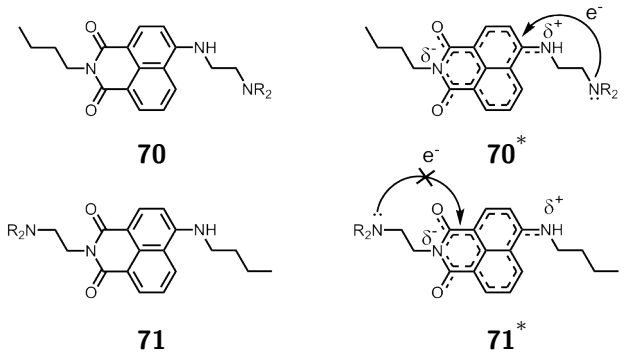

Figure **4.5** A pair of regioisomers demonstrating the effect of an intramolecular electric field upon PeT, * denoting first excited state.[4]

Intramolecular electric fields have also been proposed to explain the differences between PeT pathways within two regioisomeric small molecules which were proposed as pH sensors, in work by A. P. de Silva.[4] The distribution of charge in the excited states of compounds **70** and **71** (Figure 4.5) has an effect on the feasibility of PeT. In **70**, the transfer of the electron from the peripheral amine occurs towards the δ^+ region of the excited state. When the amine is not protonated, PeT thus occurs and the fluorophore is quenched. If the amine is protonated, its ability to act as electron donor is greatly reduced and the fluorophore is not quenched. However PeT in compound **71** is inhibited by the δ^- region of the excited state of the fluorophore, and the fluorescence intensity remains constant regardless of whether the amine is protonated or not.[4]

Further, strong electric fields established in α-helical sections of proteins have been found to be important in nature's own PeT processes. The dipole of each amino acid residue contributes to a net negative charge at the C-terminus and a net positive charge at the N-terminus, and an electric field of 10^9 V/m.[23] In one literature example the effect of this field was tested by comparing the extent of fluorescence quenching in compounds **72** and **73**, where the donor-acceptor pair is positioned such that PeT occurs either against or

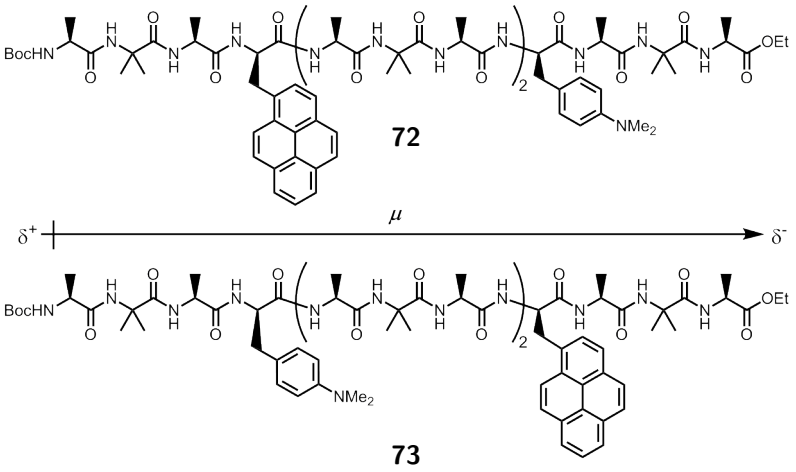

Figure **4.6** The electric field $\vec{\mu}$ generated by the peptide chain accelerates PeT in compound **72** compared to **73**.[23]

with the electric field $\vec{\mu}$ as shown (Figure 4.6). It was observed that the quantum yield and lifetime of compound **72** was reduced relative to **73**, attributable to the electric field encouraging PeT in **72**.[23] The two peptide oligomers were confirmed to adopt the same conformation in solution. Recent papers have reached similar conclusions when exploring the effect of protonation of amino acid residues on the electric field in a peptide chain.[24]

The examples in this section represent a small selection of studies into the electric field sensitivity of PeT. They all suggest that an appropriately designed PeT system could sense changes in membrane potential by the direct effect of the electric field upon the electron transfer efficiency.

4.3 Designing PeT voltage probes

4.3.1 Theoretical factors

In this section, I will continue to draw from the literature in order to rationalise a PeT voltage probe design. In 2007 a theoretical paper from Liang-shi Li modelled that an appropriately designed VSD based upon PeT could ex-

hibit large changes in fluorescence quantum yield with changes in membrane potential.[25]

The various processes of a PeT voltage sensor and their rate constants are shown in Figure 4.7. Li assumed that the only effect of a change in electric field upon PeT would be the modulation of the free-energy change of the eT step (ΔG_E) from its value in the absence of a field (ΔG_0) by the inclusion of the interaction of the change in dipole moment upon forming the CS state ($\Delta\vec{\mu}$) with the electric field ($\vec{E}$):

$$\Delta G_E = \Delta G_0 - \Delta\vec{\mu} \cdot \vec{E} \tag{4.4}$$

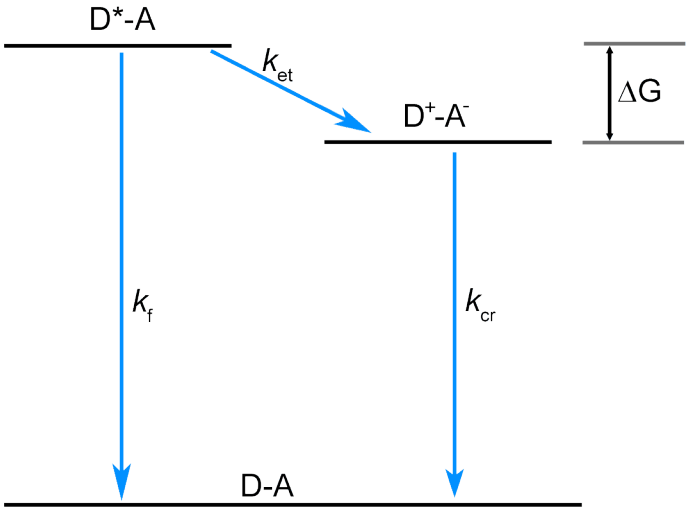

Figure **4.7** The key transitions in a PeT VSD from the excited state D^*-A and their rate constants: fluorescence (k_f), electron transfer (k_{et}) and charge recombination (k_{cr}).

A semi-classical derivative of Marcus theory was then used by Li to model the dependence of k_{et} upon ΔG. The equation contains V, the electronic coupling matrix element between the donor and acceptor, λ_m the reorganisation energy of the surrounding medium, ω_c the average frequency of the high-frequency vibrational modes of the molecule that facilitate the electron transfer process,

and S_c the electron-phonon coupling strength of these modes:

$$k_{\text{et}} = e^{-S_c} \left\{ \sum_{n=0}^{+\infty} \frac{S_c^n}{n!} \exp \left[- \frac{(\Delta G_E + \lambda_m + nh\omega_c)^2}{4\pi_m k_B T} \right] \right\} \tag{4.5}$$

$$\text{where } A = V^2 \left(\frac{4\pi^2}{h} \right) \left(\frac{1}{4\pi\lambda_m k_B T} \right)^{1/2}$$

The equation above was used to derive the free energy *vs.* eT rate curve shown in Figure 4.8. Li asserts that if a probe has a ΔG_0 lying in one of the green regions of the curve, it should be highly sensitive to changes in electric field as a large change in eT rate is observed with changes in ΔG_E. Conversely, a probe whose ΔG_0 is in the red region would be less sensitive as the same change in ΔG_E would lead to a smaller change in k_{et}. Highly sensitive PeT voltage sensors should 'pair up' donors and acceptors such that ΔG_0 lies in a highly sensitive region of this Marcus-type curve.

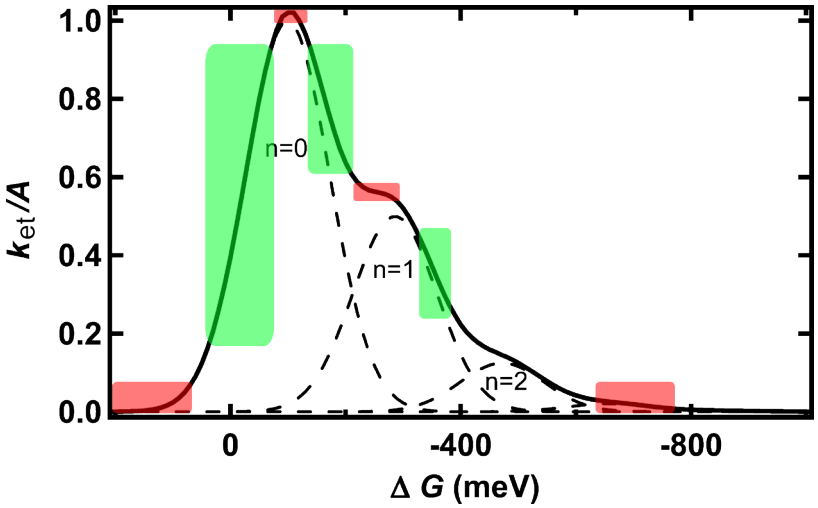

Figure **4.8** The change in eT rate with free energy according to Equation 4.5. Adapted with permission from reference 25. Copyright 2007 American Chemical Society.

With the parameters used in Li's analysis, a $\Delta S/S$ of up to 30% was predicted, for a probe where k_{et}^0, the eT rate in the absence of a field, is 100 × greater than k_{f}. However, such a dominating PeT process results in a very low quantum yield of fluorescence and a poor photon count, and to achieve this

30% sensitivity thus comes at the expense of low overall signal and poor SNR. Compromising sensitivity for higher signal can ease this problem, with predicted sensitivities in the range 10 to 25% for a ratio of $k_{\mathrm{et}}^0/k_{\mathrm{f}}$ in the range 1 to 10. Our rational design conclusion from this prediction is to choose a fluorophore with a high quantum yield as a starting point, as even at a low $k_{\mathrm{et}}^0/k_{\mathrm{f}}$ ratio of 1, the quantum yield of fluorescence will be approximately halved by the competing PeT process.[b]

Encouragingly, the values obtained in Li's analysis are for an eT distance of only 1.25 nm, as little as one quarter of the maximum width of the targeted membrane bilayers. There is thus scope for increased sensitivity by increasing the eT distance (increased $\Delta\vec{\mu}$, Equation 4.4 on Page 165). It is of note, however, that the other parameters (V, λ_m, ω_c and S_c) may have been wrongly assumed[c] and may in themselves be field sensitive. V has been dismissed by some reports as only being weakly field sensitive,[26] but others have found that changes in V provided a better match between modelled and measured field-sensitive PeT than the effect of the change in dipole (Equation 4.4 on Page 165).[27–29] Neither of these conclusions seem consistent with the highly interrelated nature of V and ΔG, and they highlight the lack of consensus in this area. In order to rationalise a molecular design from Li's theory, values for the quantities V, λ_m, ω_c and S_c would need to be known or readily calculable, which is not the case. All of these parameters are highly dependent upon the choice of donor, acceptor and molecular wire spacer. With little agreement in the literature over the effect of an electric field upon these parameters, in this chapter we adopt an empirical approach towards developing PeT voltage sensors.

[b] In this discussion, k_{f} could be more accurately expressed as $k_{\mathrm{f}} + k_{\mathrm{nr}}$ where k_{nr} is the non-radiative decay processes of the excited state.

[c] The latter three of these were taken from values used in modelling of eT in the photosynthetic reaction centre without any justification. The value of V is not discussed.

4.3.2 Molecular design

4.3.2.1 Design requirements

Although Li predicted that PeT VSDs with exceptional sensitivity are feasible, the precedence does not translate directly into a molecular design. In this section we propose a modular molecular design and a convergent synthesis, which will allow the important quantities determining PeT, particularly ΔG_0, to be varied by varying the donor and acceptor.

While some of the design requirements are unclear from the theory of field-sensitive PeT, several are less contestable. A fluorophore with a high quantum yield is a sensible start, and a fluorophore with a high molar extinction coefficient is also beneficial to ensure a high brightness ($\Phi_f \epsilon$). The general requirements of amphiphilicity and biocompatibility are in common with any VSD, thus the design will feature hydrophilic and lipophilic ends.

A specific requirement of the PeT mechanism is for a long spacer to separate the donor and the acceptor, in order that as much of the electric field as possible is sensed (which is particularly important if Equation 4.4 describes the voltage sensitive PeT process well).[25] Attention will be first given to the nature of eT in molecular wire spacers, something neglected in Li's treatment.[25]

4.3.2.2 Molecular wire spacer requirements

Concerning the design of the molecular wire spacer, it is vital to consider whether a stepwise or single-step eT is preferable in achieving high voltage sensitivity. A stepwise or 'hopping' eT process involves the transient formation of one or more intermediate CS states (D^+–S^-–A) between the initial (D–S–A) and the final (D^+–S–A^-), with the electron localised on a site S on the spacer (Scheme 4.1 on the next page). Such a stepwise eT process is characterised by high rates and low distance dependence. The single-step or superexchange

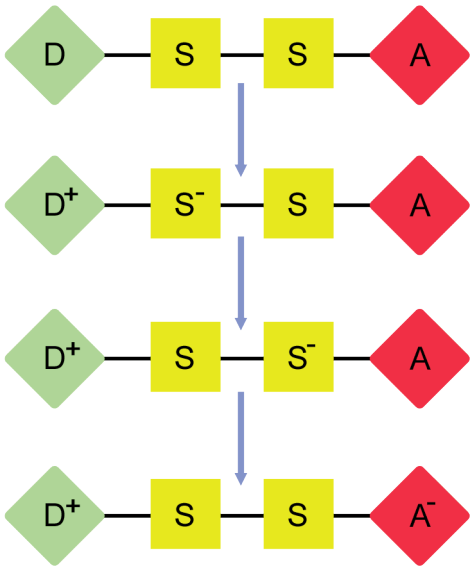

Scheme **4.1** Stepwise separation of charge onto subsequent units in the molecular wire in the 'hopping' eT mechanism.

mechanism involves electron tunnelling from the donor to the acceptor. As it is mediated by the spacer, the spacer is not directly reduced during the eT. This type of eT is more rapidly attenuated with increasing distance.

Either of these mechanisms can be engineered in an eT system by pertinent design.[30] The step-wise process requires a thermodynamically favourable CS intermediate, and thus a spacer with a suitable reduction potential such that D^+–S^-–A can form. The superexchange mechanism requires a spacer with a low-lying LUMO to allow mixing with the donor and acceptor frontier orbitals, but the LUMO energy must be above that of the donor and acceptor so that direct reduction remains energetically unfeasible.[31]

For the application of voltage-sensing *via* PeT, the superexchange mechanism is preferred. Each step in a stepwise eT process will only experience a fraction of the total electric field, and thus its rate will not be modulated much by the field (based on the change in dipole model, Equation 4.4). A stronger field effect is therefore expected in a long distance single-step eT. The spacer will therefore be chosen based upon literature precedence after a suitable flu-

orophore has been chosen.

4.3.2.3 Choice of fluorophore

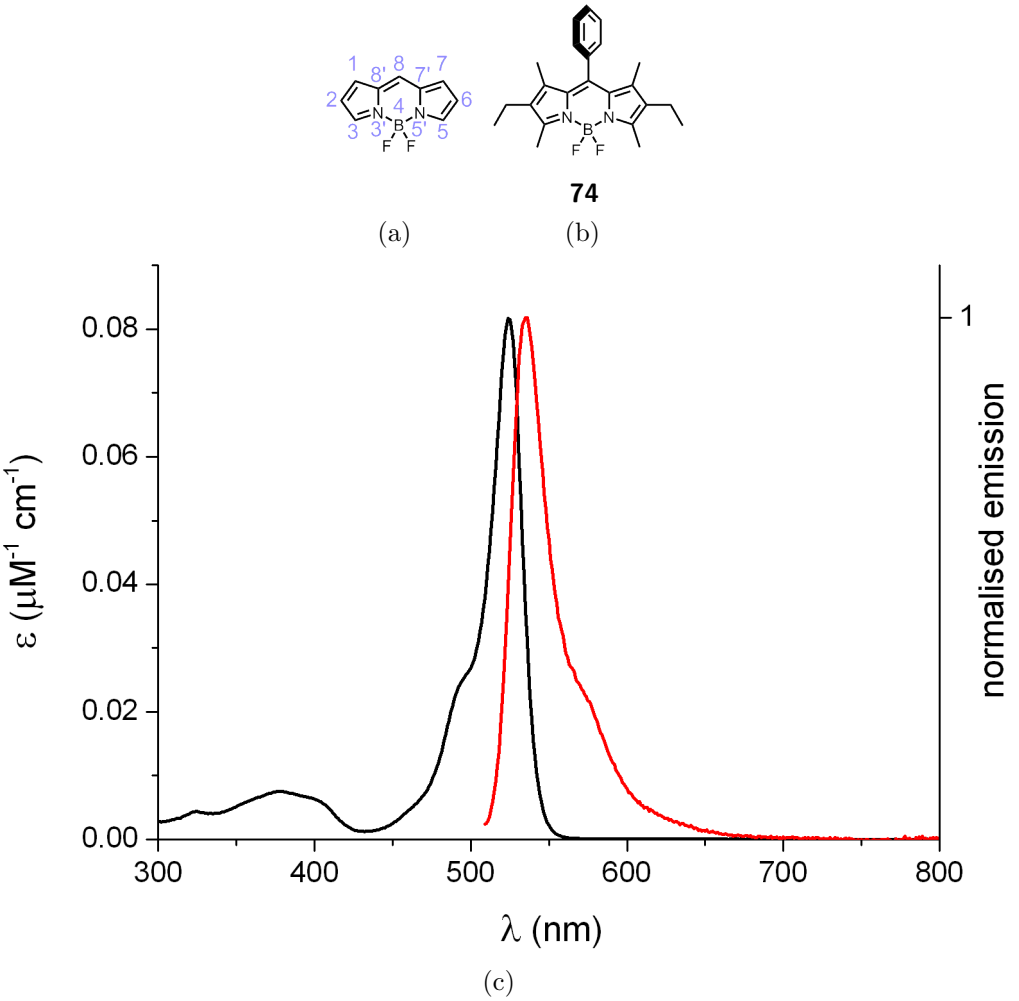

Figure **4.9** (a) The numbering of the basic BODIPY skeleton; (b) A BODIPY made from kryptopyrrole with the commonly-used phenyl group in the 8-position; (c) Absorption (black) and emission (red) spectra of the dye shown in (b) (solvents THF (abs) and EtOH (em), λ_{ex} = 490 nm).

4,4-Difluoro-4-bora-3a,4a-diaza-*s*-indacene, more commonly known as boron dipyrromethane or BODIPY, was chosen as the starting point for translating the design requirements into a molecular design. This compact chromophore has recently proven itself to be a highly versatile dye with many desirable properties. BODIPYs have a high fluorescence quantum yield (for example Φ_f = 0.89 in CH_3OH[32], compound **74**), thanks to the rigidity provided to

the dipyrrin by the coordination of BF_2, combined with a good extinction coefficient ($\sim$ 80,000 M^{-1} cm^{-1} at 525 nm in THF, compound **74**), giving a high brightness. With the reactive positions of its pyrrole rings protected (often with hydrophobic solubilising groups), BODIPY is highly chemically and photochemically stable.[33]

Many synthetic modifications can be made to BODIPY, to modulate its electronic properties, solubility, and biocompatibility.[34–36] BODIPYs have been modified at each of the possible pyrrole positions (1-3, 5-7, see Figure 4.9(a) on the preceding page), at the B−F/4 position, and at the *meso*/8 position.[35] The typical synthesis *via* condensation of two equivalents of a pyrrole with an aldehyde allows a variety of functional groups to be introduced at the beginning of a synthesis. Electrophilic substitution also permits sulfonation, halogenation and nitration of the pyrrole positions after the initial condensation, with halogens in particular opening up the possibility of further functionalisation by Pd-catalysed C−C coupling reactions or nucleophilic aromatic substitution.[35,37] This diversity has resulted in numerous functional BODIPYs,[38–40] particularly BODIPY-based biosensors and fluorescent tags (such as viscousity sensors,[39,41] pH sensors,[5,42] polarity sensors,[7] fluorescent lipids,[43–47] and protein labels[48,49]).

The redox potentials of a typical BODIPY suggest it can be used as the electron donor or acceptor in a molecular PeT system, and it has been previously employed either way in PeT systems in the literature.[7,50] As the chromophore is naturally hydrophobic, we chose the BODIPY as the membrane-bound component in this molecular design.

Having chosen BODIPY as the fluorophore on which to base our VSD design, we were inspired by work from Ulrich and Ziessel featuring a BODIPY as the electron donor, a molecular wire spacer and a pyridinium group as the electron acceptor (**76**, Figure 4.10 on the next page).[50] Comparing compound

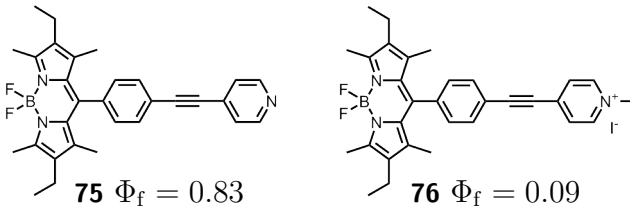

75 $\Phi_f = 0.83$ **76** $\Phi_f = 0.09$

Figure **4.10** The difference in fluorescence quantum yield between these two compounds reflects the better electron-accepting ability of the pyridinium group. OPE is shown to be a suitable molecular wire.[50]

75 with **76** shows that when an acceptor of suitable reduction potential is attached to the spacer (achieved by methylation of the pyridine to form pyridinium), PeT partially quenches fluorescence.[d] As is common in BODIPY PeT sensors, this molecular design has a large dihedral angle between the BODIPY and the adjacent phenyl of the spacer, and as such the conjugation of the dye to the bridge is weak.[51] The spacer is assumed to operate in the superexchange eT regime, based upon the competition between PeT and fluorescence, consistent with other literature on the oligo-*p*-phenylene ethynylene (OPE) molecular wire.[13,31,52,53] Compound **76** is also amphiphilic by virtue of the charged pyridinium headgroup.

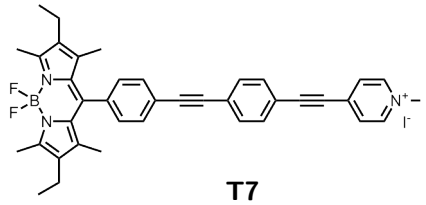

T7

Figure **4.11** The first target dye **T7**.

Based upon this, our first target dye **T7** (Figure 4.11) also bears an OPE as the molecular wire spacer, but an additional phenylene ethynylene (PE) unit is added compared to compound **76** in order to aim towards the maximum 5 nm eT distance (the upper limit of the thickness of lipid bilayer membranes in cells). The eT length of this design is modelled to be $\sim$ 2 nm. The use of

[d]It is noted that in reference 50 the authors are not designing or making VSDs. Their fundamental investigations were not applied in any way.

OPE as the spacer fits the brief for a modular 'building block' design: ethynyl groups are ideal synthetically as Sonogashira coupling can be used to assemble the dyes.

4.3.2.4 Synthetic disconnections

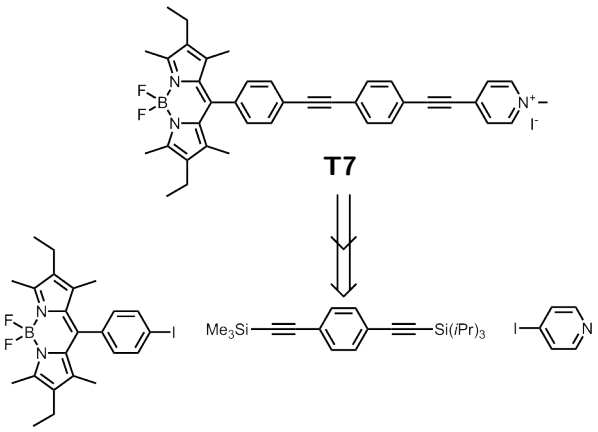

Scheme **4.2** A proposed disconnection strategy for **T7**.

A convenient disconnection of target dye **T7** is shown in Scheme 4.2. In order to provide an iodoaryl for Sonogashira assembly, the first phenyl ring at the donor end of the OPE spacer is included with the fluorophore component. A phenyl is readily incorporated into the BODIPY at the condensation step of the synthesis. The spacer component features silyl protecting groups which can be orthogonally deprotected. The appropriate synthetic building block for the headgroup is 4-iodopyridine, which can be similarly coupled to the spacer. The pyridinium is best formed as the final step of the dye synthesis, as *N*-methyl-4-iodopyridinium iodide is unstable.[e]

Two alternative electron acceptors were also chosen. Both feature a different extent of conjugation in their link to the spacer, but the electron acceptor is still a pyridinium. These are proposed to offer slight variations in reduction potential which may reveal more significant differences in voltage sensitivity

[e]J. E. Reeve and H. L. Anderson, unpublished results

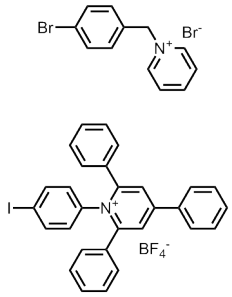

Figure **4.12** The two other pyridinium-based electron acceptors selected.

(according to the curves in Figure 4.8 on Page 166). Both can be attached by organometallic C−C coupling using the building blocks shown (Figure 4.12).

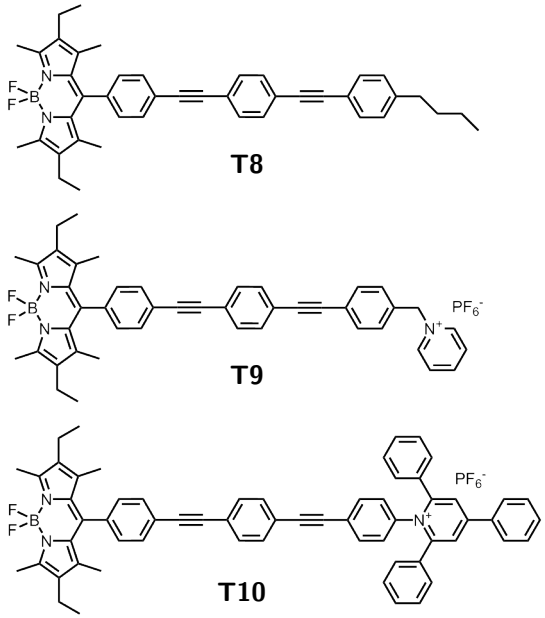

Figure **4.13** The three further first generation target dyes.

A reference dye was also conceived (**T8**, Figure 4.13). The simple attachment of a benzene ring provides a mimic of the donor-acceptor dyes but no favourable PeT pathway. This dye would allow the observation of voltage-sensitive PeT to be confidently assigned to this mechanism. 4-*n*-Butyliodobenzene is a convenient, commercially available building block.

Electrochemistry was performed on compounds **77** and **92** to allow a check of the suitability of the headgroups chosen to be made using the Rehm-Weller

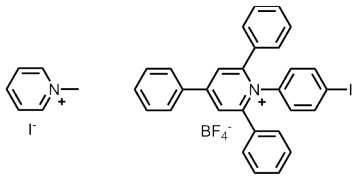

77 **92**

headgroup	E_{red}[a] (V)	ΔG[b] (eV)
77	-1.75	0.12
92	-1.37	-0.26

a) electrochemical data are referenced to internal ferrocene (Fc/Fc^+) as 0 V, and were acquired using square wave voltammetry in THF containing Bu_4NPF_6 (0.1 M). b) Rehm-Weller analysis was performed to estimate ΔG using $E_{ox} = 0.70$ V and $E_{00} = 2.33$ eV, the values measured for BODIPY **74**.

Figure **4.14** Electrochemical analysis was used to assess the suitability of the electron acceptor choices.

equation (4.1). Using electrochemical data measured for **74** as the PeT donor, the feasibility of eT was estimated. The results shown in Figure 4.14 suggest that acceptor **92** seems a suitable match from the analysis, with a negative ΔG. However, the estimate indicates that *N*-methylpyridinium iodide is not a suitable PeT acceptor, but this analysis ignores the effect that conjugating this acceptor to a molecular wire bridge will have; the reduced fluorescence quantum yield observed in compound **76** compared to compound **75** (Figure 4.10 on Page 172) suggests that ΔG will be negative for this electron acceptor also.

4.4 First generation dyes

Having chosen a fluorophore and met the other design criteria, the first generation of dyes was next synthesised. The aim was to test the suitability of the length of the OPE spacer and the headgroups chosen before adapting the de-

signs to enhance the amphiphilicity, generating dyes suitable for typical VSD testing methods.

4.4.1 Synthesis

4.4.1.1 The BODIPY fluorophore and the molecular wire spacer

The BODIPY fluorophore was synthesised in 3 steps (Scheme 4.3) from commercial starting materials following modified literature procedures.[54–56] 4-Acetyl-3,5-dimethylpyrrole carboxylic acid **78** was decarboxylated under basic conditions to give 3-acetyl-2,4-dimethylpyrrole **79**. This was reduced with $LiAlH_4$ to obtain kryptopyrrole **80**, the electron-rich ring facilitating the elimination of the alcohol intermediate.[56] Condensation with 4-iodobenzoyl chloride yielded the dipyrrin which was then coordinated to BF_2 in the presence of base to give the fluorophore building block **81**.

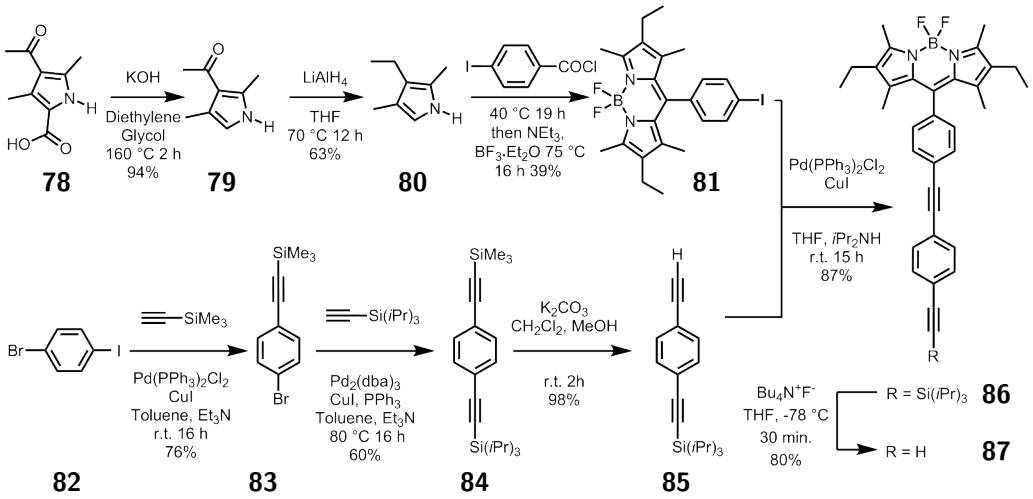

Scheme **4.3** Synthesis of the key intermediate **87**.

The segment of the spacer was synthesised by taking advantage of the different rates of Sonogashira coupling to an aryl iodide and an aryl bromide. First, one equivalent of trimethylsilylacetylene was coupled to the more reactive iodide position of 4-bromoiodobenzene. The subsequent reaction with

triisopropylsilylacetylene to form the asymmetric bridge segment proceeded at higher temperature at the less reactive bromide position.

The key intermediate **87** was accessed by coupling the singly-desilylated spacer component **85** to the iodine of the fluorophore component **81**, followed by desilylation with $Bu_4N^+F^-$.

4.4.1.2 The headgroups

Conjugated pyridinium dye **T7** was prepared by first coupling 4-iodopyridine to **87** to give pyridine intermediate **88**, and then quaternarising with iodomethane to form the pyridinium target (Scheme 4.4).

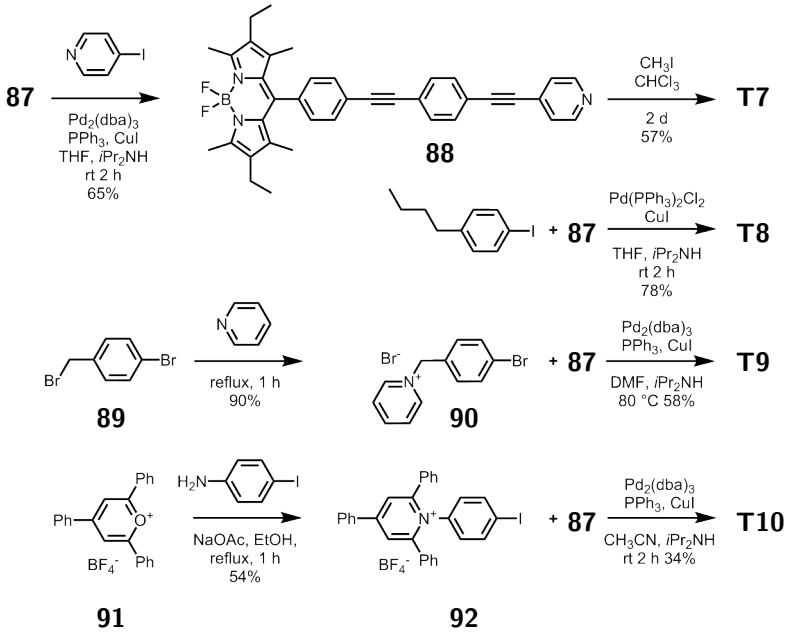

Scheme **4.4** Synthesis of the first generation target dyes from the key intermediate **87**.

For target dyes **T9** and **T10**, the headgroups were prepared separately and coupled to the building block **87** in the final step of the synthesis. 1-(4-Bromobenzyl)pyridinium bromide **90** was formed as a precipitate when heating 4-bromobenzylbromide in pyridine. 2,4,6-Triphenyl-*N*-(4-iodo-phenyl)-pyridinium tetrafluoroborate **92** was formed by refluxing the relevant pyrylium with NaOAc in ethanol before adding 4-iodoaniline. The desired product precipitated out

of solution over 1 hour. These two headgroups were then readily coupled to the BODIPY-spacer moiety **87** to give **T9** and **T10**. The reference dye **T8** was similarly accessed from the key intermediate **87** by coupling to 4-iodo-1-*n*-butylbenzene.

4.4.2 Optical and electrochemical Characterisation

4.4.2.1 Absorption spectroscopy

The absorption spectra (Figure 4.15) of the series of dyes were measured in THF and mainly differ at the UV end, due to the structural variation between the spacers. There are negligible changes in the energies of the spectra in the BODIPY region (450-550 nm) compared to each other and reference BODIPY **74** (Figure 4.9(c) on Page 170), as expected due to the decoupling of the spacer and the chromophore resulting from the twist of the *meso*-phenyl relative to the BODIPY.

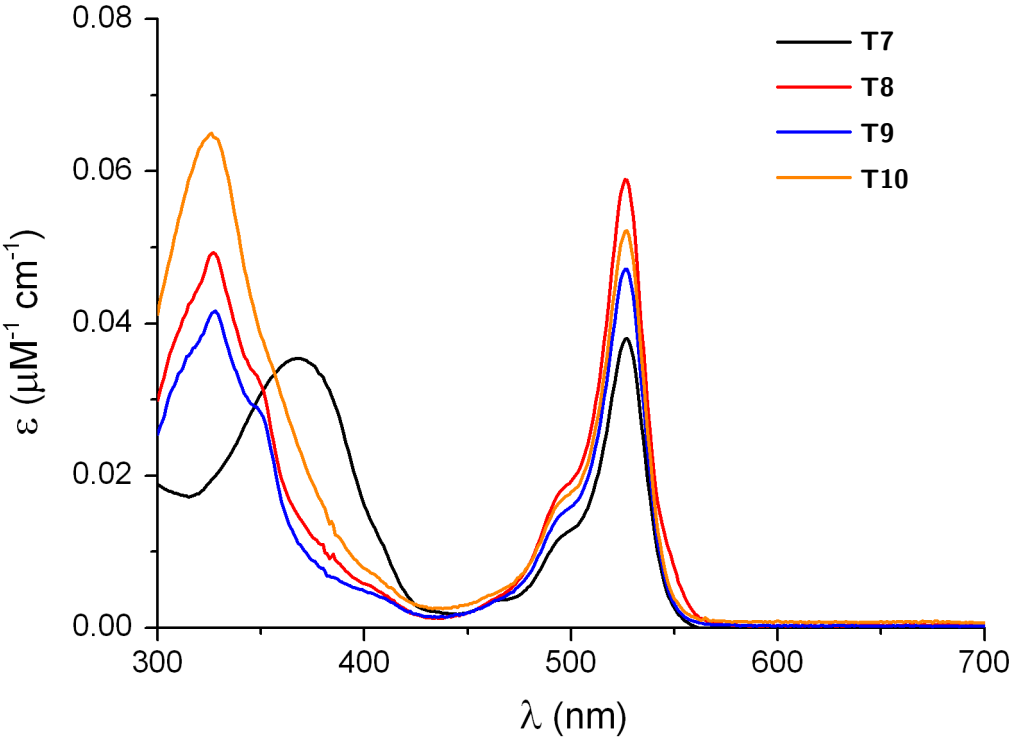

Figure **4.15** Extinction coefficients of the family of BODIPY dyes, measured in THF.

4.4.2.2 Fluorescence spectroscopy

Emission spectra were also acquired in THF, and the fluorescence quantum yields (Table 4.1) were established by comparison with a standard, BODIPY **74**. To confirm the validity of the literature values of the standard's fluorescence quantum yield, the standard was cross-checked against Rhodamine 6G, and found to match within ±10%.

dye	Φ_f[a]	τ_1 (ns)[b] [α_1 (%)]	τ_2 (ns) [α_2 (%)]
T7	0.07	0.49 [37]	2.9 [60]
T8	0.48	–	3.6 [95]
T9	0.37	–	3.6 [94]
T10	0.23	n.m.	n.m

a) $\lambda_{ex} = 490$ nm. b) Lifetime data acquired by Dr. Maria Izquierdo Arcusa, Imperial College London. τ_i and α_i come from multi-exponential fitting of the intensity as a function of time $I(t)$ of the fluorescence decay curve to the equation $I(t) = I(0)\sum_i \alpha_i e^{-t/\tau_i}$. Components lower than 5% have been ignored, indicated by '–'. 'n.m.' indicates not measured.

Table **4.1** Data from fluorescence spectroscopy for the first generation BODIPYs in THF.

Compared to the reference dye **T8**, the three dyes bearing an electron acceptor all exhibit lower fluorescence quantum yields, presumably due to competitive PeT. The fluorescence quantum yields show a correlation between the extent of conjugation of the electron acceptor to the ring and the extent of PeT quenching. All three of the donor-acceptor dyes operate in a regime where PeT competes with fluorescence but does not completely quench it, and thus meet one of the key design considerations.

The fluorescence lifetime is measured from the decay in emission signal with time following a short excitation pulse. Fluorescence lifetimes were measured by Dr. Maria Izquierdo Arcusa and Dr. Marina Kuimova, Imperial College London. τ_2 for compounds **T8** and **T9** is a typical emission lifetime for a

BODIPY fluorophore.[50,57] This is reduced accordingly in **T7**, consistent with the strongly quenched fluorescence and a competitive PeT process. The appearance of a shorter lifetime component τ_1 for this dye implies the presence of another emissive state, for example a charge-transfer state.

4.4.2.3 Electrochemistry and estimating ΔG

In order to use the most relevant and accurate redox values in the Rehm-Weller analysis (Equation 4.1 on Page 159), voltammetry was performed on the target dyes rather than their unconnected components. The results are displayed in Table 4.2.

The data reveal very little variation in oxidation potential, as expected from these electronically decoupled systems: in each case, the oxidation is that of the BODIPY, which is unperturbed by the spacer or acceptor. The first reduction potentials represent the reduction of the electron acceptor (or of BODIPY in the case of the reference dye). There is a clear correlation between the extent of conjugation of the pyridinium to the bridge and the reduction potential, the most conjugated pyridinium group of **T7** being the easiest to reduce. The reduction potentials of the D−A dyes span a range of $\sim$ 0.35 eV; as E_{00} is identical for each dye, ΔG calculated using Equation 4.1 on Page 159 also spans a range of $\sim$ 0.35 eV for this family. As expected, a correlation between the thermodynamic feasibility of PeT and the fluorescence quantum yields is found, but the electronic coupling of the acceptor to the bridge also has a role to play in determining Φ_f: **T7** and **T10** have similar estimated ΔG for the electron transfer, but the fluorescence of **T7** is more fully quenched, reflecting the stronger coupling of the pyridinium to the molecular wire.

dye	E_{ox}[a] (V)	E_{red}[a] (V)	E_{00}[b] (eV)	ΔG (eV)	Φ_f
T7	0.65	-1.30	2.33	-0.39	0.07
T8	0.67	-1.74	2.33	–[c]	0.48
T9	0.66	-1.64	2.33	-0.03	0.37
T10	0.67	-1.34	2.33	-0.33	0.23

a) electrochemical data are referenced to internal ferrocene (Fc/Fc^+) as 0 V, and were acquired using square wave voltammetry in THF containing Bu_4NPF_6 (0.1 M). b) Taken as the energy of intersection of the normalised absorption and emission curves. c) ΔG was not calculated for this reference dye as E_{ox} and E_{red} are both for the BODIPY (by comparison with compound **74**), and there is thus no feasible PeT process.

Table **4.2** The first reduction and oxidation potentials and predicted ΔG for the first generation BODIPY dyes, compared to their fluorescence quantum yields.

4.4.3 Conclusions on the first generation dyes

With the fluorescence behaviour of these first generation BODIPY dyes characterised, we were satisfied that PeT was occurring to an appropriate extent; there was a competition between PeT and fluorescence, but the fluorescence was not fully quenched. However, these dyes were not sufficiently water-soluble to introduce to a VSD testing setup. Such experiments are described in more detail in Section 4.6, but in general require an aqueous solution of a dye to be added to an aqueous bath containing a model membrane or a cell. A second generation of dyes is next designed and synthesised to overcome this limitation.

4.5 Second generation dyes

Taking forward the two dyes at the extremes of PeT efficiency, **T7** and **T9**, along with the reference no-PeT dye **T8**, the next step was to design and synthesise analogues of these with enhanced water-solubility. The synthetic transformations to achieve this were chosen to have minimal effect on the

electron accepting ability of each headgroup, and thus to maintain the ΔG and Φ_f of dyes **T7**, **T8** and **T9**.

4.5.1 Synthesis

4.5.1.1 A more amphiphilic version of T7

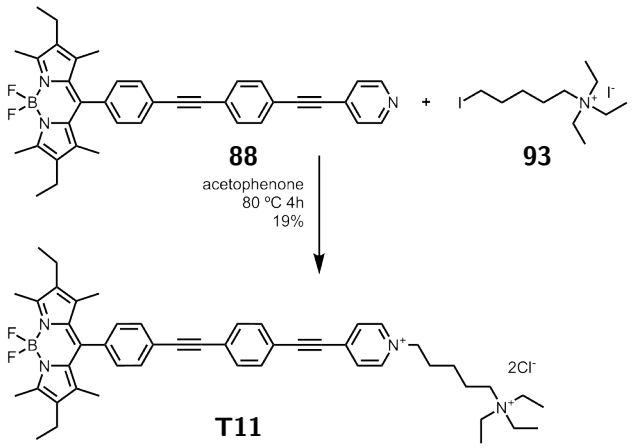

Scheme **4.5** Synthesis of dye **T11**, an analogue of **T7** with enhanced amphiphilicity.

Inspired by literature precedent for pyridinium-containing dyes,[58–61] dye **T7** was made more amphiphilic by using a singly-charged reagent for the quaternarisation step with intermediate **88**, resulting in a doubly-charged product (Scheme 4.5). The properties of the donor-acceptor system are assumed to be unperturbed by this change. Upon treating intermediate **88** with an excess of **93**, the new compound **T11** was formed. The cleanest material was more easily obtained when reaction times were kept below that required to reach completion. Nonetheless, isolation required chromatography on normal phase silica with an exotic eluent mixture[f] followed by careful aqueous washing of a chloroform solution of the eluted mixture to separate the starting salt from the product. **T11** exhibits water-solubility, but conveniently partitions more

[f]The eluent mixture referred to is methanol : NH_4Cl (2 M aq.) : nitromethane in the ratio 5:3:2.

readily into chloroform. Despite the apparent simplicity of this redesign, the actualisation of it suffered from tedious purification.

4.5.1.2 More amphiphilic versions of **T8** and **T9**

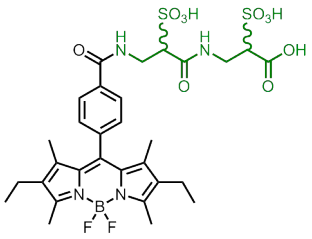

94

Figure **4.16** A disulfonated peptide moiety appended to a carboxylic acid, providing water-solubility to a BODIPY.[62]

Hydrophobic reference dye **T8** and amphiphilic dye **T9** were less trivial to adapt into dyes with enhanced amphiphilicity. The chosen strategy was selected on the basis that the water-solubilising groups must be separated from the aromatic system in order to maintain the electronic properties of the first generation dyes. Also, as the isolation of clean samples of the doubly-charged amphiphilic compound **T11** had proved challenging, carboxylic acids were picked as water-solubilising groups as these provide good water-solubility for BODIPYs for biological application,[37,63–67] but their polarity can be partially masked until the end of the synthesis using a suitable ester protecting group. Carboxylic acids could also be further appended with further solubilising groups, such as the disulfonated peptidyl chain shown in green in compound **94** from the work of Anthony Romieu and Raymond Ziessel (Figure 4.16).[62] Based on published dyes, it was anticipated that the use of two carboxylic acid groups per dye would provide sufficient water-solubility. Tertiary butyl protecting groups were chosen to mask the polarity throughout the synthesis, as these can be removed under mild conditions known to be compatible with

the BODIPY moiety.[68] The proposed headgroups for this work are shown in Figure 4.17.

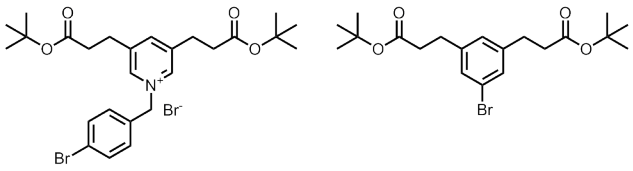

Figure **4.17** New headgroups featuring masked solubilising groups.

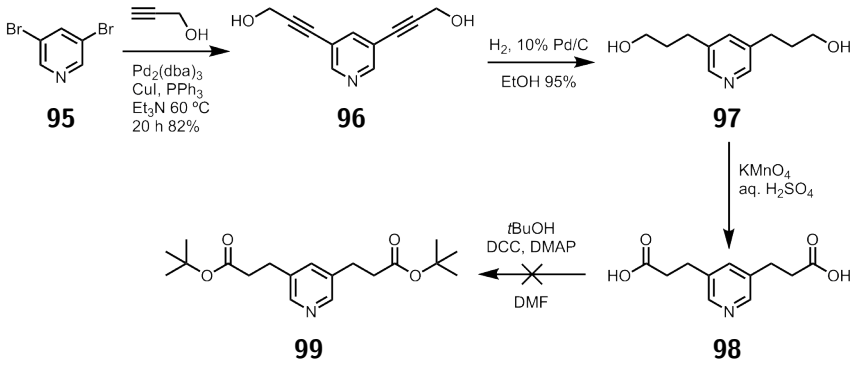

Scheme **4.6** The first route attempted towards a pyridine modified with protected carboxylic acids.

Keen to exploit similar routes for both targets, 3,5-dibromopyridine and 1,3,5-tribromobenzene were identified as good starting points for adding alkyl chains to the existing designs *via* Sonogashira coupling and subsequent reduction of the alkyne. An initial investigation (Scheme 4.6) into making compound **99** *via* a route precedented up until the conversion of **98** into **99** failed due to the poor solubility of acid intermediate **98** under conditions to attach the *t*Bu protecting groups.

To avoid this problem, the shortest readily available alkynoic acid, 5-pentynoic acid **100**, was used instead of propargyl alcohol. The acid was protected with the *t*Bu group as the first step of a synthesis, and then successfully carried through a similar route to the target headgroup (Scheme 4.7 on the next page).

The headgroup for the reference compound was synthesised using a similar route (Scheme 4.8), the key difference being the statistical Sonogashira cou-

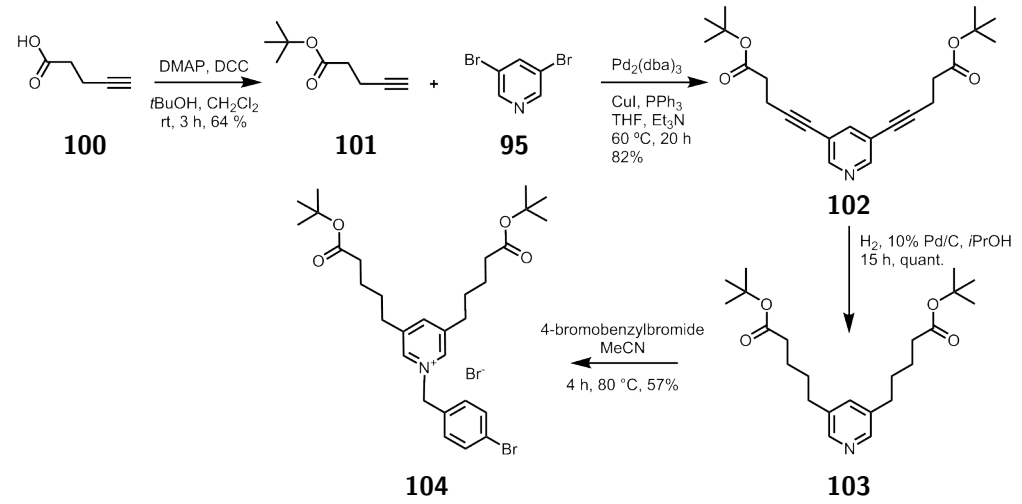

Scheme **4.7** Synthesis of an analogue of headgroup **90** with masked enhanced water-solubilising groups.

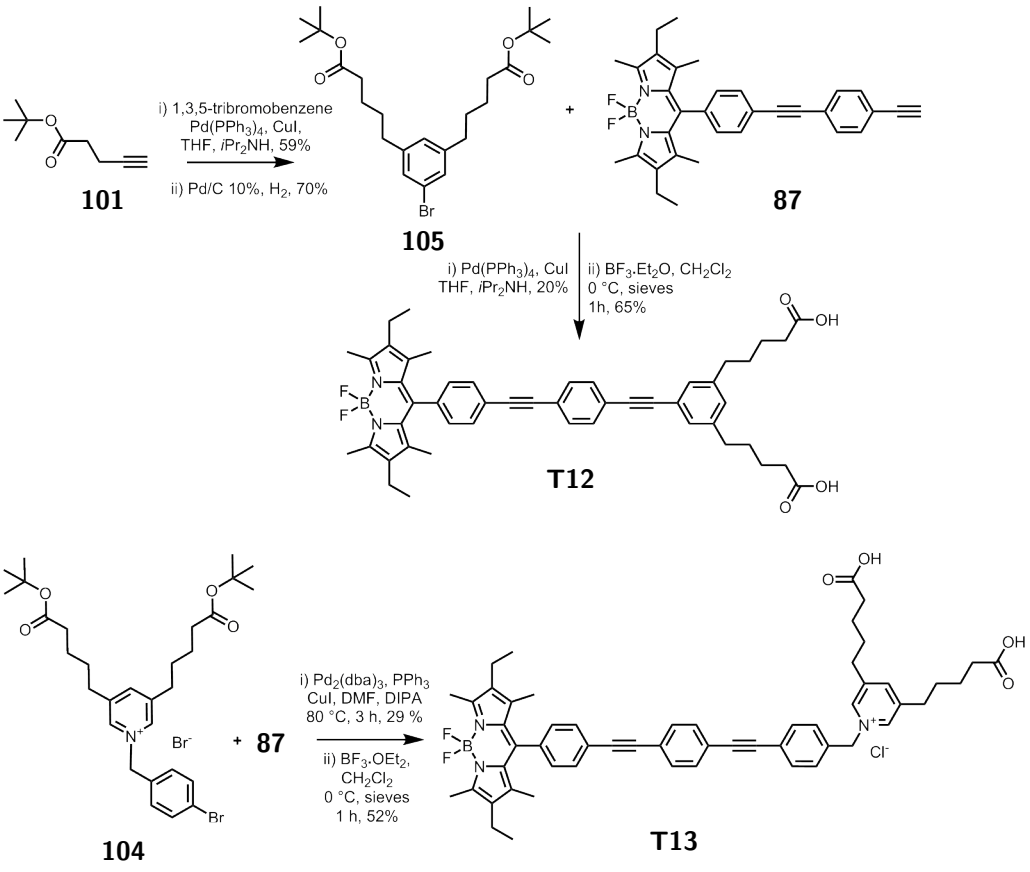

Scheme **4.8** Synthesis of two more dyes with enhanced amphiphilicity, **T12** and **T13**.

pling step attaching **101** to tribromobenzene. Both of these headgroups were attached to the rest of the dye framework by Pd-catalysed coupling to terminal

alkyne intermediate **87**. Removal of the *t*Bu protecting groups was achieved using literature conditions, and purification of the amphiphilic product was limited to extraction and precipitation once the method was optimised. The avoidance of doubly-charged final products for the second generation dyes **T12** and **T13** compared to **T11** pleasingly resulted in more readily achievable isolation of pure target dyes.

4.5.2 A synthetic aside

However, the presence of the pyridinium group in the last few steps of the synthesis of **T13** made purification trickier than hoped, probably due to the positive charge of the pyridinium. An alternative disconnection which would allow quaternarisaion of the pyridine as the final or penultimate step of a synthesis was thus investigated. The desired synthon for this route possesses an electrophilic leaving group in the benzylic position at the acceptor end of the dye, as shown in Scheme 4.9.

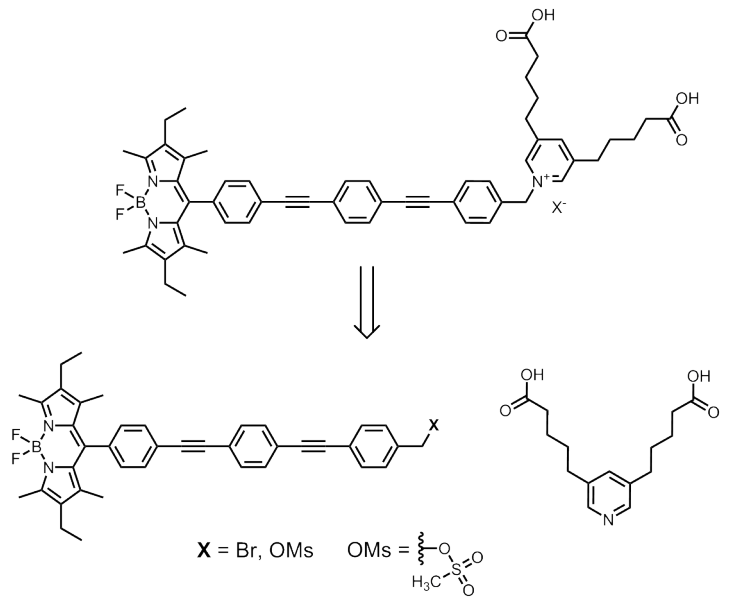

Scheme **4.9** A potential alternative disconnection that could be used to access **T13**.

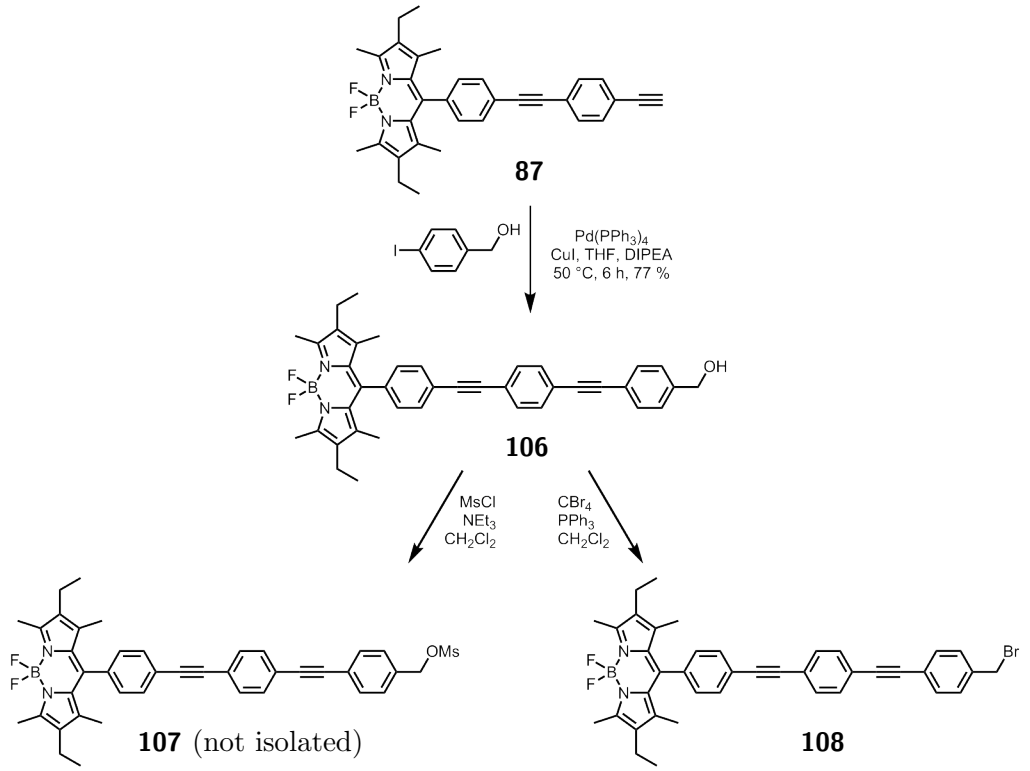

Scheme **4.10** Synthesis of useful intermediate **108**.

The first approach to this synthon was to attempt to couple 4-bromobenzylbromide **89** to BODIPY intermediate **87** using Sonogashira conditions. Diisopropylethylamine was used as a base for these attempts, as less bulky bases typically employed in such reactions (Et_3N, iPr_2NH) were expected to quaternarise by nucleophilic attack at the benzylic position. A complicated mixture of products was obtained. The major product was not fully characterised, but was clearly less fluorescent than the starting material, suggesting a successful coupling had taken place but subsequent quaternarisation at the benzylic position resulted in a product with a PeT pathway and quenched fluorescence.

Instead, 4-iodobenzylalcohol was coupled to **87** (Scheme 4.10). The intermediate **106** presented the opportunity of conversion either to the benzyl methanesulfonate (OMs) or the benzyl bromide. Both conversions took place successfully according to mass spectrometry, but **107** could not be isolated, suggesting the compound was too reactive. The Appel reaction gave the bro-

mide version which was isolated, and later employed in several test reactions with a pyridine derivative. Clean conversion was observed and this route is thus concluded to be promising for further synthetic studies.

4.5.3 Characterisation of second generation dyes

The absorption and emission spectra of the second generation dyes are identical to the relevant first generation dyes as expected (Figure 4.18). The fluorescence quantum yields (Table 4.3 on the following page) are lower for **T13** and **T12** than for the first generation counterparts, perhaps reflecting additional non-radiative processes from the embellished molecular architectures.

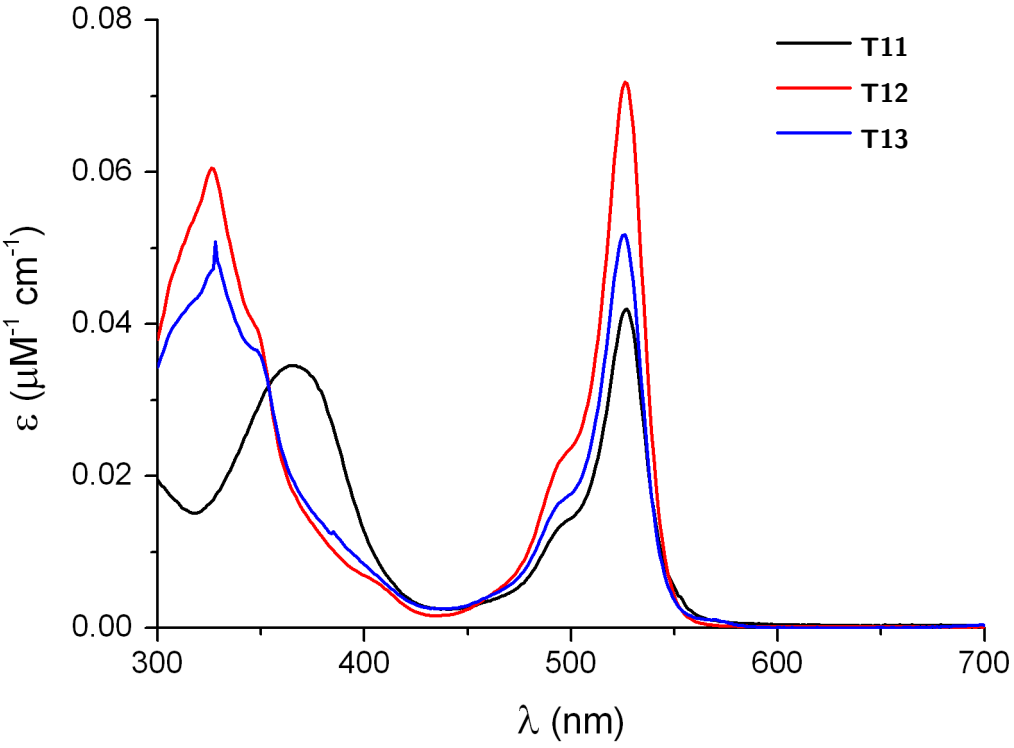

Figure **4.18** Extinction coefficients of the enhanced amphiphilicity BODIPY dyes, measured in THF.

dye	Φ_f
T11	0.09
T12	0.30
T13	0.19

Table **4.3** Data from fluorescence spectroscopy for the second generation BODIPYs, measured in THF with $\lambda_{ex} = 490$ nm.

4.6 Initial voltage-sensitivity testing

4.6.1 Model membrane system

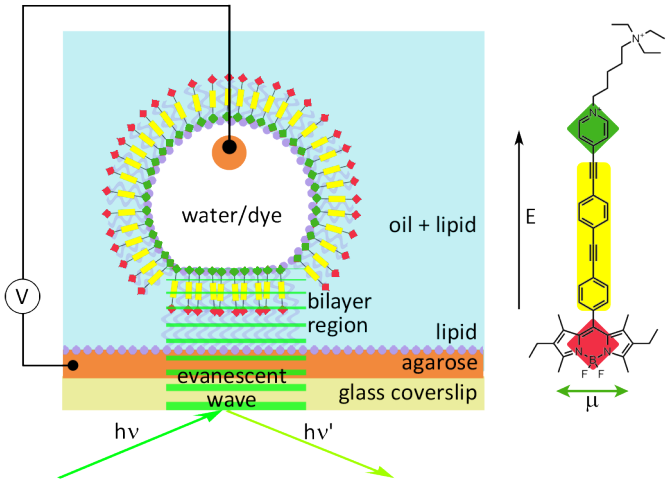

Figure **4.19** The TIRFm/DHB setup used for VSD characterisation.[69–71] The polarisation of the transition dipole of the BODIPY fluorophore is labelled on **T11**.[72]

With a family of three amphiphilic donor-acceptor fluorophores available, initial attempts at characterising the voltage sensitivity were made in a model membrane setup. Specifically, a TIRFm platform was used to image a DHB (Figure 4.19). A DHB is a micrometer-scale segment of lipid bilayer formed at the intersection of a mobile water droplet in a bath of oil on top of an

agarose (hydrogel) layer. One half of the bilayer is formed by the lipids at the agarose/oil interface, and the other half at the water/oil interface. The water droplet is lowered into the oil until a bilayer forms at the interface between the two aqueous phases (agarose/water droplet interface). Electrodes embedded in the agarose layer and the syringe used to form the water droplet allow a potential to be applied across the bilayer. The incident laser light of the TIRFm method causes an evanescent wave to propagate into the DHB sample, allowing membrane-embedded fluorophores to be excited.[69–71] Fluorophores are introduced *via* the water droplet, hence the requirement for water-soluble dyes to be synthesised.

Experiments were performed in collaboration with Dr. Bríd Cronin, Jason Sengel and Dr. Mark Wallace. The Wallace group had previously shown that the DHB/TIRFm setup can be used to observe voltage-sensitive fluorescence from electrochromic dye **Di-8-ANEPPS** (Figure 1.12 on Page 18). Amphiphilic dyes **T11** and **T13** were introduced individually to bilayers from the aqueous droplet at μM concentration. Strong fluorescence was observed from the bilayer, suggesting good membrane localisation of the dyes. Qualitatively, the relative fluorescence quantum yields of the two dyes were preserved. In each experiment, a square-wave voltage sequence of $\pm$100 mV was applied to each bilayer, changing sign each second. The fluorescence intensity was summed over the entire frame of each image. In these experiments, no change in fluorescence intensity was observed with the changing membrane potential.

This disappointing result could be explained by any of a number of factors which cause the dyes not to be voltage-sensitive as expected. Design choices may prove to be flawed, for example, the strong conjugation of the pyridinium to the molecular wire bridge in compound **T11** might reduce the distance of the eT process and limit its voltage-sensitivity. Their may also be factors causing the dyes to not have 'tested positive' during these experiments. Two causes

specific to these experiments will be discussed here, but these aside the results suggest that the dyes are in fact not voltage sensitive.

Firstly, as discussed in the introduction, competition between the desired mechanism and other mechanisms, such as repartitioning or reorientation, could result in a cancellation of the VS PeT signal. Long timescale measurements, such as these experiments which were restricted to one second voltage changes, are particularly susceptible to such complications due to the number of mechanisms which could operate within this time period. Fast electro-optic mechanisms should be observable on a sub-microsecond with sufficiently bright dyes and sensitive equipment.

Secondly, the dyes may localise in the region of the bilayer with strong surface or dipole potentials. These may interfere with the donor, spacer or acceptor to shield them from the changing electric field of the transmembrane potential. Further experiments in bilayers of different lipids or lipid compositions would help to rule this out, although the scope of lipid choice would be limited due to the need to form a stable DHB. Varying the headgroup designs, for example by using a charge-neutral sultone headgroup on **T11** or by changing the length of the alkyl spacer between the carboxylic acids and the pyridinium of **T13**, would also allow this factor to be tested, as these tweaks may change the membrane penetration depth.

To deduce the exact reasons for this result could require many different avenues of exploration, including a strong reliance upon imaging collaborators, for example in estimating the depth of membrane penetration and the orientation of the chromophore compared to the membrane normal, both of which would need to be measured at high time resolution with a varying membrane potential. Such experiments would be novel for fluorescent dyes,[73] but could be necessary to fully deduce the reasons for the negative results obtained so far. Alternatively the 'brute-force' approach of synthesising a large library of dyes

to test each variable might prove fruitful more rapidly. The work described in Chapter 5 was aimed towards facilitating this approach.

4.6.2 Cell viability

Although the voltage-sensitivity is the key part of characterising these dyes, biocompatibility is also a strongly desirable property. We thus desired to perform some preliminary tests with the compounds to assess their membrane localisation and toxicity. In experiments performed by Dr. Maria Izquierdo Arcusa and Dr. Marina Kuimova, both of the donor-acceptor second generation dyes were found to effectively stain the cell membrane of SK-OV-3 cells.

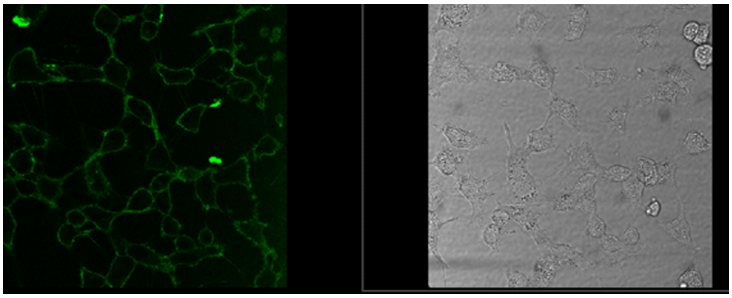

Figure **4.20** Fluorescence (left, $\lambda_{ex} = 488$ nm, $\lambda_{em} = 500 - 700$ nm) and bright field (right) microscope images of SK-OV-3 cells stained with **T13** for 20 minutes. Images acquired by Dr. Maria Izquierdo Arcusa, Imperial College London.

Bright fluorescence was observable from the cell membranes with low background signal, after the cells were incubated for five minutes with the dyes introduced to the aqueous culture bath at 2 μM. **T11** was found to be significantly more toxic to cells even at the start of the imaging experiments, suggesting a dark toxicity. Both dyes exhibited phototoxic effects upon the cells, preventing imaging beyond thirty minutes after the start of incubation. These results imply that the amphiphilicity of these dyes has been achieved as hoped, but that **T11** may be limited in applicability to cells if the toxicity observed in SK-OV-3 cells is representative.

4.7 Conclusion to Chapter 4

While I was carrying out the initial voltage-sensitivity experiments described in this chapter, work was published by Roger Y. Tsien and coworkers which proved for the first time that voltage-sensitive PeT can be applied to imaging membrane potential. Dyes **109** and **110** (Figure 4.21) consist of an *n*-butylaniline electron donor, a dichlorosulfofluorescein fluorophore and electron acceptor, and an oligo-*p*-phenylene vinylene (OPV) spacer. A $\Delta S/S$ of 25% was measured for **110**.[74] Although their work lacks an amphiphilic reference dye as a control to support the observed voltage sensitivity, the entire width of the fluorescence emission band was collected and thus changes in the fluorescence intensity were being observed, supporting the PeT mechanism. They also found little dependence of $\Delta S/S$ upon excitation wavelength, as expected for the PeT mechanism and a clear indication against an electrochromic mechanism operating. Appropriately fast time responses were also observed, and the dye featuring the longer eT distance has the higher sensitivity, consistent with expectations for voltage-sensitive PeT.

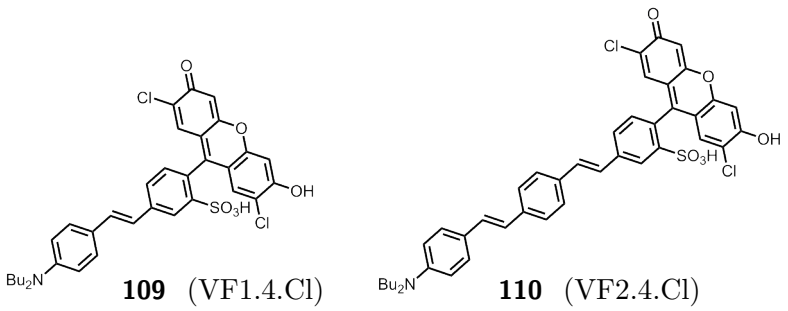

109 (VF1.4.Cl) **110** (VF2.4.Cl)

Figure **4.21** The first examples of PeT voltage probes in the literature.[74]

Comparing their VSD design to the one employed in this chapter may provide an explanation for the possible absence of voltage sensitivity observed in our dyes. The approach they adopted is conceptually very similar to the one outlined in this chapter: an electron donor and acceptor are separated by a molecular wire spacer, and the molecule is amphiphilic. Three key differences

are found between their design and ours: the fluorophore is the electron acceptor rather than the donor, the fluorophore is the hydrophilic rather than the hydrophobic part, and the lower-attenuation oligo-*p*-phenylene vinylene (OPV) molecular wire is used. The first two of these differences are unlikely to suggest a flaw in the BODIPY VSD design: as PeT is known to occur with the fluorophore as either electron donor or acceptor, the role of the fluorophore in PeT will not effect the voltage sensitivity. The direction of eT is the same in both their design and the design in this chapter, *from* the donor inside the bilayer membrane outwards to the acceptor. Nevertheless, the direction of eT should be irrelevant, as during an action potential the electric field across the membrane changes sign twice. At a given stage of the AP, either direction of eT will be either with or against the electric field, and thus exhibit enhanced or decreased PeT efficiency. Thus the location of the fluorophore, and the direction of eT relative to the transmembrane potential, should not matter as either direction will modulate the PeT efficiency (hence the four permutations of PeT VSD design in Figure 1.21 on Page 31).

The latter of the differences between the two designs could prove to be critical. The OPV spacer in Tsien's compounds has a lower attenuation than the OPE spacer employed in our design, and therefore provides stronger electronic coupling between the electron donor and the electron acceptor. The OPV spacer is more likely to result in a stepwise 'hopping' eT mechanism,[75,76] but this is not studied in their work. The precise attenuation behaviour of a particular spacer is a function not only of the spacer but of the whole eT system and thus will vary with the donor and the acceptor also. In order to deduce the effect of the spacer, an empirical approach attaching the same donor and acceptor pair to different spacers of equivalent length is necessary. It thus remains to be seen if the choice of the OPV spacer is a crucial difference between Tsien's dyes and the dyes in this chapter. This exciting report in the literature

proves that VS PeT can contend in the competitive area of IMP,[74] but does not assist in diagnosing the possible lack of sensitivity in the BODIPY-based dyes.

In summary, a family of novel amphiphilic donor-spacer-acceptor dyes were designed and synthesised, and PeT was found to compete with fluorescence. These designs were carried forward to more amphiphilic dyes with similar PeT behaviour. The second generation dyes were then characterised for voltage sensitivity and biocompatibility. While the results for the latter property were clear, further work is required to establish if these dyes are voltage sensitive or not. Similarly designed voltage sensors have irrevocably established this VS mechanism as an important player in this area, and suggest that the design described in this chapter might also contribute to the field of IMP. Extra investigation is required to fully test the voltage probes designed, synthesised and characterised in this chapter.

4.8 Experimental for Chapter 4

Compound numbers correspond to those used in this chapter, except those labelled 4-A, -B etc. which are not featured in the main text. Novel compounds are denoted by an asterisk (*) after the name. General experimental details can be found in Section 2.12 on Page 80.

79 3-Acetyl-2,4-dimethylpyrrole

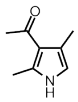

This compound was prepared by modification of a literature procedure.[56] 4-Acetyl-3,5-dimethylpyrrole carboxylic acid **78** (5.00 g, 27.6 mmol) and KOH (3.09 g, 54.5 mmol) were dissolved in ethane-1,2-diol (20 mL). The mixture was refluxed at 160 °C under N_2 for 3 h. The mixture was allowed to cool before extracting with $CHCl_3$ (3 × 50 mL), washing the organic fraction with water then brine (2 × 50 mL each) and drying over $MgSO_4$. Solvents removed under vacuum. Precipitation from $CHCl_3$/ petrol ether yielded **79** as a biege powder (3.5 g, 94%).^{1}H NMR (200 MHz, $CDCl_3$) δ 8.50 (br. s., 1 H, **N-H**), 6.37 (q, J=0.9 Hz, 1 H, **C1-H**), 2.50 (s, 3 H, **C4-Me**), 2.43 (s, 3 H, **Acetyl**), 2.28 (d, J=0.9 Hz, 3 H, **C2-Me**). ^{13}C NMR (50 MHz, $CDCl_3$) δ 195.8, 135.8, 120.8, 120.5, 114.8, 30.9, 15.2, 13.6. MS Calcd for $C_8H_{11}NO$ (M+H): 138.08. Found (TOF ES+): 138.10.

80 3-Ethyl-2,4-dimethylpyrrole (Kryptopyrrole)

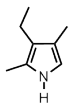

This compound was prepared by modification of a literature procedure.[56] **79** (3.00 g, 21.9 mmol) was dissolved in THF (30 mL) in a pre-dried flask under

N_2. THF (30 mL) was added to $LiAlH_4$ (1.50 g, 26.3 mmol) in a pre-dried flask under N_2. To this stirring suspension, the solution of **79** was added slowly *via* syringe. The mixture was refluxed at 68 °C for 16 h. The reaction was quenched *via* slow addition of propan-2-ol (2 mL), then MeOH (2 mL) then of aq. sat. Na_2SO_4 (2 mL). The mixture was extracted with $CHCl_3$ (100 mL). The solvents were evaporated. The product was distilled under reduced pressure (48-55 °C , 0.3 mbar) to yield 1.7 g (63%) of **80** as a light green oil which darkened rapidly upon exposure to air. ^{1}H NMR (400 MHz, $CDCl_3$) δ 7.49 (br. s., 1 H, **N-H**), 6.40 (s, 1 H, **C1-H**), 2.40 (q, J=7.6 Hz, 2 H, **Et-CH$_2$**), 2.18 (s, 3 H, **C4-Me**), 2.05 (d, J=0.9 Hz, 3 H, **C2-Me**), 1.09 (t, J=7.6 Hz, 3 H, **Et-CH$_3$**). ^{13}C NMR (50 MHz, $CDCl_3$) δ 123.7, 121.0, 118.3, 113.2, 17.9, 16.1, 11.6, 10.8. MS Calcd for $C_8H_{13}N$: 123.1048. Found (TOF FI+): 123.1045.

74 2,6-diethyl-4,4-difluoro-1,3,5,7-tetramethyl-8-(4-phenyl)-4-bora-3',5'-diaza-s-indacene

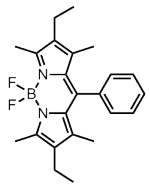

A literature procedure was followed.[3] Benzaldehyde (106 mg, 1.00 mmol) and **80** (246 mg, 2.00 mmol) were dissolved in CH_2Cl_2 (50 mL) under N_2 and pump-purge degassed. TFA (4 μL, 0.05 mmol) was added *via* syringe and the mixture stirred for 18 h, after which time the aldehyde was no longer observable by TLC. DDQ (227 mg, 1.00 mmol) was added the mixture stirred for a 1 h. Et_3N was added and the mixture stirred for 30 min before $BF_3 \cdot Et_2O$ was added. After 3 d, the reaction was worked up by washing with 2 M. aq. NaOH. The product was extracted into CH_2Cl_2 and dried over $MgSO_4$. After concentration the crude residue was purified on silica eluting with CH_2Cl_2 : hexanes 2 : 1. The product was crystallised as fine red needles from layered addition of ethanol

to CH_2Cl_2 (230 mg, 60%). ^{1}H NMR (400 MHz, $CDCl_3$) δ 7.45 - 7.50 (m, 3 H, **Aryl**), 7.27 - 7.31 (m, 2 H, **Aryl**), 2.54 (s, 6 H, **C3-Me, C5-Me**), 2.30 (q, J=7.5 Hz, 4 H, **Et-CH_2**), 1.28 (s, 6 H, **C1-Me, C7-Me**), 0.98 (t, J=7.6 Hz, 6 H, **Et-CH_3**). ^{13}C NMR (101 MHz, $CDCl_3$) δ 153.7, 140.2, 138.4, 135.8, 132.7, 130.8, 129.0, 128.7, 128.2, 17.1, 14.6, 12.5, 11.6. MS Calcd for $C_{23}H_{27}BF_2N_2$: 380.22. Found (MALDI TOF+): 380.01. λ_{max}/nm (log ϵ) in THF: 524 (4.91) 497 (4.41).

83 4-(Bromophenylethynyl)trimethylsilane

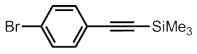

This compound was prepared by modification of a literature procedure.[80] 4-Bromoiodobenzene **82** (2.50 g, 8.84 mmol), CuI (25.3 mg, 1.33 mmol) and $Pd(PPh_3)_2Cl_2$ (245 mg, 0.350 mmol) were dried in a pre-dried flask under vacuum. The flask was pump-purge degassed and filled with N_2. Toluene (33 mL) and triethylamine (3 mL) were added *via* syringe. Trimethylsilylacetylene (1.37 mL, 9.72 mmol) was added *via* syringe and the mixture freeze-pump-thaw degassed thoroughly. Stirred under N_2 in the dark for 16 h. Solvents removed. Residue purified by flash chromatography on silica, eluting with petrol ether. Solvents removed to yield 2.1 g (95%) of **83** as a yellow solid. ^{1}H NMR (200 MHz, $CDCl_3$) δ 7.44 (dt, J=8.7, 2.0 Hz, 2 H), 7.33 (dt, J=8.7, 2.0 Hz, 2 H), 0.29 (s, 9 H). ^{13}C NMR (50 MHz, $CDCl_3$) δ 133.4, 131.6, 122.8, 122.2, 104.0, 95.6, 0.0. MS Calcd for $C_{11}H_{13}BrSi$: 251.9970. Found (TOF FI+): 251.9974.

84 1-(Triisopropylsilanylethynyl)-4-trimethylsilanylethynylbenzene

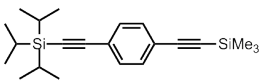

This compound was prepared by modification of a literature procedure.[80] **83** (800 mg, 3.16 mmol), CuI (90.0 mg, 0.470 mmol), $Pd_2(dba)_3$ (58.0 mg, 63.0

μmol) and PPh_3 (393 mg, 1.50 mmol) were dried in a pre-dried flask under vacuum. The flask was pump-purge degassed and filled with N_2. Toluene (13 mL) and triethylamine (1.3 mL) were added *via* syringe. Triisopropylsilylacetylene (0.75 mL, 3.3 mmol) was added *via* syringe and the mixture freeze-pump-thaw degassed thoroughly. Stirred under N_2 in the dark at 80 °C for 16 h. Solvents removed. Residue purified by flash chromatogrpahy on silica, eluting with petrol ether. Solvents removed to yield 0.67 g (60%) of **84** as a white solid. ^{1}H NMR (200 MHz, $CDCl_3$) δ 7.40 (s, 4 H), 1.13 (s, 21 H), 0.26 (s, 9 H). ^{13}C NMR (50 MHz, $CDCl_3$) δ 131.9, 131.8, 123.6, 123.0, 106.6, 104.7, 96.2, 92.9, 18.7, 11.4, 0.0. MS Calcd for $C_{22}H_{34}Si_2$: 354.2199. Found (TOF FI+): 354.2207.

85 (4-Ethynylphenylethynyl)triisopropylsilane

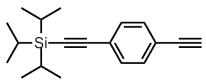

This compound was prepared by following a literature procedure.[79] **84** (100 mg, 0.280 mmol) and K_2CO_3 (42.9 mg, 0.310 mmol) were added to a 10 mL flask and purged with N_2. MeOH (2 mL) and CH_2Cl_2 (2 mL) were added and the flask purged with N_2. The solution was stirred under N_2 for 2 h. The product was extracted with CH_2Cl_2 (2 × 10 mL) and washed with water (2 × 10 mL). Solvents removed to yield **85** (78 mg, 98%) as a white solid. ^{1}H NMR (200 MHz, $CDCl_3$) δ 7.43 (br. s, 4 H), 3.17 (s, 1 H), 1.14 (s, 21 H). ^{13}C NMR (50 MHz, $CDCl_3$) δ 130.9, 123.0, 120.9, 105.4, 92.0, 82.2, 77.8, 17.6, 10.3. MS Calcd for $C_{19}H_{26}Si$: 282.1804. Found (TOF FI+): 282.1805.

81 2,6-diethyl-4,4-difluoro-1,3,5,7-tetramethyl-8-(4-iodophenyl)-4-bora-3',5'-diaza-s-indacene

This reaction was carried out following a procedure modified from the literature.[54,55] 4-iodobenzoyl chloride was distilled before use. 4-Iodobenzoyl chloride (1.08 g, 4.06 mmol) and kryptopyrrole **80** (1.00 g, 8.12 mmol) were dissolved in CH_2Cl_2 (50 mL) in a pre-dried flask under N_2. The mixture was

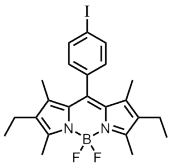

freeze-pump-thaw degassed and stirred at 40 °C for 19 h. The solvent was removed and the residue purified on silica, eluting with CH_2Cl_2 : 0-5% MeOH. The most polar fraction (dark red) corresponds to the dipyrrin. The dipyrrin was dissolved in toluene (50 mL) and triethylamine (2.25 mL, 16.1 mmol) under N_2. The mixture was freeze-pump-thaw degassed 3 ×. After 30 min, $BF_3 \cdot Et_2O$ (4.10 mL, 32.5 mmol) was added *via* syringe and the mixture heated to 75 °C. After 16 h, the mixture was allowed to cool. The reaction was washed with aq. sat. $NaHCO_3$, water and brine. The solvents were removed and the crude product purified by flash chromatography on silica, eluting with $CHCl_3$. The solvents were removed to give **81** as a dark red solid (0.80 g, 39%). ^{1}H NMR (200 MHz, $CDCl_3$) δ 7.84 (dt, J=8.4, 2.0 Hz, 2 H, **Aryl**), 7.05 (dt, J=8.4, 2.0 Hz, 2 H, **Aryl**), 2.53 (s, 6 H, **C3-Me, C5-Me**), 2.31 (q, J=7.6 Hz, 4 H, **Et-CH_2**), 1.33 (s, 6 H, **C1-Me, C7-Me**), 0.99 (t, J=7.6 Hz, 6 H, **Et-CH_3**). ^{13}C NMR (50 MHz, $CDCl_3$) δ 154.6, 139.0, 138.7, 138.6, 135.8, 133.5, 130.9, 130.7, 94.9, 17.5, 15.1, 13.0, 12.4. MS Calcd for $C_{23}H_{26}BFN_2I$ (M-F): 488.1. Found (MALDI TOF+): 486.3. λ_{max}/nm (log ϵ) in THF: 526 (4.92) 500 (4.44) 378 (3.90).

86 2,6-diethyl-4,4-difluoro-1,3,5,7-tetramethyl-8-(4-[4-(triisopropylsilylethynyl)phenyl]-ethynylphenyl)-4-bora-3',5'-diaza-s-indacene

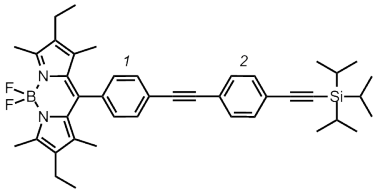

This reaction was carried out following a modified literature procedure.[50] **81** (65.0 mg, 0.130 mmol), **85** (40.0 mg, 0.140 mmol), $Pd(PPh_3)_2Cl_2$ (5.4 mg, 8.0 μmol) and CuI (2.5 mg, 13 μmol) were dried in a pre-dried Schlenk tube. THF (5 mL) and diisopropylamine (1 mL) were added under N_2, and the mixture was freeze-pump-thaw degassed. The mixture was stirred at 50 °C under N_2 for 1.5 h. The solvents were removed, and the residue purified by flash chromatography on silica, eluting with petrol ether : $CHCl_3$ 75 : 25 - 0 : 100. The solvents were removed, and the product precipitated from CH_2Cl_2/ethanol (75 mg, 87%). ^{1}H NMR (400 MHz, $CDCl_3$) δ 7.67 (d, J=8.0 Hz, 2 H, **Aryl-1**), 7.45 - 7.53 (m, 4 H, **Aryl-2**), 7.30 (d, J=8.0 Hz, 2 H, **Aryl-1**), 2.54 (s, 6 H, **C3-Me, C5-Me**), 2.31 (q, J=7.5 Hz, 4 H, **Et-CH_2**), 1.34 (s, 6 H, **C1-Me, C7-Me**), 1.15 (s, 21 H, **Si(CH(CH_3)$_2$)$_3$**), 0.99 (t, J=7.5 Hz, 6 H, **Et-CH_3**). ^{13}C NMR (126 MHz, $CDCl_3$) δ 154.0, 139.2, 138.2, 136.0, 132.9, 132.2, 132.0, 131.4, 130.5, 128.5, 123.7, 123.6, 122.6, 106.5, 93.1, 90.5, 90.3, 18.6, 17.0, 14.6, 12.5, 11.9, 11.3. ^{19}F NMR (377 MHz, $CDCl_3$) δ -145.76 (q, J=33 Hz). ^{11}B NMR (160 MHz, $CDCl_3$) δ 0.83 (t, J=34 Hz). MS Calcd for $C_{42}H_{51}BF_2N_2Si$: 661.40. Found (MALDI TOF+): 659.40. λ_{max}/nm (log ϵ) in THF: 526 (4.91) 498 (4.40) 308 (4.72).

90 1-(4-bromobenzyl)pyridinium bromide

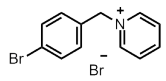

To a 100 mL flask purged with N_2 was added 4-bromobenzylbromide **89** (2.00 g, 8.00 mmol) and pyridine (50 mL). The mixture was pump-purge degassed and refluxed under N_2 for 90 mins. The solution was observed to become light yellow upon heating, and a white precipitate formed upon cooling. The product was filtered, washed with toluene and dried to give **90** (2.4 g, 90%) as a white solid. ^{1}H NMR (400 MHz, DMSO−d_6) δ 9.28 (d, J=5.8 Hz, 2 H,

Pyridinium C2-H, C6-H), 8.65 (t, J=7.8 Hz, 1 H, **Pyridinium C4-H**), 8.21 (t, J=7.1 Hz, 2 H, **Pyridinium C3-H, C5-H**), 7.67 (d, J=8.4 Hz, 2 H, **Aryl**), 7.56 (d, J=8.4 Hz, 2 H, **Aryl**), 5.92 (s, 2 H, **Benzyl**). ^{13}C NMR (50 MHz, DMSO$-d_6$) δ 146.1, 144.8, 133.6, 132.1, 131.2, 128.5, 122.9, 62.2. MS Calcd for $C_{12}H_{11}BrN$ (M +): 248.0, 250.0. Found (TOF ES+): 248.0, 250.0.

87 2,6-diethyl-4,4-difluoro-1,3,5,7-tetramethyl-8-(4-[4-ethynylphenyl]-ethynylphenyl)-4-bora-3',5'-diaza-s-indacene

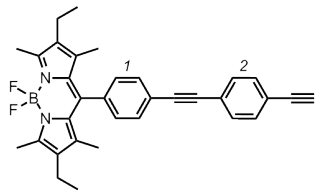

This reaction was carried out following a modified literature procedure.[55] **86** (60.0 mg, 90.0 μmol) was dried in a pre-dried flask under vacuum and then pump-purge degassed. THF (2.0 mL) was added to the flask *via* syringe under N_2 and the solution cooled to -78 °C. $Bu_4N^+F^-$ (1.0 M in THF, 450 μL, 0.450 mmol) added *via* syringe. Mixture stirred under N_2 at -78 °C for 1 h. The reaction mixture was allowed to warm to room temperature, then AcOH (10 μL, 0.18 mmol) was added *via* syringe. The mixture was passed through a silica plug, eluting with $CHCl_3$. Solvents removed. Precipitation from CH_2Cl_2/ethanol gave **87** (30 mg, 66%) as a red powder. ^{1}H NMR (400 MHz, $CDCl_3$) δ 7.67 (d, J=8.0 Hz, 2 H, **Aryl-1**), 7.47 - 7.55 (m, 4 H, **Aryl-2**), 7.31 (d, J=8.2 Hz, 2 H, **Aryl-1**), 3.21 (s, 1 H, **Acetylene**), 2.54 (s, 6 H, **C3-Me, C5-Me**), 2.31 (q, J=7.5 Hz, 4 H, **Et-CH_2**), 1.34 (s, 6 H, **C1-Me, C7-Me**), 0.99 (t, J=7.5 Hz, 6 H, **Et-CH_3**). ^{13}C NMR (126 MHz, $CDCl_3$) δ 154.0, 139.1, 138.2, 136.1, 132.9, 132.2, 132.1, 131.5, 130.5, 128.6, 123.5, 123.3, 122.2, 90.7, 90.0, 83.1, 79.1, 17.0, 14.6, 12.5, 11.9. MS Calcd for $C_{33}H_{31}BF_2N_2$: 504.25. Found (MALDI TOF+): 504.03. λ_{max}/nm (log ϵ) in THF: 526 (4.90) 498 (4.40) 302 (4.64).

T8 **2,6-diethyl-4,4-difluoro-1,3,5,7-tetramethyl-8-(4-[4-(4-*n*-butylphenyl)-ethynylphenyl]-ethynylphenyl)-4-bora-3',5'-diaza-s-indacene***

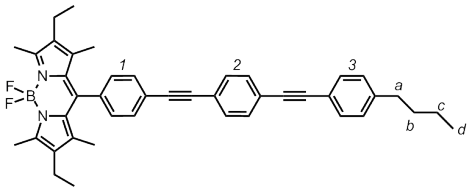

This reaction was carried out following a modified literature procedure.[50] **87** (10.0 mg, 20.0 μmol), $Pd(PPh_3)_2Cl_2$ (0.84 mg, 1.2 μmol) and CuI (0.38 mg, 2.0 μmol) were dried in a pre-dried flask under vacuum. THF (0.75 mL) and diisopropylamine (150 μL) were added to the flask *via* syringe under N_2. The mixture was freeze-pump-thaw degassed 3 × then 4-iodo-1-*n*-butylbenzene (4 μL, 0.022 mmol) was added *via* syringe under N_2. The mixture was stirred in the dark at room temperature for 2 h. Solvents removed. Residue purified on a silica column, eluting with petrol ether : $CHCl_3$ 1 : 3. $CHCl_3$ was used to assist the loading of the column. Solvents removed. Precipitation from CH_2Cl_2/MeOH gave **T8** as a red powder (10 mg, 78%). ^{1}H NMR (400 MHz, $CDCl_3$) δ 7.67 (d, J=8.4 Hz, 2 H, **Aryl-1**), 7.50 - 7.56 (m, 4 H, **Aryl-2**), 7.45 (d, J=8.2 Hz, 1 H, **Aryl-3**), 7.31 (d, J=8.4 Hz, 2 H, **Aryl-1**), 7.19 (d, J=8.4 Hz, 2 H, **Aryl-3**), 2.64 (t, J=7.8 Hz, 2 H, **Butyl-a**), 2.54 (s, 6 H, **C3-Me, C5-Me**), 2.32 (q, J=7.6 Hz, 4 H, **Et-CH_2**), 1.57 - 1.67 (m, 2 H, **Butyl-b**), 1.35 - 1.41 (m, 2 H, **Butyl-c**), 1.34 (s, 6 H, **C1-Me, C7-Me**), 0.99 (t, J=7.5 Hz, 6 H, **Et-CH_3**), 0.94 (t, J=7.3 Hz, 3 H, **Butyl-d**). ^{13}C NMR (126 MHz, $CDCl_3$) δ 154.0, 143.8, 139.2, 138.2, 136.0, 132.9, 132.2, 131.5, 130.5, 128.6, 128.5, 123.7, 123.6, 122.4, 120.0, 91.8, 90.4, 90.4, 88.4, 35.6, 33.4, 22.3, 17.1, 14.6, 13.9, 12.5, 11.9. ^{11}B NMR (160 MHz, $CDCl_3$) δ 0.84 (t, J= 33.3 Hz). ^{19}F NMR (377 MHz, $CDCl_3$) δ -145.75 (q, J=33.3 Hz). MS Calcd for $C_{43}H_{43}BF_2N_2$: 636.35. Found (MALDI TOF+): 634.83. λ_{max}/nm (log ϵ) in THF: 526 (4.77)

498 (4.27) 327 (4.69). $\lambda_{em,max}$/nm in THF: 538; Φ_f= 0.48.

T9 2,6-diethyl-4,4-difluoro-1,3,5,7-tetramethyl-8-(4-[4-(4-(benzyl-pyridinium)-phenyl)-ethynylphenyl]-ethynylphenyl)-4-bora-3',5'-diaza-s-indacene hexafluorophosphate*

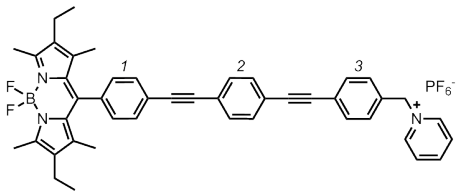

To a dried flask were added **87** (10.0 mg, 20 μmol), **90** (32.5 mg, 0.100 mmol), $Pd_2(dba)_3$ (0.92 mg, 1.0 μmol), PPh_3 (0.50 mg, 2.0 μmol) and CuI (0.2 mg, 1.0 μmol). The reagents were dried under vacuum for 0.5 h before the flask was purged with N_2. DMF (1.5 mL) and diisopropylamine (0.5 mL) were added *via* syringe and the mixture was freeze-pump-thaw degassed successively. The reaction was heated at 80 °C and completion was observed by TLC after 75 mins. The solvents were removed and the residue purified on silica eluting with $CHCl_3$: MeOH 0-20%. The desired fraction was redissolved in 2 mL of MeOH and 20 eq. of NH_4PF_6 were added to yield the product as the PF_6 salt. The compound was dissolved in $CHCl_3$ and washed with water 3 × to remove any excess NH_4PF_6, giving 9 mg of **T9** (55%) as a red powder. ^{1}H NMR (400 MHz, DMSO−d_6) δ 9.24 (d, J=5.6 Hz, 2 H, **Pyridinium C2-H, C6-H**), 8.66 (t, J=7.6 Hz, 1 H, **Pyridinium C4-H**), 8.22 (t, J=6.8 Hz, 2 H, **Pyridinium C3-H, C5-H**), 7.76 (d, J=8.0 Hz, 2 H, **Aryl-1**), 7.57 - 7.71 (m, 8 H, **Aryl-2, Aryl-3**), 7.46 (d, J=7.9 Hz, 2 H, **Aryl-1**), 5.92 (s, 2 H, **Benzyl**), 2.45 (s, 6 H, **C3-Me, C5-Me**), 2.31 (q, J=7.3 Hz, 4 H, **Et-CH_2**), 1.31 (s, 6 H, **C1-Me, C7-Me**), 0.95 (t, J=7.4 Hz, 6 H, **Et-CH_3**). ^{13}C NMR (126 MHz, DMSO−d_6) δ 153.5, 146.1, 145.0, 139.5, 138.0, 135.3, 134.9, 132.8, 132.3, 132.2, 131.8, 131.8, 129.7, 129.2, 128.8, 128.6, 123.0, 122.7, 122.4, 122.3, 90.9, 90.7, 90.0, 89.9, 79.2,

16.4, 14.5, 12.3, 11.5. ^{11}B NMR (160 MHz, DMSO−d_6) δ 0.6 (t, J=33.3 Hz). ^{19}F NMR (470 MHz, DMSO−d_6) δ -70.15 (d, J=714.4 Hz), -142.94 (q, J=33.3 Hz). MS Calcd for $C_{45}H_{41}BF_2N_3$: 672.3364. Found (TOF ESI+): 672.3348. $\lambda_{em,max}$/nm in THF: 538; Φ_f= 0.37.

88 2,6-diethyl-4,4-difluoro-1,3,5,7-tetramethyl-8-(4-[4-(4-pyridine)-ethynylphenyl]-ethynylphenyl)-4-bora-3',5'-diaza-s-indacene*

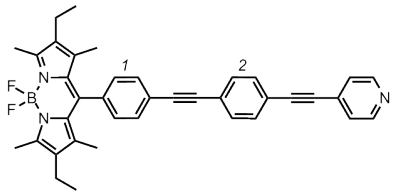

A Schlenk tube was dried under vacuum and **87** (10.0 mg, 20 μmol), 4-iodopyridine (43.0 mg, 200 μmol), $Pd(PPh_3)_2Cl_2$ (1.30 mg, 2.00 μmol) and CuI (0.38 mg, 2.0 μmol) were added. The vessel was purged with N_2 and THF (750 μL) and diisopropylamine (150 μL) were added *via* syringe. The mixture was freeze-pump-thaw degassed successively and stirred at ambient temperature under N_2. After 30 mins, the solvents were removed and the residue purified on silica eluting with $CHCl_3$: MeOH 0-5% to yield **88** as a red powder (7.5 mg, 65%) after precipitation from CH_2Cl_2/MeOH. ^{1}H NMR (400 MHz, $CDCl_3$) δ 8.63 (d, J=5.5 Hz, 2 H, **Pyridine C2-H, C6-H**), 7.68 (d, J=8.4 Hz, 2 H, **Aryl-1**), 7.55 - 7.60 (m, 4 H, **Aryl-2**), 7.40 (d, J=6.1 Hz, 1 H, **Pyridine C3-H, C5-H**), 7.32 (d, J=8.4 Hz, 2 H, **Aryl-1**), 2.55 (s, 6 H, **C3-Me, C5-Me**), 2.32 (q, J=7.5 Hz, 4 H, **Et-CH_2**), 1.34 (s, 6 H, **C1-Me, C7-Me**), 0.99 (t, J=7.6 Hz, 6 H, **Et-CH_3**). ^{13}C NMR (126 MHz, $CDCl_3$) δ 162.5, 154.1, 149.9, 139.1, 138.1, 136.2, 133.0, 132.3, 131.9, 131.7, 130.5, 128.6, 125.5, 123.7, 123.4, 122.1, 93.5, 91.1, 90.0, 88.5, 17.0, 14.6, 12.5, 11.9. ^{11}B NMR (160 MHz, $CDCl_3$) δ 0.83 (t, J= 33.3 Hz). ^{19}F NMR (470 MHz, $CDCl_3$) δ -145.74 (q, J= 33.3 Hz). MS Calcd for $C_{38}H_{34}BF_2N_3$: 582.29. Found (MALDI TOF+): 581.84. λ_{max}/nm (log ϵ) in THF: 527 (4.85) 500 (4.37) 323 (4.74).

T7 **2,6-diethyl-4,4-difluoro-1,3,5,7-tetramethyl-8-(4-[4-(4-methylpyridinium)-ethynylphenyl]-ethynylphenyl)-4-bora-3',5'-diaza-s-indacene hexafluorophosphate***

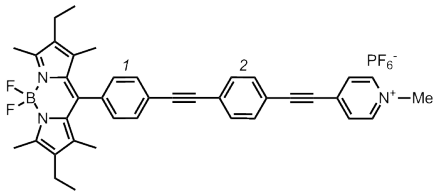

^{1}H NMR (400 MHz, DMSO−d_6) δ 9.02 (d, J=6.5 Hz, 2 H, **Pyridinium C2-H, C6-H**), 8.28 (d, J=6.5 Hz, 2 H, **C3-H, C5-H**), 7.73 - 7.84 (m, 6 H, **Aryl-1, Aryl-2**), 7.48 (d, J=8.0 Hz, 2 H, **Aryl-1**), 4.33 (s, 3 H, **Pyridinium *N*-Me**), 2.45 (s, 6 H, **C3-Me, C5-Me**), 2.31 (q, J=7.8 Hz, 4 H, **Et-CH_2**), 1.31 (s, 6 H, **C1-Me, C7-Me**), 0.95 (t, J=7.6 Hz, 6 H, **Et-CH_3**). ^{13}C NMR (126 MHz, DMSO−d_6) δ 153.6, 145.7, 139.4, 138.0, 137.9, 135.6, 132.8, 132.7, 132.3, 132.1, 129.7, 129.0, 128.8, 124.5, 122.5, 120.1, 101.0, 92.0, 89.7, 87.1, 16.4, 14.5, 12.3, 11.5. ^{11}B NMR (160 MHz, DMSO−d_6) δ 0.60 (t, J= 33.3 Hz). ^{19}F NMR (470 MHz, DMSO−d_6) δ -70.15 (d, J=710.9 Hz), -142.93 (q, J= 33.3 Hz). MS Calcd for $C_{39}H_{37}BF_2N_3$: 596.3050. Found (TOF ESI+): 596.3040. $\lambda_{em,max}$/nm in THF: 538; Φ_f= 0.07.

92 **2,4,6-Triphenyl-N-(4-iodophenyl)-pyridinium tetrafluoroborate**

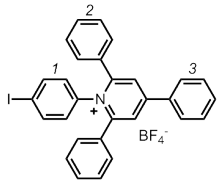

This reaction was carried out according to a modified literature procedure.[78] 2,4,6-Triphenylpyrylium tetrafluoroborate **91** (500 mg, 1.26 mmol) and NaOAc (450 mg, 5.49 mmol) were added to a pre-dried flask under N_2. Ethanol (8 mL) was added *via* syringe and the suspension stirred at 60 °C for 5 minutes. A

solution of 4-iodoaniline (240 mg, 1.10 mmol) in ethanol (2 mL) was added dropwise *via* syringe to the suspension. The mixture was heated at reflux for 1 h, during which the solution had turned yellow and a precipitate had formed. The solution was stored at 4 °C for 3 d and the precipitate was filtered off. The precipitate was dissolved in CH_2Cl_2 and washed with water. The solvent was removed and the product precipitated from CH_2Cl_2/ethanol to give **92** (356 mg, 54%). ^{1}H NMR (400 MHz, MeOD) δ 8.12 (s, 2 H, **Pyridinium C3-H, C5-H**), 7.89 (d, J=7.3 Hz, 2 H, **Aryl-3, ortho**), 7.60 (d, J=7.0 Hz, 1 H, **Aryl-3, para-H**), 7.56 (d, J=7.9 Hz, 2 H, **Aryl-2, para-H**), 7.45 (d, J=8.6 Hz, 2 H, **Aryl-1**), 7.26 - 7.41 (m, 10 H, **Aryl-2 ortho/meta, Aryl-3 meta**), 6.97 (d, J=8.9 Hz, 2 H, **Aryl-1**). ^{13}C NMR (101 MHz, MeOD) δ 158.1, 157.0, 138.9, 138.5, 134.5, 132.9, 132.8, 130.9, 130.4, 130.1, 129.9, 129.0, 128.7, 126.5, 96.4. MS Calcd for $C_{29}H_{21}NI$: 510.07. Found (TOF ESI+): 511.60.

T10 2,6-diethyl-4,4-difluoro-1,3,5,7-tetramethyl-8-(4-[4-(4-(2,4,6-triphenylpyridinium)-phenyl)-ethynylphenyl]-ethynylphenyl)-4-bora-3',5'-diaza-s-indacene hexafluorophosphate*

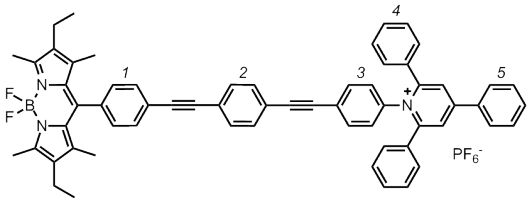

87 (10.0 mg, 20.0 μmol), **92** (11.8 mg, 20.0 μmol), $Pd_2(dba)_3$ (0.90 mg, 1.0 μmol), PPh_3 (0.52 mg, 2.0 μmol) and CuI (0.20 mg, 1.0 μmol) were added to a dried flask under N_2. Acetonitrile (1 mL) and diisopropylamine (150 μL) were added *via* syringe and the mixture freeze-pump-thaw degassed thoroughly. After 2 h, the solution was purified on silica eluting with $CHCl_3$: MeOH 0-1%. The desired fraction was dissolved in MeOH and the product precipitated upon addition of an excess of NH_4PF_6 to yield **T10** (6.0 mg, 34%) ^{1}H NMR (400 MHz, $CDCl_3$) δ 8.09 (s, 2 H, **Pyridinium C3-H, C5-H**), 7.87 (d, J=7.0

Hz, 2 H, **Aryl-5, ortho**), 7.66 (d, J=8.2 Hz, 2 H, **Aryl-1**), 7.61 (d, J=7.2 Hz, 1 H, **Aryl-5, para**), 7.57 (d, J=7.7 Hz, 2 H, **Aryl-4, para**), 7.54 (d, J=8.0 Hz, 2 H, **Aryl-2**), 7.47 (d, J=8.4 Hz, 2 H, **Aryl-2**), 7.28 - 7.44 (m, 14 H, **Aryl-3, Aryl-4 ortho/meta, Aryl-5 meta**), 7.22 (d, J=8.7 Hz, 2 H, **Aryl-1**), 2.54 (s, 6 H, **C3-Me, C5-Me**), 2.31 (q, J=7.4 Hz, 4 H, **Et-CH_2**), 1.33 (s, 6 H, **C1-Me, C7-Me**), 0.99 (t, J=7.5 Hz, 6 H, **Et-CH_3**). ^{13}C NMR (126 MHz, $CDCl_3$) δ 158.4, 156.6, 154.1, 139.1, 138.2, 138.1, 136.2, 134.4, 132.9, 132.5, 132.3, 132.2, 132.1, 131.7, 131.6, 130.5, 129.8, 129.6, 128.7, 128.6, 128.6, 128.4, 126.5, 125.1, 123.5, 123.4, 122.2, 91.8, 91.1, 90.0, 89.2, 17.0, 14.6, 12.5, 11.9. ^{11}B NMR (160 MHz, $CDCl_3$) δ 0.83 (t, J= 33.3 Hz). ^{19}F NMR (470 MHz, $CDCl_3$) δ -73.27 (d, J=710.9 Hz) -145.77 (q, J= 32.9 Hz). MS Calcd for $C_{62}H_{51}BF_2N_3$: 886.4149. Found (TOF ESI+): 886.4148. $\lambda_{em,max}$/nm in THF: 538; Φ_f= 0.23.

93 1-Iodo-5-(triethylammonium)-pentane iodide

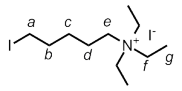

1,5-Diiodopentane (2.23 mL, 15.0 mmol) and triethylamine (1.39 mL, 10.0 mmol) were added *via* syringe to Et_2O (1.5 mL) in a flask purged with N_2 and the mixture stirred for 18 h. A white precipitate formed, which was filtered and washed with Et_2O (100 mL) to give **93** (0.87 g, 20%). ^{1}H NMR (400 MHz, DMSO−d_6) δ 3.30 (t, J=6.7 Hz, 2 H, **e**), 3.23 (q, J=7.3 Hz, 6 H, **f**), 3.09 - 3.16 (m, 2 H, **a**), 1.82 (quin, J=7.1 Hz, 2 H, **d**), 1.55 - 1.66 (m, 2 H, **b**), 1.32 - 1.42 (m, 2 H, **c**), 1.17 (t, J=7.3 Hz, 9 H, **g**). ^{13}C NMR (101 MHz, DMSO−d_6) δ 56.7, 52.9, 33.1, 27.7, 20.8, 9.4, 8.1. MS Calcd for $C_{11}H_{25}IN$: 298.10. Found (TOF ESI+): 298.11.

T11 2,6-Diethyl-4,4-difluoro-1,3,5,7-tetramethyl-8-(4-[4-(4-(5-(triethylammonium)-pentyl)-pyridinium)-ethynylphenyl]-ethynylphenyl)-4-bora-3',5'-diaza-s-indacene dichloride*

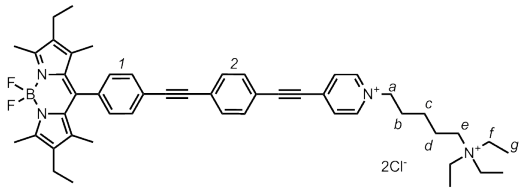

To a flask purged with N_2 were added **88** (15.0 mg, 26.0 μmol), **93** (219 mg, 0.520 mmol) and acetophenone (3 mL). The mixture was heated to 80 °C for 4 h. The solvent was removed and the crude residue purified on silica, eluting the starting material first with $CHCl_3$: 5% MeOH then the product with MeOH : NH_4Cl (2 M aq.) : nitromethane 5 : 3 : 2. The solvents were removed and the residue dissolved in $CHCl_3$ ($\sim$ 5 mL) in a centrifuge tube. Water ($\sim$ 55 mL) was layered over the solution and the tube was centrifuged (10 min, 3500 rpm). The water was removed and the process repeated 10 ×, after which complete removal of the excess of **93** was confirmed by NMR. **T11** was isolated as a red powder by precipitation from $CHCl_3$/petrol ether (4.0 mg, 19%). ^{1}H NMR (400 MHz, $CDCl_3$) δ 9.70 (d, J=5.8 Hz, 2 H, **Pyridinium C2-H, C6-H**), 7.97 (d, J=5.8 Hz, 2 H, **Pyridinium C3-H, C5-H**), 7.69 (d, J=8.2 Hz, 2 H, **Aryl-1**), 7.61 - 7.67 (m, 4 H, **Aryl-2**), 7.33 (d, J=8.2 Hz, 2 H, **Aryl-1**), 5.05 (t, J=7.3 Hz, 2 H, **a**), 3.49 (t, J=8.3 Hz, 2 H, **e**), 3.43 (q, J=7.3 Hz, 6 H, **f**), 2.54 (s, 6 H, **C3-Me, C5-Me**), 2.39 - 2.50 (m, 2 H, **b**), 2.31 (q, J=7.5 Hz, 4 H, **Et-CH_2**), 2.03 - 2.15 (m, 2 H, **d**), 1.78 - 1.90 (m, 2 H, **c**), 1.40 (t, J=7.3 Hz, 9 H, **g**), 1.34 (s, 6 H, **C1-Me, C7-Me**), 0.99 (t, J=7.4 Hz, 6 H, **Et-CH_3**). ^{13}C NMR (126 MHz, $CDCl_3$) δ 154.1, 144.8, 140.5, 139.0, 138.1, 136.5, 133.0, 132.8, 132.3, 131.9, 130.5, 129.5, 128.7, 126.0, 123.1, 119.8, 104.9, 92.5, 89.7, 86.7, 60.3, 58.1, 53.5, 30.8, 22.8, 21.9, 17.0, 14.6, 12.5, 11.9, 8.1. ^{11}B NMR (160 MHz, $CDCl_3$) δ 0.83 (t, J=32.3 Hz). ^{19}F NMR (377 MHz, $CDCl_3$) δ 1-

45.76 (q, J=32.3 Hz). MS Calcd for $[C_{49}H_{59}BF_2N_4]^{2+}$: 376.2399. Found (TOF ESI+): 376.2395. λ_{max}/nm (log ϵ) in THF: 527 (4.62) 500 (4.16) 366 (4.54). $\lambda_{em,max}$/nm in THF: 538; Φ_f= 0.09.

101 ***tert*-butyl pent-4-ynoate**

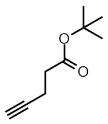

This reaction was carried out according to a literature method.[77] 4-Pentynoic acid **100** (1.00 g, 10.1 mmol), *tert*-butanol (1.93 mL, 20.2 mmol), *N,N*-dimethylaminopyridine (50.0 mg, 0.410 mmol) and *N,N*'-dicyclohexylcarbodiimide (2.29 g, 11.1 mmol) were stirred in dry CH_2Cl_2 (6 mL) under N_2 for 3 h. The reaction mixture was washed twice with 0.5 M HCl, twice with sat. $NaHCO_3$ and extracted with CH_2Cl_2. The solvent was removed and the crude residue purified by flash chromatography on silica, eluting with CH_2Cl_2. The solvent was removed to give **101** as a colourless oil (0.99 g, 64%). ^{1}H NMR (400 MHz, $CDCl_3$) δ 2.43 - 2.49 (m, 4 H), 1.95 - 1.99 (m, 1 H), 1.45 (br. s, 9 H). ^{13}C NMR (50 MHz, $CDCl_3$) δ 171.5, 83.2, 81.3, 69.2, 34.9, 28.5, 14.9.

102 **Di-*tert*-butyl 5,5'-(pyridine-3,5-diyl)bis(pent-4-ynoate)***

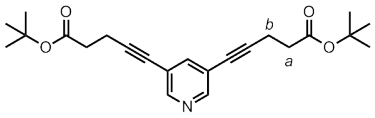

3,5-Dibromopyridine **95** (460 mg, 1.95 mmol), $Pd_2(dba)_3$ (36.0 mg, 39.0 μmol), CuI (7.4 mg, 39 μmol) and PPh_3 (42.0 mg, 0.160 mmol) were added to a dried Schlenk tube purged with N_2 and dried under vacuum for 30 mins. Triethylamine (1.5 mL) and tetrahydrofuran (15 mL) were added under N_2. The mixture was freeze-pump-thaw degassed before **101** (900 mg, 5.84 mmol) was added *via* syringe. The reaction was stirred at 40 °C for 15 h. The solvents

were removed and the residue purified on silica, eluting with CH_2Cl_2 : ethyl acetate 0-10%. The bis-substituted title compound was isolated as a yellow-brown solid (330 mg, 44%). ^{1}H NMR (400 MHz, $CDCl_3$) δ 8.35 (br. s, 2 H, **Pyridine C2-H, C6-H**), 7.50 (t, J=2.1 Hz, 1 H, **Pyridine C4-H**), 2.56 (t, J=7.2 Hz, 4 H, **a**), 2.40 (t, J=7.2 Hz, 4 H, **b**), 1.34 (s, 18 H, ***t*-Bu**). ^{13}C NMR (50 MHz, $CDCl_3$) δ 171.4, 151.0, 141.1, 120.7, 92.9, 81.4, 77.6, 34.9, 28.5, 16.0. MS Calcd for $C_{23}H_{29}NO_4$ (M +Na): 406.1989. Found (TOF ESI+): 406.1988.

103 Di-*tert*-butyl 5,5'-(pyridine-3,5-diyl)dipentanoate*

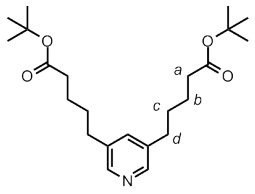

10% Pd/C (8.3 mg, 0.078 mmol) and **102** (300 mg, 0.782 mmol) were added to a dried flask under N_2. Propan-2-ol (20 mL) was added *via* syringe and the mixture pump-purge degassed 3 × with N_2 then 3 × with H_2. After 15 h, completion was observed by TLC. The flask was purged with N_2. The solution was passed through celite eluting with propan-2-ol. The solvent was removed to yield **103** as a yellow-brown oil (306 mg, 100%). ^{1}H NMR (400 MHz, $CDCl_3$) δ 8.26 (d, J=1.9 Hz, 2 H, **Pyridine C2-H, C6-H**), 7.28 (t, J=1.9 Hz, 1 H, **Pyridine C4-H**), 2.55 - 2.63 (m, 4 H, **d**), 2.21 - 2.28 (m, 4 H, **a**), 1.58 - 1.66 (m, 8 H, **b, c**), 1.43 (s, 18 H, ***t*-Bu**). ^{13}C NMR (50 MHz, $CDCl_3$) δ 173.3, 147.9, 137.4, 136.1, 80.6, 35.7, 33.1, 31.0, 28.5, 25.1. MS Calcd for $C_{23}H_{38}NO_4$: 392.2795. Found (TOF ESI+): 392.2786.

104 1-(4-iodobenzyl)-3,5-bis(5-(*tert*-butoxy)-5-oxopentyl)-pyridinium bromide*

To a dry flask were added **103** (306 mg, 0.782 mmol), 4-bromobenzylbromide (1.95 g, 7.82 mmol) and dry acetonitrile (10.0 mL). The mixture was pump-purge degassed 3 × then brought to reflux under N_2 for 4 h. The solvents

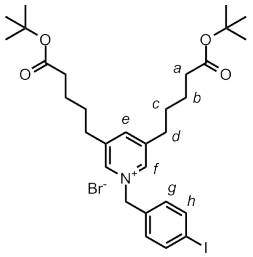

were removed and the crude residue purified on silica, eluting with CH_2Cl_2 : MeOH 5-10%. **104** was isolated as a viscous brown oil (0.28 g, 57%). ^{1}H NMR (400 MHz, $CDCl_3$) δ 9.27 (d, J=1.2 Hz, 2 H, **f**), 7.96 (br. s, 1 H **e**), 7.73 (dt, J=8.5, 2.3 Hz, 2 H, **g**), 7.48 (dt, J=8.4, 2.3 Hz, 2 H,**h**), 6.22 (s, 2 H, **Benzyl**), 2.84 (t, J=7.6 Hz, 4 H, **d**), 2.28 (t, J=7.0 Hz, 4 H, **a**), 1.69 - 1.79 (m, 4 H, **c**), 1.61 - 1.67 (m, 4 H, **b**), 1.44 (s, 21 H, ***t*-Bu**). ^{13}C NMR (101 MHz, $CDCl_3$) δ 172.6, 144.5, 143.2, 141.8, 138.5, 133.1, 131.5, 96.2, 80.3, 62.5, 34.7, 32.3, 29.4, 28.1, 24.2. MS Calcd for $C_{30}H_{43}INO_4$ (M+): 608.22. Found (TOF ESI+): 608.83.

4-A 2,6-diethyl-4,4-difluoro-1,3,5,7-tetramethyl-8-(4-[4-([4-benzyl]-3,5-bis[5-(*tert*-butoxy)-5-oxopentyl]pyridinium)-ethynylphenyl]-ethynylphenyl)-4-bora-3',5'-diaza-s-indacene chloride*

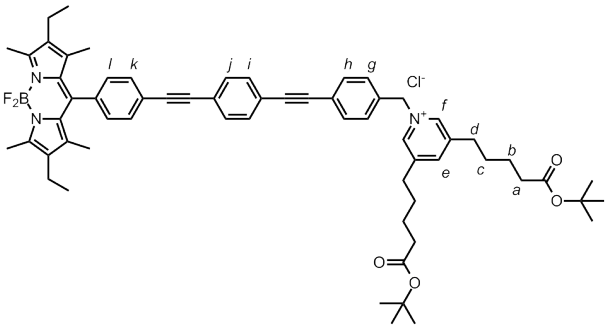

87 (26.0 mg, 51.5 μmol), **104** (166 mg, 0.259 mmol), $Pd_2(dba)_3$ (2.4 mg, 2.6 μmol), PPh_3 (1.4 mg, 5.3 μmol) and CuI (0.5 mg, 3 μmol) were dried under vacuum in a pre-dried flask under N_2. *N,N*-Dimethylformamide (5 mL) and DIPA (0.5 mL) were added *via* syringe, the mixture was freeze-pump-thaw degassed 3 ×, and then heated to 80 °C for 3 h. The solvents were removed

and the crude residue purified by flash chromatography on silica, eluting with CH_2Cl_2 : 1-10% MeOH (0.1 M NH_4Cl). This afforded a mixture of the desired product and **104** which were separated using size exclusion chromatography (Biobeads eluting with $CHCl_3$). The solvents were removed and the product precipitated from CH_2Cl_2/petrol ether (60-80) to give a red solid (15 mg, 29%). ^{1}H NMR (400 MHz, $CDCl_3$) δ 9.05 (s, 2 H, **f**), 8.02 (s, 1 H, **e**), 7.67 (d, J=8.4 Hz, 4 H, **g, k**), 7.58 (d, J=8.2 Hz, 2 H, **h**), 7.51 - 7.56 (m, 4 H, **i, j**), 7.30 (d, J=8.4 Hz, 2 H, **l**), 6.18 (s, 2 H, **Benzyl**), 2.89 (t, J=7.6 Hz, 4 H, **d**), 2.54 (s, 6 H, **C3-Me, C5-Me**), 2.26 - 2.35 (m, 8 H, **Et-CH_2, a**), 1.72 - 1.82 (m, 4 H, **c**), 1.63 - 1.70 (m, 4 H, **b**), 1.45 (s, 18 H, ***t*-Bu**), 1.33 (s, 6 H, **C1-Me, C7-Me**), 0.99 (t, J=7.6 Hz, 6 H, **Et-CH_3**). ^{13}C NMR (126 MHz, $CDCl_3$) δ 172.7, 154.0, 144.5, 143.3, 142.0, 139.1, 138.2, 136.1, 132.9, 132.6, 132.2, 131.7, 131.6, 130.5, 129.7, 128.6, 124.7, 123.5, 123.0, 122.9, 90.8, 90.6, 90.4, 90.2, 80.4, 63.7, 34.7, 32.4, 29.7, 29.3, 28.1, 24.2, 17.0, 14.6, 12.5, 11.9. MS Calcd for $C_{63}H_{73}BF_2N_3O_4$ (M+): 984.5662. Found (TOF ESI+): 984.5667. λ_{max}/nm (log ϵ) in THF: 526 (4.68) 498 (4.21) 328 (4.67).

T13 2,6-diethyl-4,4-difluoro-1,3,5,7-tetramethyl-8-(4-[4-([4-benzyl]-3,5-bis(4-carboxybutyl)-pyridinium-ethynylphenyl]-ethynylphenyl)-4-bora-3',5'-diaza-s-indacene chloride*

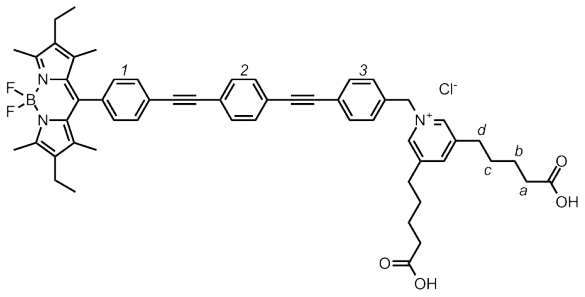

This transformation was effected by following a modified literature procedure.[68] A solution of **4-A** (5.0 mg, 5.0 μmol) was stirred at 0 °C in CH_2Cl_2 (2 mL) under N_2. To this solution were added 4 Ä molecular sieve beads ($\sim$ 80 mg) and $BF_3 \cdot Et_2O$ (200 μL, 10% vol/vol). After 40 min, complete loss of starting

material was observed by TLC, along with the formation of a polar product. The reaction was quenched by the addition of sat. aq. $NaHCO_3$. The product was extracted with $CHCl_3$ and washed successively with water. The solvents were removed and the crude product precipitated from ($CHCl_3$: MeOH 1 : 1)/pentane to yield **T13** (6.5 mg, 52%). ^{1}H NMR (400 MHz, DMSO−d_6) δ 9.02 (s, 2 H, **Pyridinium C2-H, C6-H**), 8.46 (br. s., 1 H, **Pyridinium C4-H**), 7.76 (d, J=8.3 Hz, 2 H, **Aryl-1**), 7.60 - 7.70 (m, 6 H, **Aryl-2, Aryl-3**), 7.55 (d, J=8.3 Hz, 2 H, **Aryl-3**), 7.46 (d, J=7.9 Hz, 2 H, **Aryl-1**), 5.81 (br. s., 2 H, **Benzyl**), 2.79 (t, J=7.0 Hz, 4 H, **d**), 2.45 (s, 6 H, **C3-Me, C5-Me**), 2.31 (q, J=7.6 Hz, 4 H, **Et-CH_2**), 2.07 - 2.16 (m, 4 H, **a**), 1.62 - 1.73 (m, 4 H, **c**), 1.42 - 1.51 (m, 4 H, **b**), 1.31 (s, 6 H, **C1-Me, C7-Me**), 0.95 (t, J=7.5 Hz, 6 H, **Et-CH_3**). ^{13}C NMR (126 MHz, DMSO−d_6 : $CDCl_3$ 2 : 1) δ 174.1, 153.3, 145.4, 142.9, 141.7, 139.2, 137.8, 135.3, 132.6, 132.0, 131.5, 131.4, 129.8, 128.8, 128.8, 128.4, 123.4, 123.0, 122.6, 122.4, 90.7, 90.4, 89.9, 89.8, 63.0, 33.2, 31.5, 29.1, 23.7, 16.5, 14.4, 12.1, 11.5. MS Calcd for $C_{55}H_{57}BF_2N_3O_4$ (M+): 872.4414. Found (TOF ESI+): 872.4412. λ_{max}/nm (log ϵ) in THF: 526 (4.71) 498 (4.24) 328 (4.71). $\lambda_{em,max}$/nm in THF: 538; Φ_f= 0.19.

4-B di-*tert*-butyl 5,5'-(5-bromo-1,3-phenylene)bis(pent-4-ynoate)*

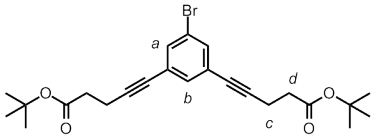

To a pre-dried flask were added 1,3,5-tribromobenzene (500 mg, 1.58 mmol), $Pd(PPh_3)_4$ (91 mg, 79 μmol) and CuI (15 mg, 79 μmol). THF (8 mL) and diisopropylamine (2 mL) were added and the mixture freeze-pump-thaw degassed 2 ×. The flask was purged with N_2 and **101** (537 mg, 3.48 mmol) was added *via* syringe. The mixture was further freeze-pump-thaw degassed 2 × then heated to 60 °C for 90 min, after which consumption of the 1,3,5-

tribromobenzene was observed by TLC (CH_2Cl_2). The mixture was filtered and concentrated. The crude residue was purified on silica, eluting with CH_2Cl_2. **4-B** was isolated as a yellow oil (430 mg, 59% vs. 1,3,5-tribromobenzene). ^{1}H NMR (400 MHz, $CDCl_3$) δ 7.42 (d, J=1.5 Hz, 2 H, **a**), 7.30 (t, J=1.5 Hz, 1 H, **b**), 2.67 (t, J=7.4 Hz, 4 H, **c**), 2.52 (t, J=7.4 Hz, 4 H, **d**), 1.47 (s, 18 H, ***t*-Bu**). ^{13}C NMR (50 MHz, $CDCl_3$) δ 171.5, 134.1, 133.6, 125.9, 122.0, 90.8, 81.3, 35.0, 28.5, 15.9 (unknown impurity at 79.6 ppm). MS Calcd for $C_{24}H_{29}BrO_4$ (M+Na): 483.1141. Found (TOF ESI+): 483.1138.

105 di-*tert*-butyl 5,5'-(5-bromo-1,3-phenylene)dipentanoate*

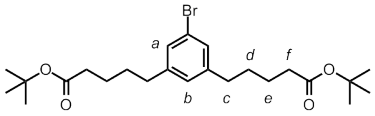

To a dry flask were added **4-B** (0.42 g, 0.91 mmol), 10% Pd/C (39 mg, 0.36 mmol) and propan-2-ol (1 mL). The flask was pump-purge degassed 3 × with N_2 then 3 × with H_2 and stirred under balloon pressure of H_2 for 5 h. The reaction mixture was passed through celite, eluting with propan-2-ol, and concentrated. The crude mixture was purified on silica, eluting with $CHCl_3$ to yield **105** as a colourless oil (300 mg, 70%). ^{1}H NMR (400 MHz, $CDCl_3$) δ 7.12 - 7.16 (m, 2 H, **a**), 6.88 - 6.90 (m, 1 H, **b**), 2.51 - 2.60 (m, 4 H, **f**), 2.20 - 2.27 (m, 4 H, **c**), 1.57 - 1.66 (m, 8 H, **d, e**), 1.44 (br. s, 18 H, ***t*-Bu**). ^{13}C NMR (50 MHz, $CDCl_3$) δ 173.4, 144.9, 129.2, 127.8, 122.7, 35.7 (assigned to two carbon environments by HSQC) 31.1, 28.6, 25.1 (unknown impurity at 80.7 ppm). MS Calcd for $C_{24}H_{37}BrO_4$ (M+Na): 491.1767. Found (TOF ESI+): 491.1757.

4-C 2,6-diethyl-4,4-difluoro-1,3,5,7-tetramethyl-8-(4-[4-(3,5-bis[5-(*tert*-butoxy)-5-oxopentyl])-ethynylphenyl]-ethynylphenyl)-4-bora-3',5'-diaza-s-indacene*

To a pre-dried schlenk were added **87** (20 mg, 40 μmol), **105** (94.0 mg, 200 μmol), $Pd(PPh_3)_4$ (4.7 mg, 4.0 μmol) and CuI (0.8 mg, 4 μmol). The reagents

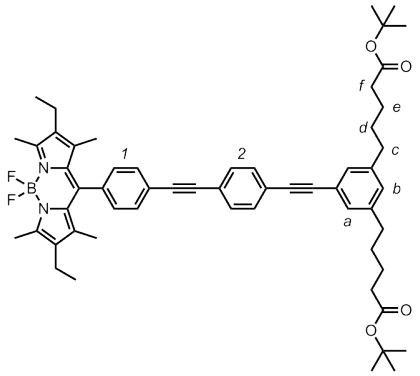

were dried for 30 mins under vacuum before THF (1 mL) and $i\mathrm{Pr_2NH}$ (0.1 mL) were added *via* syringe. The mixture was freeze-pump-thaw degassed 3 × then brought to 60 °C under N_2 for 3 h, when TLC indicated complete consumption of starting material **87**. The solvents were removed and the crude residue purified on silica, eluting first with toluene then $CHCl_3$: 0-5% MeOH. The product fractions still contained excess starting material **105**, which was separated efficiently using size-exclusion chromatography. Precipitation from CH_2Cl_2/petrol ether (60-80) yielded **4-C** in 20% yield (7 mg). ^{1}H NMR (200 MHz, $CDCl_3$) δ 7.67 (d, J=8.4 Hz, 2 H, **Aryl-1**), 7.54 (s, 4 H, **Aryl-2**), 7.31 (d, J=8.4 Hz, 2 H, **Aryl-1**), 7.20 (d, J=1.7 Hz, 2 H, **a**), 6.97 - 7.00 (m, 1 H, **b**), 2.57 - 2.70 (m, 4 H, **f**), 2.55 (s, 6 H, **C3-Me, C5-Me**), 2.20 - 2.39 (m, 8 H, **c**, **Et-CH_2), 1.59 - 1.71 (m, 8 H, d,e**), 1.45 (s, 18 H, ***t*-Bu**), 1.34 (s, 6 H, **C1-Me, C7-Me**), 1.00 (t, J=7.5 Hz, 6 H, **Et-CH_3**).

T12 2,6-diethyl-4,4-difluoro-1,3,5,7-tetramethyl-8-(4-[4-(3,5-bis[4-carboxybutyl])-ethynylphenyl]-ethynylphenyl)-4-bora-3',5'-diaza-s-indacene*

This transformation was effected by following a modified literature procedure.[68] **4-C** (7 mg, 8 μmol) was added to a dry flask containing 4 Ä molecular sieve beads ($\sim$ 80 mg) and dried under vacuum. CH_2Cl_2 (1 mL) was added *via* syringe under N_2 and the stirring solution was cooled to 0 °C before $BF_3 \cdot Et_2O$ (100 μmol, 10% vol/vol) was added *via* syringe. After 30 mins, the reaction was complete by TLC. $NaHCO_3$ sat. aq. solution (1 mL) was added and the

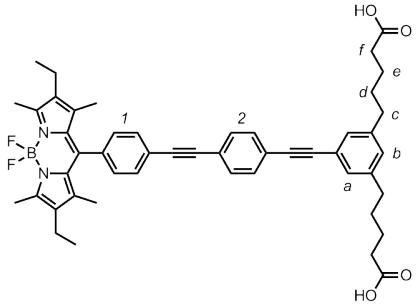

mixture stirred for 15 mins. The product was then extracted with $CHCl_3$ and washed with water 2 ×. The solvents were removed and the product precipitated from CH_2Cl_2/petrol ether (60-80) as a red powder (4 mg, 65%). ^{1}H NMR (400 MHz, $CDCl_3$) δ 7.67 (d, J=8.2 Hz, 2 H, **Aryl-1**), 7.50 - 7.57 (m, 4 H, **Aryl-2**), 7.30 (d, J=8.4 Hz, 2 H, **Aryl-1**), 7.17 - 7.23 (m, 2 H, **a**), 7.00 - 7.03 (m, 1 H, **b**), 2.63 (t, J=6.8 Hz, 4 H, **f**), 2.54 (s, 6 H, **C3-Me, C5-Me**), 2.40 (t, J=6.7 Hz, 4 H, **c**), 2.31 (q, J=7.5 Hz, 4 H, **Et-CH_2), 1.60 - 1.76 (m, 8 H, d, e**), 1.34 (s, 6 H, **C1-Me, C7-Me**), 0.99 (t, J=7.6 Hz, 6 H, **Et-CH_3**) ^{13}C NMR (126 MHz, $CDCl_3$) δ 179.1, 154.0, 142.2, 139.2, 138.2, 136.0, 132.9, 132.2, 131.6, 131.5, 130.5, 129.3, 129.1, 128.6, 123.6, 122.7, 122.5, 91.9, 90.5, 90.3, 88.5, 35.1, 33.7, 30.3, 24.0, 17.0, 14.6, 12.5, 11.9 (1 aromatic signal not found). MS Calcd for $C_{49}H_{50}BF_2N_2O_4$: 779.3845. Found (TOF ESI-): 779.3831. λ_{max}/nm (log ϵ) in THF: 526 (4.86) 500 (4.38) 326 (4.78). $\lambda_{em,max}$/nm in THF: 538; Φ_f= 0.30.

106 2,6-diethyl-4,4-difluoro-1,3,5,7-tetramethyl-8-(4-[4-(4-[methanol]phenyl)-ethynylphenyl]-ethynylphenyl)-4-bora-3',5'-diaza-s-indacene*

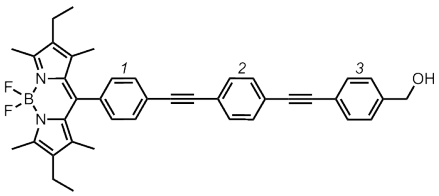

To a dried flask were added **87** (30 mg, 60 μmol), 4-iodobenzylalcohol (280

mg, 1.2 mmol), $Pd(PPh_3)_4$ (18 mg, 16 μmol) and CuI (1.5 mg, 7.5 μmol). The reagents were dried under vacuum for 30 mins then THF (4 mL) and DIPEA (0.4 mL) were added *via* syringe under N_2. The mixture was freeze-pump-thaw degassed 3 × and stirred at 50 °C for 6 h. The solvents were removed and the residue purified on silica eluting with $CHCl_3$ 0-2.5% MeOH. The excess 4-iodobenzylalcohol was then separated using size-exclusion chromatography in $CHCl_3$. The solvents were removed and **106** precipitated as a red powder from CH_2Cl_2/petrol ether (60-80) (28 mg, 77%). ^{1}H NMR (400 MHz, $CDCl_3$) δ 7.67 (d, J=8.2 Hz, 2 H, **Aryl-1**), 7.55 (s, 4 H, **Aryl-2**), 7.55 (d, J=8.0 Hz, 2 H, **Aryl-3**), 7.38 (d, J=8.0 Hz, 2 H, **Aryl-3**), 7.31 (d, J=8.2 Hz, 2 H, **Aryl-1**), 4.75 (d, J=5.5 Hz, 2 H, **Benzyl**), 2.54 (s, 6 H, **C3-Me, C5-Me**), 2.32 (q, J=7.6 Hz, 4 H, **Et-CH_2**), 1.34 (s, 6 H, **C1-Me, C7-Me**), 0.99 (t, J=7.5 Hz, 6 H, **Et-CH_3**), (overlapping multiplets proven by COSY). ^{13}C NMR (126 MHz, $CDCl_3$) δ 154.0, 141.3, 139.2, 138.2, 136.0, 132.9, 132.2, 131.8, 131.6, 131.6, 130.5, 128.6, 126.8, 123.6, 123.4, 122.6, 122.2, 91.3, 90.6, 90.3, 89.0, 64.9, 17.1, 14.6, 12.5, 11.9. MS Calcd for $C_{40}H_{37}BF_2N_2O$: 611.31. Found (MALDI TOF+): 610.98. λ_{max}/nm (log ϵ) in THF: 526 (4.88) 499 (4.39) 328 (4.79).

108 2,6-diethyl-4,4-difluoro-1,3,5,7-tetramethyl-8-(4-[4-(4-[bromomethyl]phenyl)-ethynylphenyl]-ethynylphenyl)-4-bora-3',5'-diaza-s-indacene*

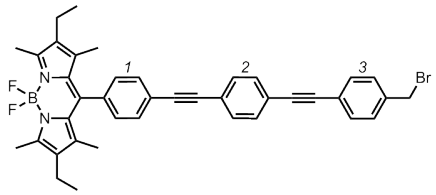

A flask was charged with **106** (15 mg, 25 mmol), CBr_4 (24 mg, 75 mmol), PPh_3 (20 mg, 75 mmol) and DCM (300 μL) and the mixture stirred at room temperature. After 1 h, the solvents were removed and the crude residue purified on silica, eluting $CHCl_3$. The solvents were removed and precipitation from

CH_2Cl_2/petrol ether (60-80) gave **108** as red needles (10 mg, 60%). ^{1}H NMR (400 MHz, $CDCl_3$) δ 7.67 (d, J=8.2 Hz, 2 H, **Aryl-1**), 7.55 (m, 4 H, **Aryl-2**), 7.52 (d, J=8.2 Hz, 2 H, *Aryl-3*), 7.40 (d, J=8.2 Hz, 2 H, **Aryl-3**), 7.31 (d, J=8.2 Hz, 2 H, **Aryl-1**), 4.51 (s, 2 H, **Benzyl**), 2.55 (s, 6 H, **C3-Me, C5-Me**), 2.32 (q, J=7.5 Hz, 4 H, **Et-CH_2**), 1.34 (s, 6 H, **C1-Me, C7-Me**), 1.00 (t, J=7.5 Hz, 6 H, **Et-CH_3**). ^{13}C NMR (126 MHz, $CDCl_3$) δ 154.0, 139.1, 138.2, 138.1, 136.0, 132.9, 132.2, 132.0, 131.6, 131.6, 130.5, 129.1, 128.6, 123.6, 123.2, 123.1, 122.8, 90.9, 90.7, 90.3, 89.8, 32.9 (confirmed as benzylic position by HSQC), 17.1, 14.6, 12.5, 11.9. MS Calcd for $C_{40}H_{36}BrBF_2N_2$: 675.22. Found (MALDI TOF+): 673.72. λ_{max}/nm (log ϵ) in THF: 526 (4.92) 500 (4.46) 329 (4.90).

4.9 Bibliography

1 Tsien, R. Y. *Biochemistry* **1980**, *19*, 2396–2404.
2 Gunnlaugsson, T.; Kruger, P. E.; Lee, T.; Parkesh, R.; Pfeffer, F. M.; Hussey, G. M. *Tetrahedron Lett.* **2003**, *44*, 6575–6578.
3 Gabe, Y.; Urano, Y.; Kikuchi, K.; Kojima, H.; Nagano, T. *J. Am. Chem. Soc.* **2004**, *126*, 3357–3367.
4 de Silva, A. P.; Gunaratne, H. Q. N.; Habib-Jiwan, J.-L.; McCoy, C. P.; Rice, T. E.; Soumillion, J.-P. *Angew. Chem. Int. Ed. Engl.* **1995**, *34*, 1728–1731.
5 Hall, M. J.; Allen, L. T.; O'Shea, D. F. *Org. Biomol. Chem.* **2006**, *4*, 776–780.
6 Kowada, T.; Kikuta, J.; Kubo, A.; Ishii, M.; Maeda, H.; Mizukami, S.; Kikuchi, K. *J. Am. Chem. Soc.* **2011**, *133*, 17772–17776.
7 Sunahara, H.; Urano, Y.; Kojima, H.; Nagano, T. *J. Am. Chem. Soc.* **2007**, *129*, 5597–5604.
8 Greenfield, S. R.; Svec, W. A.; Gosztola, D.; Wasielewski, M. R. *J. Am. Chem. Soc.* **1996**, *118*, 6767–6777.
9 Kawabata, H.; Nishimura, Y.; Yamazaki, I.; Iwai, K.; Ohta, N. *J. Phys. Chem. A* **2001**, *105*, 10261–10270.
10 Zhou, J.; Lukin, L. V.; Braun, C. L. *J. Phys. Chem. A* **2008**, *112*, 7507–7513.
11 Davis, W. B.; Svec, W. A.; Ratner, M. A.; Wasielewski, M. R. *Nature* **1998**, *396*, 60–63.
12 Craig, D. C.; Lawson, J. M.; Oliver, A. M.; Paddon-Row, M. N. *J. Chem. Soc., Perkin Trans. 1* **1990**, 3305–3315.

13 Wasielewski, M. R. *J. Org. Chem.* **2006**, *71*, 5051–5066.
14 Rehm, D.; Weller, A. *Isr. J. Chem.* **1970**, *8*, 259–271.
15 Marcus, R. A.; Sutin, N. *Bioch. et Biophys. Acta - Bioenergetics* **1985**, *811*, 265–322.
16 Wasielewski, M. R. *Chem. Rev.* **1992**, *92*, 435–461.
17 Marcus, R. A. *Angew. Chem. Int. Ed. Engl.* **1993**, *32*, 1111–1121.
18 Debreczeny, M. P.; Svec, W. A.; Wasielewski, M. R. *Science* **1996**, *274*, 584–587.
19 Gosztola, D.; Yamada, H.; Wasielewski, M. R. *J. Am. Chem. Soc.* **1995**, *117*, 2041–2048.
20 Gosztola, D.; Niemczyk, M. P.; Wasielewski, M. R. *J. Am. Chem. Soc.* **1998**, *120*, 5118–5119.
21 Lukas, A. S.; Miller, S. E.; Wasielewski, M. R. *J. Phys. Chem. B* **2000**, *104*, 931–940.
22 Hayes, R. T.; Wasielewski, M. R.; Gosztola, D. *J. Am. Chem. Soc.* **2000**, *122*, 5563–5567.
23 Galoppini, E.; Fox, M. A. *J. Am. Chem. Soc.* **1996**, *118*, 2299–2300.
24 Gao, J.; Mller, P.; Wang, M.; Eckhardt, S.; Lauz, M.; Fromm, K. M.; Giese, B. *Angew. Chem. Int. Ed.* **2011**, *50*, 1926–1930.
25 Li, L.-s. *Nano Lett.* **2007**, *7*, 2981–2986.
26 Lin, S.; Yeh, C.; Wu, G. Y. *Chem. Phys. Lett.* **1990**, *166*, 195–202.
27 Ito, T.; Yamazaki, I.; Ohta, N. *Chem. Phys. Lett.* **1997**, *277*, 125–131.
28 Ito, T.; Yamazaki, I.; Ohta, N. *J. Phys. Chem. B* **2002**, *106*, 895–898.
29 Murgida, D. H.; Hildebrandt, P. *J. Phys. Chem. B* **2002**, *106*, 12814–12819.
30 Bixon, M. *J. Chem. Phys.* **1997**, *107*, 5154–5170.
31 Wenger, O. S. *Acc. Chem. Res.* **2010**, *44*, 25–35.
32 Chaudhuri, T.; Mula, S.; Chattopadhyay, S.; Banerjee, M. *Spectrochim. Acta A: Mol. and Biomol. Spec.* **2010**, *75*, 739–744.
33 Ziessel, R.; Bonardi, L.; Ulrich, G. *Dalton Trans.* **2006**, 2913–2918.
34 Ziessel, R.; Ulrich, G.; Harriman, A. *New J. Chem.* **2007**, *31*, 496–501.
35 Loudet, A.; Burgess, K. *Chem. Rev.* **2007**, *107*, 4891–4932.
36 Ulrich, G.; Ziessel, R.; Harriman, A. *Angew. Chem. Int. Ed.* **2008**, *47*, 1184–1201.
37 Li, L.; Han, J.; Nguyen, B.; Burgess, K. *J. Org. Chem.* **2008**, *73*, 1963–1970.
38 El-Khouly, M. E.; Fukuzumi, S.; D'Souza, F. *ChemPhysChem* **2014**, *15*, 30–47.
39 Benniston, A. C.; Copley, G. *Phys. Chem. Chem. Phys.* **2009**, *11*, 4124–4131.
40 Boens, N.; Leen, V.; Dehaen, W. *Chem. Soc. Rev.* **2012**, *41*, 1130–1172.
41 Levitt, J. A.; Kuimova, M. K.; Yahioglu, G.; Chung, P.-H.; Suhling, K.; Phillips, D. *J. Phys. Chem. C* **2009**, *113*, 11634–11642.
42 Han, J.; Loudet, A.; Barhoumi, R.; Burghardt, R. C.; Burgess, K. *J. Am. Chem. Soc.* **2009**, *131*, 1642–1643.
43 Stckl, M.; Herrmann, A. *Bioch. et Biophys. Acta - Biomem.* **2010**, *1798*,

1444–1456.
44 Sachl, R.; Boldyrev, I.; Johansson, L. B. A. *Phys. Chem. Chem. Phys.* **2010**, *12*, 6027–6034.
45 Kaiser, R. D.; London, E. *Bioch. et Biophys. Acta - Biomem.* **1998**, *1375*, 13–22.
46 Johnson, I. D.; Kang, H. C.; Haugland, R. P. *Anal. Biochem.* **1991**, *198*, 228–237.
47 Boldyrev, I. A.; Zhai, X.; Momsen, M. M.; Brockman, H. L.; Brown, R. E.; Molotkovsky, J. G. *J. Lipid Res.* **2007**, *48*, 1518–1532.
48 Wang, D.; Fan, J.; Gao, X.; Wang, B.; Sun, S.; Peng, X. *J. Org. Chem.* **2009**, *74*, 7675–7683.
49 Krumova, K.; Cosa, G. *J. Am. Chem. Soc.* **2010**, *132*, 17560–17569.
50 Ulrich, G.; Ziessel, R. *J. Org. Chem.* **2004**, *69*, 2070–2083.
51 Kollmannsberger, M.; Gareis, T.; Heinl, S.; Daub, J.; Breu, J. *Angew. Chem. Int. Ed. Engl.* **1997**, *36*, 1333–1335.
52 Wielopolski, M.; Atienza, C.; Clark, T.; Guldi, D.; Martn, N. *Chem. Eur. J.* **2008**, *14*, 6379–6390.
53 Kaliginedi, V.; Moreno-Garca, P.; Valkenier, H.; Hong, W.; Garca-Surez, V. M.; Buiter, P.; Otten, J. L. H.; Hummelen, J. C.; Lambert, C. J.; Wandlowski, T. *J. Am. Chem. Soc.* **2012**, *134*, 5262–5275.
54 Coskun, A.; Akkaya, E. U. *J. Am. Chem. Soc.* **2006**, *128*, 14474–14475.
55 Azov, V. A.; Schlegel, A.; Diederich, F. *Bull. Chem. Soc. Jpn.* **2006**, *79*, 1926–1940.
56 Mula, S.; Ray, A. K.; Banerjee, M.; Chaudhuri, T.; Dasgupta, K.; Chattopadhyay, S. *J. Org. Chem.* **2008**, *73*, 2146–2154.
57 Kollmannsberger, M.; Rurack, K.; Resch-Genger, U.; Daub, J. *J. Phys. Chem. A* **1998**, *102*, 10211–10220.
58 Wu, Y.; Yeh, F. L.; Mao, F.; Chapman, E. R. *Biophys. J.* **2009**, *97*, 101–109.
59 Fluhler, E.; Burnham, V. G.; Loew, L. M. *Biochemistry* **1985**, *24*, 5749–5755.
60 Reeve, J. E.; Collins, H. A.; Mey, K. D.; Kohl, M. M.; Thorley, K. J.; Paulsen, O.; Clays, K.; Anderson, H. L. *J. Am. Chem. Soc.* **2009**, *131*, 2758–2759.
61 Reeve, J. E. Ph.D. thesis, University of Oxford, 2012.
62 Niu, S. L.; Ulrich, G.; Ziessel, R.; Kiss, A.; Renard, P.-Y.; Romieu, A. *Org. Lett.* **2009**, *11*, 2049–2052.
63 Li, Z.; Mintzer, E.; Bittman, R. *J. Org. Chem.* **2006**, *71*, 1718–1721.
64 Matsui, M.; Funabiki, K.; Nakaya, K.-i. *Bull. Chem. Soc. Jpn.* **2005**, *78*, 464–467.
65 Ueno, Y.; Jose, J.; Loudet, A.; Perez-Bolivar, C.; Anzenbacher, P.; Burgess, K. *J. Am. Chem. Soc.* **2010**, *133*, 51–55.
66 Meltola, N.; Soini, A.; Hnninen, P. *J. Fluoresc.* **2004**, *14*, 129–138.
67 Meltola, N. J.; Wahlroos, R.; Soini, A. E. *J. Fluoresc.* **2004**, *14*, 635–647.
68 Li, Z.; Bittman, R. *J. Org. Chem.* **2007**, *72*, 8376–8382.
69 Thompson, J. R.; Heron, A. J.; Santoso, Y.; Wallace, M. I. *Nano Lett.*

2007, *7*, 3875–3878.

70 Heron, A. J.; Thompson, J. R.; Cronin, B.; Bayley, H.; Wallace, M. I. *J. Am. Chem. Soc.* **2009**, *131*, 1652–1653.

71 Heron, A. J.; Thompson, J. R.; Mason, A. E.; Wallace, M. I. *J. Am. Chem. Soc.* **2007**, *129*, 16042–16047.

72 Bergstrm, F.; Mikhalyov, I.; Hgglf, P.; Wortmann, R.; Ny, T.; Johansson, L. B.-A. *J. Am. Chem. Soc.* **2002**, *124*, 196–204.

73 Pons, T.; Mongin, O.; Mertz, J.; Blanchard-Desce, M.; Moreaux, L. *J. Biomed. Opt.* **2003**, *8*, 428–431.

74 Miller, E. W.; Lin, J. Y.; Frady, E. P.; Steinbach, P. A.; Kristan, W. B.; Tsien, R. Y. *Proc. Nat. Acad. Sci.* **2012**, *109*, 2114–2119.

75 Ricks, A. B.; Solomon, G. C.; Colvin, M. T.; Scott, A. M.; Chen, K.; Ratner, M. A.; Wasielewski, M. R. *J. Am. Chem. Soc.* **2010**, *132*, 15427–15434.

76 Ricks, A. B.; Brown, K. E.; Wenninger, M. K.; Karlen, S. D.; Berlin, Y. A.; Co, D. T.; Wasielewski, M. R. *J. Am. Chem. Soc.* **2012**, *134*, 4581–4588.

77 Fischer, G. M.; Jungst, C.; Isomaki-Krondahl, M.; Gauss, D.; Moller, H. M.; Daltrozzo, E.; Zumbusch, A. *Chem. Commun.* **2010**, *46*, 5289–5291.

78 Fortage, J.; Tuyras, F.; Ochsenbein, P.; Puntoriero, F.; Nastasi, F.; Campagna, S.; Griveau, S.; Bedioui, F.; Ciofini, I.; Lain, P. P. *Chem. Eur. J.* **2010**, *16*, 11047–11063.

79 Fortage, J.; Boixel, J.; Blart, E.; Hammarstrm, L.; Becker, H. C.; Odobel, F. *Chem. Eur. J.* **2008**, *14*, 3467–3480.

80 Weil, T.; Reuther, E.; Beer, C.; Müllen, K. *Chem. Eur. J.* **2004**, *10*, 1398–1414.

Chapter 5: A New approach to assessing the voltage-sensitivity of molecular probes

Noting the reliance of voltage-sensitive dye testing methods upon lipid bilayer membranes, and the resultant requirement for amphiphilic dyes to be synthesised for testing, the research in this chapter details a new testing setup. Steps are taken towards actualising this novel technique, which features dyes bound to a surface and sandwiched between two electrodes. This provides a useful approach to testing pyridinium-containing VSDs, bypassing the need to isolate amphiphilic dyes. The precursor of a known VSD is also synthesised via *a new route with milder conditions than the literature route.*

5.1 Introduction

A drawback of all of the available VSD testing methods is that amphiphilic, water-soluble dyes are required. In the work described in Chapter 4, this restriction called for the synthesis of a second generation of dyes in order for the underlying molecular design to be testable. As dyes of increased amphiphilicity are generally harder to purify, due to chromatographic methods favouring either hydrophobic or hydrophilic molecules, from a synthetic standpoint the availability of a VSD testing method which does not require such a strongly amphiphilic dye is desirable. In this chapter we therefore review methods which could be applied to this problem, before suggesting and carrying out initial steps towards a novel solution.

5.2 How the voltage-sensitivity of voltage-sensitive dyes is assessed

The methods used for studying the voltage-sensitivity of VSDs have naturally and rightly been dominated by the incorporation of a VSD into a lipid bilayer membrane, and the application of a controlled potential across this membrane (voltage-clamping). The membranes of live cells, both cultures and brain slices, and cell models have been used. The earliest VSDs were characterised in voltage-clamped giant squid axons,[1] but with vast improvements in microscopy, much smaller cells have been used in more recent years.[2–4] Patch clamping, an electrophysiological tool used to apply a voltage across a cell membrane (see Figure 1.4 on Page 6), is necessary to characterise VSDs in cells, as the optical signal needs to be measured against a known transmembrane potential. As mentioned in Section 1.2.1, patch clamping is a practically challenging technique. Ironically, one of the motivating factors behind the development of VSDs is to avoid patch clamping in the measurement of mem-

brane potential, yet patch clamping is required for the initial characterisation of VSDs.

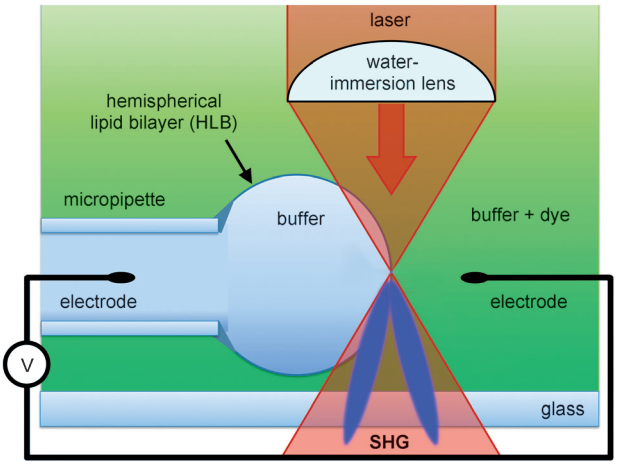

Figure **5.1** A hemispherical lipid bilayer experimental setup for testing VSDs (specifically SHG dyes in this example). VSDs insert into the outer leaflet of the HLB from the buffer bath. Adapted from reference 5 with permission, copyright 2013 WILEY-VCH Verlag GmbH & Co. KGaA, Weinheim.

Hemispherical lipid bilayers (HLBs) (Figure 5.1) are the most often employed model membrane system. Model membranes such as these have been particularly useful, as polarised transmission or emission data can be more readily collected from these geometrically well-defined models than *in vitro* or *ex vivo*. The accessibility of this polarised data has been significant in inspecting VSD mechanisms and in optimising VSDs.[6] An alternative model system was employed in Chapter 4, but in common with the HLB approach and experiments on cells, the dyes to be tested must be introduced as an aqueous solution. All of the model testing methods rely on aqueous dye solutions to ensure the dye can be incorporated asymmetrically into the bilayer (a prerequisite for electrochromic, SHG and PeT dyes, see Sections 1.3.4, 3.2 and 4.3.2). It is not possible to achieve this asymmetry by mixing a hydrophobic dye with the lipid before bilayer formation, as upon formation of the bilayer the dye will be equally partitioned into both membrane leaflets; as such, amphiphilic dyes are required.

A further weakness of the existing VSD testing methods is their reliance upon lipid bilayer membranes. Although lipid membranes are the final intended target of VSD application, such membranes limit the electric field that can be applied before instability becomes an issue.[7,8]

Further, as shown in Figure 1.13 on Page 19, lipid bilayers have an inherently complicated electrostatic potential profile because of the surface and dipole potentials of the lipids.[9–11] These potentials can interfere with the intended operation of VSDs,[9] and could even completely obscure the voltage-sensitivity of a dye. The variation in the dipole and surface potentials of a membrane from cell to cell and species to species, due to the different lipid compositions of the cell membrane, probably contributes to the poor transferability of existing VSDs.

Supported lipid bilayers (SLB) or tethered lipid bilayer (TLB) membranes have become popular in the wider field of chemical biology because of their stability compared to HLBs and giant unilamellar vesicless (GUVs).[12] They feature a lipid bilayer covalently joined to a surface by a spacer (Figure 5.2 on the following page).[13] An advantageous property of these bilayers is the opportunity to apply surface structural techniques to biochemical problems.[12] Like the TIRFm/DHB setup used in Section 4.6, SLBs have been used to study the electrical behaviour of ion channels in membranes, and could be applied to VSD testing. However, the restrictions outlined above of other lipid-based techniques apply to SLBs and TLBs also.

A lipid-free method of testing VSDs is thus appealing for studying fundamental field sensitive optical behaviour in the absence of the limitations detailed in this section. I next detail the literature precedence for such a system, propose advances in design and describe my research towards the conceived solution.

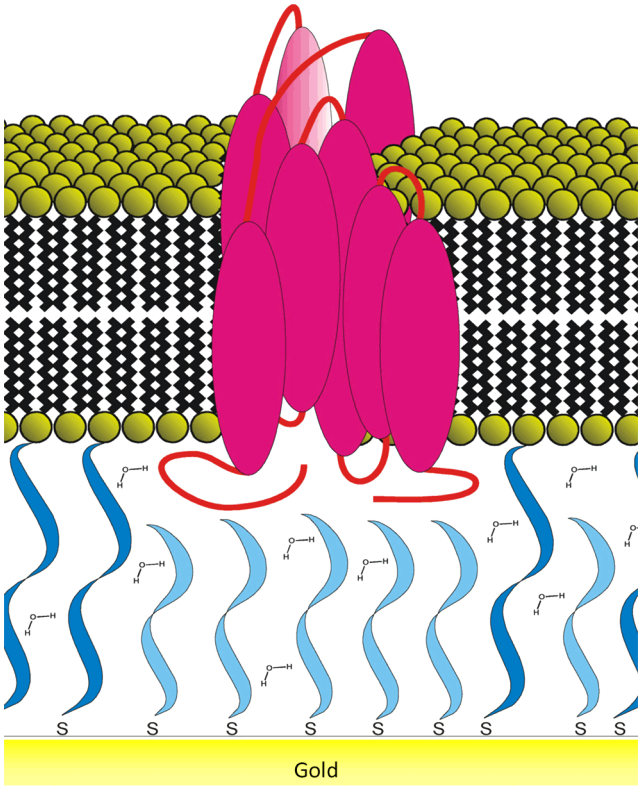

Figure **5.2** A tethered lipid bilayer containing an ion channel. The gold surface can be used as an electrode and the system immersed in a water bath for performing electrochemical measurements. The lower layer of lipids are modified with a thiol-terminated covalent linker, represented by the blue ribbon. Adapted from reference 13 with permission from Elsevier.

5.3 Alternative methods for VSD testing

Langmuir-Blodgett (L-B) films (Figure 5.3) are a possible technique that could be used in VSD characterisation. These multilayer structures composed of organic monolayers have been used in studies of distance and field-dependent PeT by sequentially transferring an electron donor layer, a molecular wire layer, then an electron acceptor layer to a solid support.[14,15] When the solid support is a suitable electrode, a sandwich device can be constructed with a second electrode, an electric field can be applied across the layers and PeT can be studied. However, despite this system being lipid-free, L-B films can only be made from amphiphilic components, as each monolayer is deposited on top of the previous monolayer from a water-air interface.[16]

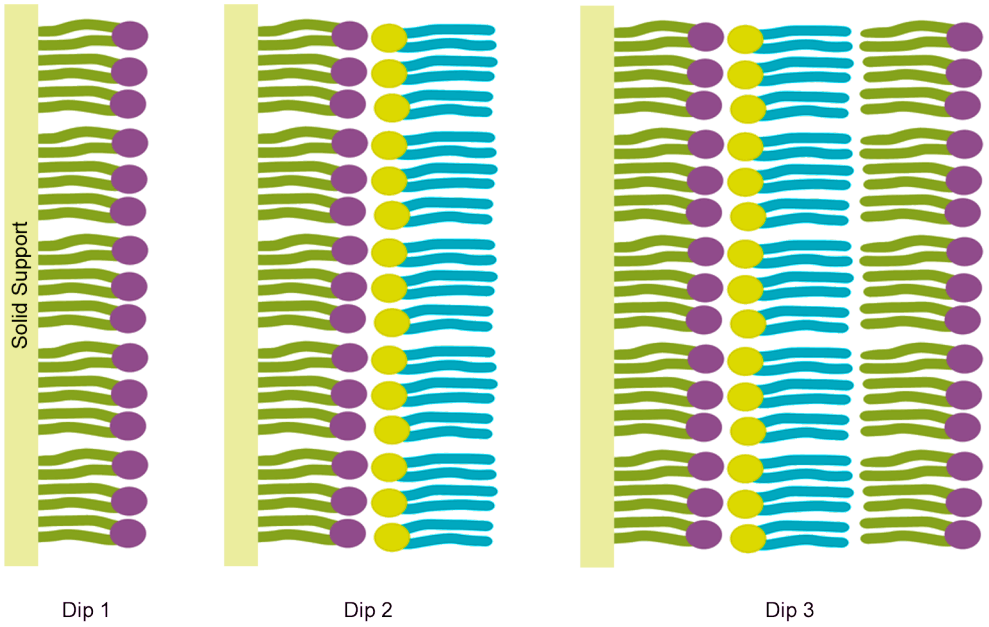

Figure **5.3** Multiple layers of amphiphiles being built up on a hydrophobic solid support using Langmuir-Blodgett transfer.

An additional spectroscopic approach relevant to VSD testing is the Stark spectroscopy method developed by Steven G. Boxer (Stanford University). The cell depicted in Figure 5.4 is used to study the Stark effect, the effect of an applied external electric field upon the absorption and emission spectra of chromophores, from small molecular chromophores through to complex proteins. A potential difference is applied between the plates of two transparent electrodes, generating a strong electric field. A frozen glassy matrix of solvent is used to simplify data analysis by fixing the orientation of each chromophore in the sample. The optical polarisation is varied to selectively target chromophores of each orientation relative to the direction of the electric field.[17] The equipment can allow a field of 10^8 V m^{-1} to be applied, $\sim 10\times$ greater than the field change during an action potential. This method has not been applied to testing VSDs but the authors of reference 17 have acknowledged the opportunity.

The major restriction of this technique in relation to PeT voltage sensors

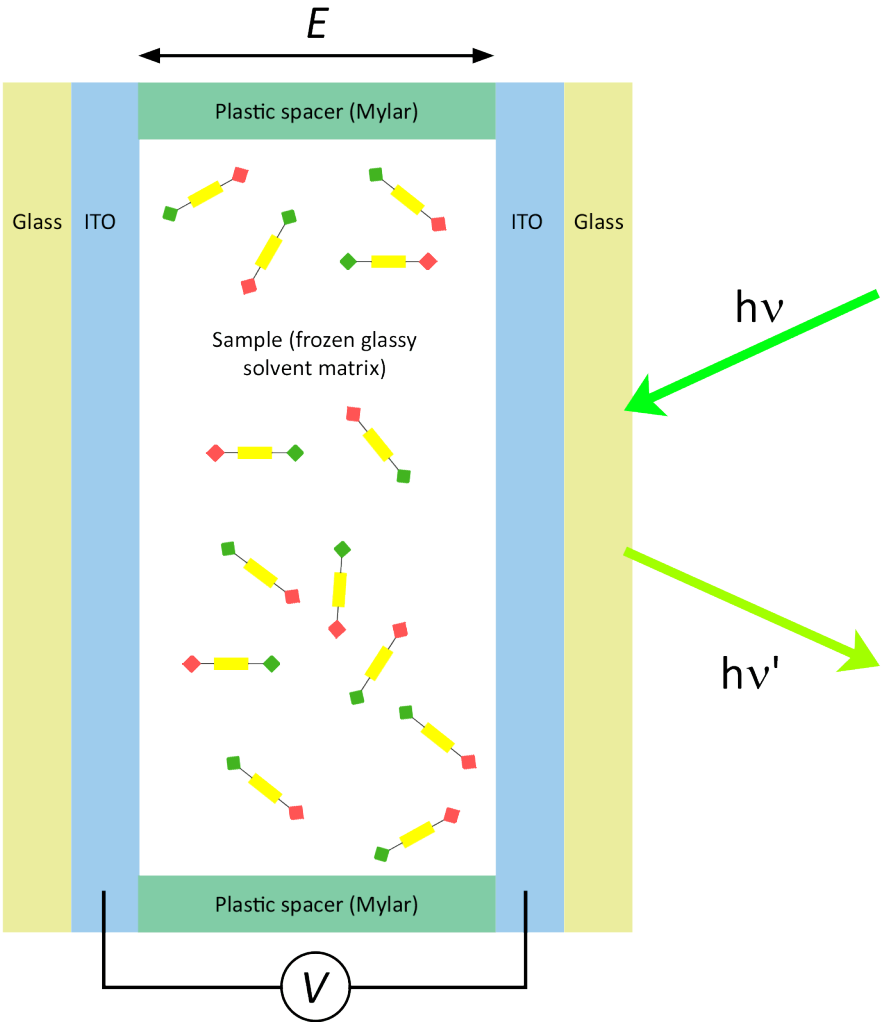

Figure **5.4** The Boxer cell used for Stark spectroscopy of randomly-oriented chromophores. E denotes the electric field as a result of the applied potential V.

is that a change in polarisation does not discriminate between different alignments of the electron transfer process with the electric field. This system is not only intuitively far removed from the final application of a VSD; for PeT sensors, it does not generate meaningful results. A further restriction of this technique is that the dipoles of the frozen solvent molecules create strong localised electric fields,[17] that could interfere with VSD testing much like phospholipid dipoles. Low temperature is also necessary for the solvent to be frozen, which might require specialised spectroscopic instruments to accommodate, although the use of a viscous polymer (as in Section 2.10) could circumvent this issue.

5.4 Proposing a new VSD testing method

The proposed solution to the problems and shortcomings of existing VSD testing methods is a hybrid of Boxer's Stark spectroscopy cell and recent advances in surface chemistry and organic electronics (Figure 5.5 on the next page). It is based upon the routine observation of fluorescence from monolayers of dyes attached to surfaces. The solution is thus more conceptually similar to an asymmetrically-labelled lipid bilayer membrane than the Stark cell method. The dye will be attached to a flat surface using a chemically grafted monolayer (CGM) technique. Two electrode plates allow a potential difference to be applied across a layer of polymer separating the electrodes. At least one of the electrodes will be transparent to allow fluorescence measurements to be performed.[a]

CGMs have attracted interest over recent years because of their use in biosensors, nanotechnology and organic electronics.[18,19] They are most commonly constructed from a post-functionalisation reaction with a self-assembled monolayer (SAM) already on a surface, for example a silane SAM on an oxide surface (glass, silicon, or a transparent conducting oxide (TCO)), or a thiol SAM on a gold surface. Silanes have the upper-hand in terms of physical and chemical stability, but the sensitivity of the chlorosilane or alkoxysilane precursors to water make their handling difficult compared to thiols.[19] It is due to the difficulty of purifying silane and thiol derivatives of compounds for surface attachment that silanes and thiols with reactive functional groups have been developed to allow CGM formation via reaction with an existing SAM (Scheme 5.1 on Page 232). Nucleophilic substitution, 'click' chemistry (N_3 and C≡C terminated SAMs), Diels-Alder cycloaddition and native chemical ligation (NCL) (the formation of an amide bond between *N*-terminal cysteine of

[a]With two transparent electrodes, SHG and transmission spectroscopy would be possible, increasing the scope of this method. This chapter will focus on a device initially for fluorescence only.

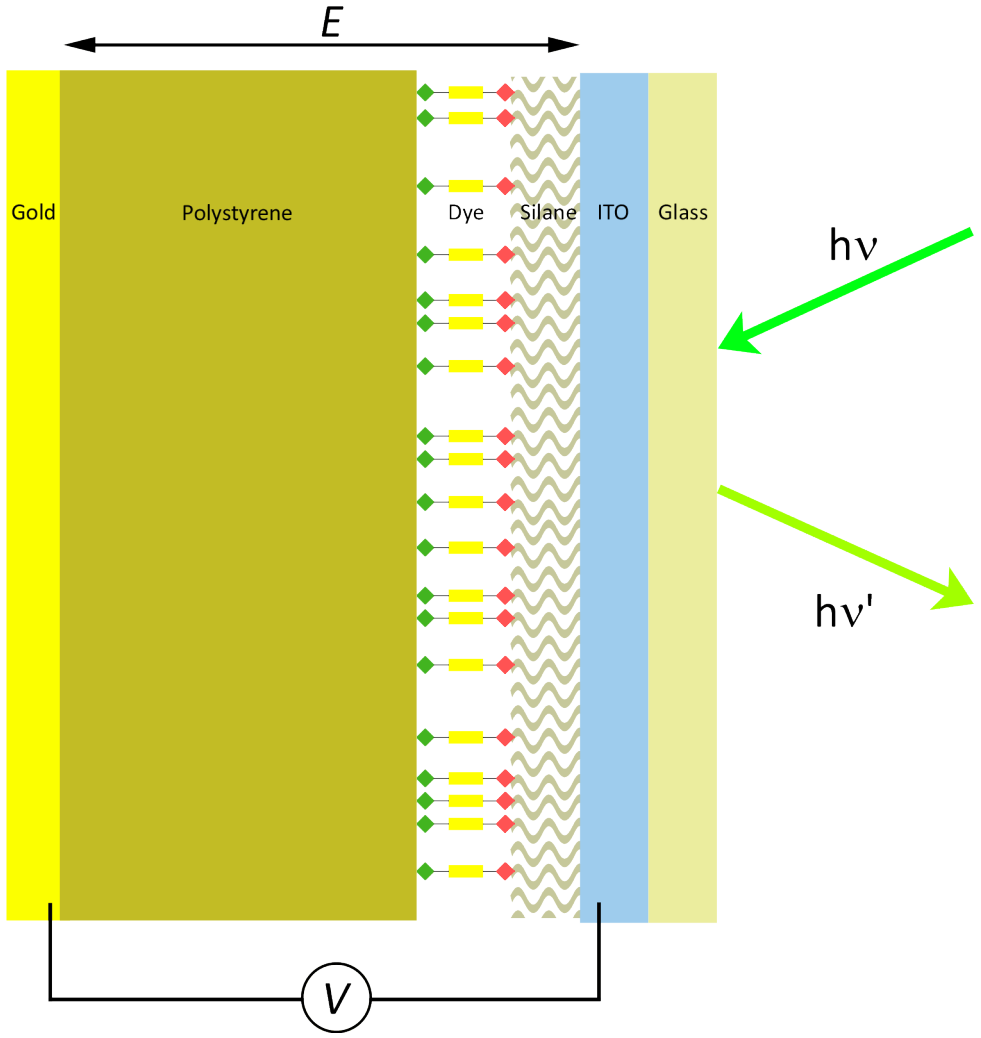

Figure **5.5** The side profile of the design proposed in this section. E denotes the electric field as a result of the applied potential V.

a peptide and a thioester)[20] have all been employed to permit the covalent attachment of the desired molecule to a self-assembled monolayer. As well as this scope for different reactions, the final surface coverage of CGMs can also be tuned by concentration or reaction time changes,[20] or the coadsorption of molecules lacking a reactive group in the initial SAM, limiting the extent of further functionalisation.[18,21]

We decided to use a silane-based SAM on a TCO surface, as gold surfaces have previously been found to quench fluorescence of surface-bound dyes.[22] The stability advantages of silane monolayers are also noted, and

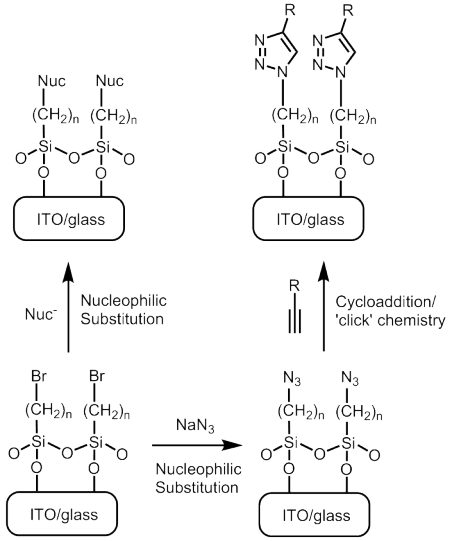

Scheme **5.1** Some of the general surface functionalisation reactions that have been published.[18,19]

post-functionalisation of a silanised surface minimises the problem of handling silanes. Indium-doped tin oxide (ITO) on glass was selected as the transparent oxide surface, as it is readily commercially available, and silane chemistry has been applied to indium-doped tin oxide (ITO) in an identical manner as to glass.[23–27]

The vast majority of currently used VSDs feature a pyridinium group as an electron acceptor (see Figure 2.1 on Page 43). The syntheses of these dyes almost invariably ends with quaternarisation of a pyridine to form the final compound. This step endows these dyes with amphiphilicity, and results in tricky purification. An ideal tool for testing pyridinium-containing VSDs without having to isolate amphiphilic dyes would use this quaternarisation step as the surface grafting reaction. In this way, the need to handle amphiphilic dyes before their voltage-sensitivity has been tested can be removed. A suitable silane for this tool is compound **111** (Scheme 5.2 on the following page), as used by Tobin Marks and coworkers to post-functionalise silicon surfaces, by the quaternarisation of a pyridine-containing dye *via* nucleophilic substitution at the benzylic position.[28]

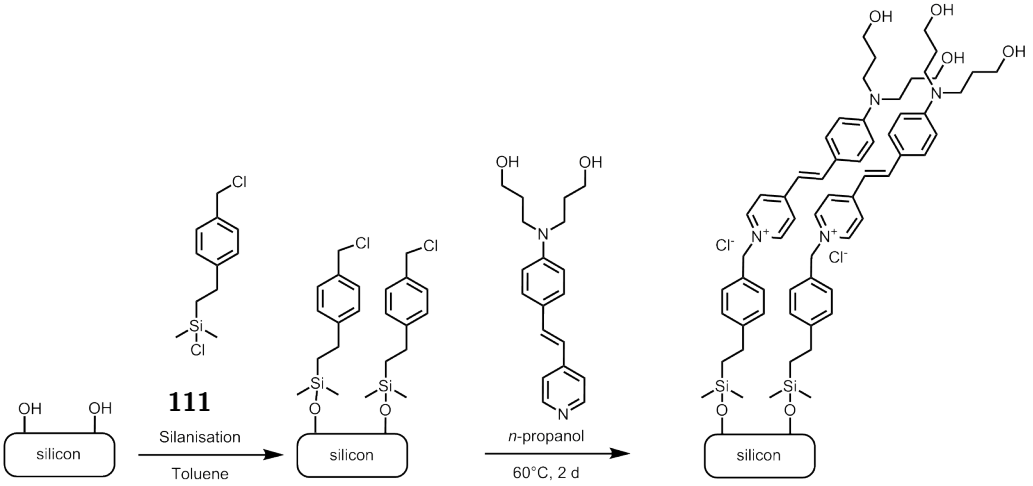

Scheme **5.2** Forming a pyridinium CGM by post-functionalising silane **111** at the benzylic position.[28]

Due to the surface roughness of ITO,[29,30] a polymer layer was to be used to separate the two electrodes, both to prevent short-circuits between them and reduce the error in calculating the electric field experienced by the dye monolayer. Polystyrene (PS) was chosen for this role, as its high dielectric strength (the measure of the potential difference that can be maintained without a breakdown leading to conductance) would allow the device to act as a capacitor, sustaining a potential difference between the two electrodes so that the VSD experiences an electric field. The second electrode of the initial design is a layer of gold, which can be evaporated onto the polystyrene (PS) layer, a commonly used technique in organic electronics.[31,32]

5.5 Development of the proposed VSD testing device

5.5.1 Silane synthesis

The silane **111** was prepared according to a literature procedure (Scheme 5.3 on the next page).[28] The role of phenothiazine in the catalyst mix as a 'promoter' and 'β-director' is asserted but not proven in the literature.[33] The crude mixture was judged by NMR to contain the two isomers in the ratio

6 : 1 β : α. Careful distillation of the product mixture gave the desired β regioisomer in reasonable purity (> 90% β, < 10% α).

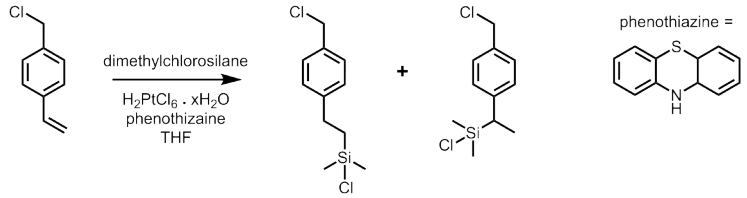

111 (β) (α)

Scheme **5.3** Synthesis of the silane chosen for forming the initial SAM layer.

5.5.2 Functionalising glass surfaces

As an initial test of the intended surface functionalisation method, glass surfaces were used as they are cheaper than ITO-coated glass. The steps are illustrated in Scheme 5.4 on the following page. Glass microscope slides were cleaned on one face using standard methods ('Piranha' solution, 7 : 3 c.H_2SO_4 : 30-35% aq.H_2O_2),[20,28] then silanisation of this face was performed by immersing each slide in a solution of the silane in the presence of a *N,N*-diisopropylethylamine (DIPEA), a non-nucleophilic base.[20,28] Crude 'naked eye' contact angle measurements were used to confirm the wetting and dewetting properties expected of cleaned and silanised surfaces respectively. A water droplet with a high contact angle could be deposited on surfaces before cleaning or after silanisation, whereas clean surfaces were wetted with a thin film of water. Nucleophilic substitution at the benzylic position of the silane with pyridine dye **88** was found to be best performed in refluxing toluene, at 1 mM concentration.[20,28] This reaction was slower at the lower reflux temperature of $CHCl_3$. After washing the functionalised slides, UV-visible absorption spectroscopy proved the presence of surface-bound dye by comparison of the spectra with a control slide, which had not been treated with the silane before treating with the dye.

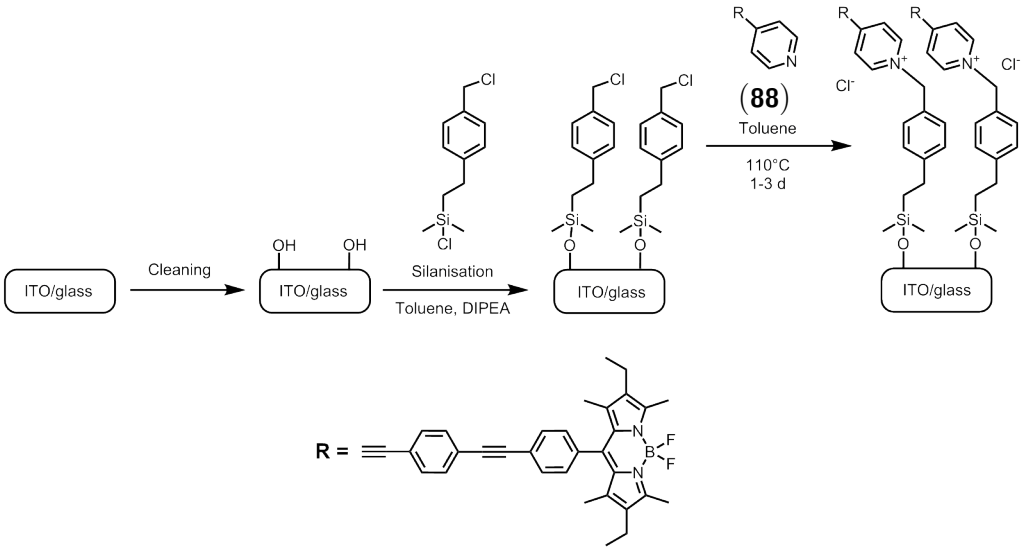

Scheme **5.4** The steps involved in functionalising glass or ITO-coated glass surfaces.

5.5.3 Functionalising ITO-coated glass surfaces

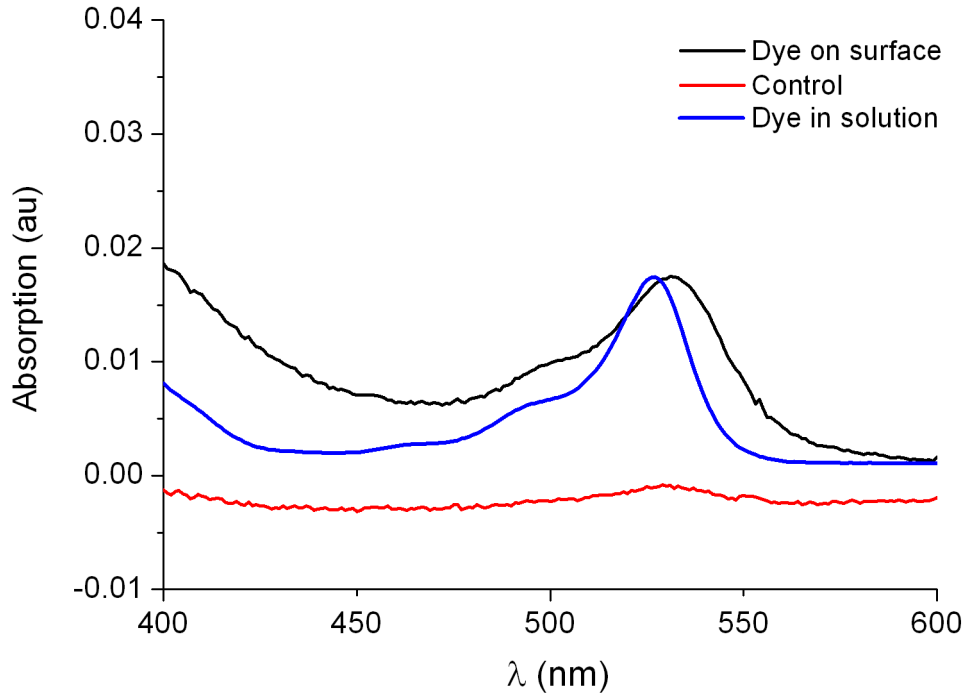

Figure **5.6** Grafting of the dye onto the silanised ITO surface was judged to be occurring by changes in absorption compared to a control ITO surface which was not silanised. A normalised overlay of the absorption of the equivalent dye in $CHCl_3$ solution is included for comparison.

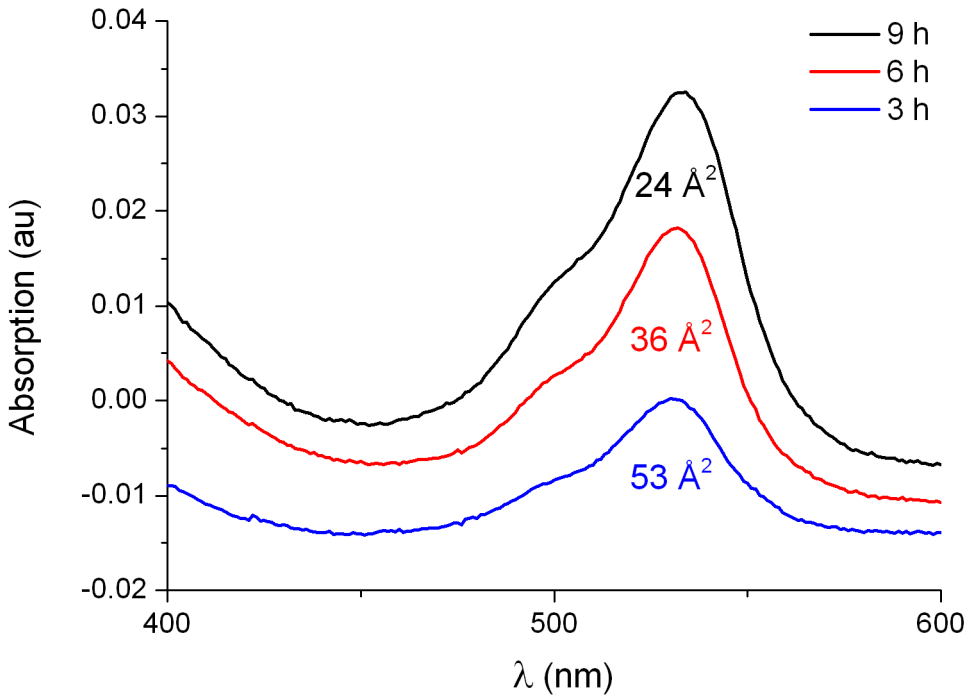

Figure **5.7** Absorption and area per chromophore after 3, 6 and 9 hours of dye functionalisation.

This successful procedure was then applied to functionalising ITO surfaces, the only difference being the cleaning method used for these slides: to prevent the removal of the ITO coating, degreasing with organic solvents was followed by oxygen plasma treatment.[27,29,30,34] Contact angle tests were again used to confirm the efficacy of this process.

Following the same silanisation and dyeing procedures as before, UV-visible absorption spectra showed that the surface functionalisation was occurring as expected (Figure 5.6 on the page before). The broadening and bathochromic shift of the absorption compared to the solution spectrum is indicative of excitonic coupling between proximate dyes on the surface.[35] On these slides, the dye grafting reaction was studied in more detail, for example by looking at the dependence between reaction time and surface coverage (Figure 5.7). The coverage was estimated by comparison of the integrated absorption spectra on the

surface and at known concentration in solution.[35] The area per molecule found suggests that the functionalisation nears completion, assuming that the long axis of each molecule lies perpendicular to the surface, based upon Hyperchem modelling of **88** (Figure 5.8). Fluorescence (emission and excitation, Figure 5.9 on the following page) measurements were also performed, and again confirm the identity of the surface-bound dye.

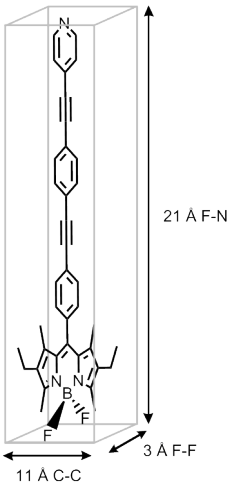

Figure **5.8** Modelling of **88** suggests an area of 33 Å^2 if the dye is aligned perpendicular to the surface, and an area of 60–220 Å^2 if the dye lies flat on the surface.

5.5.4 Device construction

The steps described in this section are illustrated in Scheme 5.5 on Page 239. With functionalised slides in hand, preliminary trials at applying the polymer layer were undertaken next. Spin-coating was used as it is a readily available technique leading to a high-quality polymer layer.[36–38] In this technique, a volume of a polymer solution is applied to the substrate to be coated, and the substrate is then spun for a short period (for example one minute), during which time the solution is spread evenly across the substrate, and the polymer is deposited as the solvent evaporates. Literature relationships between spin speed, polymer properties (such as average molecular weight and polydispersity) and polymer concentration are noted.[39,40] Toluene is regarded as

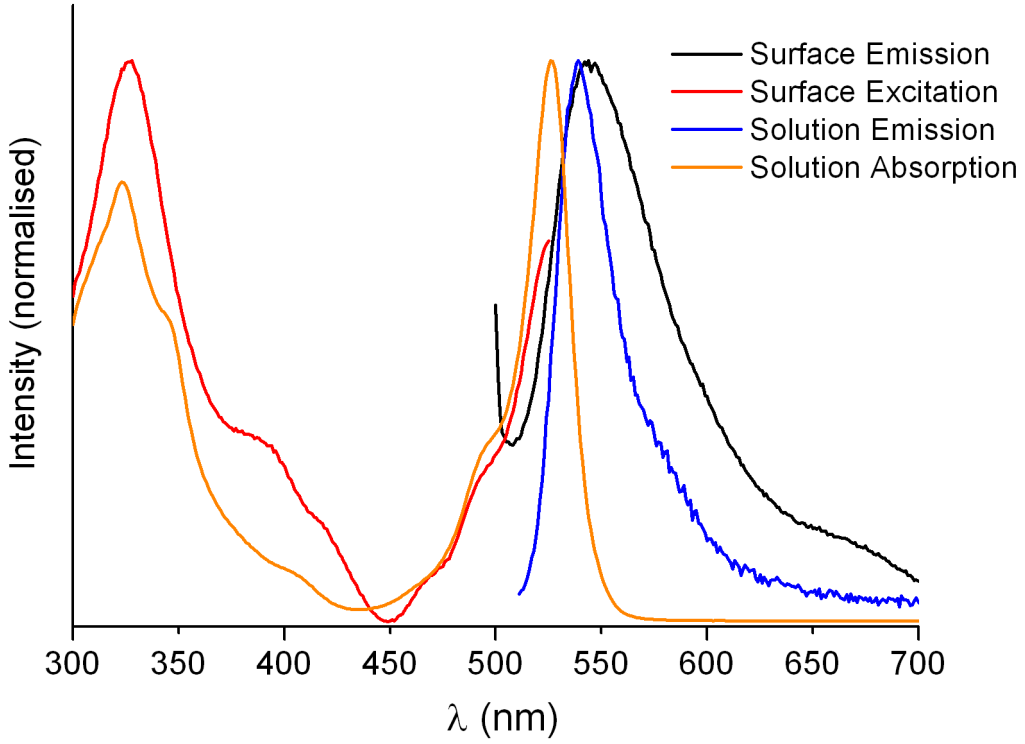

Figure **5.9** Normalised emission and excitation measurements performed on a dye-functionalised ITO surface, compared to the emission and absorption measured in solution.

a good solvent for spin-coating, with smoother polymer layers found by researchers compared to those formed from more volatile solvents like CH_2Cl_2.[40] A polymer with M_w in the range 10^4-10^5 will give a thicker polymer film with higher mechanical integrity than a lower M_w polymer.[40] Considering the desired thickness, a film over 100 nm is preferable on the grounds of stability (some defect-forming mechanisms are less likely to operate)[41] and a film over 200 nm is beneficial because of the ITO surface roughness.[29,30] However, in the absence of specific data pertaining to currently available PS samples, ellipsometry (performed by Dr. Robert Jacobs) was used to compare solutions of weight percentage 1-8% M_w 192,000 PS in toluene. To simplify the ellipsometry, the solutions were spun onto silicon wafers instead of onto functionalised ITO slides. The 8% solution gave films with thicknesses in the range 400-500 nm.

Using this method to apply a polymer layer to a partially silanised and dyed

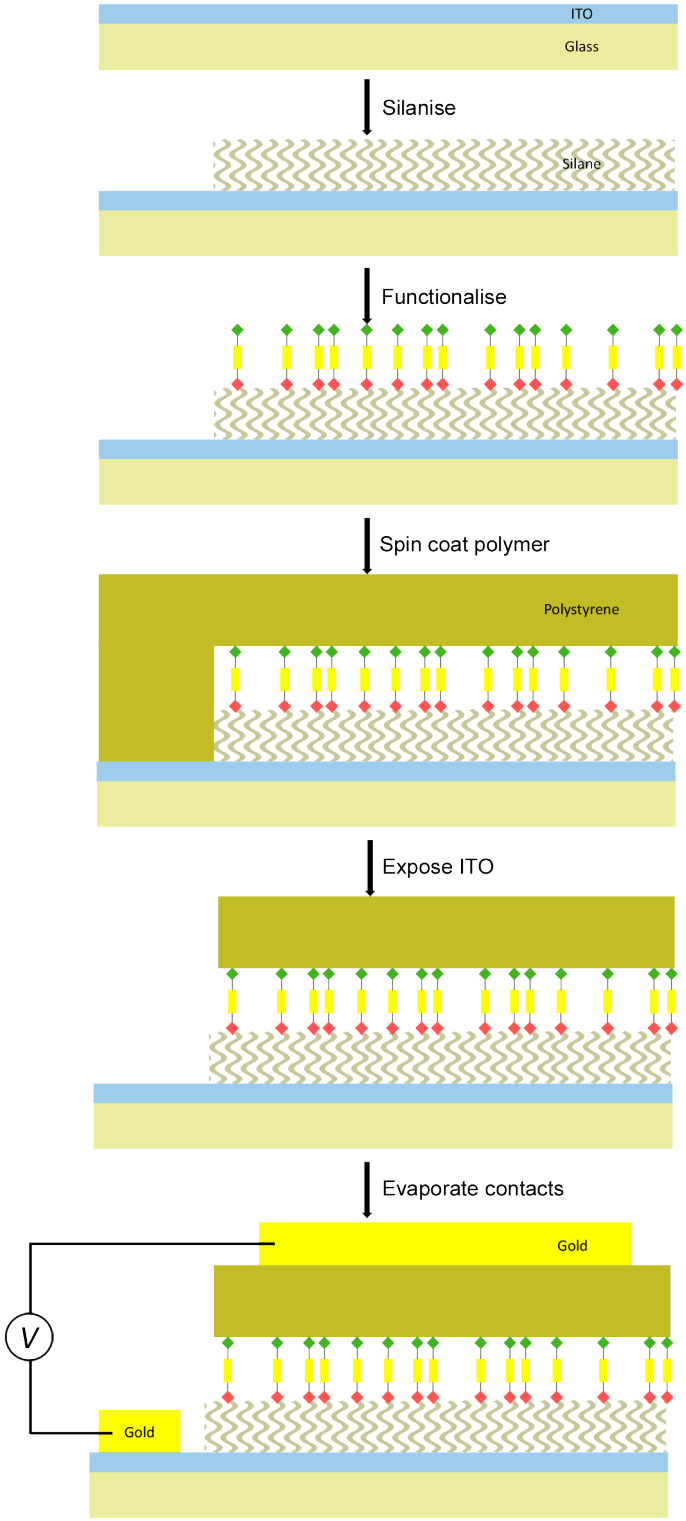

Scheme **5.5** A step-by-step schematic of the VSD testing device construction.

ITO slide, the polymer was then carefully removed from the undyed section of the slide using solvent, exposing some ITO. Gold contacts were then evapo-

rated onto the exposed ITO and the polymer to allow the device to be tested (evaporation performed by Dr. Robert Jacobs). Unfortunately, resistance measurements revealed short circuits in these pilot devices, preventing their operation as capacitors. Optical microscopy of the polymer layers revealed defects, most likely arising from the presence of dust. PS is expected to provide a good surface energy match with the hydrophobic BODIPY dye, so a surface energy mismatch is not the most probable source of the defects seen.[42] It is also not expected that the polymer is adversely affected by the evaporation of gold contacts onto it.[31,32] The first step to bypassing this problem would be to repeat the device construction in a controlled dust-free environment. If the polymer layer continued to display the same flaw under these conditions, different polymers would be tested, as polymer dewetting in the absence of dust is indicative of a poor surface energy match between the polymer and the underlying dye layer.

5.6 Synthesis of a dye to test the proposed testing device

In parallel with developing the new VSD testing device, a pyridine precursor of a known pyridinium VSD was synthesised (compound **115**, Scheme 5.6 on the following page). This precursor could provide further experimental evidence of successful CGM formation *via* post-functionalisation of the surface by quaternarisation of a pyridine-containing dye. The availability of this precursor was also deemed to be necessary in order to allow devices to be made that would provide a positive control that the method is suitable for testing voltage-sensitivity.

The published synthesis of **Di-4-ANEPPS** (Scheme 5.6 on the next page) and related dyes features a high temperature and high pressure Bucherer reac-

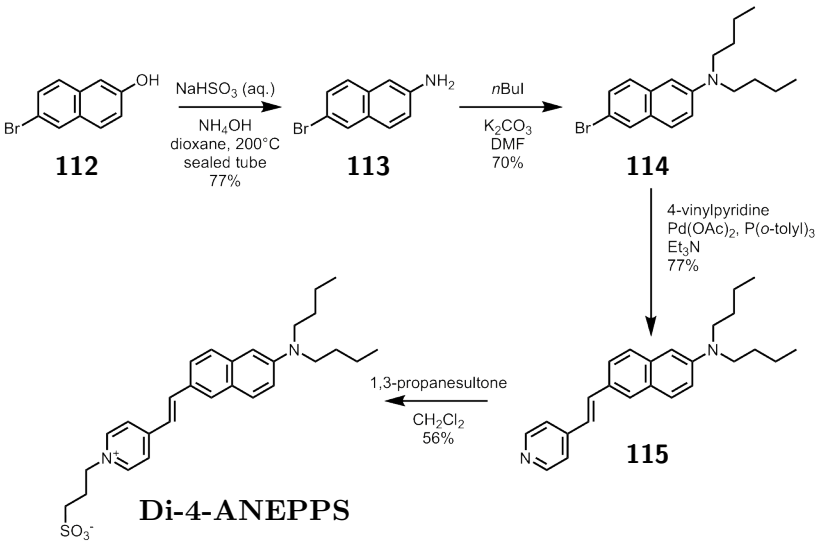

Scheme **5.6** The original synthesis of **Di-4-ANEPPS**.[43,44]

tion to convert the starting material (6-bromo-2-naphthol, **112**) into 6-bromo-2-aminonaphthalene **113**.[43,44] The amine is then alkylated, and Heck coupling used to attached the 4-vinylpyridine before the final quaternarisation step.[43]

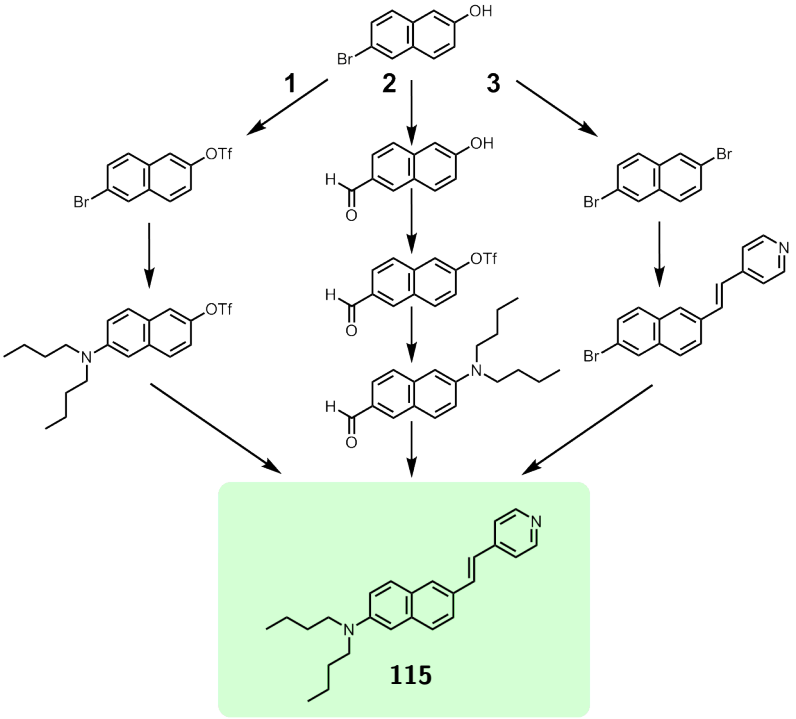

Scheme **5.7** Three possible alternative routes to the pyridine precursor of **Di-4-ANEPPS**.

The tremendous improvements in organometallic coupling reactions since the original synthesis of **Di-4-ANEPPS** was published prompted the investigation into an alternative synthetic route that would circumvent the need to use the potentially dangerous Bucherer conditions. Three general approaches to the precursor **115** (Scheme 5.7 on the preceding page) seemed possible based on literature searches: first, the triflation of 6-bromo-2-naphthol followed by a selective Buchwald coupling on the bromo position, giving a similar intermediate to the original route, completed by Heck coupling to add the 4-vinylpyridine at the triflate position; second, formylation with CO/H_2 or CO and a silane under Pd-catalysed conditions to give 6-hydroxy-2-naphthaldehyde,[45,46] followed by triflation, Buchwald coupling to the amine and then a Knoevenagel reaction to add the 4-vinylpyridine; third, conversion of 6-bromo-2-naphthol into 2,6-dibromonaphthalene, followed by a statistical Buchwald or Heck reaction, then a Heck or Buchwald reaction respectively to give **115**.

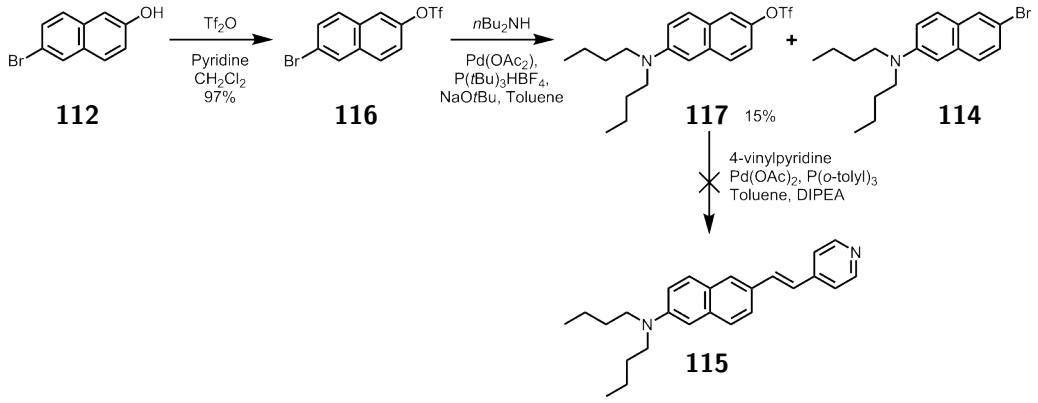

Scheme **5.8** The first route attempted towards the **Di-4-ANEPPS** precursor **115**.

Attempting route one first (Scheme 5.8), the triflation of the naphthol starting material **112** proceeded cleanly, and a Buchwald cross-coupling with dibutylamine was then expected to selectively functionalise at the bromo position, as reported for other amines (diphenylamine and benzamide) with this reactant.[47,48] However, clean samples of the desired compound **117** were only

obtainable in 15% yield, due to difficulties separating it from the starting material **116** and the byproduct **114**. This complication is in contrast with the high yield and high selectivity of the literature reports, but Buchwald reactions can be very sensitive to substrate changes. Test reactions of the unprecedented attachment of 4-vinylpyridine to the triflate position of **116** using Heck conditions consistently resulted in recovered starting material **116**.

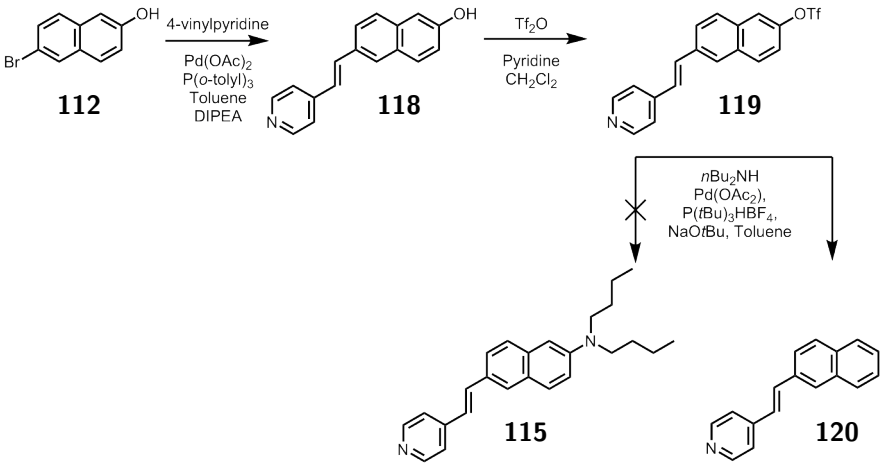

Scheme **5.9** A variation on the first route towards **115**.

This route was then tried in a different order (Scheme 5.9). First, 4-vinylpyridine was coupled to the bromo position of **112** to give **118**. The naphthol position was then triflated, and the Buchwald attempted at this position. Unfortunately, the Buchwald conditions replaced the triflate with a hydrogen to give compound **120**, rather than coupling the amine at this position.

As route three carried more overlap with route one than route two did, it was attempted next (Scheme 5.10 on the next page). 2,6-Dibromonaphthalene **121** was first prepared from **112** following a literature method. This step was achieved in low yield but on a large scale (2 grams of isolated product). Based on the experiences of route one, the less reactive Heck step seemed the best first choice for the statistical step, and the mono-substituted product **122** was formed in 29% yield, along with 40% recovered starting material and 22% of the bis-substituted product **123**. The Buchwald reaction to couple the amine

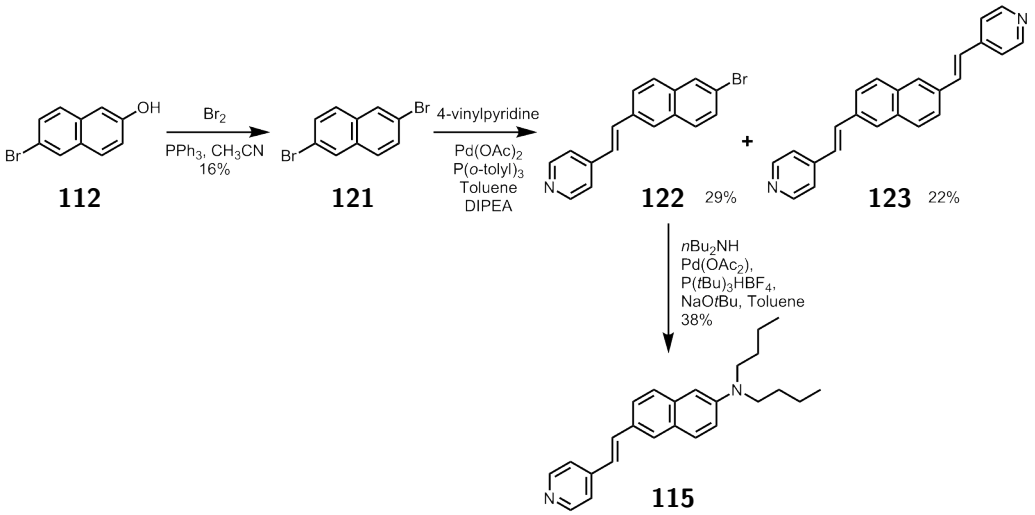

Scheme **5.10** The third route successfully yielded the desired compound **115**.

to **122** requires optimising, but yielded 38% of the targeted **Di-4-ANEPPS** precursor **115**.

With appropriate optimisation, the route established will prove to be a useful preparation of **115** for research into the VSD testing method proposed in this chapter, or for researchers needing access to a **Di-4-ANEPPS** analogue with an alternative headgroup without a commercial source.

The second route was not pursued as it required more synthetic conversions, and the Knoevenagel step is reported to be best performed using a 4-methyl-*N*-methylpyridinium rather than 4-methyl-pyridine as desired here.[43]

5.7 Conclusion to Chapter 5

The work in this chapter presents first steps towards a new testing method for VSDs which may prove to be a useful tool, especially for the screening of pyridinium-based dyes. The design provides a lipid-free method for orientating chromophores in an electric field, and does not require an amphiphilic dye to be used, but rather the pyridine precursor of an amphiphilic dye. This eliminates the troublesome purification associated with charged, amphiphilic

compounds, and enables studies of voltage-sensitive behaviour to be made before the commitment of synthesising amphiphilic dyes. It also lifts the limit of the electric field that can be applied ten-fold compared to lipid bilayer membranes, a useful feature for studying novel voltage sensors. The system as reported is restricted to pyridine-based dyes, but the wide scope of surface functionalisation reactions will allow other types of dyes to be tested also after suitable modification. A test dye for this system was also synthesised, utilising milder reactions than the literature precedence for this type of compound. With the correct optimisation, both of these avenues of investigation will prove useful in facilitating research into VSDs.

5.8 Experimental for Chapter 5

Compound numbers correspond to those used in this chapter, except those labelled 5-A, -B etc. which are not featured in the main text. Novel compounds are denoted by an asterisk (*) after the name. General experimental details can be found in Section 2.12 on Page 80.

111 Chloro(4-[chloromethyl]phenethyl)dimethylsilane

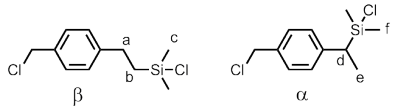

This compound was made according to a literature procedure.[28] THF was added to a pre-dried flask under N_2. 4-Vinylbenzylchloride (5.0 mL, 36 mmol), $H_2PtCl_6 \cdot xH_2O$ (100 mg, ~0.25 mmol) and phenothiazine (88 mg, 0.44 mmol) were added under N_2, the mixture freeze-pump-thaw degassed 3 × and purged with N_2. Dimethylchlorosilane (5.1 mL, 46 mmol) was added dropwise at 0 °C from a dropping funnel over 30 mins. The mixture was stirred for 21 h at room temperature before the solvent was removed under vacuum. The product was distilled from the crude mixture under reduced pressure (0.05 mbar, 82-84 °C) using a Vigreux fractionating column and then re-distilled to give an oil consisting of 91 : 9.0 β : α (2.7 g, 30%). ^{1}H NMR (400 MHz, $CDCl_3$) δ 7.35 (d, J=8.0 Hz, 2 H, β-**aryl**), 7.28 - 7.33 (m, 0.18 H, α-**aryl**), 7.25 (d, J=7.9 Hz, 2 H, β-**aryl**), 7.16 (d, J=7.9 Hz, 0.19 H, α-**aryl**), 4.61 (s, 2 H, **benzylic**), 2.76 - 2.83 (m, 2 H, **a**), 2.48 (q, J=7.5 Hz, 0.086 H, **d**), 1.50 (d, J=7.5 Hz, 0.30 H, **e**), 1.19 - 1.25 (m, 2 H, **b**), 0.46 (s, 6 H, **c**), 0.38 (d, J=10.8 Hz, 0.56 H, **f**). ^{13}C NMR (101 MHz, $CDCl_3$) δ 144.2, 135.1, 128.8, 128.3, 46.2, 28.9, 20.8, 1.7. MS Calcd for $C_{11}H_{16}Cl_2Si$: 246.0398. Found (TOF FI+): 246.0406.

121 2,6-Dibromonapthalene

A literature prep was followed on a modified scale.[49] Two flasks were dried un-

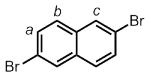

der vacuum. Triphenylphosphine (14.1 g, 53.8 mmol) was added to one flask, 6-bromo-2-naphthol (10.0 g, 44.8 mmol) to the other, and both dried under vacuum. Dry acetonitrile (20 mL) was added to each flask under N_2. The triphenylphosphine solution was cooled to 0 °C and bromine (2.53 mL, 49.3 mmol) was added dropwise *via* syringe. The mixture was stirred at room temperature for 30 min before the brown 6-bromo-2-naphthol solution was added *via* canula. The resulting mixture was stirred at 70 °C for 2 hours, during which the solution turned orange. The solvent was removed by heating to 140 °C, and the residue was heated to 300 °C for 1 hour. The resulting black tar was allowed to cool to 100 °C before dissolving the product in toluene. The cooled toluene solution (orange) was washed with 1 M NaOH and water then dried over $MgSO_4$. The solvent was evaporated, the residue dissolved in MeOH and the precipitate filtered and washed with MeOH to yield 2.1 g (16%) of the desired product. ^{1}H NMR (400 MHz, $CDCl_3$) δ 7.98 (d, J=1.8 Hz, 2 H, **c**), 7.63 (d, J=8.8 Hz, 2 H, **b**), 7.58 (dd, J=8.8, 1.8 Hz, 2 H, **a**). ^{13}C NMR (101 MHz, $CDCl_3$) δ 132.8, 130.3, 129.9, 128.6, 120.2. MS Calcd for $C_{10}H_6Br_2$: 285.8816. Found (TOF FI+): 285.8825.

122 (*E*)-4-(2-(6-Bromonaphthalen-2-yl)vinyl)pyridine*

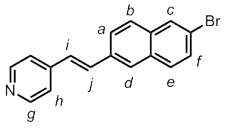

To a pre-dried Schlenk tube were added **121** (300 mg, 1.05 mmol), $Pd(OAc)_2$ (10.2 mg, 45.4 μmol) and tris(*o*-tolyl)phosphine (27.3 mg, 89.6 μmol). These were dried under vacuum and the flask was purged with N_2. Toluene (2 mL), diisopropylamine (2 mL) and 4-vinylpyridine (126 μL, 1.17 mmol) were added

via syringe and the mixture was freeze-pump-thaw degassed 3 ×. The reaction was stirred at 110 °C for 3 h, after which 2 products were observed by TLC. The mixture was concentrated and dried under high vacuum before purification on silica, eluting with $CHCl_3$: 1% MeOH. The solvents were removed from the first fraction to give the desired product as a yellow powder (95 mg, 29%). The bis-substituted product was also isolated (79 mg, 22%), and starting material recovered also (119 mg, 40%), total recovery 91%. ^{1}H NMR (400 MHz, MeOD) δ 8.47 (d, J=6.3 Hz, 2 H, **g**), 7.96 (d, J=1.5 Hz, 1 H, **d**), 7.86 (s, 1 H, **c**), 7.74 (d, J=2.3 Hz, 1 H, **e**), 7.71 (d, J=9.1 Hz, 1 H, **b**), 7.56 - 7.60 (m, 1 H, **f**), 7.50 - 7.55 (m, 1 H, **a**), 7.48 (d, J=6.1 Hz, 2 H, **h**), 7.47 (d, J=16.9 Hz, 1 H, **j**), 7.15 (d, J=16.2 Hz, 1 H, **i**)

115 (*E*)-*N*,*N*-dibutyl-6-(2-(pyridin-4-yl)vinyl)naphthalen-2-amine

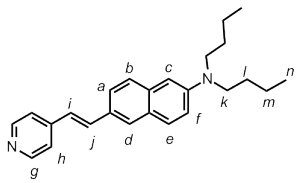

To a pre-dried Schlenk tube were added **122** (45.0 mg, 145 μmol), NaOtBu (70.0 mg, 725 μmol), $Pd(OAc)_2$ (1.6 mg, 7.3 μmol) and $P(t\text{Bu})_3HBF_4$ (4.2 mg, 15 μmol). These were dried under vacuum and the flask was purged with N_2. THF (1.5 mL) and $n\text{Bu}_2\text{NH}$ (244 μL, 1.45 mmol) were added, freeze-pump-thaw degassed and heated to 70 °C under N_2. After 90 mins, the mixture was concentrated then dried under high vacuum. The residue was purified on silica eluting with 1 : 1 petrol ether : ethyl acetate. The desired product was obtained as an orange solid (20 mg, 38%). ^{1}H NMR (400 MHz, $CDCl_3$) δ 8.56 (d, J=5.6 Hz, 2 H, **g**), 7.72 (br. s, 1 H, **d**), 7.68 (d, J=9.2 Hz, 1 H, **e**), 7.57 - 7.64 (m, 2 H, **a, b**), 7.41 (d, J=16.2 Hz, 1 H, **i**), 7.38 (d, J=5.8 Hz, 2 H, **h**), 7.07 (dd, J=9.0, 2.6 Hz, 1 H, **f**), 7.01 (d, J=16.4 Hz, 1 H, **j**), 6.81 (d, J=2.2 Hz, 1 H, **c**), 3.39 (t, J=7.7 Hz, 4 H, **k**), 1.60 - 1.69 (m, 4 H, **l**), 1.41 (dq, J=15.0, 7.4

Hz, 4 H, **m**), 1.00 (t, J=7.3 Hz, 6 H, **n**) ^{13}C NMR (101 MHz, $CDCl_3$) δ 149.9, 146.8, 145.4, 135.6, 134.0, 129.3, 129.1, 128.0, 126.5, 125.7, 123.6, 123.3, 120.6, 116.0, 105.0, 50.9, 29.5, 20.4, 14.0. MS Calcd for 359.25: C25H31N2. Found (TOF ESI+): 359.3. λ_{max}/nm (log ϵ) in THF: 394 (4.44).

5.8.1 General surface chemistry procedures

Slides were cut to $\sim$ 15 mm $\times$ 25 mm with a diamond-tipped pen before use. Glass slides were standard microscope slides, and were first cleaned by immersion in a Petri dish (one face touching the bottom of the dish) containing freshly mixed Piranha solution (7 : 3 c.H_2SO_4 : 30-35% aq.H_2O_2) for 90 mins and then rinsed copious amounts of deionised water, sonicated in deionised water, dried under a flow of N_2 then under vacuum in an oven held at 160 °C for a minimum of 15 mins. ITO-coated glass substrates (Sigma-Aldrich, 70-100 Ω/sq) require milder cleaning procedures,[29] and were cleaned by sonication in acetone (10 mins), CH_2Cl_2 (10 mins), dried under a flow of N_2 then cleaned by oxygen plasma treatment in a Bio-Rad PT7125 Barrel Plasma Etcher at 150 W for 15 mins. Slides were stored under N_2 in a dessicator prior to use. After cleaning, slides were handled exclusively with tweezers. It is assumed that these cleaning protocols only clean the exposed face of the slide, and thus that subsequent silanisation only occurs on one face also.

All reactions were followed by sonication of the slides in a beaker of dry toluene, and the slides were then dried under a flow of N_2 and stored in a dessicator in the dark under N_2 prior to further use or characterisation.

Cleaning, silanisation and spin-coating procedures were all confirmed to be successful by the appropriate change in hydrophobicity of the surface, as judged by a 'naked eye' contact angle measurement.

5.8.2 Adsorption of silane **111** onto glass or ITO

This surface reaction was carried out at room temperature in 7 mL vials in a dessicator purged with N_2. Each slide was partially immersed in a toluene solution of the silane **111** (5% v/v) and DIPEA (1% v/v) for 30 min in an individual vial. The silanisation solution was handled under a flow of N_2 to limit water content.

5.8.3 Functionalisation with dye **88**

This reaction required refluxing solvent and was thus conducted in a two-neck flask, the wider neck used to insert slides under a flow of N_2, and the narrow neck equippped with a condensor. The silanised slides were immersed in a 1 mM toluene solution of **88**, and brought to reflux under N_2 after pump-purge degassing. Reaction times were varied from 30 min to 3 days.

5.8.4 Device preparation

A slide with satisfactory dye coverage (as judged by UV/vis absorption spectroscopy) had the polymer layer applied by spin-coating. The slide was held on the rotating table by vacuum and rubber seal, the polymer solution (125 μL, 8% by weight, M_w 192,000 PS) was applied using an Eppendorf pippette, and the slide was spun at 1500 revolutions per min (acceleration time $\sim$ 1 s) for a period of 1 min. Following spinning, the slide stood for 2 h in a dessicator under N_2, before transfer to a vacuum oven for a further 2 h (60 °C, 0.15 mbar). Polymer coating the edge of the slide without silane/dye (see Scheme 5.5 on Page 239) was removed using a cotton bud soaked in acetone. Gold contacts were then evaporated under vacuum onto the ITO and the polymer as illustrated in Scheme 5.5 (This experiment was performed by Dr. Robert Jacobs using an Edwards Auto 306 Cryo Evaporator). The initial test of this completed device was a simple check of resistance across the two gold contacts

using a micrometer. The gold electrode on top of the polymer was contacted using a fine strip of foil to avoid applying pressure to the polymer layer.

5.9 Bibliography

1 Cohen, L. B.; Salzberg, B. M.; Davila, H. V.; Ross, W. N.; Landowne, D.; Waggoner, A. S.; Wang, C. H. *J. Membr. Biol.* **1974**, *19*, 1–36.
2 Acker, C. D.; Yan, P.; Loew, L. M. *Biophys. J.* **2011**, *101*, L11–L13.
3 Holthoff, K.; Zecevic, D.; Konnerth, A. *J. Physiol.* **2010**, *588*, 1085–1096.
4 Zhou, W.-L.; Yan, P.; Wuskell, J. P.; Loew, L. M.; Antic, S. D. *J. Neurosci. Meth.* **2007**, *164*, 225–239.
5 Reeve, J. E.; Corbett, A. D.; Boczarow, I.; Kaluza, W.; Barford, W.; Bayley, H.; Wilson, T.; Anderson, H. L. *Angew. Chem. Int. Ed.* **2013**, *52*, 9044–9048.
6 Loew, L. M. *J. Biochem. Biophys. Methods* **1982**, *6*, 243–260.
7 Weaver, J. C.; Mintzer, R. A. *Phys. Lett. A* **1981**, *86*, 57–59.
8 Tung, L.; Troiano, G. C.; Sharma, V.; Raphael, R. M.; Stebe, K. J. *Ann. N. Y. Acad. Sci.* **1999**, *888*, 249–265.
9 Gross, E.; Bedlack, R. S.; Loew, L. M. *Biophys. J.* **1994**, *67*, 208–216.
10 Przybylo, M.; Borowik, T.; Langner, M. *J. Fluoresc.* **2010**, *20*, 1139–1157.
11 Peterka, D. S.; Takahashi, H.; Yuste, R. *Neuron* **2011**, *69*, 9–21.
12 Chan, Y.-H. M.; Boxer, S. G. *Curr. Opin. Chem. Biol.* **2007**, *11*, 581–587.
13 Knoll, W.; Köper, I.; Naumann, R.; Sinner, E.-K. *Electrochim. Acta* **2008**, *53*, 6680–6689.
14 Ito, T.; Yamazaki, I.; Ohta, N. *J. Phys. Chem. B* **2002**, *106*, 895–898.
15 Ito, T.; Yamazaki, I.; Ohta, N. *Chem. Phys. Lett.* **1997**, *277*, 125–131.
16 Ariga, K.; Yamauchi, Y.; Mori, T.; Hill, J. P. *Adv. Mater.* **2013**, *25*, 6477–6512.
17 Bublitz, G. U.; Boxer, S. G. *Annu. Rev. Phys. Chem.* **1997**, *48*, 213–242.
18 Samanta, D.; Sarkar, A. *Chem. Soc. Rev.* **2011**, *40*, 2567–2592.
19 Haensch, C.; Hoeppener, S.; Schubert, U. S. *Chem. Soc. Rev.* **2010**, *39*, 2323–2334.
20 Anderson, S. *Langmuir* **2008**, *24*, 13962–13968.
21 Sekar, M. M. A.; Hampton, P. D.; Buranda, T.; López, G. P. *J. Am. Chem. Soc.* **1999**, *121*, 5135–5141.
22 Ding, L.; Fang, Y. *Chem. Soc. Rev.* **2010**, *39*, 4258–4273.
23 Armstrong, N. R.; Shepard Jr., V. R. *J. Electroanal. Chem. and Interfac. Electrochem.* **1980**, *115*, 253–265.
24 Okahata, Y.; Yokobori, M.; Ebara, Y.; Ebato, H.; Ariga, K. *Langmuir* **1990**, *6*, 1148–1153.
25 Schlapak, R.; Armitage, D.; Saucedo-Zeni, N.; Hohage, M.; Howorka, S. *Langmuir* **2007**, *23*, 10244–10253.

26 Chen, L.-J.; Shah, S. S.; Verkhoturov, S. V.; Revzin, A.; Schweikert, E. A. *Surf. Interface Anal.* **2011**, *43*, 555–558.
27 Jain, S.; Tanwar, V.; Dixit, V.; Verma, S.; Samanta, S. *App. Surf. Sci.* **2001**, *182*, 350–356.
28 Roscoe, S. B.; Kakkar, A. K.; Marks, T. J.; Malik, A.; Durbin, M. K.; Lin, W.; Wong, G. K.; Dutta, P. *Langmuir* **1996**, *12*, 4218–4223.
29 Moore, E.; O'Connell, D.; Galvin, P. *Thin Solid Films* **2006**, *515*, 2612–2617.
30 Markovich, I.; Mandler, D. *J. Electroanal. Chem.* **2001**, *500*, 453–460.
31 Yoon, M.-H.; Facchetti, A.; Marks, T. J. *Proc. Nat. Acad. Sci.* **2005**, *102*, 4678–4682.
32 DiBenedetto, S. A.; Facchetti, A.; Ratner, M. A.; Marks, T. J. *J. Am. Chem. Soc.* **2009**, *131*, 7158–7168.
33 Chuang, V. T. *U.S. Patent* **1975**, US3925434A.
34 Choi, Y.; Noh, J. *Mol. Cryst. Liq. Cryst.* **2008**, 165/[529]–171/[535].
35 McCallien, D. W. J.; Burn, P. L.; Anderson, H. L. *J. Chem. Soc., Perkin Trans. 1* **1997**, 2581–2586.
36 Schubert, D. *Polymer Bulletin* **1997**, *38*, 177–184.
37 Na, M.; Rhee, S.-W. *Org. Electr.* **2006**, *7*, 205–212.
38 Park, J. H.; Hwang, D.; Lee, J.; Im, S.; Kim, E. *Thin Solid Films* **2007**, *515*, 4041–4044.
39 Hall, D. B.; Underhill, P.; Torkelson, J. M. *Polym. Eng. Sci.* **1998**, *38*, 2039–2045.
40 Spangler, L. L.; Torkelson, J. M.; Royal, J. S. *Polym. Eng. Sci.* **1990**, *30*, 644–653.
41 Stange, T. G.; Evans, D. F.; Hendrickson, W. A. *Langmuir* **1997**, *13*, 4459–4465.
42 Al Akhrass, S.; Reiter, G.; Hou, S. Y.; Yang, M. H.; Chang, Y. L.; Chang, F. C.; Wang, C. F.; Yang, A. C.-M. *Phys. Rev. Lett.* **2008**, *100*, 178301–178304.
43 Hassner, A.; Birnbaum, D.; Loew, L. M. *J. Org. Chem.* **1984**, *49*, 2546–2551.
44 Takakura, H.; Sasakura, K.; Ueno, T.; Urano, Y.; Terai, T.; Hanaoka, K.; Tsuboi, T.; Nagano, T. *Chem. Asian J.* **2010**, *5*, 2053–2061.
45 Brennführer, A.; Neumann, H.; Beller, M. *Synlett* **2007**, 2537–2540.
46 Klaus, S.; Neumann, H.; Zapf, A.; Strübing, D.; Hübner, S.; Almena, J.; Riermeier, T.; Gross, P.; Sarich, M.; Krahnert, W.-R.; Rossen, K.; Beller, M. *Angew. Chem. Int. Ed.* **2006**, *45*, 154–158.
47 Tam, V. K.; Liu, Q.; Tor, Y. *Chem. Commun.* **2006**, 2684–2686.
48 Shaibu, B. S.; Lin, S.-H.; Lin, C.-Y.; Wong, K.-T.; Liu, R.-S. *J. Org. Chem.* **2011**, *76*, 1054–1061.
49 Kaku, T.; Matsunaga, N.; Ojida, A.; Tanaka, T.; Hara, T.; Yamaoka, M.; Kusaka, M.; Tasaka, A. *Bioorg. Med. Chem.* **2011**, *19*, 1751–1770.